DEPARTAMENT DE BIOLOGIA CEL·LULAR I ANATOMIA PATOLÒGICA

FACULTAT DE MEDICINA, UNIVERSITAT DE BARCELONA

IMPLICACIÓN DE LOS FACTORES NEUROTRÓFICOS EN LA FISIOPATOLOGÍA Y PROTECCIÓN DE LA ENFERMEDAD DE HUNTINGTON

Tesis presentada por José Ramón Pineda Martí

para optar al título de Doctor en Biología

RESULTADOS

Primer trabajo

"Brain-Derived Neurotrophic Factor Regulates the Onset and Severity of Motor Dysfunction Associated with Enkephalinergic Neuronal Degeneration in Huntington's Disease"

Publicado en *The Journal of Neuroscience*

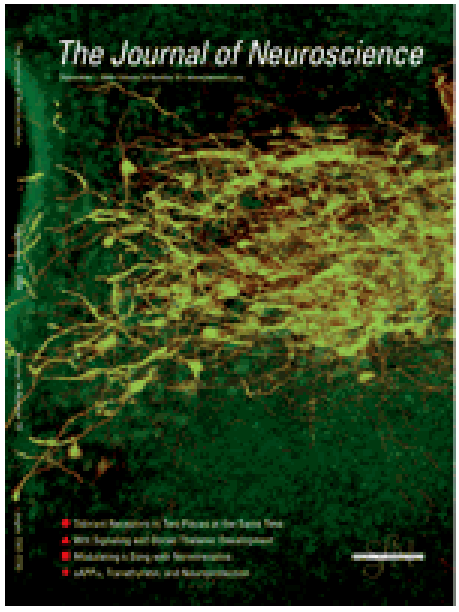

The Journal of Neuroscience, September 1, 2004 • 24(35):7727–7739 • 7727

Neurobiology of Disease

Brain-Derived Neurotrophic Factor Regulates the Onset and Severity of Motor Dysfunction Associated with Enkephalinergic Neuronal Degeneration in Huntington's Disease

Josep M. Canals,[1] José R. Pineda,[1] Jesús F. Torres-Peraza,[1] Miquel Bosch,[1] Raquel Martín-Ibañez,[1] M. Teresa Muñoz,[1] Guadalupe Mengod,[2] Patrik Ernfors,[3] and Jordi Alberch[1]

[1]Departament de Biologia Cel·lular i Anatomia Patològica, Facultat de Medicina, Institut d'Investigacions Biomèdiques August Pi i Sunyer, Universitat de Barcelona, and [2]Department of Neurochemistry, Institut d'Investigacions Biomèdiques de Barcelona–Consejo Superior de Investigaciones Cientificas, Institut d'Investigacions Biomèdiques August Pi i Sunyer, E-08036 Barcelona, Spain, and [3]Laboratory of Molecular Neurobiology, Department of Medical Biochemistry and Biophysics, Karolinska Institute, S-17177 Stockholm, Sweden

The mechanism that controls the selective vulnerability of striatal neurons in Huntington's disease is unclear. Brain-derived neurotrophic factor (BDNF) protects striatal neurons and is regulated by Huntingtin through the interaction with the neuron-restrictive silencer factor. Here, we demonstrate that the downregulation of BDNF by mutant Huntingtin depends on the length and levels of expression of the CAG repeats in cell cultures. To analyze the functional effects of these changes in BDNF in Huntington's disease, we disrupted the expression of *bdnf* in a transgenic mouse model by cross-mating *bdnf*$^{+/-}$ mice with R6/1 mice. Thus, we compared transgenic mice for mutant Huntingtin with different levels of BDNF. Using this double mutant mouse line, we show that the deficit of endogenous BDNF modulates the pathology of Huntington's disease. The decreased levels of this neurotrophin advance the onset of motor dysfunctions and produce more severe uncoordinated movements. This behavioral pathology correlates with the loss of striatal dopamine and cAMP-regulated phosphoprotein-32-positive projection neurons. In particular, the insufficient levels of BDNF cause specific degeneration of the enkephalinergic striatal projection neurons, which are the most affected cells in Huntington's disease. This neuronal dysfunction can specifically be restored by administration of exogenous BDNF.

Therefore, the decrease in BDNF levels plays a key role in the specific pathology observed in Huntington's disease by inducing dysfunction of striatal enkephalinergic neurons that produce severe motor dysfunctions. Hence, administration of exogenous BDNF may delay or stop illness progression.

Key words: neurotrophins; cell death; striatum; knock-out; movement disorders; polyQ

Introduction

Neurodegenerative disorders such as Parkinson's, Huntington's, or Alzheimer's diseases are characterized by the loss of specific neuronal populations. The mechanism responsible for the neurodegenerative pattern of each disease is not known. In Huntington's disease (HD), the CAG triplet expansion in the *huntingtin* gene (*htt*) causes a primary loss of striatal projection neurons that, in turn, leads to progressive motor impairment (Hickey and Chesselet, 2003). Although *htt* is widely expressed in all animal cells and its mutation is not tissue specific, the medium-sized spiny striatal neurons, which express GABA, and dopamine and cAMP-regulated phosphoprotein (DARPP)-32, undergo selective degeneration. Within the striatum, two separate subpopulations of GABAergic neurons project to the external globus pallidus or to the substantia nigra pars reticulata and the internal globus pallidus, originating the "indirect" and "direct" pathways, respectively. The first of these subpopulations expresses enkephalin and is enriched in D_2 dopamine receptors, whereas the neurons that project to the substantia nigra and the internal globus pallidus express substance P and D_1 dopamine receptors (Gerfen, 1992). The primary affected striatal neurons are the enkephalinergic and those neurons that project to the substantia nigra; however, striatal output to the internal globus pallidus is relatively preserved (Richfield et al., 1995). Striatal interneurons are also spared in this disorder (Sieradzan and Mann, 2001). This

Received March 31, 2004; revised July 1, 2004; accepted July 2, 2004.

This study was supported by Ministerio de Ciencia y Tecnología Grants SAF2002-00314 (J.A.), SAF2002-00311 (J.M.C.), and SAF1999-0123 (G.M.); Redes Temáticas de Investigación Coorporativa (G03/167, G03/210; Ministerio de Sanidad y Consumo); Fundació La Caixa; and Fundación Ramón Areces. J.R.P. is a fellow of the Ministerio de Educación, Cultura y Deporte, J.F.T.-P. is a fellow of the Fundación Gran Mariscal de Ayacucho, M.B. is a fellow of the Universitat de Barcelona, and R.M.-I. is a fellow of the Ministerio de Ciencia y Tecnologia. We thank Drs. Lydia Giménez-Llort and Mara Dierssen for their help with behavior design and analyses and for critically reading this manuscript. We are grateful to Sonia Marco, Ana López, and Francesca Calderón for technical assistance, Drs. Jordi Petriz and Isabel Sanchez (Cell Separation Unit, Institut d'Investigacions Biomèdiques August Pi i Sunyer) for their support and advice in cell sorting technique, Anna Bosch (Serveis Científico-Tècnics, Universitat de Barcelona) for her support and advice in the use of confocal microscopy, Dr. Josep Lluis Carrasco (Departament de Salut Pública, Universitat de Barcelona) for statistical analyses, and Dr. Emili Martínez for the behavior set up. We are also grateful to Dr. Amèrica Jiménez and the staff of the animal facility (Facultat de Medicina, Universitat de Barcelona) for their help with mouse care. We thank Robin Rycroft for checking the English.

Correspondence should be addressed to Dr. Jordi Alberch, Departament de Biologia Cel·lular i Anatomia Patològica, Facultat de Medicina, Institut d'Investigacions Biomèdiques August Pi i Sunyer, Universitat de Barcelona, C/Casanova, 143, E-08036 Barcelona, Spain. E-mail: alberch@ub.edu.

DOI:10.1523/JNEUROSCI.1197-04.2004

 0270-6474/04/247727-13$15.00/0

specific degeneration correlates with the appearance of choreic movements (Reiner et al., 1988). However, neuronal degeneration extends to other brain regions such as the cerebral cortex, particularly in more advanced cases (Rubinsztein, 2002).

It has been suggested that mutant Htt initiates a cascade of different events in the disease that converge in the specific cell death of striatal neurons. A large number of abnormalities have been reported in HD, including transcription deficits, energy impairment, excitotoxicity, and lack of trophic support (Sugars and Rubinsztein, 2003; Alberch et al., 2004). In this context, it has been shown recently that Htt directly modulates the expression of neuron-restrictive silencer factor (NRSF)-controlled neuronal genes, including the *brain-derived neurotrophic factor* (*bdnf*) gene (Zuccato et al., 2003). Thus, wild-type (wt) Htt stimulates the production of BDNF, a neurotrophic factor for striatal neurons (Perez-Navarro et al., 2000), whereas mutant Htt reduces it (Zuccato et al., 2001). In keeping with these findings, BDNF is decreased in brain tissue from human HD patients (Ferrer et al., 2000; Zuccato et al., 2001) and in some mice transgenic for *mutant htt* (Zuccato et al., 2001; Duan et al., 2003; Zhang et al., 2003).

Besides this evidence that mutant Htt regulates BDNF expression, it remains to be established whether downregulation of endogenous BDNF participates in the specific motor dysfunctions observed in HD. To study the function of endogenous BDNF in HD, we generated a double-mutant animal by crossing *bdnf* heterozygous mice with a model of HD. Our present data show that reduction of BDNF levels advances the age of onset and exacerbates the lack of motor control. This enlarged neurological pathology correlates with morphological alterations, which shows that BDNF plays a role in the specific degeneration of the striatal enkephalinergic population.

Materials and Methods

Cell procedures. We used the conditionally immortalized striatal derived neural stem cells, M213 (a generous gift from Dr. W. Freed, National Institute on Drug Abuse, Bethesda, MD) (Giordano et al., 1993). For all experiments, cells were grown and passaged at the permissive temperature of 33°C in DMEM (Invitrogen, Renfrewshire, Scotland) supplemented with 10% fetal calf serum (Invitrogen). Cells were transfected using the rat neural stem cells nucleofector kit as described by the manufacturer (Amaxa, Cologne, Germany). M213 cells (5×10^6) were resuspended in 200 μl of nucleofector solution (Amaxa) and mixed with 5 μg of the required cDNA for each sample. Electroporation was performed using the A-33 nucleofector program (Amaxa). We transfected three different constructs, which allowed us to express the mutant exon 1 of the *htt* gene with different CAG/CAA repeats: 47 (qp47), 72 (qp72), and 103 (qp103) (Kazantsev et al., 1999) (generously provided by Dr. George M. Lawless, Cure HD Initiative, Reagent Resource Bank of the Hereditary Disease Foundation, New York, NY).

For the study of BDNF secretion, cells were cultured in 24-well plates for 24 hr after transfection and, thereafter, positively expressing cells were purified by cell sorting. Cell sorting was performed on a fluorescence-activated cell sorting Vantage SE (Becton Dickinson, Mountain View, CA) using a single laser set at 488 nm. Cells were sorted according to the endogenous enhanced green fluorescent protein (EGFP) fluorescence intensity, and fluorescent channel 1 threshold was set to collect only cells with high levels of expression except for qp103 clones, for which the gates were adjusted to collect separately the cells with high and low levels of expression (see Fig. 1*B*, inset). Sorting conditions were as follows: drop drive of 23,000 drops per second; three drops of sorting envelope; sample rate of 500–1000 cells per second; drop delay of 12.0. Sorted cells were collected in the cell culture medium described above and seeded at a density of 10,000 cells/cm^2 onto 24-well plates. One day later, the expression of EGFP was assessed in an inverted fluorescent microscope. More than 80% of cells were positive, showing larger and more abundant aggregates in cells transfected with longer constructs. The levels of *mutant htt* directly correlate to the levels of EGFP, because both are expressed as a fusion protein. Six days after plating, the cell culture was removed and processed for the quantification of the BDNF levels. Proteins from cell lysates were quantified to normalize the levels of BDNF with respect to the microgram of protein from cells for each well at the end of the experiment.

Mouse strains. To obtain double-mutant mice with mutant Htt and low levels of BDNF (bDM; $bdnf^{+/-}$ htt^{m}) or mice with mutant Htt and low levels of neurotrophin (NT)-3 (n3DM; $nt\text{-}3^{+/-}$ htt^{m}), we crossmated R6/1 mice (Mangiarini et al., 1996) with *bdnf* heterozygous (Ernfors et al., 1994a) or *nt-3* heterozygous mice (Ernfors et al., 1994b), respectively. F2 $bdnf^{+/+}$ htt^{m} × $bdnf^{+/-}$ htt^{wt} or F2 $nt\text{-}3^{+/+}$ htt^{m} × $nt\text{-}3^{+/-}$ htt^{wt} inbred mice were used in this study. All experiments were performed on male littermates from the F2 population to avoid strain and sex differences. Mice were housed together in numerical birth order in groups of mixed genotypes until they were 30 weeks of age with access to food and water *ad libitum* in a colony room kept at a constant temperature (19–22°C) and humidity (40–50%) on a 12 hr light/dark cycle. All experiments were conducted in a blind-coded manner with respect to genotype, and data were recorded for analysis by microchip mouse number. For developmental studies, some animals were killed 15 d after birth (n = 4–6 per genotype). All animal-related procedures were in accordance with the National Institutes of Health guide for the care and use of laboratory animals and approved by the local animal care committee of the Universitat de Barcelona (99/01) and by the Generalitat de Catalunya (99/1094). Animals were killed at 30 weeks of age, just before they drastically lost weight and died. Body weight was measured twice each week.

For genotyping, DNA was obtained from tail biopsy and processed for PCR. The primers used for DNA amplifications have been described previously (Ernfors et al., 1994b; Mangiarini et al., 1996; Agerman et al., 2003). PCR fragments were resolved in agarose gels, 2% for *bdnf* or *nt-3* amplification and 1.5% for *mutant htt* analysis.

In vivo *BDNF treatment.* Administration of exogenous BDNF was performed in 20-week-old R6/1 mice (n = 5) and in 14-week-old bDM (n = 5) at the disease onset in each genotype. BDNF (4.5 μg per day) was continuously infused using an osmotic minipump at a rate of 1 μl per hour (Alzet model 2001; Alza, Palo Alto, CA). A 28-gauge stainless steel cannula was implanted into the left striatum (coordinates: anteroposterior, +0.5; lateral, +2.0 from bregma and dorsoventral, −2.7 from dura). The cannula was fixed on the skull with anchor screws and dental cement. The metal inlet of the cannula was fitted to a tube connected to the osmotic pump filled with either BDNF (187.5 ng/μl in PBS) or PBS alone (sham controls). The Alzet minipump was previously equilibrated for 4 hr at 37°C in 0.9% NaCl. The pump was implanted subcutaneously in the back of the animal. After 1 week, animals were killed and brains were analyzed for *in situ* hybridization for neuropeptides.

Behavior analysis. Behavioral testing began at 3 weeks of age, when mice were weaned. Tests were conducted regularly until week 30 to follow the progression of each phenotype (n = 9–16 mice per group). Motor coordination and balance were evaluated on the rotarod apparatus at several revolutions per minute as described previously (Carter et al., 1999). In brief, animals were trained at a constant speed (24 rpm) for 60 sec. We performed four trials per day on three consecutive days, and the latency to fall was recorded. No differences between groups were detected during this period. After training, mice were evaluated once every 2 weeks at 16, 24, and 32 rpm starting at 6 weeks of age, and the number of falls in a total of 60 sec was recorded. The animals were put on the rotarod several consecutive times until the addition of the latency to fall off reached the total time of 60 sec. We compared the curves of the behavior pattern and calculated the percentage of rotarod impairment as described previously (Ferrante et al., 2002). The curves have been estimated through generalized linear mixed models assuming a residual distributed under a Poisson distribution. The estimation approach used was the Penalized Quasi-Likelihood, and the effects have been tested using the F-Wald test. To analyze the individual differences in each time point, we performed a one-way ANOVA followed by least significant difference (LSD; t test) *post hoc* test.

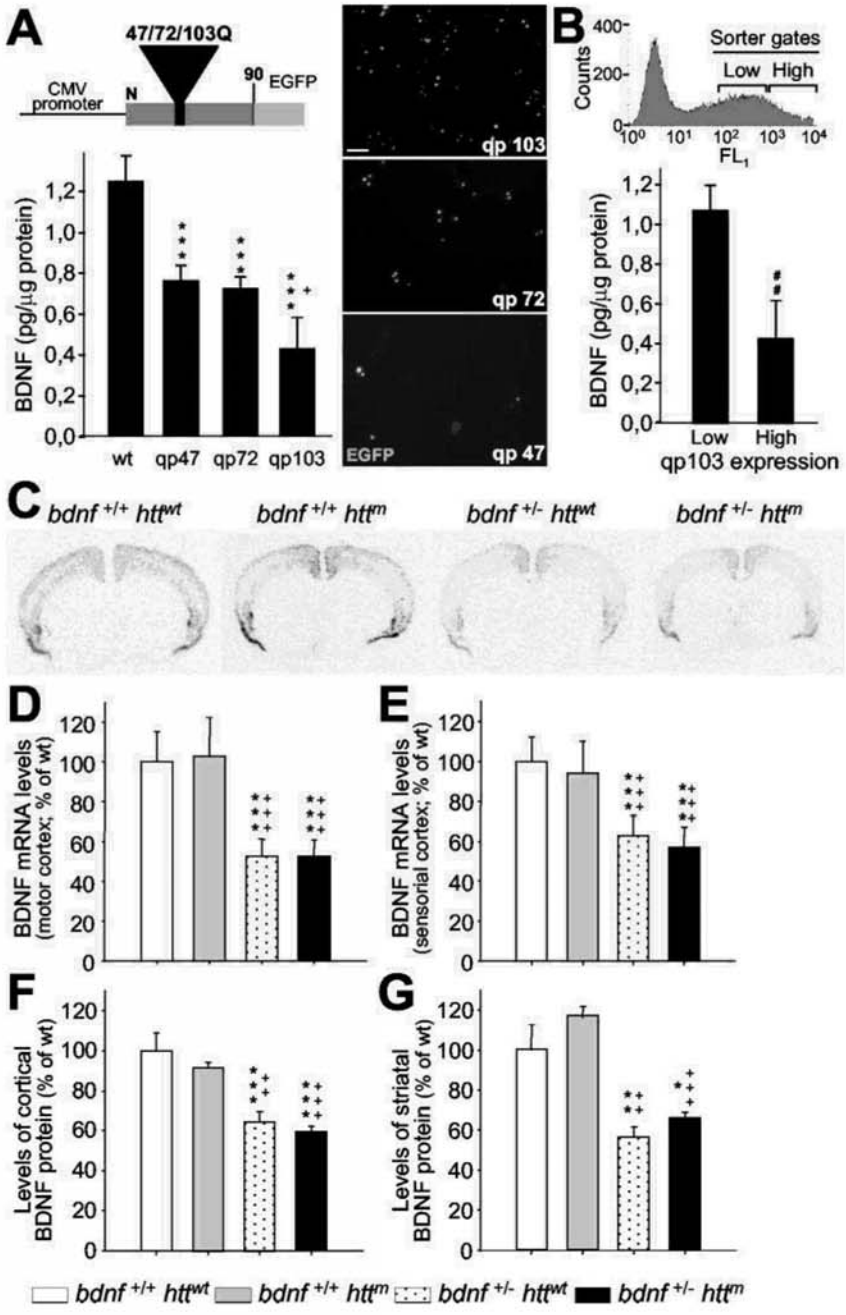

Figure 1. The number of CAG repeats and the levels of *mutant htt* expression modulate the expression of BDNF. *A*, ELISA for BDNF was performed on the culture media from wt M213 cells and subclones expressing exon 1 of *mutant htt* with 47 (qp47), 72 (qp72), and 103 CAG/CAA repeats (qp103). The expression of this neurotrophin decreases as the number of repeats is longer. The scheme at the top shows the structure of qp constructs, which expresses a fusion protein of the first 90 amino acids of the *mutant htt* and the EGFP. The right panels are photomicrographs of transfected cells with the qp47, 72, and 103 constructs, which show the *mutant htt* inclusions. CMV, Cytomegalovirus. Scale bar, 50 μm. *B*, Transfected cells that express different levels of qp103 were collected by cell sorting (inset shows sorting gates), and BDNF levels were assessed. The amount of BDNF in culture media is inversely proportional to the levels of expression of qp103. $^{***}p < 0.001$ compared with wt cells; $^{+}p < 0.05$ compared with qp47 or qp72; $^{\#\#}p < 0.005$ compared with low levels of qp103 expression. *C–G*, BDNF levels are not affected by the mutant exon 1 of Htt in R6/1 ($bdnf^{+/+}$ htt^{m}). *C–E*, *In situ* hybridization demonstrates that *mutant htt* does not change the levels of *bdnf* expression either in the motor cortex (*D*) or in the sensorial cortex (*E*). *C*, A Representative coronal section (bregma, +1.1 mm) of *bdnf in situ* hybridization of the four genotypes analyzed. *F*, *G*, In addition, the levels of BDNF protein detected by ELISA are not modified by *mutant htt* in the cortex (*F*) or in the striatum (*G*). The only changes in mRNA or protein are detected in $bdnf^{+/-}$ mice with or without *mutant htt* (*C–G*). $^{*}p < 0.05$, $^{**}p < 0.005$, and $^{***}p < 0.001$ compared with wt mice ($bdnf^{+/+}$ htt^{wt}); $^{++}p < 0.005$ and $^{+++}p < 0.001$ compared with R6/1 mice ($bdnf^{+/+}$ htt^{m}).

The walking footprint pattern, equilibrium, vision, and muscular strength were evaluated at 30 weeks of age ($n = 9–16$ mice per group). The footprint test was performed as described previously (Carter et al., 1999). Mice were trained three consecutive times to walk in a corridor that was 50 cm long and 7 cm wide. To register the experiments, the forefeet and hindfeet of the mice were painted with nontoxic black and red ink, respectively, and then given one run. The footprint pattern was analyzed for the number of steps on the white paper, the stride length was measured as the average distance of forward movement between each stride, and the forebase and hindbase widths were measured as the perpendicular distance between the left and right footprints of a given step.

Equilibrium was analyzed by placing the mice at the center of a raised (60 cm) horizontal rod (50 cm long), and their latency to fall off the rod was scored with a maximum of 60 sec. A flat wooden rod (12 mm wide) was used in trials 1 and 2, and a cylindrical wire rod (14 mm diameter) was used in trials 3 and 4. The distance covered on the cylindrical rod was also registered and analyzed. The latency to fall off the wooden rod was recorded with no differences between groups found. The visual cliff avoidance and the wire hang tests were performed as described previously (Lione et al., 1999; Gimenez-Llort et al., 2002).

For analyses of circling behavior, bDM were injected intraperitoneally with amphetamine (5 mg/kg) 1 week after unilateral BDNF infusion. Mice were placed in circular cages and connected to an automated rotometer. A computer recorded the number of complete (360°) turns made during a 5 min period. Mice were allowed 15 min to habituate to the rotometer before the administration of amphetamine. The values were expressed as net total numbers of full turns in 1 hr.

Results were expressed as the mean of several animals, and error bars represent the SEM. Statistical analysis was performed using one-way ANOVA followed by LSD *post hoc* test.

ELISA. BDNF or NT-3 contents were determined in duplicate by the Emax ImmunoAssay system (Promega, Madison, WI), as described previously (Perez-Navarro et al., 2000). For cell cultures, the cell culture media were collected after 6 d of plating cell after cell sorting. We analyzed 50 μl of supernatants from cell cultures diluted 1:1 in block and sample buffer. Values were normalized by the total protein content of the cells in each well at the end of the experiment and expressed as picogram of neurotrophin per microgram of protein. For total protein measurements, wells were washed twice with PBS and then cells were homogenized in lysis buffer (137 mM NaCl, 20 mM Tris-HCl, pH 8.0, 1% Igepal, 10% glycerol, 1 mM PMSF, 10 μg/ml Aprotinin, 1 μg/ml Leupeptin). Quantifications were performed using the Detergent Compatible Protein Assay (Bio-Rad, Hercules, CA) following the manufacturer instructions.

For analysis of BDNF levels in brain tissue, mice were deeply anesthetized in a CO_2 cham-

ber at 30 weeks of age ($n = 4$ per genotype). Their cortex and striatum were dissected out on ice and rapidly frozen using CO_2 pellets. Samples were then homogenized in lysis buffer, sonicated, and centrifuged (10 min at 14 rpm at 4°C). Supernatants were collected and the protein contents were measured as above. Total protein (300 μg) was analyzed for each point diluted 1:1.5 in block and sample buffer. Values were calculated as picogram of BDNF per milligram of tissue protein and standardized to the average of wt animals.

Western blot analysis. We analyzed the levels of wt Htt by Western blot analysis using the same monoclonal antibody against the wt Htt fragment described above (Mab2166; Chemicon, Temecula, CA). Samples ($n = 3$ per genotype and time point) were prepared and processed by Western blot as described previously (Dyer and McMurray, 2001). In brief, tissue from the cerebral cortex or striatum was homogenate by sonication in 10 μl of radioimmunoprecipitation assay buffer (150 mM NaCl, 50 mM Tris-HCl, pH 8.0, 1 mM EDTA, 1 mM EGTA, 1% Triton X-100, 0.1% SDS, 0.5% sodium deoxycholate, 1 mM PMSF, 10 μg/ml Aprotinin, 1 μg/ml Leupeptin) per milligram of tissue. After homogenation, samples were centrifuged twice at 12,000 × *g* for 10 min. Supernatant proteins (30 μg) without head denaturation were loaded in a 7.5% SDS-PAGE and transferred to Immobilon-P membranes (Millipore, Bedford, MA). Blots were blocked in 3% nonfat dry milk in TBS-T (150 mM NaCl, 20 mM Tris-HCl, pH 7.5, 0.05% Tween 20) and then incubated with 1:5000 of primary antibody in 0.5% nonfat dry milk in TBS-T. After several washes in TBS-T, blots were incubated with 1:1000 of anti-mouse IgG HRP-conjugated (Promega) and developed by ECL Western blotting analysis system (Bioscience Europe, Freiburg, Germany). As loading controls, we reincubated the membranes with a monoclonal anti-α-tubulin antibody (Sigma, St. Louis, MO).

Immunocytochemistry. To analyze the localization of wt Htt, we performed immunocytochemistry on M213 transfected with qp72. For these experiments, expressing cells were not selected by cell sorting to have a heterogenous population in each well. In addition, we analyzed qp72 cells because their smaller and less abundant aggregates allowed us to perform more accurate localization at different levels of aggregate formation. To detect wt Htt, we used a monoclonal antibody against the Htt fragment from aa 181–810 (Mab2166; Chemicon). This antibody only detects wt Htt because this sequence is not included in the qp-mutant Htt constructs used in the present study (Kazantsev et al., 1999). Cells were fixed with 4% paraformaldehyde solution in PBS. After three washes, cells were incubated with the primary antibody (1:1000 in PBT buffer: PBS with 1% bovine serum albumin and 0.3% Triton X-100) at 4°C for 16 hr. The excess of antibody was washed out with PBS and thereafter incubated with the secondary antibody (donkey anti-mouse-Texas Red conjugated 1:300; Jackson Immuno Research, West Grove, PA), washed, and mounted with Mowiol (Calbiochem, La Jolla, CA). Control avoiding the primary antibody was performed and resulted in no signal. Photomicrographs were taken using a confocal microscope.

Histology. For neurotrophin *in situ* hybridization studies, mice were killed by decapitation at 30 weeks of age, and brains were dissected out

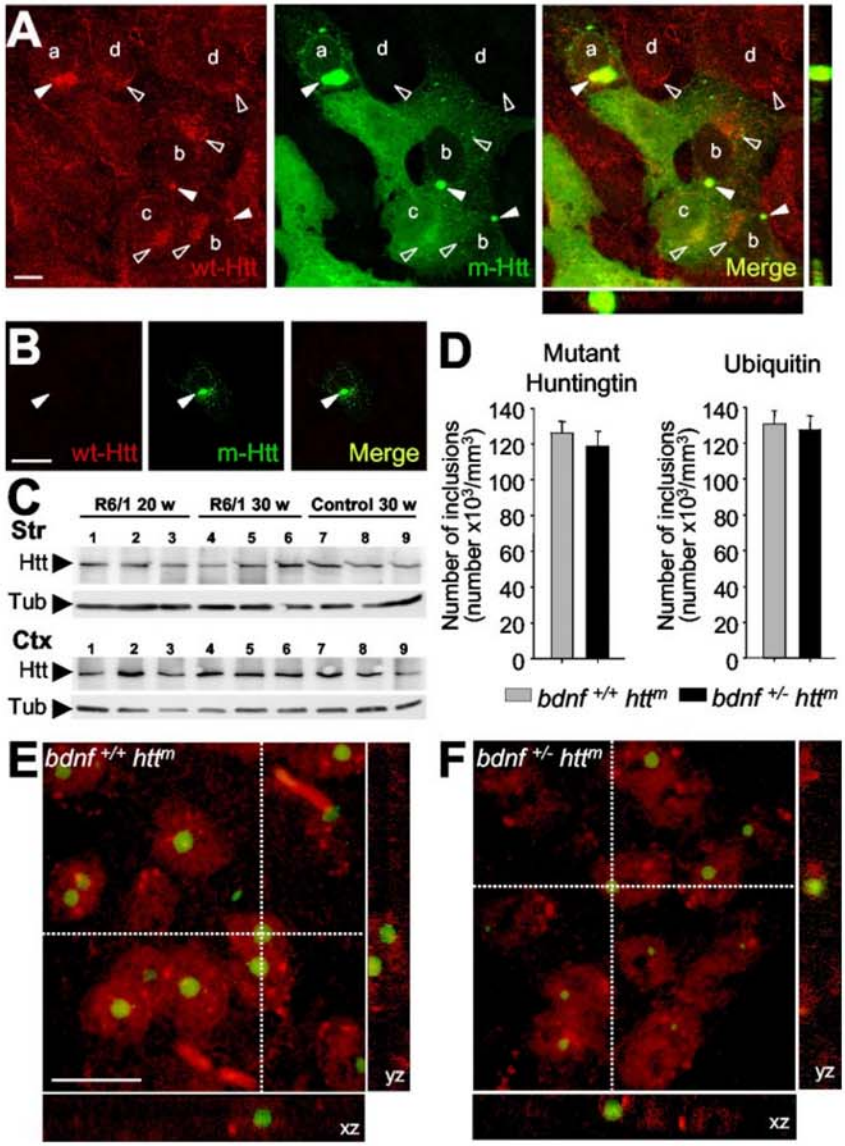

Figure 2. Sequestering wt Htt downregulates BDNF. *A*, Within nontransfected neural stem cells derived from the striatum (M213; *d*), wt Htt localizes in endocytic structures (open arrowheads). This localization is also detected in cells transfected with the exon 1 of *htt* with 72 repeats (qp72) that do not present aggregates (*c*) or that present small aggregates (*b*). However, in cells that express the qp72 construct and present large aggregates (*a*), wt Htt is only detected into the aggregates (filled arrowheads). We used the monoclonal antibody Mab2166 (Chemicon) to detect wt Htt (red; wt-Htt), whereas the mutant Htt was detected by the endogenous EGFP of the fusion protein (green; m-Htt). *B*, No signal for wt Htt was detected in the aggregates (filled arrowheads) in experiments avoiding the primary antibody. *C*, Western blot showing the levels of wt Htt in the cerebral cortex (Ctx) and in the striatum (Str) from R6/1 animals at 20 weeks (lanes 1–3) or at 30 weeks (lanes 4–6) or from wild-type mice at 30 weeks (lanes 7–9). Note that there are no changes in the levels of wt Htt (Htt) in R6/1. The levels of α-tubulin (Tub) are shown as a loading control. *D–F*, The levels of BDNF in *mutant htt* mice do not modify the number or morphological aspects of the intranuclear inclusions. Animals with *mutant htt* had intranuclear inclusions, which can be detected by mutant Htt or ubiquitin immunohistochemistry. *D*, The same density of aggregates was detected in both immunostaining patterns per genotype. In addition, similar results are shown in both R6/1 mice ($bdnf^{+/+}$ htt^m) and bDM ($bdnf^{+/-}$ htt^m), without significant differences between the two groups. *E*, *F*, Double immunohistochemistry against NeuN (red) and ubiquitin (green) demonstrated the same intranuclear location in both genotypes, containing *mutant htt*, with normal levels of BDNF (R6/1 mice; *E*) or with lower *bdnf* expression (bDM; *F*). Scale bars: *A*, 10 μm; *B*, 15 μm; (in *E*) *E*, *F*, 10 μm.

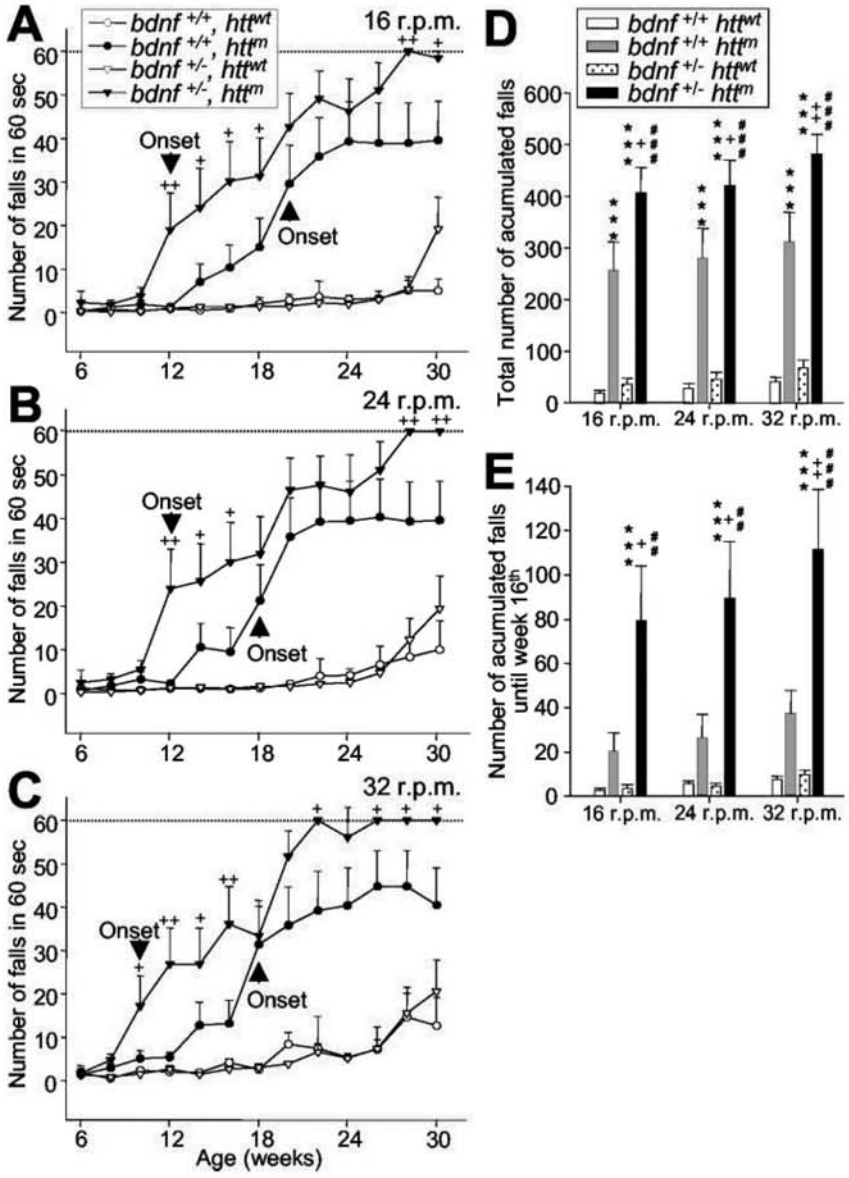

Figure 3. Lower BDNF levels cause earlier onset and more severe motor dysfunctions in *mutant htt* mice. *A–C*, bDM (*bdnf* $^{+/-}$ *htt*^{m}) show more deficits on the rotarod than R6/1 mice (*bdnf* $^{+/+}$ *htt*^{m}) tested at 16 rpm (*A*), 24 rpm (*B*), or 32 rpm (*C*) ($p <$ 0.001; F-Wald test). $^{+}p < 0.05$ and $^{++}p < 0.005$ compared with R6/1 mice (*bdnf* $^{+/+}$ *htt*^{m}). bDM show earlier symptoms at all revolutions assayed, and the onset of motor deficits (expressed as the first significant time point with respect to control animals; *A–C*, arrowhead) showed advances from 6–8 weeks with respect to R6/1 mice (*bdnf* $^{+/+}$ *htt*^{m}; *A–C*). *D*, In addition, bDM show more severe symptoms. The total number of accumulated falls in the period examined is significantly different between *mutant htt* mice with normal or low levels of BDNF. *E*, During early stages, the differences in the severity of motor deficits (measured as the total number of falls up to the age of 16 weeks) between R6/1 mice and bDM are very large. *D*, *E*, $^{***}p < 0.001$ compared with wt mice (*bdnf* $^{+/+}$ *htt*^{wt}); $^{+}p < 0.05$ and $^{++}p < 0.005$ compared with R6/1 mice (*bdnf* $^{+/+}$ *htt*^{m}); $^{\#\#}p < 0.005$ and $^{\#\#\#}p < 0.001$ compared with *bdnf* heterozygous mice (*bdnf* $^{+/-}$ *htt*^{wt}).

and frozen in dry-ice cooled isopentane ($n = 4$). Serial coronal cryostat sections (14 μm) were processed for hybridization with radioactive riboprobes (Ibanez et al., 1992; Laurenzi et al., 1994; Lindefors et al., 1995) as described previously (Canals et al., 2001). Antisense cRNA probe to detect the transcripts of neurotrophins was prepared by *in vitro* transcription using T3 or T7 RNA polymerase (Promega) and [^{33}P]-UTP (Bioscience Europe). For control experiments, sense cRNA probes were obtained by *in vitro* transcription using the opposite RNA polymerase. After deproteination and acetylation slices were incubated for 16 hr in a humidified chamber at 53°C with 3×10^{5} cpm of antisense probes in 150 μl of hybridization mixture (50% formamide, 20 mM Tris-HCl, pH 7.6, 1 mM EDTA, pH 8.0, 0.3 M NaCl, 0.1 M dithiothreitol, 0.5 mg/ml yeast tRNA, 0.1 mg/ml polyA RNA, 1× Denhardt's solution, and 10% dextran sulfate). After hybridization, slices were washed at high stringency, dried, and exposed to Biomax MR (Kodak, Rochester, NY) for 10 d.

Cresyl violet staining and immunohistochemistry assays were performed on paraformaldehyde fixed material as described previously (Canals et al., 2001). Animals were transcardially perfused with 4% paraformaldehyde solution in 0.1 M sodium phosphate, pH 7.2, at 15 d and 30 weeks of age. The brains were postfixed for 2 hr in the same solution, cryoprotected in incrementing 10–30% sucrose/PBS, and frozen in dry-ice cooled isopentane. Serial horizontal cryostat sections (30 μm) separately (0.3 mm) were processed for cresyl violet staining or immunohistochemistry.

Sections were processed as free-floating for immunohistochemistry. To block endogenous peroxidases, sections were incubated for 30 min with PBS containing 10% methanol and 3% H_2O_2. Sections were then washed three times in PBS and blocked for 1 hr with 2–10% normal serum in PBS. Tissue was then incubated with the appropriated primary antibody in PBS containing 2% normal goat serum for 16 hr at 4°C, except for DARPP-32, which was incubated at room temperature. The following antibodies were used: anti-neuronal-specific nuclear protein (NeuN) 1:100 (Chemicon); anti-DARPP-32, 1:10,000 (a generous gift from Dr. H. C. Hemming, Rockefeller University, New York, NY); anti-parvalbumin, 1:1250 (Sigma); anti-ubiquitin, 1:800 (Dako, High Wycombe, UK), and anti-mutant Htt, 1:50 (EM48; Chemicon). Sections were washed three times and incubated with a biotinylated secondary antibody (1/220; Pierce, Rockford, IL) for 1–2 hr at room temperature in the same buffer as the primary antibody. The immunohistochemical reaction was developed using the ABC kit (Pierce). No signal was detected in controls avoiding the primary antibodies.

For double-labeling immunohistochemistry, slides were coincubated with the primary antibodies anti-ubiquitin and anti-NeuN overnight at 4°C. After three washes in PBS, the sections were coincubated with both secondary antibodies (anti-rabbit FITC conjugated, 1:100, Vector Laboratories, Burlingame, CA; and anti-mouse Texas Red conjugated, 1:200, Jackson ImmunoResearch), washed, and mounted with Mowiol (Calbiochem). Double-labeling analysis was performed using a confocal microscope.

For enkephalin and substance P analyses, sections were processed by nonisotopic *in situ* hybridization as described previously (Serrats et al., 2003). Frozen tissue sections were air dried, fixed in 4% paraformaldehyde in PBS for 20 min at 4°C, washed once in 3× PBS and twice in 1× PBS for 5 min each, and incubated for 2 min at 21°C in a freshly prepared solution of predigested Pronase (Calbiochem) at a final concentration of 24 U/ml in 50 mM Tris-HCl, pH 7.5, 5 mM EDTA. Enzyme activity was stopped by immersion for 30 sec in 2 mg/ml glycine in PBS. Tissues were finally rinsed in PBS and dehydrated through a graded series of ethanol. Tissue sections were then covered

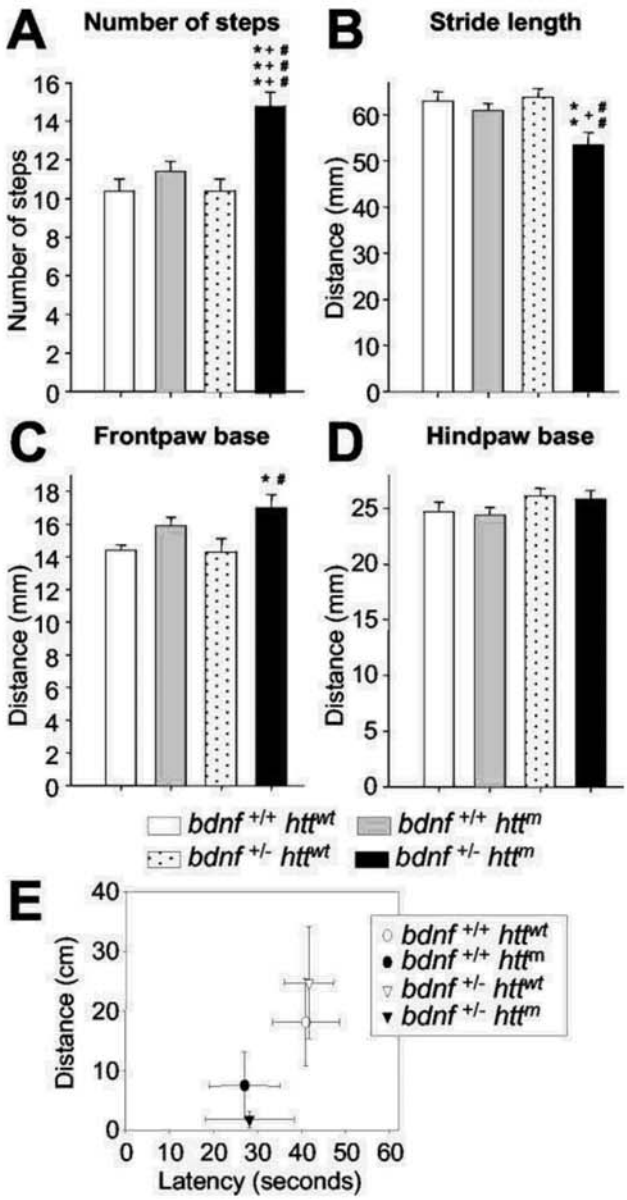

Figure 4. BDNF levels control motor coordination in *mutant htt* mice. *A–D*, The decrease of *bdnf* in *mutant htt* mice produces an uncoordinated walking footprint pattern. We analyzed the following four parameters of footprints: *A*, the number of steps; *B*, the distance between two consecutive steps; *C*, *D*, the distance between right and left frontbase and hindbase path, respectively. bDM shows differences in the number and distance of steps (*A*, *B*) and in the frontbase width (*C*). No differences were found in the hindbase pattern (*D*). $^{*}p < 0.05$, $^{**}p < 0.005$, and $^{***}p < 0.001$ compared with wt mice ($bdnf^{+/+}$ htt^{wt}); $^{+}p < 0.05$ and $^{+++}p < 0.001$ compared with R6/1 mice ($bdnf^{+/+}$ htt^{m}); $^{\#}p < 0.05$, $^{\#\#}p < 0.005$, and $^{\#\#\#}p < 0.001$ compared with *bdnf* heterozygous mice ($bdnf^{+/-}$ htt^{wt}). *E*, The levels of BDNF do not affect the mouse's ability to walk on a wire rod. Although we did not find statistical differences between groups, animals with *mutant htt* and with normal or lower levels of BDNF had a higher tendency to fall off the rod. The distance covered by the animals on the rod also shows the same effect, with shorter runs in those animals expressing *mutant htt*.

with 100 μl of hybridization buffer containing the probes, overlaid with Nescofilm coverslips (Bando Chemical, Kobe, Japan), and incubated overnight in humidified boxes at 42°C. Digoxigenin (DIG)-labeled probes were diluted in hybridization solution: 50% formamide, 4× SSC (1× SSC: 150 mM NaCl, 15 mM sodium citrate), 1× Denhardt's solution, 10% dextran sulfate, 1% Sarkosyl, 20 mM phosphate buffer, pH 7.0, 250 μg/ml yeast tRNA and 500 μg/ml salmon sperm DNA to a final concentration of 1.5 nM. The oligodeoxyribonucleotide probes used were as follows: the enkephalin probe was complementary to bases 513–542 of the enkephalin sequence (GenBank accession number K02807) and was synthesized on a 380 Applied Biosystem DNA synthesizer (Foster City Biosystem, Foster City, CA), and the substance P probe was complementary to bases 223–270 from the preprotachykinin A sequence (GenBank accession number M34183) and synthesized by Isogen Bioscience BV (Maarssen, The Netherlands). They were 3′-end labeled with terminal deoxynucleotidyltransferase and DIG-11-dUTP (Roche, Mannheim, Germany) as described previously (Schmitz et al., 1991). DIG-labeled oligonucleotides were purified by ethanol precipitation and resuspended in 200 μl of TE (10 mM Tris-HCl, pH 7.5, 1 mM EDTA, pH 8.0). After hybridization, sections were washed four times (45 min each) in a buffer containing 0.6 M NaCl and 10 mM Tris-HCl, pH 7.5, at 60°C.

Nonradioactive hybridization signal was developed as described previously (Landry et al., 2000). Briefly, after washing, the slides were immersed for 30 min in a buffer containing 0.1 M Tris-HCl, pH 7.5, 1 M NaCl, 2 mM $MgCl_2$, and 0.5% bovine serum albumin and incubated overnight at 4°C in the same solution with alkaline phosphate-conjugated anti-digoxigenin-F(ab) fragments (1:5000; Roche). They were then washed three times in the same buffer and twice in an alkaline buffer (0.1 M Tris-HCl, pH 9.5, 0.1 M NaCl, and 5 mM $MgCl_2$). Alkaline phosphatase activity was developed by incubating the sections with 3.3 mg of nitroblue tetrazolium and 1.65 mg of bromochloroindolyl phosphate (Invitrogen) dissolved in 10 ml of alkaline buffer. The enzymatic reaction was stopped by extensive rinsing in alkaline buffer with the addition of 1 mM EDTA. The sections were then dehydrated and air-dried.

Quantification of neurotrophin expression. The expression levels of different neurotrophins [nerve growth factor (NGF), BDNF, NT-3, and NT-4/5] were quantified on *in situ* hybridization films ($n = 4$). Consecutive sections (23–29 sections per animal) were scanned, and mRNA levels were analyzed using the ImageJ program (National Institute of Mental Health, Bethesda, MD). The intensity in a squared area of 152.4 μm^2 was quantified, and the background signal of the same adjacent area outside of the brain was subtracted. Results were expressed as the mean of several mice, and error bars represent the SEM. Statistical analysis was performed using one-way ANOVA followed by the LSD *post hoc* test.

Cell and inclusion counting. Brain, cortical, and striatal volumes were measured by using Image tool program (The University of Texas Health Center, San Antonio, TX) on a computer attached to an Olympus (Ballerup, Denmark) microscope. Consecutive sections (14–16 sections per animal) were visualized, and the borders of the anatomical landmarks were outlined. The volumes were calculated by multiplying the sum of all sectional areas (square millimeters) by the distance between successive sections (0.3 mm) as described previously (Canals et al., 2001).

All cell counts were performed blind with respect to genotype in 30-week-old mice ($n = 4–7$ per each group and staining). Unbiased stereological counts of striatal cells were obtained from the entire neostriatum using the computer-assisted stereology toolbox software (Olympus). The dissector counting method was used to analyze coronal sections spaced 300 μm apart. The counting frames were randomly sampled. We counted the neuron-like cells in cresyl violet staining as the cells with a large nonpyknotic nucleus with clear nucleoli. DARPP-32 neuron areas were analyzed using the program AnalySIS Auto (Soft Imaging System, Münster, Germany).

For intranuclear aggregate counting, three fields of 0.035 mm^2 were analyzed in each section separated by 0.3 mm ($n = 4$). The number of inclusions was expressed in density. To obtain the number per cubic millimeter, we divided the counts by the area corresponding to each field examined and multiplied by the thickness of the section.

All results were expressed as the mean and the SEM of different mice. Statistical analysis was performed using ANOVA followed by the LSD *post hoc* test or a Student's *t* test for independent samples.

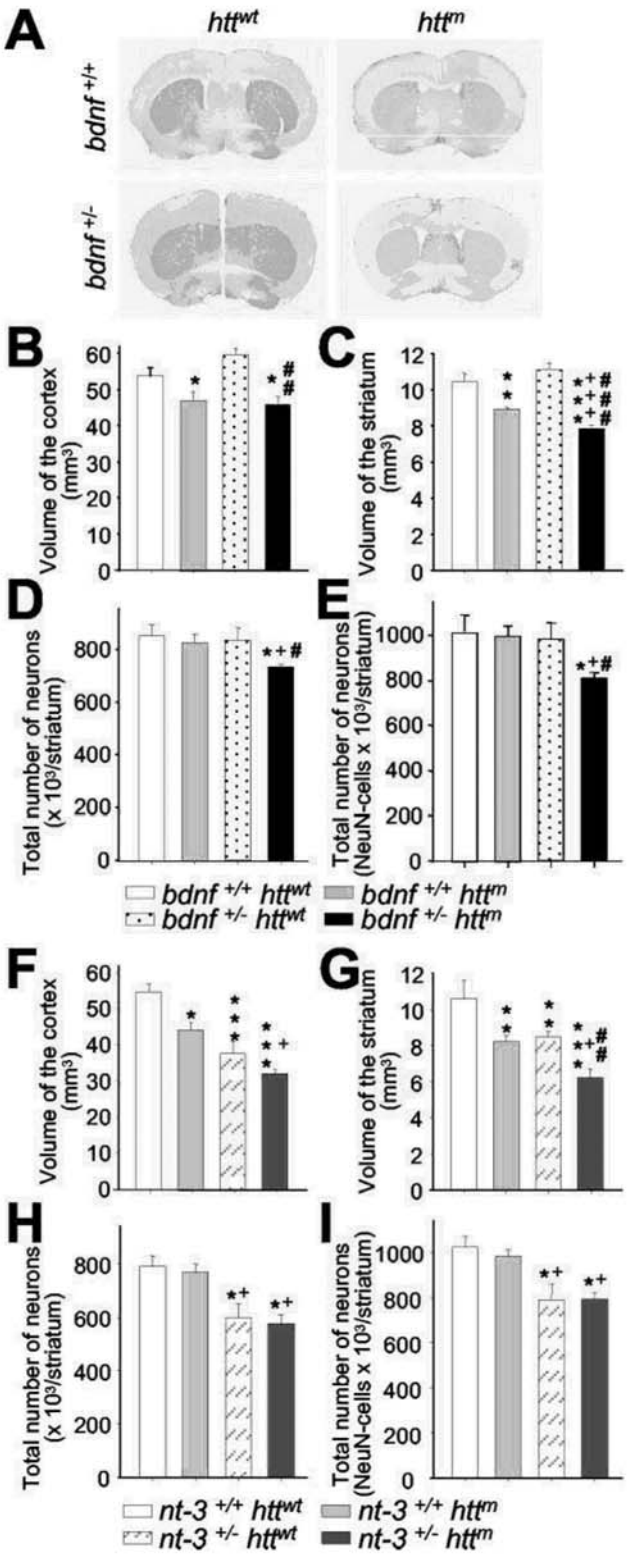

Figure 5. Reduction of BDNF levels in *mutant htt* mice produces neuronal loss in the striatum. *A*, Representative sections of DARPP-32 immunohistochemistry on wt mice ($bdnf^{+/+}$ htt^{wt}), R6/1 mice ($bdnf^{+/+}$ htt^{m}), *bdnf* heterozygous mice ($bdnf^{+/-}$ htt^{wt}), and bDM ($bdnf^{+/-}$ htt^{m}). *B*, *C*, We used DARPP-32 immunostaining to measure the volume of the cerebral cortex (*B*) and the striatum (*C*). *B*, The cerebral cortex shows the same atrophy in both genotypes with *mutant htt*. *C*, In contrast, the striatal volume is significantly lower in bDM with respect to R6/1 mice, indicating that the insufficient levels of this neurotrophin produce more severe striatal degeneration. *D*, *E*, At 30 weeks, bDM have striatal neuronal loss, counted by neuronal morphology in cresyl violet staining (*D*) or by NeuN immunohistochemistry (*E*). No decrease in neurons was detected in other genotypes. *F*, *G*, In n3DM ($nt\text{-}3^{+/-}$ htt^{m}), the effects observed result from the addition of striatal and cortical reduction observed in individual genotypes, *mutant htt* and $nt\text{-}3^{+/-}$. *H*, *I*, No differences in cell loss were observed between *nt-3* heterozygous with or without *mutant htt*. Both genotypes ($nt\text{-}3^{+/-}$ htt^{wt} and $nt\text{-}3^{+/-}$ htt^{m}) present a ~25% reduction. $^{*}p < 0.05$, $^{**}p < 0.005$, and $^{***}p < 0.001$ compared with wt mice ($bdnf^{+/+}$ htt^{wt} or $nt\text{-}3^{+/+}$ htt^{wt}); $^{+}p < 0.05$ and $^{+++}p < 0.001$ compared with $bdnf^{+/+}$ htt^{m} or $nt\text{-}3^{+/+}$ htt^{m} mice; $^{\#}p < 0.05$, $^{\#\#}p < 0.005$, and $^{\#\#\#}p < 0.001$ compared with *bdnf* or *nt-3* heterozygous mice, respectively.

Results

The length and levels of CAG-repeat expression regulate BDNF *in vitro*

Here, we examined whether the number of repeats and the levels of *mutant htt* expression affect the production of BDNF (Fig. 1*A*,*B*). The levels of BDNF in supernatants of immortalized striatal neurons transfected with constructs of exon 1 of *mutant htt* containing 47 or 72 CAG repeats (qp47and qp72) were reduced similarly (Fig. 1*A*) (qp47, 63.01 ± 5.43%; qp72, 61.64 ± 3.63% of parental cells). However, supernatants from cells transfected with exon 1 of the *mutant htt* with 103 repeats (qp103) was significantly lower than qp47 and qp72 (Fig. 1*A*) (34.55 ± 12.95% of parental cells and 59.38 ± 12.25% with respect to qp72). In addition, the amount of BDNF was inversely proportional to the levels of expression of qp103 (Fig. 1*B*). In cells expressing low qp103 levels, BDNF production was similar to that found in supernatants from parental cells without significant differences. These findings may help to explain the differences in BDNF levels observed in distinct mouse models of HD. To evaluate the specificity of this effect, we also measured the levels of NT-3 in supernatants from qp103 transfected cells, and we did not observe modifications of this protein (104.52 ± 18.9% of parental cells).

Generation of transgenic *mutant htt* mice with different levels of BDNF

To analyze the role of BDNF in HD progression and to explore whether the decrease of its expression is involved in the selective vulnerability, we generated a bDM line by crossing R6/1 mice (Mangiarini et al., 1996) with *bdnf* heterozygous mice (Ernfors et al., 1994b) as described in Materials and Methods. We did not detect any difference in life span between wt and $bdnf^{+/-}$ mice. However, R6/1 mice showed shorter survival as described by Mangiarini et al. (1996). We examined the levels of BDNF, mRNA, and protein in the cerebral cortex and striatum from 30-week-old mice ($n = 4$ per genotype). We found that $bdnf^{+/+}$ htt^{m} mice, the equivalent genotype to R6/1, have similar levels of BDNF mRNA and protein to wt mice (Fig. 1*C–G*). *In situ* hybridization for *bdnf* showed that the expression of this neurotrophin was only lower in *bdnf* heterozygous animals ($bdnf^{+/-}$ htt^{wt} and $bdnf^{+/-}$ htt^{m}) (Fig. 1*C–E*). In addition, BDNF protein levels analyzed by ELISA (Fig. 1*F*,*G*) showed the same levels in the cerebral cortex and in the striatum of the two genotypes with $bdnf^{+/+}$ (in picogram per milligram of protein; striatum: wt, 46.81 ± 5.97 and R6/1 genotype, 54.70 ± 3.24; cerebral cortex: wt, 61.90 ± 5.52 and $bdnf^{+/+}$ htt^{m}, 56.96 ± 1.67). To rule out a genetic background effect, we also evaluated R6/1 mice. These mice showed no changes in BDNF levels (data not shown). In addition, bDM ($bdnf^{+/-}$ htt^{m}; in picogram per milligram of protein; striatum: 30.96 ± 1.41; cortex: 36.78 ± 1.70) showed the same decrease in BDNF levels as $bdnf^{+/-}$ littermates with normal *htt* ($bdnf^{+/-}$ htt^{wt}; in picogram per milligram of protein; striatum: 26.42 ± ←

2.98; cortex: 40.24 ± 3.49) (Fig. 1*F,G*). We next analyzed whether other neurotrophins compensate for the insufficient levels of BDNF by modifying their levels of expression. *In situ* hybridizations against NGF, NT-3, or NT-4/5 did not show changes in the mRNA levels of these neurotrophins in any genotype studied (data not shown).

BDNF regulation is downstream of the aggregate formation

It has been proposed that this wt Htt-mediated BDNF regulation can be associated to the sequestering of wt Htt into aggregates. Our results showed that in nontransfected M213 cells, wt Htt is localized in endocytic compartments, as described previously (Kegel et al., 2000) (Fig. 2*A*). However, in M213 cells transfected with *mutant htt*, wt Htt is also localized into aggregates, and in cells with large aggregates, the endocytic wt Htt labeling disappeared (Fig. 2*A*). No signal was observed avoiding primary antibody (Fig. 2*B*).

To test a correlation between the expression of BDNF and the levels of wt Htt *in vivo*, we examined the levels of the endogenous wt form in symptomatic R6/1 at 20 and 30 weeks in the cerebral cortex and the striatum ($n = 3$). Our results demonstrated that the levels of the protein of wt Htt were not modified in the R6/1 compared with 30-week-old wt mice (Fig. 2*C*).

Our results also showed that modification of BDNF levels did not alter the number and the localization of ubiquitinated aggregates (Fig. 2*D–F*). We counted the density of aggregates containing mutant Htt by immunohistochemistry against mutant Htt or ubiquitin in the striatum of both *mutant htt* genotypes, R6/1 mice and bDM at 30 weeks of age ($n = 4$). The number of aggregates per cubic millimeter was not modified by decreased *bdnf* expression [mutant Htt-positive aggregates per cubic millimeter: R6/1 ($bdnf^{+/+}$ htt^{m}), 126,100 ± 6540; bDM ($bdnf^{+/-}$ htt^{m}), 118,722 ± 8169] (Fig. 2*D*). Similarly, the ubiquitination of these aggregates showed no inter-group differences [ubiquitin-positive aggregates per cubic millimeter: R6/1 ($bdnf^{+/+}$ htt^{m}), 130,751 ± 7416; bDM ($bdnf^{+/-}$ htt^{m}), 127,695 ± 7600] (Fig. 2*D*). We also performed double immunohistochemistry to locate these inclusions. Aggregates in both genotypes had the same distribution pattern with a main intranuclear location (Fig. 2*E,F*). Most striatal cells had at least one intranuclear aggregate (Fig. 2*E,F*). Similar results were observed in the cerebral cortex (data not shown). Together, present findings suggest that BDNF regulation is downstream of the aggregate formation.

The reduction of BDNF induces advanced and more severe motor deficits in *mutant htt* mice

All animals that expressed *mutant htt* displayed a progressive neurological phenotype. However, bDM showed more severe symptoms. bDM had more tremors at rest and sudden movements that resembled chorea (supplemental material, available at www.jneurosci.org). The behavioral analyses of their motor abilities on the rotarod apparatus showed that R6/1 mice began to show significant differences from wt mice at 18 weeks at 24 and 32 rpm (Fig. 3*B,C*) and at 20 weeks of age at 16 rpm (Fig. 3*A*). However, bDM showed significant motor alterations with respect to wt or *bdnf* heterozygous mice from 10 weeks of age at 32 rpm (Fig. 3*C*) and 12 weeks at 16 and 24 rpm (Fig. 3*A,B*). Therefore, the onset of motor disorders advanced between 6 and 8 weeks (at 24 rpm and 16 or 32 rpm, respectively) in animals with a life span of 34 weeks (Mangiarini et al., 1996). The severity of motor dysfunction was also affected in bDM. The progression of movement deficits in bDM ($bdnf^{+/-}$ htt^{m}) was more severe than in R6/1 mice ($bdnf^{+/+}$ htt^{m}; $p < 0.001$; F-Wald test). Furthermore, the total number of falls during the entire period (30 weeks) was significantly higher in bDM ($bdnf^{+/-}$ htt^{m}) than in R6/1 mice ($bdnf^{+/+}$ htt^{m}) (Fig. 3*D*). The impairment of rotarod performance resulting from a decrease of BDNF in *mutant htt* mice was 154%. This effect was especially drastic in the initial period: up to 16 weeks of age, bDM showed 340% of rotarod test impairment (Fig. 3*E*). The progression of motor dysfunction was rapid in bDM, which were the only mice to reach the top number of falls (Fig. 3*A–C*). Remarkably, *bdnf* heterozygous mice did not show differences with respect to wt mice, indicating that the decrease of BDNF per se does not produce motor disturbances.

The instability of animals on the moving cylinder of the rotarod may be attributable to the lack of motor coordination or because of deficits in equilibrium, vision, or muscular strength. Thus, we next measured walking coordination by quantitative analysis of the footprint patterns (Fig. 4*A–D*). At 30 weeks of age, R6/1 mice did not show alterations in the number of steps (Fig. 4*A*), stride length (Fig. 4*B*), frontbase width (Fig. 4*C*), or hindbase width (Fig. 4*D*). However, bDM showed significant differences in all parameters studied except hindbase width (Fig. 4*A–D*), suggesting that the lack of coordination contributes to rotarod disturbance. We also analyzed other behavioral parameters that might affect motor dysfunction. Equilibrium was assessed for the four different genotypes (Fig. 4*E*). The groups did not differ in their performance on a cylindrical wire rod, although fall latency in *mutant htt* animals with normal or reduced BDNF levels tended to go down (Fig. 4*E*). Similarly, no differences in the visual cliff avoidance test or in muscular strength evaluated by the wire hang test were observed between groups (data not shown).

We could not perform motor behavior analysis in n3DM because all *nt-3* heterozygous mice were unable to perform the tasks. Motor deficits in these mice have been described previously (Ernfors et al., 1994b).

Neuronal cell loss in the striatum of bDM

Although all animals with *mutant htt* had less brain volume, modification of *bdnf* alleles did not affect these changes ($n = 4–7$; brain volume: $bdnf^{+/+}$ htt^{wt}, 100 ± 8.83%; $bdnf^{+/+}$ htt^{m}, 81.75 ± 6.80%; $bdnf^{+/-}htt^{wt}$, 97.29 ± 12.82%; $bdnf^{+/-}htt^{m}$, 82.43 ± 13.81% with respect to wt). Similarly, the levels of *bdnf* expression did not affect the volume of the cortex, which was less in both groups with *mutant htt* (Fig. 5*A,B*). In contrast, degeneration of the striatum was observed in the bDM (Fig. 5*A,C*). These animals showed a volume of 75.43 ± 1.12% with respect to wt animals (100 ± 5.17%), which was significantly lower than the volume in R6/1 striata (85.32 ± 0.68% with respect to wt). In addition, a decrease in BDNF levels caused neuronal loss in the striatum of *mutant htt* transgenic mice. The estimated number of total neurons counted by cresyl violet was down to 85.64 ± 1.29% in bDM with respect to wt mice (Fig. 5*D*). Similarly, the number of NeuN-positive cells was 79.60 ± 2.35% in bDM with respect to wt mice (Fig. 5*E*). No differences were detected in the other genotypes, either in cresyl violet or in NeuN-positive counts (cresyl violet: $bdnf^{+/+}$ htt^{wt}, 100 ± 0.87%; $bdnf^{+/+}$ htt^{m}, 96.93 ± 3.72%; $bdnf^{+/-}$ htt^{wt}, 97.44 ± 5.54% with respect to wt; NeuN-positive cells: $bdnf^{+/+}$ htt^{wt}, 100 ± 7.04%; $bdnf^{+/+}$ htt^{m}, 98.31 ± 4.01%; $bdnf^{+/-}$ htt^{wt}, 95.80 ± 8.90% with respect to wt).

To demonstrate the specific effect of BDNF, we generated a n3DM line in which transgenic mice present different levels of NT-3, another neurotrophin with protective effects on striatal neurons (Perez-Navarro et al., 2000). The analyses of n3DM revealed a decrease in the volume of both cortex and striatum (Fig. 5*F,G*) [cerebral cortex: $nt\text{-}3^{+/-}htt^{m}$, 59.02 ± 2.13% with respect

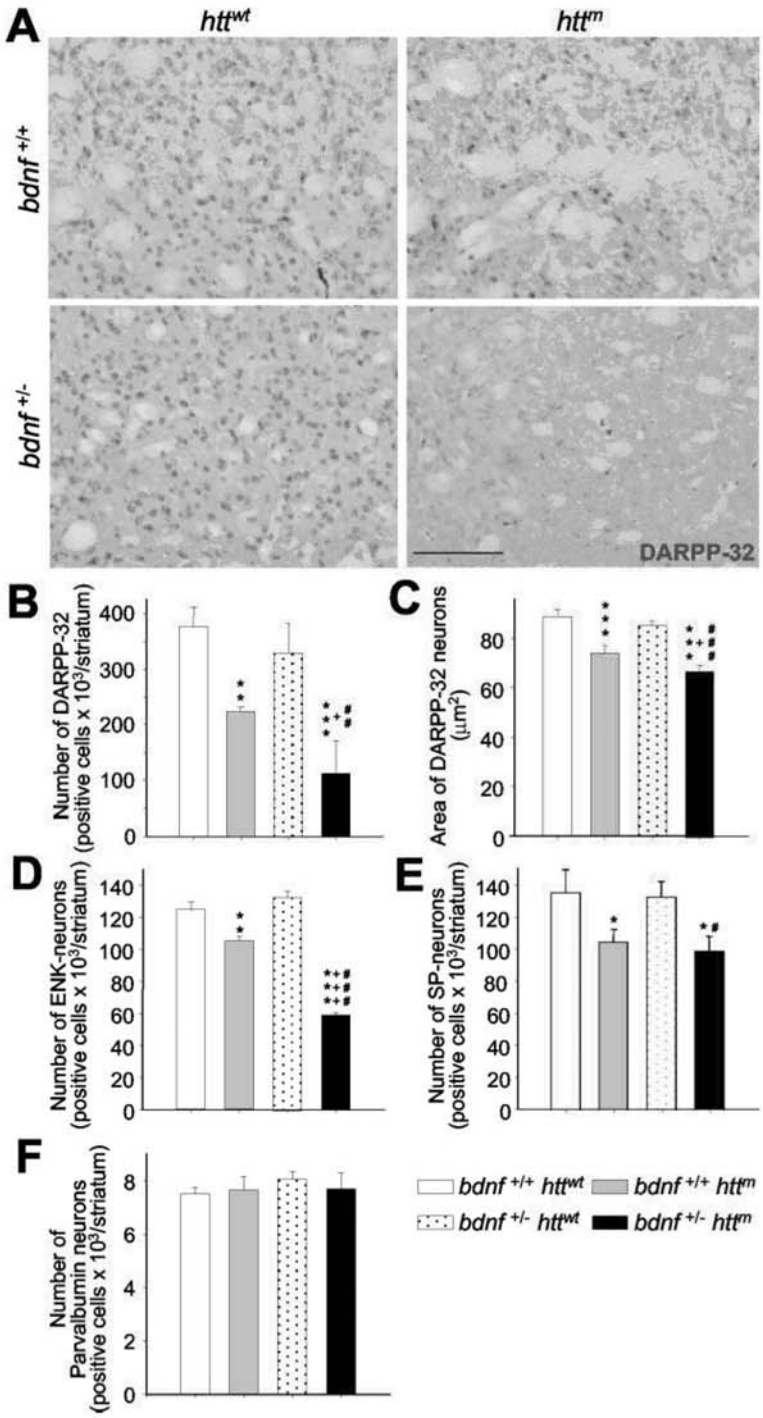

Figure 6. The striatal cells lost in bDM are enkephalin-positive neurons. *A–C*, At 30 weeks of age, bDM ($bdnf^{+/-}$ htt^m) had great atrophy of medium-sized striatal projection neurons, as demonstrated by DARPP-32 immunostaining. The number of DARPP-32-positive neurons decreased in all *mutant htt* mice (*B*). However, the lowest number of DARPP-32-positive neurons was detected in bDM. *C*, The cross-sectional area of DARPP-32 neurons decreased in all animals that express *mutant htt*, although the area is significantly smaller in bDM. *D*, *E*, The two neuronal subpopulations of medium-sized spiny neurons in the striatum were characterized by *in situ* hybridization. *D*, The number of enkephalin-positive neurons (ENK) was dramatically less in bDM. The number of ENK-positive neurons was also less in R6/1 mice ($bdnf^{+/+}$ htt^m) than in wt mice but only by a small amount. *E*, The differences between the two *mutant htt* groups are statistically significant. In contrast, the decrease in substance P-positive neurons (SP) is similar in R6/1 mice ($bdnf^{+/+}$ htt^m) and bDM ($bdnf^{+/-}$ htt^m), without significant differences. *F*, We also analyzed the number of striatal interneurons by parvalbumin immunohistochemistry. No differences were found between the four genotypes analyzed. $^*p < 0.05$, $^{**}p < 0.005$, and $^{***}p < 0.001$ compared with wt mice ($bdnf^{+/+}$ htt^{wt}); $^+p < 0.05$ and $^{+++}p < 0.001$ compared with R6/1 mice ($bdnf^{+/+}$ htt^m); $^\#p < 0.05$, $^{\#\#}p < 0.005$, and $^{\#\#\#}p < 0.001$ compared with *bdnf* heterozygous mice ($bdnf^{+/-}$ htt^{wt}). Scale bar, 100 μm.

to wt ($nt\text{-}3^{+/+}$ htt^{wt}, 100 ± 4.18%); striatum: $nt\text{-}3^{+/-}$ htt^m, 62.30 ± 4.50% with respect to wt ($nt\text{-}3^{+/+}$ htt^{wt}, 100 ± 8.26%)]. However, this decrease in volume results from the addition of the independent effects observed in R6/1 mice and *nt-3* heterozygous mice (Fig. 5*F*,*G*) [cerebral cortex: R6/1 mice ($nt\text{-}3^{+/+}$ htt^m), 82.57 ± 4.59%; $nt\text{-}3^{+/-}$ htt^{wt}, 68.90 ± 9.4% with respect to wt; striatum: R6/1 mice ($nt\text{-}3^{+/+}$ htt^m), 78.52 ± 1.84%; $nt\text{-}3^{+/-}$ htt^{wt}, 81.38 ± 2.68% with respect to wt]. Therefore, the effect of *mutant htt* is similar in *nt-3* heterozygous mice ($nt\text{-}3^{+/-}$ htt^m with respect to $nt\text{-}3^{+/-}$ htt^{wt}: cortex, 85.65 ± 3.1%; striatum, 76.55 ± 5.5%) and in mice with normal NT-3 levels ($nt\text{-}3^{+/+}$ htt^m with respect to wt: cortex, 82.57 ± 4.59%; striatum, 78.52 ± 1.8%). The effect of this neurotrophin on striatal neurons is similar in both NT-3 heterozygous genotypes in which the number of neurons is reduced ~25% (Fig. 5*H*,*I*) (cresyl violet: $nt\text{-}3^{+/+}$ htt^{wt}, 100 ± 4.98%; $nt\text{-}3^{+/+}$ htt^m, 97.34 ± 3.76%; $nt\text{-}3^{+/-}$ htt^{wt}, 75.59 ± 6.79%; $nt\text{-}3^{+/-}$ htt^m, 72.80 ± 4.45% with respect to wt; NeuN-positive cells: $nt\text{-}3^{+/+}$ htt^{wt}, 100 ± 4.69%; $nt\text{-}3^{+/+}$ htt^m, 96.68 ± 3.46%; $nt\text{-}3^{+/-}$ htt^{wt}, 77.03 ± 3.50%; $nt\text{-}3^{+/-}$ htt^m, 77.76 ± 2.70% with respect to wt).

We next analyzed whether neuronal loss in the striatum is because of a deficit during development or progressive degeneration. bDM showed no neuronal alterations in the striatum at postnatal day 15 (n = 4–6 per genotype). The striatal volume of bDM was 104 ± 4.18% with respect to wt, and the number of NeuN-positive neurons was 109.93 ± 5.01% with respect to wt. In addition, we analyzed the striatal volume and neurons of animals that had complete knock-out of the *bdnf* gene. These animals showed a striatal volume of 98.87 ± 3.53%, and the number of NeuN-positive neurons was 105.49 ± 6.06% with respect to wt.

Specific degeneration of enkephalin striatal subpopulation is controlled by BDNF

One of the pathological characteristics of HD is its specific pattern of degeneration. Here, we show that the number of medium-sized neurons immunostained with DARPP-32 was reduced in R6/1 mice (59 ± 2% with respect to wt; 100 ± 9%) (Fig. 6*A*,*B*). However, DARPP-32-positive neurons were fewer in bDM (30 ± 16% with respect to wt) (Fig. 6*A*,*B*). We calculated the effect attributed to lower BDNF levels in animals with *mutant htt* by standardizing values for the R6/1

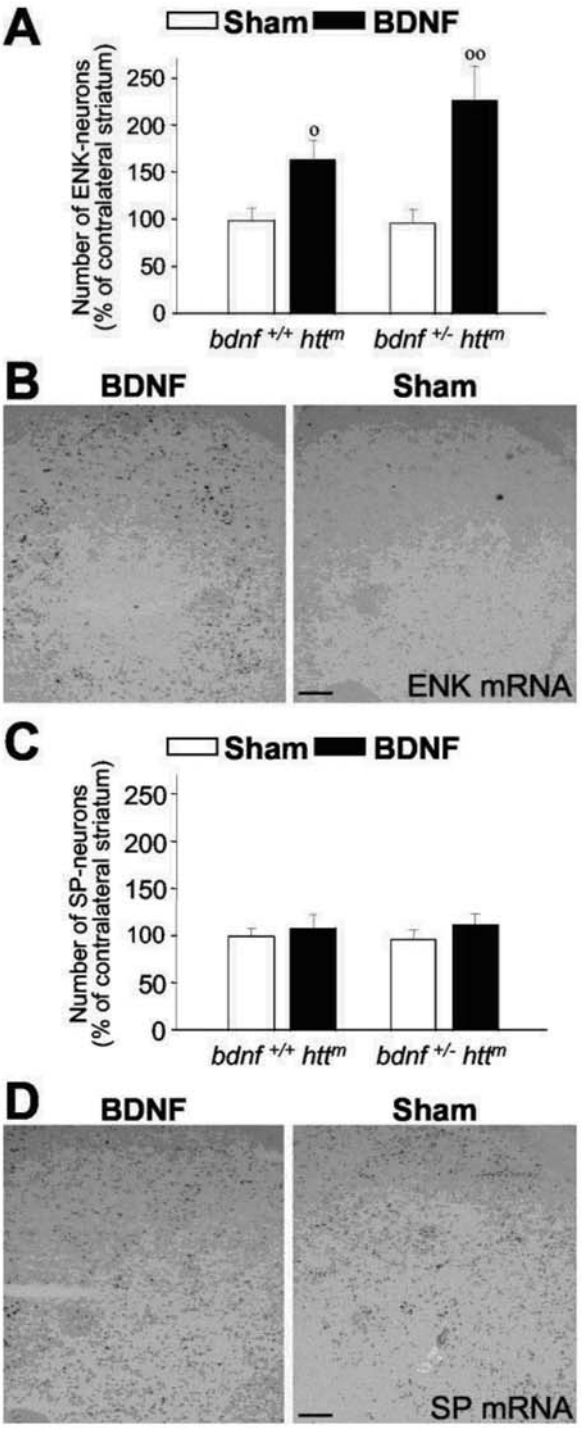

Figure 7. Exogenous BDNF restores the enkephalin loss in *mutant htt* mice. *A*, *B*, Continuous intrastriatal administration of BDNF (4.5 μg per day) during 1 week produces an increase in the number of enkephalin-positive cells (ENK). This effect may be caused by the enhancement in the enkephalin mRNA levels in both R6/1 mice ($bdnf^{+/+}$ htt^{m}) and bDM ($bdnf^{+/-}$ htt^{m}). *C*, *D*, However, intrastriatal administration of BDNF in the same animals does not modify the levels of substance P-positive neurons (SP). No differences were observed in PBS-infused animals (sham) with respect to untreated animals, either in enkephalin- or in substance P-positive neurons (data not shown). *B*, *D*, Representative photomicrographs of *in situ* hybridization for enkephalin (ENK) and substance P (SP) in bDM injected with BDNF or PBS (Sham). Note that after BDNF treatment, the enkephalin-positive neurons were detected around the injection site but not in the injection core (*B*). $^{o}p < 0.05$ and $^{oo}p < 0.005$ compared with sham-operated mice (Student's *t* test). Scale bars: *B*, *D*, 100 μm.

mice, showing a reduction of 50 ± 13% in bDM with respect to R6/1 mice. No differences in the number of DARPP-32-positive neurons were observed in *bdnf* heterozygous mice (87 ± 14% with respect to wt) (Fig. 6*A*,*B*).

The cross-sectional area of DARPP-32-positive neurons showed a small reduction in R6/1 mice ($bdnf^{+/+}$ htt^{m}, 85 ± 3% with respect to wt; 100 ± 3%) (Fig. 6*C*). However, in bDM, medium-sized cells were more atrophied with a significantly lower soma area (72 ± 1.9% with respect to wt) (Fig. 6*C*). In contrast, we did not find loss of parvalbumin-positive interneurons in any genotype analyzed ($bdnf^{+/+}$ htt^{wt}, 100 ± 3.2%; $bdnf^{+/+}$ htt^{m}, 95.6 ± 9.2%; $bdnf^{+/-}$$htt^{wt}$, 107.29 ± 4.0%; $bdnf^{+/-}$$htt^{m}$, 102.6 ± 7.9% with respect to wt) (Fig. 6*F*).

We next characterized the subpopulations of striatal projection neurons by *in situ* hybridization (Fig. 6*D*,*E*). In bDM, the number of enkephalin-positive neurons drastically fell to 47.20 ± 0.99% with respect to wt (100 ± 4.39%), whereas in R6/1, the number of enkephalin-positive neurons decreased to only 84.32 ± 2.10% with respect to wt (Fig. 6*D*). In contrast, the number of substance P-positive neurons in the two genotypes expressing *mutant htt* was not significantly different ($bdnf^{+/+}$ htt^{wt}, 100 ± 10.75%; $bdnf^{+/+}$ htt^{m}, 77.10 ± 7.02%; $bdnf^{+/-}$$htt^{wt}$, 97.91 ± 7.41%; $bdnf^{+/-}$$htt^{m}$, 73.04 ± 6.83% with respect to wt) (Fig. 6*E*).

To further study the specific effect of BDNF on enkephalinergic neurons, we administered 4.5 μg of BDNF per day into the striatum of 20-week-old R6/1 mice during 1 week ($n = 5$) (Fig. 7). This treatment enhanced the number of enkephalin-positive neurons to 60.28 ± 24.07% above the sham-R6/1 mice (Fig. 7*A*). We also administered BDNF to 14-week-old bDM in which exogenous BDNF increased the number of enkephalinergic neurons 127.09 ± 31.42% above sham-bDM (Fig. 7*A*,*B*). However, BDNF treatment did not alter the number of substance P-positive neurons in R6/1 mice (12.86 ± 15.25% above sham) or in bDM (19.18 ± 10.34% above sham) (Fig. 7*C*,*D*). In addition, preliminary behavioral analysis showed that bDM, which received unilateral administration of BDNF, showed asymmetric rotations induced by amphetamine (5 mg/kg). These mice showed 65.00 ± 20.57 contralateral net rotations, whereas sham-bDM showed −40.00 ± 23.18 ipsilateral net rotations ($p = 0.0137$). Thus, present results suggest that BDNF restores some striatal functions related to the increase in enkephalin expression.

Discussion

In the present study, we disrupted the expression of *bdnf* in an HD mouse model by cross-mating $bdnf^{+/-}$ (Ernfors et al., 1994b) and R6/1 mice (Mangiarini et al., 1996). The characterization of these mice demonstrates that endogenous BDNF regulates the onset and the severity of motor dysfunction. These effects are caused by selective degeneration of enkephalin-positive neurons in the striatum, which can be restored by administration of exogenous BDNF.

It has been postulated that mutant Htt may act as a dominant-negative over wt protein by capturing it into aggregates (Dyer and McMurray, 2001). This effect could result in the loss of wt Htt function in NRSF inhibition (Zuccato et al., 2003), causing BDNF alterations. We observed that wt Htt colocalizes with mutant Htt into the aggregates in cells that express *mutant htt* gene, supporting the idea of a dominant-negative role for mutant Htt in cell cultures. In addition, a decrease in mutant Htt-mediated BDNF depends not only on the number of CAG repeats but also on its levels of expression, because low amounts of mutant Htt did not produce a decrease in BDNF levels. These data may ex-

plain the differences observed in distinct *mutant htt* transgenic mouse models. In fact, our findings showed that the transgenic R6/1 mice, which express only one copy of the mutant 5′-end of the human *htt* gene carrying $(CAG)_{115}$ (Mangiarini et al., 1996), have normal levels of BDNF, which correlates with the normal levels of wt Htt detected in these mice. However, R6/2 mice, which express the transgene three times more than R6/1 and carry 150 CAG repeats (Mangiarini et al., 1996), have decreased levels of free wt Htt, which reduces BDNF concentrations (Zhang et al., 2003). Within knock-in mouse lines, a dose-dependent Htt-mediated BDNF decrease has also been established (Zuccato et al., 2001). Our results also demonstrate that decreasing the levels of BDNF in R6/1 mice does not alter the number or localization of intranuclear aggregates *in vivo*. Similar results have been described previously in cell culture (Saudou et al., 1998). Together, all of these findings suggest that the number of CAG repeats and its levels of expression modify the amount of wt Htt available to retain the NRSF and consequently produce changes in *bdnf* expression.

Besides this interaction between the expression of *mutant htt* and BDNF, no evidence has correlated the decrease in BDNF with the HD neuropathology. Our results show that the decrease in BDNF levels produced more severe symptoms in an HD model. bDM showed an early onset of motor dysfunction with significant motor alterations 6–8 weeks before their littermates, R6/1 mice. In addition, the progression of movement deficits in bDM was faster and more severe than in R6/1. We also found motor disorders in the analysis of footprint patterns, which demonstrated that only bDM have deficits in walking coordination. Note that although *bdnf* knock-outs have alterations of sensory neurons (Ernfors et al., 1994a; Jones et al., 1994), $bdnf^{+/-}$ mice with *wt htt* or *mutant htt* did not show deficits in the equilibrium, visual test, or muscular strength. In addition, it has been shown recently that the conditional BDNF-null mutant mice, which lack this neurotrophin in the striatum, do not have motor alterations (Baquet et al., 2004). These findings demonstrate that BDNF affects brain nuclei that control motor coordination only in the presence of *mutant htt*.

We next examined the neuronal populations that are affected by BDNF in HD. The lower BDNF levels of bDM reduced striatal volume without affecting the cerebral cortex. Similarly, neuronal loss in the cerebral cortex has not been observed in transgenic *mutant htt* mouse models (Mangiarini et al., 1996; Hodgson et al., 1999; Shelbourne et al., 1999; Yamamoto et al., 2000; Slow et al., 2003). These results indicate that downregulation of cortical *bdnf* mRNA found in animal models and patients with HD (Zuccato et al., 2001) primarily affects striatal neurons but not cortical structures. In fact, it has been described that BDNF protein only decreases in the striatum of HD patients and not in the cerebral cortex (Ferrer et al., 2000). In support of this view, it has been shown that cortical BDNF is transported anterogradely to the striatum (Altar et al., 1997), and it can protect striatal neurons from excitotoxicity (Martinez-Serrano and Bjorklund, 1996; Perez-Navarro et al., 1999, 2000; Canals et al., 2001; Alberch et al., 2002). Therefore, a decrease in the expression of cortical *bdnf* participates in selective striatal damage.

HD advances to higher grades (1–4) when specific striatal cell death occurs (Vonsattel et al., 1985). We show that the specific decrease of striatal volume in bDM is caused by a loss of striatal neurons, which was only observed in our bDM model at 30 weeks. These findings are consistent with previous reports that show that R6/1 (Mangiarini et al., 1996) and $bdnf^{+/-}$ mice (Jones et al., 1994; Ivkovic et al., 1997) have the same number of striatal neurons as wt mice. Thus, the lack of BDNF per se does not induce degeneration of striatal neurons, but, together with the presence of *mutant htt*, it produces striatal cell loss. This neuronal loss is not attributable to a deficit during development, because we did not observe alterations of the number of striatal neurons in 15-d-old bDM. In addition, the effect of BDNF on striatal neurons of HD mice is specific because no differences were detected in *nt-3* heterozygous mice with or without *mutant htt*. Our results are in agreement with the decrease of BDNF, but not NT-3, in the transgenic yeast artificial chromosome models (Zuccato et al., 2001), which present loss of striatal neurons (Hodgson et al., 1999). Similarly, reduced levels of BDNF are also detected in R6/2 (Zhang et al., 2003), which show a rapid disease progression and striatal degeneration (Menalled and Chesselet, 2002). It has been demonstrated that *mutant htt* causes context-dependent neurodegeneration mediated by different N-terminal Htt fragments in transgenic mice (Yu et al., 2003), similar to what we observed for the regulation of BDNF expression.

Motor deficits in R6/1 animals are attributed to neuronal dysfunction of DARPP-32-positive neurons rather than to cell death, because no loss of striatal neurons was observed in these mice. DARPP-32 is downregulated in R6/1 mice, whereas calbindin immunolabeling, another marker for medium-sized projection neurons, is not modified (van Dellen et al., 2000). However, the drastic decrease in DARPP-32-positive cells observed in bDM is attributed to downregulation of the cellular marker and neuronal death, because this population represents 95% of striatal neurons. bDM showed a 50% reduction in DARPP-32-positive neurons without any change in the number of parvalbumin-positive interneurons. These striatal DARPP-32-positive neurons project to the globus pallidus and substantia nigra via two separate subpopulations, enkephalin- and substance P-positive neurons, respectively, which have different sensitivity to *mutant htt*. The analysis of each subpopulation demonstrated that the number of enkephalin-positive neurons fell drastically in bDM. In contrast, the levels of BDNF did not affect the number of substance P-positive neurons. These results are coincident with previous studies with R6/2 mice, which present a decrease of BDNF levels (Zhang et al., 2003) and a 50% reduction of enkephalin mRNA but not of the levels of substance P expression (Bibb et al., 2000).

In view of our results, which show that the deficit of endogenous BDNF specifically regulates the levels of enkephalin in HD, we next examined the effect of administration of this neurotrophin in *mutant htt* transgenic mice. The intrastriatal treatment with BDNF produced a reversion of the loss of the enkephalinergic phenotype in R6/1 and in bDM. This increase in the number of enkephalinergic neurons is attributable to the recovery of mRNA expression because only 20% of neurons are lost in bDM, and no cell death is observed in R6/1 mice. These findings suggest that atrophic or dysfunctional striatal neurons are recovered by BDNF administration. Consistent with these results is the observation that 1 week administration of BDNF *in vivo* leads to overall increased expression of enkephalin as well as an increase in the number of striatal cells expressing enkephalin (Perez-Navarro et al., 1999). In addition, our results from the circling behavior induced by amphetamine administration suggest that increasing enkephalin expression via BDNF administration may have functional implication in HD mouse models. However, additional experiments are required to improve the dose and the administration strategies to perform long-term bilateral treatments.

In conclusion, our results demonstrate that BDNF plays a pivotal role in the pathophysiology of HD. Although BDNF is not an inductor of HD and the initial steps of this disorder may occur

without BDNF alterations, we show that BDNF regulates the age of onset and the severity of motor dysfunctions through the control of the survival of striatal enkephalinergic neurons. In addition, BDNF treatment restores the enkephalin levels in striatal projection neurons, one of the most affected populations in HD. Therefore, administration of BDNF or increasing endogenous levels in HD patients may stop or delay illness progression.

References

Agerman K, Hjerling-Leffler J, Blanchard MP, Scarfone E, Canlon B, Nosrat C, Ernfors P (2003) BDNF gene replacement reveals multiple mechanisms for establishing neurotrophin specificity during sensory nervous system development. Development 130:1479–1491.

Alberch J, Perez-Navarro E, Canals JM (2002) Neuroprotection by neurotrophins and GDNF family members in the excitotoxic model of Huntington's disease. Brain Res Bull 57:817–822.

Alberch J, Perez-Navarro E, Canals JM (2004) Neurotrophic factors in Huntington's disease. Prog Brain Res 146:195–229.

Altar CA, Cai N, Bliven T, Juhasz M, Conner JM, Acheson AL, Lindsay RM, Wiegand SJ (1997) Anterograde transport of brain-derived neurotrophic factor and its role in the brain. Nature 389:856–860.

Baquet ZC, Gorski JA, Jones KR (2004) Early striatal dendrite deficits followed by neuron loss with advanced age in the absence of anterograde cortical brain-derived neurotrophic factor. J Neurosci 24:4250–4258.

Bibb JA, Yan Z, Svenningsson P, Snyder GL, Pieribone VA, Horiuchi A, Nairn AC, Messer A, Greengard P (2000) Severe deficiencies in dopamine signaling in presymptomatic Huntington's disease mice. Proc Natl Acad Sci USA 97:6809–6814.

Canals JM, Checa N, Marco S, Akerud P, Michels A, Perez-Navarro E, Tolosa E, Arenas E, Alberch J (2001) Expression of brain-derived neurotrophic factor in cortical neurons is regulated by striatal target area. J Neurosci 21:117–124.

Carter RJ, Lione LA, Humby T, Mangiarini L, Mahal A, Bates GP, Dunnett SB, Morton AJ (1999) Characterization of progressive motor deficits in mice transgenic for the human Huntington's disease mutation. J Neurosci 19:3248–3257.

Duan W, Guo Z, Jiang H, Ware M, Li XJ, Mattson MP (2003) Dietary restriction normalizes glucose metabolism and BDNF levels, slows disease progression, and increases survival in huntingtin mutant mice. Proc Natl Acad Sci USA 100:2911–2916.

Dyer RB, McMurray CT (2001) Mutant protein in Huntington disease is resistant to proteolysis in affected brain. Nat Genet 29:270–278.

Ernfors P, Lee KF, Jaenisch R (1994a) Mice lacking brain-derived neurotrophic factor develop with sensory deficits. Nature 368:147–150.

Ernfors P, Lee KF, Kucera J, Jaenisch R (1994b) Lack of neurotrophin-3 leads to deficiencies in the peripheral nervous system and loss of limb proprioceptive afferents. Cell 77:503–512.

Ferrante RJ, Andreassen OA, Dedeoglu A, Ferrante KL, Jenkins BG, Hersch SM, Beal MF (2002) Therapeutic effects of coenzyme Q10 and remacemide in transgenic mouse models of Huntington's disease. J Neurosci 22:1592–1599.

Ferrer I, Goutan E, Marin C, Rey MJ, Ribalta T (2000) Brain-derived neurotrophic factor in Huntington disease. Brain Res 866:257–261.

Gerfen CR (1992) The neostriatal mosaic: multiple levels of compartmental organization. Trends Neurosci 15:133–139.

Gimenez-Llort L, Fernandez-Teruel A, Escorihuela RM, Fredholm BB, Tobena A, Pekny M, Johansson B (2002) Mice lacking the adenosine A1 receptor are anxious and aggressive, but are normal learners with reduced muscle strength and survival rate. Eur J Neurosci 16:547–550.

Giordano M, Takashima H, Herranz A, Poltorak M, Geller HM, Marone M, Freed WJ (1993) Immortalized GABAergic cell lines derived from rat striatum using a temperature-sensitive allele of the SV40 large T antigen. Exp Neurol 124:395–400.

Hickey MA, Chesselet MF (2003) The use of transgenic and knock-in mice to study Huntington's disease. Cytogenet Genome Res 100:276–286.

Hodgson JG, Agopyan N, Gutekunst CA, Leavitt BR, LePiane F, Singaraja R, Smith DJ, Bissada N, McCutcheon K, Nasir J, Jamot L, Li XJ, Stevens ME, Rosemond E, Roder JC, Phillips AG, Rubin EM, Hersch SM, Hayden MR (1999) A YAC mouse model for Huntington's disease with full-length mutant huntingtin, cytoplasmic toxicity, and selective striatal neurodegeneration. Neuron 23:181–192.

Ibanez CF, Hallbook F, Godeau F, Persson H (1992) Expression of neurotrophin-4 mRNA during oogenesis in *Xenopus laevis*. Int J Dev Biol 36:239–245.

Ivkovic S, Polonskaia O, Farinas I, Ehrlich ME (1997) Brain-derived neurotrophic factor regulates maturation of the DARPP-32 phenotype in striatal medium spiny neurons: studies *in vivo* and *in vitro*. Neuroscience 79:509–516.

Jones KR, Farinas I, Backus C, Reichardt LF (1994) Targeted disruption of the BDNF gene perturbs brain and sensory neuron development but not motor neuron development. Cell 76:989–999.

Kazantsev A, Preisinger E, Dranovsky A, Goldgaber D, Housman D (1999) Insoluble detergent-resistant aggregates form between pathological and nonpathological lengths of polyglutamine in mammalian cells. Proc Natl Acad Sci USA 96:11404–11409.

Kegel KB, Kim M, Sapp E, McIntyre C, Castano JG, Aronin N, DiFiglia M (2000) Huntingtin expression stimulates endosomal-lysosomal activity, endosome tubulation, and autophagy. J Neurosci 20:7268–7278.

Landry M, Holmberg K, Zhang X, Hokfelt T (2000) Effect of axotomy on expression of NPY, galanin, and NPY Y1 and Y2 receptors in dorsal root ganglia and the superior cervical ganglion studied with double-labeling *in situ* hybridization and immunohistochemistry. Exp Neurol 162:361–384.

Laurenzi MA, Barbany G, Timmusk T, Lindgren JA, Persson H (1994) Expression of mRNA encoding neurotrophins and neurotrophin receptors in rat thymus, spleen tissue and immunocompetent cells. Regulation of neurotrophin-4 mRNA expression by mitogens and leukotriene B4. Eur J Biochem 223:733–741.

Lindefors N, Brodin E, Metsis M (1995) Spatiotemporal selective effects on brain-derived neurotrophic factor and trkB messenger RNA in rat hippocampus by electroconvulsive shock. Neuroscience 65:661–670.

Lione LA, Carter RJ, Hunt MJ, Bates GP, Morton AJ, Dunnett SB (1999) Selective discrimination learning impairments in mice expressing the human Huntington's disease mutation. J Neurosci 19:10428–10437.

Mangiarini L, Sathasivam K, Seller M, Cozens B, Harper A, Hetherington C, Lawton M, Trottier Y, Lehrach H, Davies SW, Bates GP (1996) Exon 1 of the HD gene with an expanded CAG repeat is sufficient to cause a progressive neurological phenotype in transgenic mice. Cell 87:493–506.

Martinez-Serrano A, Bjorklund A (1996) Protection of the neostriatum against excitotoxic damage by neurotrophin-producing, genetically modified neural stem cells. J Neurosci 16:4604–4616.

Menalled LB, Chesselet MF (2002) Mouse models of Huntington's disease. Trends Pharmacol Sci 23:32–39.

Perez-Navarro E, Alberch J, Neveu I, Arenas E (1999) Brain-derived neurotrophic factor, neurotrophin-3 and neurotrophin-4/5 differentially regulate the phenotype and prevent degenerative changes in striatal projection neurons after excitotoxicity *in vivo*. Neuroscience 91:1257–1264.

Perez-Navarro E, Canudas AM, Akerund P, Alberch J, Arenas E (2000) Brain-derived neurotrophic factor, neurotrophin-3, and neurotrophin-4/5 prevent the death of striatal projection neurons in a rodent model of Huntington's disease. J Neurochem 75:2190–2199.

Reiner A, Albin RL, Anderson KD, D'Amato CJ, Penney JB, Young AB (1988) Differential loss of striatal projection neurons in Huntington disease. Proc Natl Acad Sci USA 85:5733–5737.

Richfield EK, Maguire-Zeiss KA, Vonkeman HE, Voorn P (1995) Preferential loss of preproenkephalin versus preprotachykinin neurons from the striatum of Huntington's disease patients. Ann Neurol 38:852–861.

Rubinsztein DC (2002) Lessons from animal models of Huntington's disease. Trends Genet 18:202–209.

Saudou F, Finkbeiner S, Devys D, Greenberg ME (1998) Huntingtin acts in the nucleus to induce apoptosis but death does not correlate with the formation of intranuclear inclusions. Cell 95:55–66.

Schmitz GG, Walter T, Seibl R, Kessler C (1991) Nonradioactive labeling of oligonucleotides *in vitro* with the hapten digoxigenin by tailing with terminal transferase. Anal Biochem 192:222–231.

Serrats J, Artigas F, Mengod G, Cortes R (2003) GABAB receptor mRNA in the raphe nuclei: co-expression with serotonin transporter and glutamic acid decarboxylase. J Neurochem 84:743–752.

Shelbourne PF, Killeen N, Hevner RF, Johnston HM, Tecott L, Lewandoski M, Ennis M, Ramirez L, Li Z, Iannicola C, Littman DR, Myers RM (1999) A Huntington's disease CAG expansion at the murine Hdh locus is unstable and associated with behavioural abnormalities in mice. Hum Mol Genet 8:763–774.

Sieradzan KA, Mann DM (2001) The selective vulnerability of nerve cells in Huntington's disease. Neuropathol Appl Neurobiol 27:1–21.

Slow EJ, Van Raamsdonk J, Rogers D, Coleman SH, Graham RK, Deng Y, Oh R, Bissada N, Hossain SM, Yang YZ, Li XJ, Simpson EM, Gutekunst CA, Leavitt BR, Hayden MR (2003) Selective striatal neuronal loss in a YAC128 mouse model of Huntington disease. Hum Mol Genet 12:1555–1567.

Sugars KL, Rubinsztein DC (2003) Transcriptional abnormalities in Huntington disease. Trends Genet 19:233–238.

van Dellen A, Welch J, Dixon RM, Cordery P, York D, Styles P, Blakemore C, Hannan AJ (2000) N-Acetylaspartate and DARPP-32 levels decrease in the corpus striatum of Huntington's disease mice. NeuroReport 11:3751–3757.

Vonsattel JP, Myers RH, Stevens TJ, Ferrante RJ, Bird ED, Richardson Jr EP (1985) Neuropathological classification of Huntington's disease. J Neuropathol Exp Neurol 44:559–577.

Yamamoto A, Lucas JJ, Hen R (2000) Reversal of neuropathology and motor dysfunction in a conditional model of Huntington's disease. Cell 101:57–66.

Yu ZX, Li SH, Evans J, Pillarisetti A, Li H, Li XJ (2003) Mutant huntingtin causes context-dependent neurodegeneration in mice with Huntington's disease. J Neurosci 23:2193–2202.

Zhang Y, Li M, Drozda M, Chen M, Ren S, Mejia Sanchez RO, Leavitt BR, Cattaneo E, Ferrante RJ, Hayden MR, Friedlander RM (2003) Depletion of wild-type huntingtin in mouse models of neurologic diseases. J Neurochem 87:101–106.

Zuccato C, Ciammola A, Rigamonti D, Leavitt BR, Goffredo D, Conti L, MacDonald ME, Friedlander RM, Silani V, Hayden MR, Timmusk T, Sipione S, Cattaneo E (2001) Loss of huntingtin-mediated BDNF gene transcription in Huntington's disease. Science 293:493–498.

Zuccato C, Tartari M, Crotti A, Goffredo D, Valenza M, Conti L, Cataudella T, Leavitt BR, Hayden MR, Timmusk T, Rigamonti D, Cattaneo E (2003) Huntingtin interacts with REST/NRSF to modulate the transcription of NRSE-controlled neuronal genes. Nat Genet 35:76–83.

Segundo trabajo

"Brain-Derived Neurotrophic Factor modulates dopaminergic deficits in a transgenic mouse model of Huntington's Disease"

Publicado en *Journal of Neurochemistry*

Journal of Neurochemistry, 2005, **93**, 1057–1068 doi:10.1111/j.1471-4159.2005.03047.x

Brain-derived neurotrophic factor modulates dopaminergic deficits in a transgenic mouse model of Huntington's disease

José R. Pineda,*,† Josep M Canals,*,† Miquel Bosch,*,† Albert Adell,†,‡ Guadalupe Mengod,†,‡ Francesc Artigas,†,‡ Patrik Ernfors,§ and Jordi Alberch*,†

*Departament de Biologia Cel·lular i Anatomia Patològica, Facultat de Medicina, Universitat de Barcelona, Spain

†Institut d'Investigacions Biomèdiques August Pi i Sunyer, Barcelona, Spain

‡Department of Neurochemistry, Institut d'Investigacions Biomèdiques de Barcelona-Consejo Superior de Investigaciones Científicas (IIBB-CSIC), Barcelona, Spain

§Laboratory of Molecular Neurobiology, Department of Medical Biochemistry and Biophysics, Karolinska Institute, Stockholm, Sweden

Abstract

Dysfunction of dopaminergic neurons may contribute to motor impairment in Huntington's disease. Here, we study the role of brain-derived neurotrophic factor (BDNF) in alterations of the nigrostriatal system associated with transgenics carrying mutant huntingtin. Using huntingtin-BDNF$^{+/-}$ double-mutant mice, we analyzed the effects of reducing the levels of BDNF expression in a model of Huntington's disease (R6/1). When compared with R6/1 mice, these mice exhibit an increased number of aggregates in the substantia nigra *pars compacta*. In addition, reduction of BDNF expression exacerbates the dopaminergic neuronal dysfunction seen in mutant huntingtin mice, such as the decrease in retrograde labelling of dopaminergic neurons and striatal dopamine content. However, mutant huntingtin mice with normal or lowered BDNF expression show the same decrease in the anterograde transport, number of dopaminergic neurons and nigral volume. In addition, reduced BDNF expression causes decreased dopamine receptor expression in mutant huntingtin mice. Examination of changes in locomotor activity induced by dopamine receptor agonists revealed that, in comparison with R6/1 mice, the double mutant mice exhibit lower activity in response to amphetamine, but not to apomorphine. In conclusion, these findings demonstrate that the decreased BDNF expression observed in Huntington's disease exacerbates dopaminergic neuronal dysfunction, which may participate in the motor disturbances associated with this neurodegenerative disorder.

Keywords: amphetamine, axonal transport, movement disorders, neuronal dysfunction, neurotrophins, substantia nigra.
J. Neurochem. (2005) **93,** 1057–1068.

Neurodegenerative disorders are characterized by a progressive and specific loss of neurons. Huntington's disease (HD) is an autosomal dominant inherited neurodegenerative disorder caused by unstable expanded CAG repeats in the 5′-coding region of the huntingtin (*htt*) gene (The Huntington's Disease Collaborative Research Group 1993). The primary brain region affected in HD is the striatum, where a selective degeneration of GABAergic projection neurons occurs. However, neuronal degeneration also extends to other brain areas, including the cerebral cortex, substantia nigra (SN), globus pallidus and subthalamic nucleus as the disease progresses (Rubinsztein 2002; Browne and Beal 2004).

The important role of the SN dopaminergic system in the control of motor function suggests that dysfunctional dopaminergic transmission may play a role in motor disturbances, the most common feature of HD (Hickey *et al.* 2002). In fact, reduced expression of dopamine receptors and

Received August 6, 2004; revised manuscript received December 10, 2004; accepted December 14, 2004.

Address correspondence and reprint requests to Dr J. Alberch, Departament de Biologia Cel·lular i Anatomia Patològica, Facultat de Medicina, Universitat de Barcelona, C/Casanova, 143 E-08036 Barcelona, Spain. E-mail: alberch@ub.edu

Abbreviations used: BDA, biotinylated dextran amine; bDM, BDNF-mutant *htt* mice; BDNF, brain-derived neurotrophic factor; BSA, bovine serum albumin; DOPAC, 3,4-dihydroxyphenylacetic acid; FG, Fluorogold; HD, Huntington's disease; *htt*, huntingtin gene; LSD, least significant difference; OD, optical density; PBS, phosphate-buffered saline; PMSF, phenylmethylsulphonyl fluoride; SDS, sodium dodecyl sulfate; SN, substantia nigra; SNpc, substantia nigra pars compacta; SNpr, substantia nigra pars reticulata; wt, wild type.

altered dopaminergic function has been described in asymptomatic and symptomatic HD patients (Antonini *et al.* 1996; Weeks *et al.* 1996; Ginovart *et al.* 1997).

Transgenic mice carrying the mutant *htt* gene have facilitated efforts to understand the pathophysiology of HD. The transgenic mouse lines R6, including R6/1 and R6/2, are the best-characterized mouse models of HD (Mangiarini *et al.* 1996). Several reports have shown that these mice reproduce some of the dopaminergic dysfunction observed in HD patients. However, dopaminergic deficits are more apparent in the R6/2 line (Bibb *et al.* 2000; Hickey *et al.* 2002; Petersen *et al.* 2002), which shows a more rapid progression of HD symptoms (Mangiarini *et al.* 1996). These dopaminergic alterations include decreased levels of D_1 and D_2 dopamine receptors (Cha *et al.* 1998), reduced dopamine content (Reynolds *et al.* 1999), and age-dependent impairment in the behavioural response to dopamine stimulants (Hickey *et al.* 2002).

The mechanism underlying HD pathogenesis remains to be elucidated, but it could involve the gain of toxic functions, the loss of beneficial functions of wild type (wt)-*htt* or both. Wt-*htt* increases the transcription of the brain-derived neurotrophic factor (BDNF) (Zuccato *et al.* 2001), a neuroprotective factor for striatal (Bemelmans *et al.* 1999; Perez-Navarro *et al.* 1999, 2000; Kells *et al.* 2004) and dopaminergic neurons (Hyman *et al.* 1991). This beneficial activity of wt-*htt* is lost when the protein is mutated as, under these conditions, BDNF expression is reduced (Ferrer *et al.* 2000; Zuccato *et al.* 2001, 2003). Furthermore, reduction of endogenous striatal BDNF levels in mutant *htt* transgenic mice results in earlier onset and enhanced severity of motor alterations (Canals *et al.* 2004). Within the SN, BDNF plays a critical role in the control of dopaminergic functions, as shown by the finding that BDNF heterozygous mice exhibit elevated dopamine concentrations (Dluzen *et al.* 2002) and increased amphetamine-stimulated locomotor behaviour (Dluzen *et al.* 2001).

In the present work, we focus on the role of BDNF in the dopaminergic system of the mutant *htt* transgenic models. We have recently developed a new R6/1 subline that expresses lower levels of BDNF, the BDNF-mutant *htt* mice (bDM; Canals *et al.* 2004). Thus, when R6/1 mice were compared with bDM, our results indicate that a decrease in the levels of this neurotrophin exacerbates the dopaminergic dysfunction observed in HD mouse models.

Material and methods

Animals

BDNF heterozygous mice ($bdnf^{+/-}$ htt^{wt}; Ernfors *et al.* 1994) were crossed with R6/1 mice ($bdnf^{+/+}$ htt^{m}; Mangiarini *et al.* 1996) to obtain bDM ($bdnf^{+/-}$ htt^{m}), as described previously (Canals *et al.* 2004). Because of the different background strains of the BDNF heterozygous mice (BalbC) and the R6/1 mice (C6CBA), we used F2 inbred mice from the same litter mates for all viable genotypes (wt: $bdnf^{+/+}$ htt^{wt}; R6/1: $bdnf^{+/+}$ htt^{m}; BDNF heterozygous: $bdnf^{+/-}$ htt^{wt}; bDM: $bdnf^{+/-}$ htt^{m}). Animals were housed together in numerical birth order in groups of mixed genotypes. All experiments were conducted with a blind-coded respect to genotype, and data were recorded for analysis by microchip mouse number. For genotyping, DNA was obtained from tail biopsy material, processed for PCR and amplified fragments were resolved on an agarose gel: 2% for BDNF (Agerman *et al.* 2003) and 1.5% for mutant *htt* (Mangiarini *et al.* 1996). Animals were maintained with access to food and water *ad libitum* in a colony room kept at a constant temperature (19–22°C) and humidity (40–50%) on a 12 : 12 h light/dark cycle. All animal-related procedures were performed in accordance with the National Institute of Health Guide for the care and use of laboratory animals and approved by the local animal care committee of the University of Barcelona and by the Generalitat de Catalunya.

Injections of axonal tracers

To study axonal transport from the SN to the striatum, intracerebral injections of both anterograde [biotinylated dextran amine (BDA); Molecular Probes, Eugene, OR, USA] or retrograde [Fluorogold (FG); Fluorochrome Inc. Denver, CO, USA] tracers were performed in 30-week-old mice ($n = 4$–5 per genotype). Animals were anaesthetized with pentobarbital solution (50 mg/kg) and placed in a stereotaxic apparatus (Stoelting Co., Wood Dale, IL, USA).

For anterograde transport studies, 0.2 μL of a BDA solution [10% in phosphate-buffered saline (PBS; pH 7.4)] was delivered into the substantia nigra pars compacta (SN*pc*) (antero-posterior (A/P) −3.2 mm, lateral (L) ± 1.3 mm from bregma; and dorso-ventral (D/V) 4.4 mm from dura; incisor bar set at −3 mm) as described elsewhere (Ramanathan *et al.* 2002). Five days after injection of the tracer, mice were transcardially perfused with 4% paraformaldehyde and 0.05% glutaraldehyde in 0.1 M phosphate buffer (PB). After 2 h of post-fixation in the same solution, sections were cryoprotected with 12% sucrose and frozen in dry-ice cooled isopentane. Coronal sections throughout the striatum were cut on a cryostat (14 μm) and revealed using the avidin-biotin-peroxidase method (ABC; Pierce, Rockford, IL, USA) with 3,3′-diaminobenzidine (DAB; Sigma, St Louis, MO, USA) as chromogen for the peroxidase reaction. No signal was detected in controls without BDA injection.

The retrograde labelling of the SN*pc* was examined injecting a FG solution (1% in PBS) into the striatum at the following coordinates: A/P +0.5 mm, L −2 mm from bregma; and D/V 2.7 mm from dura; incisor bar set at −3 mm. Two days after striatal injection, mice were perfused transcardially with 4% paraformaldehyde in PB, cryoprotected with 30% sucrose and frozen in dry-ice cooled isopentane. Coronal sections (30 μm) were cut on a cryostat and mounted with Mowiol (Calbiochem, San Diego, CA, USA).

Enzyme-linked immunosorbent assay (ELISA)

BDNF content was determined using E_{max} Immunoassay system kit (Promega, Madison, WI, USA), according to the manufacturer's instructions. Mice were deeply anaesthetized in a CO_2 chamber at 30 weeks of age ($n = 4$ per genotype). Their SN was dissected out on ice and rapidly frozen using CO_2 pellets. Samples were then

homogenized in lysis buffer (137 mM NaCl, 20 mM Tris-HCl pH 8.0, 1% Igepal, 10% glycerol, 1 mM phenylmethylsulphonyl fluoride (PMSF), 10 μg/mL aprotinin, 1 μg/mL leupeptin), sonicated and centrifuged (10 min × 16 000 *g* at 4°C). Supernatants were collected and the protein contents measured by Detergent Compatible Protein Assay (Bio-Rad, Hercules, CA, USA). Total protein (150 μg) was analyzed in duplicate for each point, diluted 1 : 1.5 in blocking and sample buffer. Serial dilutions of recombinant BDNF (0–500 pg/mL) were added to duplicate wells in each plate in order to generate a standard curve.

Western blot analysis

We analyzed the levels of wt Htt and mutant Htt by western blot using monoclonal antibodies against wt Htt [4C8 (mAb2166; Chemicon, Temecula, CA, USA)] or the poly glutamine tract of mutant Htt (1F8, a generous gift from Marcy E MacDonald, Massachusetts General Hospital, Boston, MA). Samples ($n = 3$ per genotype) were processed by western blot as described elsewhere (Persichetti *et al.* 1999; Canals *et al.* 2004). In brief, brain tissues of R6/1 or bDM were homogenated by sonication in 10 μL RIPA buffer [150 mM NaCl, 50 mM Tris-HCl, pH 8.0, 1 mM EDTA, 1 mM EGTA, 1% Triton X-100, 0.1% sodium dodecyl sulfate (SDS), 0.5% sodium deoxycholate, 1 mM PMSF, 10 μg/mL aprotinin, 1 μg/mL leupeptin] per mg tissue. After homogenation, samples were centrifuged twice at 12 000 *g* for 10 min. Twenty micrograms of supernatant proteins were loaded in a 6% SDS–polyacrylamide gel electrophoresis (PAGE) and transferred to Immobilon-P membranes (Millipore Corporation, Bedford, MA, USA). Blots were blocked in 10% non-fat dry milk in TBS-T (150 mM NaCl, 20 mM Tris-HCl, pH 7.5, 0.05% tween-20) and then incubated with the respective primary antibody (1 : 2000 for 4C8 and 1 : 10 000 for 1F8) in PBS. After several washes in TBS-T, blots were incubated with 1 : 2000 of anti-mouse IgG HRP-conjugated (Promega) and developed by ECL western blotting analysis system (Bioscience Europe GmbH, Freiburg, Germany). As loading controls, we re-incubated the membranes with a monoclonal anti-α-tubulin antibody (1 : 50 000; Sigma). The intensity of the bands were measured using the Phoretix 1D gel analysis program (Phoretix International Ltd, Newcastle-upon-Tyne, UK) and values in each lane were normalized to their respective loading control. Results were expressed as percentage with respect to R6/1 mice.

Dopamine measurements

Five mice from each genotype were deeply anaesthetized in a CO_2 chamber and killed by decapitation. As age-matched controls, five animals from each independent background strain, BalbC and C6CBA, were examined in parallel following the same protocol. Their striata were dissected out on ice, weighed and rapidly frozen using CO_2 pellets. Then, tissue was ultrasonically homogenized in 500 μL of ice-cold 0.4 M perchloric acid containing 5 mM sodium metabisulfite, 8.3 mM cysteine and 0.3 mM EDTA. After centrifugation at 12 000 *g* (30 min, 4°C), the concentration of dopamine and its acid metabolite DOPAC was analyzed using high-performance liquid chromatography (HPLC). These molecules were separated on an Ultrasphere 3-μm column (7.5 cm × 0.46 cm; Beckman, San Ramon, CA, USA) and detected with a Hewlett-Packard 1049 amperometric detector (Palo Alto, CA, USA), set at a potential of +0.75 V. The mobile phase consisted of 0.15 M KH_2PO_4, 0.46 mM octyl sodium sulfate, 0.5 mM EDTA (pH 2.8 adjusted with phosphoric acid) and 12% methanol, and was pumped at a rate of 0.6 mL/min. Under these conditions, the respective retention times of dopamine and DOPAC were approximately 7 and 9 min. Values were expressed as nmoles/g of tissue and compared with wt mice.

In situ hybridization

Thirty-week-old mice from each genotype were deeply anaesthetized in a CO_2 chamber ($n = 4$–6 per genotype) and serial coronal cryostat sections (14 μm) were obtained from unfixed frozen brains. As controls, mice from independent background strains, BalbC and C6CBA, were also analyzed ($n = 3$).

For examination of BDNF mRNA levels, we performed *in situ* hybridization with radioactive riboprobes, as described elsewhere (Canals *et al.* 2001). An antisense cRNA probe to detect the transcripts of mouse BDNF was prepared by *in vitro* transcription using T7 RNA polymerase (Promega) and ^{33}P-UTP (Bioscience Europe). For controls, a sense cRNA probe was obtained by *in vitro* transcription using T3 RNA polymerase (Promega). After deproteination and acetylation slices were incubated for 16 h in a humidified chamber at 53°C with 2.5×10^5 cpm in hybridization cocktail (50% formamide, 20 mM Tris-HCl pH 7.6, 1 mM EDTA pH 8, 0.3 M NaCl, 0.1 M dithiothreitol, 0.5 mg/mL yeast tRNA, 0.1 mg/mL polyA RNA, 1 × Denhardt's solution and 10% dextran sulfate). After hybridization, slices were washed at high stringency, dried and exposed to Biomax MR film (Eastman Kodak Company, Rochester, NY) for 2 weeks.

For D_1 and D_2 dopamine receptor *in situ* hybridization, frozen tissue sections were brought to room temperature (22°C), and fixed for 20 min at 4°C with 4% paraformaldehyde in PBS. The protocol for *in situ* hybridization was based on previously described procedures (Tomiyama *et al.* 1997). For the detection of different mRNAs, the oligodeoxyribonucleotide probes used were complementary to bases 1805–1852 for dopamine D_1 receptor mRNA (GenBank acc. no. NM_012546) and 347–388 for dopamine D_2 receptor mRNA (GenBank acc. no. NM_012547). Oligonucleotides were labelled at their 3′ end using [α-^{33}P]dATP (3000 Ci/mmol; New England Nuclear, Boston, MA, USA) and terminal deoxynucleotidyltransferase (TdT; Oncogene Research Products, San Diego, CA, USA), and purified using QIAquick Nucleotide Removal Kit (Qiagen GmbH, Hilden, Germany). Brain sections were washed three times for 5 min in PBS at room temperature, and incubated for 2 min at 21°C in a solution of predigested pronase (Calbiochem) at a final concentration of 24 U/mL in 50 mM Tris-HCl pH 7.5, 5 mM EDTA. The reaction was stopped by immersion for 30 s in 2 mg/mL glycine in PBS. Tissues were finally rinsed in PBS and dehydrated through a graded ethanol series. For hybridization, the radioactively labelled probe was diluted in a solution containing: 50% formamide, 4 × SSC (1 × SSC: 150 mM NaCl, 15 mM sodium citrate), 1 × Denhardt's solution (0.02% Ficoll, 0.02% polyvinylpyrrolidone), 0.02% bovine serum albumin (BSA), 10% dextran sulfate, 1% sarkosyl, 20 mM phosphate buffer pH 7.0, 250 μg/mL yeast tRNA and 500 μg/mL salmon sperm DNA. The final concentration of radioactive probe in the hybridization buffer was 1.5 nM. Tissue sections were covered with hybridization solution containing the labelled probe overlaid with Nescofilm coverslips (Bando Chemical Ind., Kobe, Japan) and incubated overnight at 42°C in humid boxes.

Sections were washed four times in SSC at 60°C, dehydrated and exposed to Biomax MR Kodak film (Eastman Kodak) or dipped in Ilford K5 nuclear emulsion (Ilford, Mobberly, Chesire, UK). They were then exposed in the dark at 4°C for 6 weeks, and finally developed in Kodak D19 (Eastman Kodak) for 5 min.

Immunohistochemistry

Thirty-week-old mice were deeply anaesthetized in a CO_2 chamber and transcardially perfused with 4% paraformaldehyde in PBS. Brains were post-fixed for 2 h in the same solution and cryoprotected with 30% sucrose in PBS. Serial coronal cryostat sections (30 μm), 0.3 mm apart, were processed for immunohistochemistry.

Immunohistochemistry was performed on free-floating sections. Endogenous peroxidases were blocked for 30–45 min in PBS containing 10% methanol and 3% H_2O_2. Then, non-specific protein interactions were blocked with normal serum or BSA. Tissue was then incubated overnight at 4°C with the following primary antibodies: anti-tyrosine hydroxylase (TH; 1 : 4000; Diasorin, Saluggia, Italy); anti-parvalbumin (1 : 1250; Sigma); anti-mutant htt (EM48; 1 : 50; Chemicon); and anti-ubiquitine antibody (1 : 800, Dako A/S, Glostrup, Germany). Sections were washed three times in PBS and incubated with a biotinylated secondary antibody (1 : 200; Pierce) at room temperature for between 30 min and 2 h. The immunohistochemical reaction was developed using the ABC kit (Pierce) and visualized with DAB. No signal was detected in controls in which the primary antibodies have been omitted.

Quantitative analysis

BDNF expression levels were quantified on *in situ* hybridization films ($n = 4$). Consecutive sections (7–8 sections/animal) were scanned and the signal intensity was analyzed using the ImageJ program (National Institute of Mental Health, Bethesda, MD, USA). The area of the SN*pc* was determined according to the anatomical landmarks and the intensity was quantified. The background signal of the same adjacent area outside of the brain was subtracted.

SN*pc* volume was measured using the AnalySIS programe (Software Imaging System GmbH, Münster, Germany) on a computer attached to an Olympus microscope. Consecutive sections (7–8 sections/animal) were visualized at low magnification and the borders of the nigral TH-positive immunostaining were outlined. The volumes were calculated using the Cavalieri method, multiplying the sum of all sectional areas (mm^2) by the distance between successive sections (0.3 mm), as described previously (Canals *et al.* 2001; Canudas *et al.* 2005).

For quantification of BDA-labelled fibres in the striatum, we measured the optical density on consecutive sections (9–10 sections/animal) throughout striata. Digital images were taken at low magnification, the anatomical landmarks of the striatum were outlined, and the average of signal intensity was measured using the ImageJ program after background correction as above.

Cell and aggregate counts were performed blind with respect to genotype in 30-week-old mice ($n = 3$–4 per each genotype). Unbiased stereological counts of FG- or TH-positive cells and cytoplasmic or intranuclear aggregates were obtained from the entire SN*pc* using the Computer Assisted Stereology Toolbox (CAST) software (Olympus Danmark A/S, Ballerup, Denmark). The dissector counting method was employed to analyze coronal sections spaced 180 μm apart. The counting frames were randomly sampled.

Total SN*pc* mRNA levels of striatal dopamine receptors were quantified on *in situ* hybridization films. Consecutive sections (18–20 sections/animal) were scanned and mRNA levels were analyzed using the ImageJ program (National Institute of Mental Health). The striatal area was determined according to anatomical landmarks and the intensity was quantified. The background signal of the same adjacent area outside of the brain was subtracted.

To analyze the expression of D_1 and D_2 receptors per cell, striatal images were taken in a field of 0.13 mm^2 on successive sections as above. The soma area of 10 randomly chosen cells per section was outlined and the emulsion autoradiography grains were counted using the AnalySIS program (Software Imaging System GmbH) as described elsewhere (Perez-Navarro *et al.* 1999).

Statistical analysis was performed using ANOVA followed by the least significant difference (LSD) post-hoc test. All results were normalized to wt mice and expressed as the average ± standard error of the mean (SEM) of different mice per genotype.

Behavioral measurements

Locomotor activity was measured in an open-field and recorded with a video caption system (Videotrack 512; Electronique lyonnaise, Lyon, France) in 34–57 mice at 15 and/or 30 weeks of age. Animals were placed into the register area, and left to habituate for 1 h. After this period, mice received apomorphine (0.5 mg/kg in 0.9% NaCl, s.c. 30-week-old mice: $bdnf^{+/+}$ htt^{wt}, $n = 6$; $bdnf^{+/+}$ htt^{m}, $n = 10$; $bdnf^{+/-}$ htt^{wt}, $n = 8$; $bdnf^{+/-}$ htt^{m}, $n = 10$) or amphetamine (5 mg/kg in 0.9% NaCl, i.p. 15-week-old mice: $bdnf^{+/+}$ htt^{wt}, $n = 16$; $bdnf^{+/+}$ htt^{m}, $n = 15$; $bdnf^{+/-}$ htt^{wt}, $n = 11$; $bdnf^{+/-}$ htt^{m}, $n = 15$; 30-week-old mice: $bdnf^{+/+}$ htt^{wt}, $n = 6$; $bdnf^{+/+}$ htt^{m}, $n = 10$; $bdnf^{+/-}$ htt^{wt}, $n = 8$; $bdnf^{+/-}$ htt^{m}, $n = 10$) and their behaviour was recorded over the following hour. The same mice were evaluated with both dopaminergic stimulants, although the animals analyzed at 15 and 30 weeks of age come from different litter mates. Data caption were recorded at 5-min intervals. Time spent in movement (s), and the distance covered (cm) was analyzed. To evaluate any possible behavioural influence from the genetic background, we also examined the motor activity induced by apomorphine (0.5 mg/kg, s.c.) or amphetamine (5 mg/kg, i.p.) treatment in mice from different strains (BalbC and C6CBA; $n = 5$ per strain).

We compared the curves defined for each genotype after the administration of the dopaminergic stimulants, apomorphine or amphetamine. For statistical analysis, we performed a two-way repeated measures analysis of variance (ANOVA) with the factors 'mutant htt' and 'BDNF' using the Statistica program (StatSoft Inc., Tulsa, OK, USA). We also analyzed the global effect between genotypes by calculating the total time in movement and the total distance covered after administration of the dopaminergic agonists, and values were compared using one-way ANOVA followed by LSD post-hoc test.

Results

Mutant Htt produces dysfunction of nigrostriatal axonal transport

To study how changes in BDNF expression affect the mutant *htt*-associated dysfunction of the dopaminergic system of the

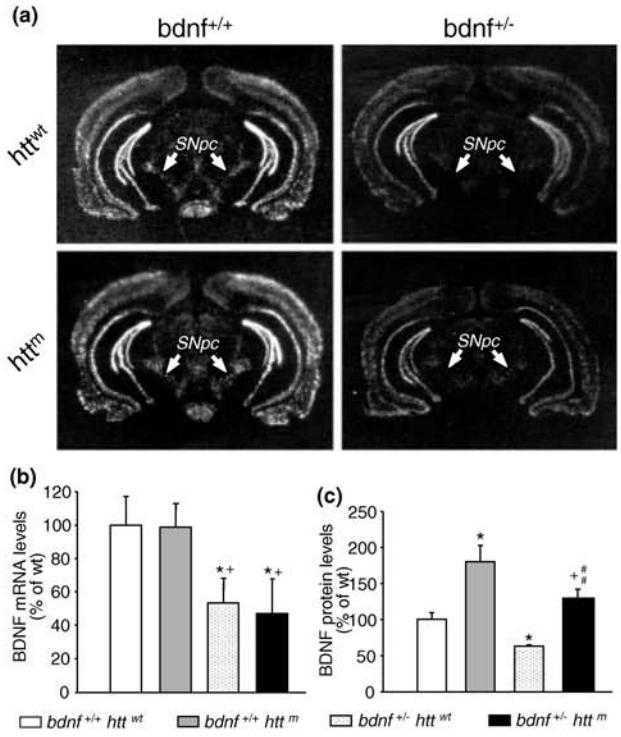

Fig. 1 BDNF is accumulated in the SN*pc* in mutant *htt* transgenic mice. (a, b) BDNF *in situ* hybridization shows lower levels of BDNF mRNA in heterozygous BDNF mice with or without mutant *htt* (BDNF heterozygous, $bdnf^{+/-}$ htt^{wt}; bDM: $bdnf^{+/-}$ htt^{m}) than in wt-BDNF mice (wt mice, $bdnf^{+/+}$ htt^{wt}; R6/1 mice, $bdnf^{+/+}$ htt^{m}). (a) Magnified view of the SN from representative coronal sections (bregma −3.0 mm) of BDNF *in situ* hybridization of the four genotypes analyzed. Arrows indicate the SN*pc*. (b) Quantification of *in situ* hybridization for BDNF mRNA in the SN*pc*. (c) Mutant *htt* mice with normal or decreased levels of BDNF expression accumulate BDNF protein in the SN. $^{*}p < 0.05$ compared with wt mice; $^{+}p < 0.05$ compared with R6/1 mice; ## $p < 0.005$ compared with BDNF heterozygous mice.

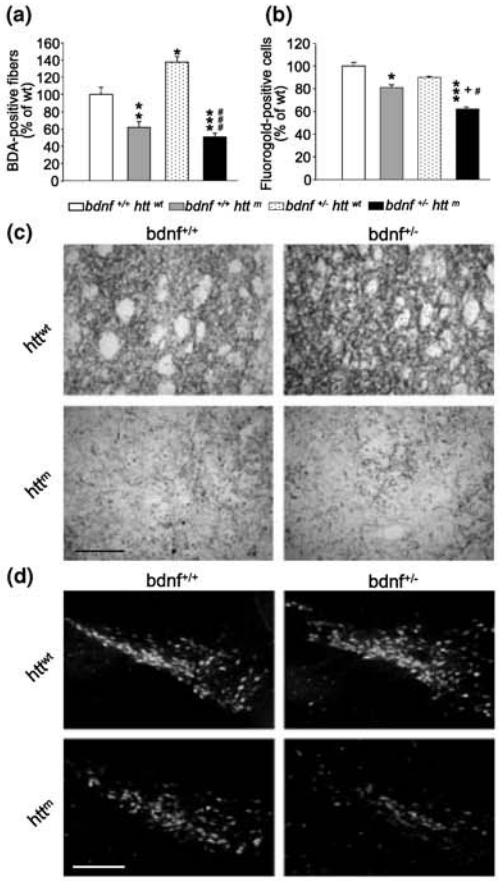

Fig. 2 Decreased levels of BDNF expression exacerbate the deficit of the nigrostriatal retrograde labelling in mutant *htt* transgenic mice. (a, c) The intranigral injection of an anterograde tracer, BDA, shows that both genotypes that express mutant *htt* have an impairment of axonal transport. (a) Quantitative studies show a significant reduction of transport in R6/1 mice ($bdnf^{+/+}$ htt^{m}) and bDM ($bdnf^{+/-}$ htt^{m}), without differences between them. $^{*}p < 0.05$, $^{**}p < 0.005$, $^{***}p < 0.001$ compared with wt mice; ###$p < 0.001$ compared with BDNF heterozygous mice. (b) Quantification of retrograde labelled neurons after striatal Fluorogold injection demonstrates that the nigrostriatal pathway is affected in 30-week-old R6/1 mice, and this effect is more severe in bDM mice. No alterations in FG retrograde labelling are observed in BDNF heterozygous mice ($bdnf^{+/-}$ htt^{wt}) with respect to wt mice ($bdnf^{+/+}$ htt^{wt}). $^{*}p < 0.05$, $^{***}p < 0.001$ compared with wt mice;$^{+}$ $p < 0.05$ compared with R6/1 mice; #$p < 0.05$ compared with BDNF heterozygous mice. (c) Images from the anterograde labelled striata after BDA injection in the SN*pc*. Scale bar: 100 μm (d) Representative images of SN*pc* labelled with FG retrograde tracer injected into the striatum. Scale bar: 200 μm.

SN*pc*, we compared R6/1 mice with normal levels of BDNF mRNA with the R6/1 subline with lowered BDNF levels (bDM; Canals *et al*. 2004). *In situ* hybridization of the SN*pc* showed low levels of BDNF mRNA in heterozygous mice for BDNF with or without mutant *htt* ($bdnf^{+/-}$ htt^{wt}, and $bdnf^{+/-}$ htt^{m}; Figs 1a and b). Nevertheless, protein levels analyzed by ELISA were increased in the SN of mutant *htt* genotypes compared with the SN of wt mice (in pg/mg of protein; $bdnf^{+/+}$ htt^{wt}, 72.8 ± 7.0; $bdnf^{+/+}$ htt^{m}, 130.8 ± 20.3; $bdnf^{+/-}$ htt^{wt}, 45.6 ± 1.84; $bdnf^{+/-}$ htt^{m}, 94.6 ± 8.5; Fig. 1c).

These results suggested an abnormal accumulation of BDNF in nigral cells because of a deficit of nigrostriatal pathway. Thus, in order to assess the functionality of the nigrostriatal pathway, we performed studies with the anterograde tracer BDA and the retrograde tracer FG (Fig. 2). We observed a large reduction in the anterograde labelling of the striatal fibres in R6/1 mice ($bdnf^{+/+}$ htt^{m}, 61.82% ± 6.76 with respect to wt mice) and in bDM ($bdnf^{+/-}$ htt^{m}, 50.76% ± 4.57 compared with wt mice). Surprisingly, the anterograde labelling was enhanced in BDNF heterozygous mice ($bdnf^{+/-}$ htt^{wt} 137.61% ± 6.60 compared with wt mice). Therefore, the accumulation of BDNF protein in the SN might be related to a dysfunction of the anterograde transport in

animals that express mutant htt. We next examined whether retrograde labelling of dopaminergic neurons was affected by mutant *htt*, by injecting the retrograde tracer FG into the striatum (Figs 2b and d). Mutant *htt* mice displayed a reduction of FG-retrograde labelled cells, which was more pronounced in bDM animals (FG-positive cells in the SN: $bdnf^{+/+}$ htt^{wt}, 20 380 ± 910; $bdnf^{+/+}$ htt^{m}, 16 450 ± 670; $bdnf^{+/-}$ htt^{wt}, 18 260 ± 250; $bdnf^{+/-}$ htt^{m}, 12 730 ± 430; Fig. 2b). This represents a 20% reduction in R6/1 and a 37% reduction in bDM with respect to wt mice. It is noteworthy that the decrease of BDNF mRNA per se did not alter the uptake or retrograde transport of Fluorogold in BDNF heterozygous mice (Figs 2b and d).

Non-ubiquitinated Htt aggregates are increased in bDM

Assessment of aggregate number and localization revealed that in the SN most of the aggregates were located in the SN*pc* and very few in the SN *pars reticulata* (SN*pr*; Fig. 3a). This specific pattern of distribution was not affected in bDM (Fig. 3b).

The decrease in BDNF expression was inversely proportional to the number of mutant Htt aggregates in the SN*pc*. Thus, the number of intranuclear aggregates in bDM was increased by 276% over those in R6/1 mice (Fig. 3c–e) and the number of mutant Htt cytoplasmic aggregates in bDM was 189% over the aggregates in the R6/1 mice (Fig. 3c, d and f). Interestingly, the number of ubiquitinated aggregates was not modified by the level of BDNF ($bdnf^{+/+}$ htt^{m}, 100 ± 29%; $bdnf^{+/-}$ htt^{m}, 85 ± 12% with respect to R6/1; Fig. 3g).

We also analyzed whether changes in BDNF levels may modify the expression of Htt. Western blot analyses against mutant and wt-Htt showed similar levels of protein in both R6/1 and bDM mice (Fig. 3h).

The reduction of BDNF expression in mutant *htt* transgenic mice does not affect the number of dopaminergic neurons at the SN

We next compared the volume of the SN*pc* between each genotype. All mice carrying the mutant *htt* showed a reduction in SN*pc* volume ($bdnf^{+/+}$ htt^{wt}, 0.319 ± 0.01; $bdnf^{+/+}$ htt^{m}, 0.181 ± 0.02; $bdnf^{+/-}$ htt^{wt}, 0.298 ± 0.02; $bdnf^{+/-}$ htt^{m}, 0.189 ± 0.02 mm^3; Fig. 4a). Thus, we did not observe any effect of BDNF on the SN*pc* volume of mutant *htt* transgenic mice. The number of TH-positive neurons was also reduced in both mutant *htt* transgenic mice expressing either normal or reduced BDNF (Fig. 4b). Here, we observed a 26% reduction in the number of dopaminergic cells in R6/1 mice and a 36% reduction in bDM mice (Fig. 4b). To assess the specificity of the effect on the SN*pc*, we also analyzed the number of parvalbumin-positive neurons in the SN*pr*. We did not observe any differences in the number of these cells between the genotypes studied (Fig. 4c).

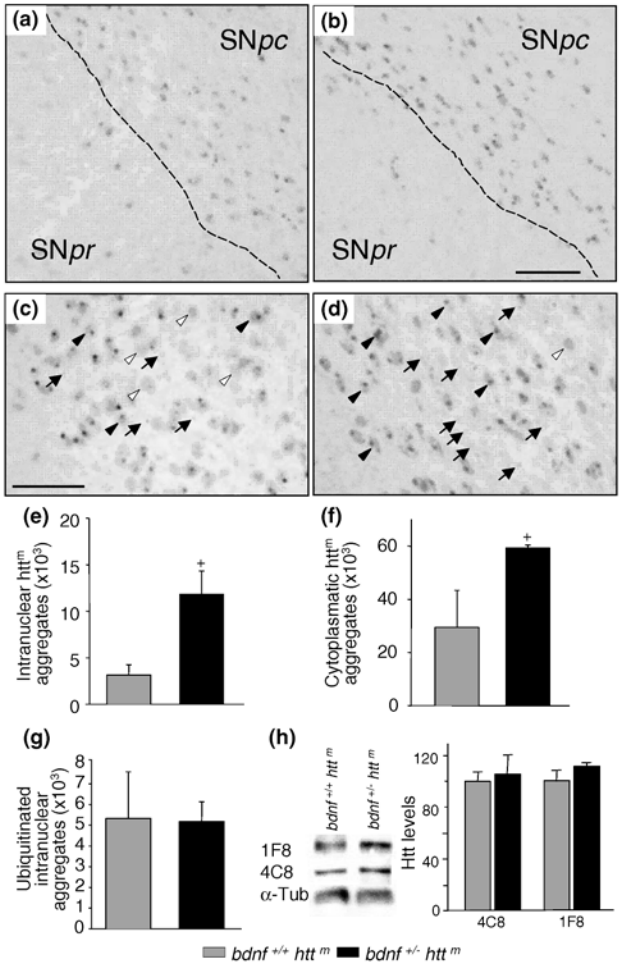

Fig. 3 The number of *htt*-positive aggregates is increased in bDM mice with respect to R6/1 mice. (a, b) Within the SN, aggregates are mainly distributed in the SN*pc* and very few are observed in the SN*pr*. (c–e) The number of intranuclear *htt*-positive inclusions (detected with EM48 antibody, arrows in c and d) is higher in bDM ($bdnf^{+/-}$ htt^{m}) than in R6/1 mice ($bdnf^{+/+}$ htt^{m}). (c, d, f) Similarly, cytoplasmic *htt*-aggregates (detected with EM48 antibody, black arrowheads in c and d) are more abundant in bDM than in R6/1 mice. The number of cells that do not have inclusions is lower in bDM than in R6/1 mice (white arrowheads in c and d). (g) However, the number of ubiquitinated intranuclear aggregates does not differ between bDM and R6/1 mice. (h) Western blot analysis shows that the different levels of BDNF between R6/1 mice and bDM do not affect the amount of wt or mutant *htt* (detected with the 4C8 or the 1F8, respectively). Scale bars: a and b, 100 μm; c and d, 50 μm. $^+p < 0.05$ compared with R6/1 mice.

Dopamine levels in the striatum are reduced in bDM

To study the regulation of dopamine metabolism, we next examined changes in dopamine and 3,4,-dihydrophenylacetic acid (DOPAC) contents induced by BDNF in mutant *htt* mice. Dopamine concentration in BDNF heterozygous mice was increased (165% with respect to wt levels). Interestingly, we found a significant reduction of both dopamine (62.5%

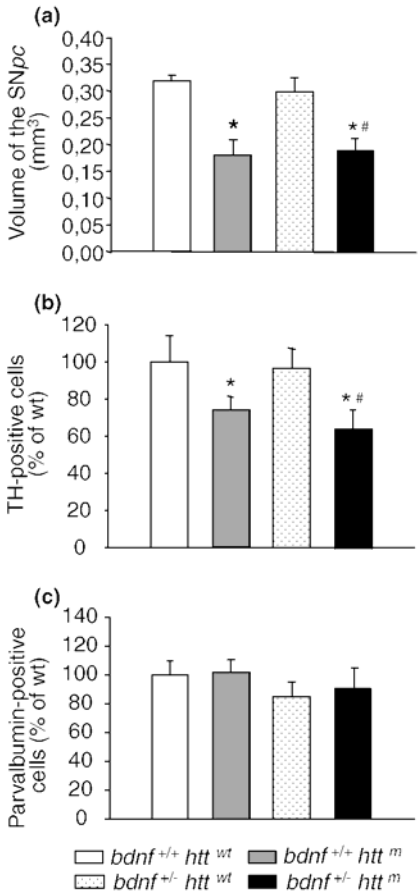

Fig. 4 Decreasing BDNF expression in mutant *htt* transgenic mice does not affect the volume of the SN or the number of TH-positive neurons. (a) The volume of the SN*pc* is significantly lower in mutant *htt* mice with normal (R6/1, $bdnf^{+/+}$ htt^{m}) or lower levels of BDNF (bDM, $bdnf^{+/-}$ htt^{m}) than in wt ($bdnf^{+/+}$ htt^{wt}) or heterozygous BDNF mice ($bdnf^{+/-}$ htt^{wt}). (b) Similarly, the number of dopaminergic neurons (TH-positive) is decreased in both R6/1 mice and bDM, with no differences between them. (c) The number of parvalbumin-positive neurons in the SN*pr* is not affected in any genotype studied. $^{*}p < 0.05$ compared with wt mice; $\#p < 0.05$ compared with BDNF heterozygous mice.

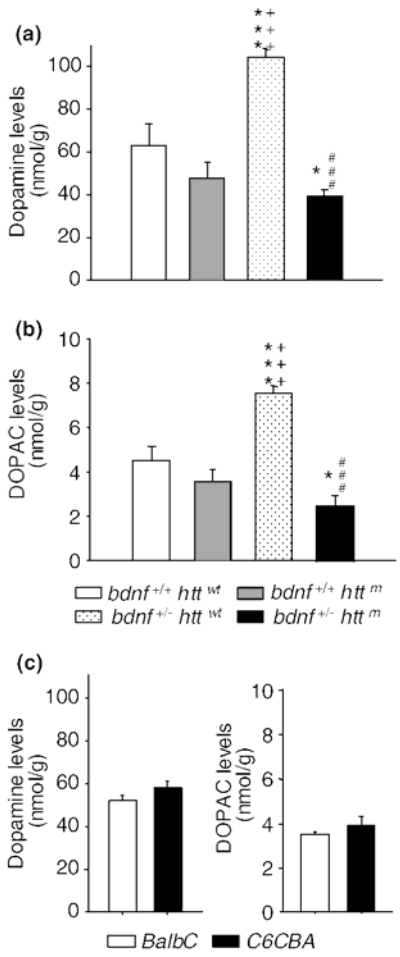

Fig. 5 bDM presents a reduction of both dopamine and DOPAC levels. (a) The levels of dopamine in R6/1 mice ($bdnf^{+/+}$ htt^{m}) show a tendency towards a decrease, whereas bDM mice ($bdnf^{+/-}$ htt^{m}) exhibit lower levels of dopamine that are significantly different from wt levels. However, the dopamine levels are increased in BDNF heterozygous mice ($bdnf^{+/-}$ htt^{wt}). (b) The levels of DOPAC are only decreased in bDM mice. (c) No differences in the levels of dopamine or DOPAC are detected between mice from independent background strains (BalbC and C6CBA). $^{*}p < 0.05$, $^{***}p < 0.001$ compared with wt mice ($bdnf^{+/+}$ htt^{wt}); $^{+++}p < 0.001$ compared with R6/1 mice; $\#\#\#p < 0.001$ compared with BDNF heterozygous mice ($bdnf^{+/-}$ htt^{wt}).

compared with wt mice and 35.6% with BDNF heterozygous mice; Fig. 5a) and DOPAC levels (55.15% with respect to wt mice and 37.7% compared with BDNF heterozygous mice; Fig. 5b) in bDM striata (dopamine in nmoles/g tissue: $bdnf^{+/+}$ htt^{wt}, 63.30 ± 9.98; $bdnf^{+/+}$ htt^{m}, 47.61 ± 7.49; $bdnf^{+/-}$ htt^{wt}, 104.43 ± 3.83; $bdnf^{+/-}$ htt^{m}, 39.10 ± 3.36; and DOPAC in nmoles/g tissue: $bdnf^{+/+}$ htt^{wt}, 4.46 ± 0.56; $bdnf^{+/+}$ htt^{m}, 3.59 ± 0.49; $bdnf^{+/-}$ htt^{wt}, 7.53 ± 0.34; $bdnf^{+/-}$ htt^{m}, 2.46 ± 0.37). Thus, decreased BDNF expression in mutant *htt* mice significantly decreased striatal dopamine and DOPAC content, which may result from a reduced dopamine synthesis in nigro-striatal dopaminergic neurons. The analysis of the independent background strains showed similar levels to our controls, without differences between strains (dopamine in nmoles/g tissue: BalbC, 52.81 ± 2.22; C6CBA, 56.59 ± 3.7 and DOPAC in nmoles/g tissue: BalbC, 3.33 ± 0.13; C6CBA, 3.76 ± 0.34).

D_1 and D_2 receptor mRNA levels are only reduced in bDM

As reduced levels of dopamine can modify the expression of dopamine receptors, we examined the mRNA levels of dopamine receptors in the striatum of all four genotypes.

In situ hybridization for D_1 receptors revealed a 47% reduction of total striatal expression in bDM compared with wt mice [optical density (OD) values: $bdnf^{+/+}$ htt^{wt},

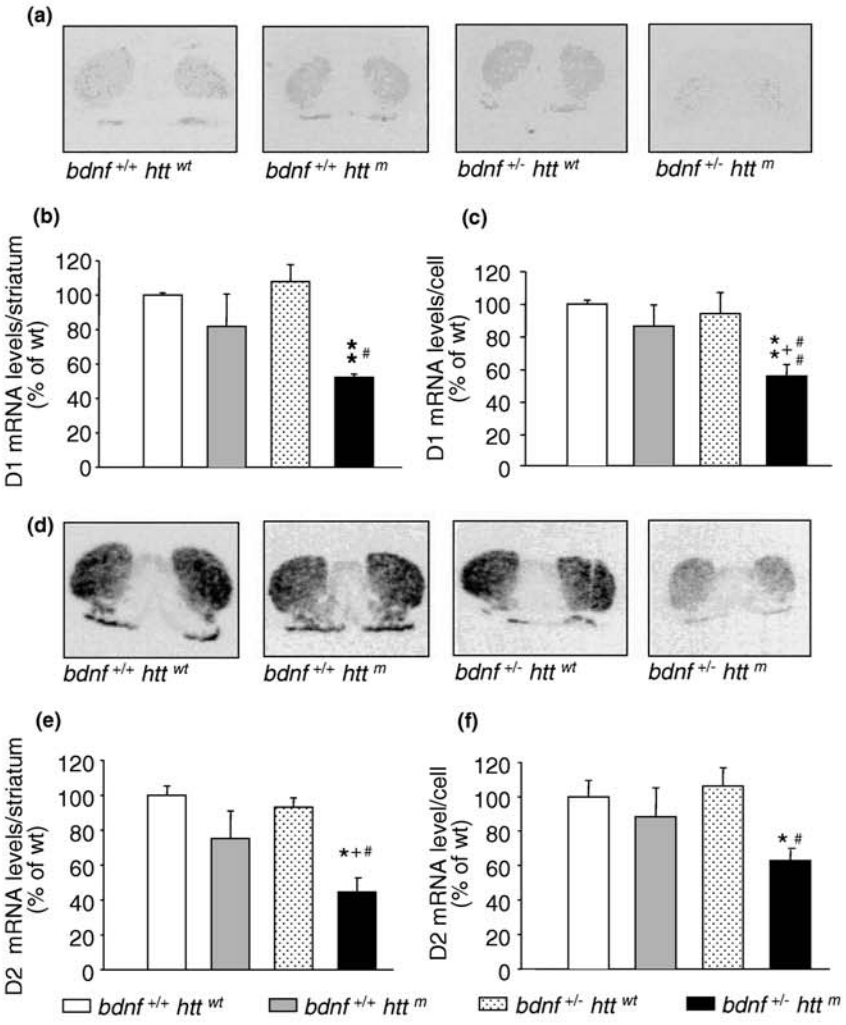

Fig. 6 Dopamine receptors expression is reduced in bDM mice. (a, d) Representative images of the *in situ* hybridization for the D_1 (a) and D_2 (d) dopamine receptors, showing the striatum of all four genotypes analyzed (wt, $bdnf^{+/+}$ htt^{wt}; R6/1, $bdnf^{+/+}$ htt^{m}; BDNF heterozygous, $bdnf^{+/-}$ htt^{wt}; and bDM, $bdnf^{+/-}$ htt^{m}). (a, b) The total levels of mRNA for the D_1 receptor are decreased in bDM mice. (c) This effect may be as a result of a reduction in expression levels and not of cell death because the levels of mRNA per cell are lower in bDM than in wt mice. No alterations of D_1 levels are detected in R6/1 or BDNF heterozygous mice. (d–f) Similarly, the levels of D_2 expression in total or per cell are reduced in bDM but not in R6/1 mice. $^{*}p < 0.05$, $^{**}p < 0.005$ compared with wt mice; $^{+}p < 0.05$ compared with R6/1 mice; $\#p < 0.05$, $\#\#p < 0.005$ compared with BDNF heterozygous mice.

18.24 ± 0.24, $bdnf^{+/+}$ htt^{m}, 14.92 ± 3.42; $bdnf^{+/-}$ htt^{wt}, 19.69 ± 1.81; $bdnf^{+/-}$ htt^{m}, 9.54 ± 0.31; Figs 6(a and b)]. Similar results were obtained for D_2 receptors, which showed a 54% reduction in bDM with respect to wt mice [OD values $bdnf^{+/+}$ htt^{wt}, 109.06 ± 8.54; $bdnf^{+/+}$ htt^{m}, 72.94 ± 7.25; $bdnf^{+/-}$ htt^{wt}, 95.28 ± 11.42; $bdnf^{+/-}$ htt^{m}, 49.85 ± 16.25; Figs 6 (d and e)]. Thus, dopamine receptors are significantly reduced in bDM striata. However, this reduction could be attributed to striatal neuronal atrophy. For this reason, we next analyzed whether the low levels of expression were as a result of cellular loss or receptor down-regulation. When we counted the expression of each receptor per cell, as described in material and methods, we observed a reduction of the expression levels of each receptor in bDM (D_1 values: $bdnf^{+/+}$ htt^{wt}, 100 ± 3%; $bdnf^{+/+}$ htt^{m}, 86 ± 13%; $bdnf^{+/-}$ htt^{wt}, 94 ± 13%; $bdnf^{+/-}$ htt^{m}, 55 ± 7% compared with wt mice; Fig. 6c; and D_2 values: $bdnf^{+/+}$ htt^{wt}, 100 ± 9%; $bdnf^{+/+}$ htt^{m}, 88 ± 17%; $bdnf^{+/-}$ htt^{wt}, 106 ± 11%; $bdnf^{+/-}$ htt^{m}, 63 ± 6% with respect to wt mice; Fig. 6f). No differences in D_1 or D_2 mRNA levels were detected between the independent background strains (OD values for D_1: BalbC, 16.42 ± 1.84; C6CBA, 19.63 ± 2.12 and OD values for D_2: BalbC, 109.81 ± 8.36; C6CBA, 107.96 ± 5.21).

BDM mice show reduced locomotor activity in response to amphetamine but not to apomorphine

Finally, locomotor activity in the open field was assessed in response to pharmacological dopaminergic agents. We first examined whether differences in stress handling could interfere with locomotion analyses. Thus, 15- and 30-week-old mice from the four genotypes were injected with vehicle (0.9% NaCl) alone and their behaviour was analyzed. These experiments showed no differences between genotypes, either at 15 weeks of age (data not shown) or at 30 weeks of age (Figs 7a and b). Next, we stimulated 30-week-old mice from the four genotypes with apomorphine and the motor activity response was recorded over the course of the next hour. We observed a rapid peak of locomotor response without any difference between genotypes (Figs 7c and e). We also analyzed locomotor activity after amphetamine

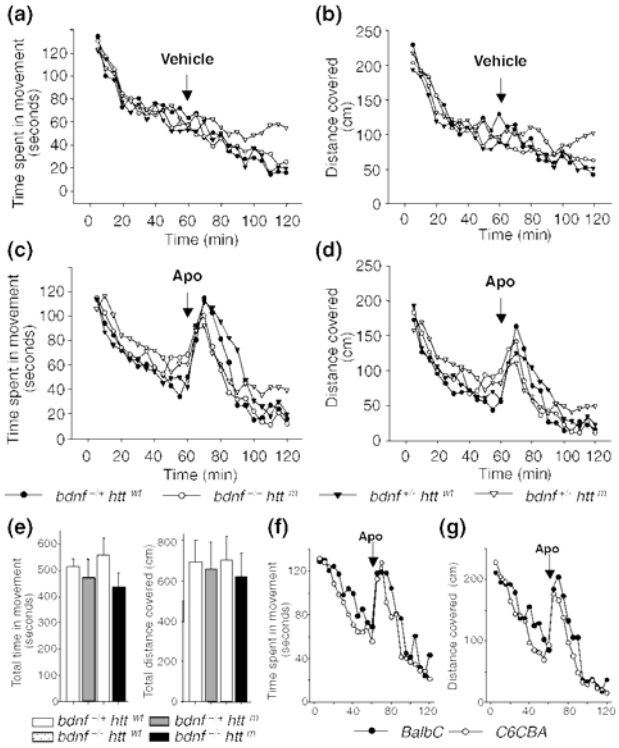

Fig. 7 No differences in apomorphine-induced locomotor activity are observed between the four genotypes studied (wt, $bdnf^{+/+}$ htt^{wt}; R6/1, $bdnf^{+/+}$ htt^{m}; BDNF heterozygous, $bdnf^{+/-}$ htt^{wt}; and bDM, $bdnf^{+/-}$ htt^{m}). (a, b) Handling stress after the injection of the vehicle (0.9% NaCl) does not alter the locomotion in any genotype examined. (c–e) However, the administration of apomorphine (Apo) induces a peak of locomotor activity at 65–75 min in all genotypes. No differences in the time spent in movement (c, e) or in the distance covered (d, e) are detected between the four groups studied. (f, g) The genetic background (BalbC and C6CBA) does not produce differences in locomotion after apomorphine administration.

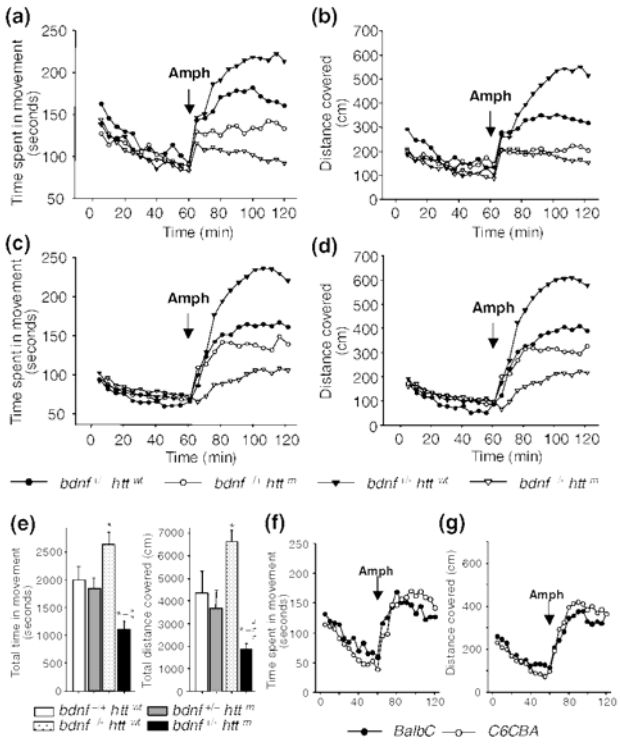

Fig. 8 bDM mice show a lower locomotor activity response than the other genotypes studied. (a, b) The response to amphetamine (Amph) was evaluated in 15-week-old mice of all four genotypes (wt, $bdnf^{+/+}$ htt^{wt}; R6/1, $bdnf^{+/+}$ htt^{m}; BDNF heterozygous, $bdnf^{+/-}$ htt^{wt}; and bDM, $bdnf^{+/-}$ htt^{m}). bDM mice exhibit a decreased response to amphetamine, although BDNF heterozygous animals with normal *htt* show a higher response to amphetamine than wt. (c–e) Higher differences are observed in 30-week-old mice. At this development stage, bDM show significant differences with respect to the other genotypes analyzed. $^{*}p < 0.05$ compared with wt mice; $^{+}p < 0.05$ compared with R6/1 mice; $\#\#p < 0.005$, $\#\#\#p < 0.001$ compared with BDNF heterozygous mice. (f, g) There are no differences in amphetamine response between mice from independent background strains (BalbC and C6CBA).

administration in 15- or 30-week-old mice. BDNF heterozygous mice showed hyperlocomotor activity while bDM mice showed a reduced response (Fig. 8). This enhancement of motor activity after amphetamine stimulation in BDNF heterozygous mice was detected in 15-week-old (Figs 8a and b; $p < 0.05$ with respect to wt mice) and 30-week-old mice (Figs 8c–e; $p < 0.05$ with respect to wt mice). BDM showed differences at 15 weeks of age with respect to wt and R6/1 with less time spend in movement (Fig. 8a; $p < 0.05$ with respect to wt and R6/1 mice and $p < 0.005$ with respect to BDNF heterozygous mice), although bDM did not show differences with R6/1 in the distance covered (Fig. 8b; $p < 0.05$ and $p < 0.005$ with respect to wt and BDNF heterozygous mice, respectively). The analysis of 30-week-old bDM showed less locomotor response compared with the other genotypes in both, the time spent in movement (Figs 8c and e; $p < 0.05$ with respect to wt and R6/1 mice and $p < 0.005$ with respect to BDNF heterozygous mice) and the distance covered (Figs 8d and e; $p < 0.05$ with respect to wt and R6/1 mice and $p < 0.001$ with respect to BDNF heterozygous mice). These findings indicate that the decrease of BDNF expression in the presence of mutant *htt* affects the presynaptic dopaminergic system, but does not have functional repercussions at the postsynaptic level. No differences between background strains were detected either after apomorphine (Figs 7f and g) or amphetamine treatment (Figs 8f and g).

Discussion

To study the role of BDNF in the nigrostriatal pathway in HD, we compared two transgenic models that differ in the expression levels of this neurotrophin, the R6/1 mice (Mangiarini *et al.* 1996) and a subline with decreased levels

of BDNF, bDM (Canals *et al.* 2004). We have demonstrated that reduction of BDNF expression in the R6/1 mouse line increases the number of both nuclear and cytoplasmic aggregates. The enhancement of the number of aggregates in the neuropil of the SN*pc* correlates with the levels of striatal dopamine and dopamine receptors. However, although R6/1 mice show a reduced number of TH-positive neurons and SN*pc* volume, the lower levels of BDNF mRNA in bDM do not influence these parameters. We also observed that decreased BDNF expression in R6/1 mice exacerbates deficits in amphetamine- but not apomorphine-induced locomotor activity.

We have shown here that R6/1 mice have normal levels of BDNF mRNA in the SN, as occurs in the striatum and cerebral cortex (Canals *et al.* 2004). However, we detected increased levels of BDNF protein in the SN of both R6/1 and bDM mice. These findings are in agreement with those that we obtained from anterograde tracer studies, which showed a deficit of nigrostriatal transport in animals that express mutant *htt*. Similarly, a recent report showed that mutant *htt* affects the vesicular transport of BDNF (Gauthier *et al.* 2004) and therefore BDNF may be accumulated in the SN, the area in which it is produced. In fact, it has been shown that BDNF is synthesized by dopaminergic neurons of the SN (Aliaga *et al.* 2000; Rite *et al.* 2003; Canudas *et al.* 2005) and transported anterogradely to the striatum by nigral afferents (Altar and DiStefano 1998). Furthermore, the inhibition of axonal transport with intracerebroventricular injections of colchicine elevates BDNF protein staining in cell bodies of cortical and nigral neurons, but depletes it within the neostriatum (Altar and DiStefano 1998). In HD patients, although BDNF mRNA is decreased in cerebral cortex (Zuccato *et al.* 2001), the amount of BDNF protein is reduced in the striatum but not in the cortex (Ferrer *et al.* 2000; Gauthier *et al.* 2004), suggesting a relative protein accumulation in the cortex.

We also observed that retrograde labelling of SN*pc* neurons was altered in R6/1. This impairment of nigrostriatal retrograde labelling is progressive in R6/1 mice. Whilst it has been shown previously that the uptake or transport of FG is intact in 16-weeks-old animals (Petersen *et al.* 2002), we observed an effect at 30 weeks of age. This effect was exacerbated in bDM mice, suggesting that the lack of BDNF contributes to the progression of the neurodegenerative process in the presence of mutant *htt*.

Although there is some controversy about the role of *htt* aggregates, many authors propose, on the basis that Htt interacts with proteins associated to cytoskeleton-based transport (Li *et al.* 1995; Kalchman *et al.* 1997; Wanker *et al.* 1997; Li *et al.* 1998), that their presence in the neuropil is implicated in disturbances of axonal transport (Li *et al.* 2001). Our present findings show that decreasing BDNF expression in the R6/1 mouse line increases the number of non-nuclear aggregates, which could be related to the enhanced dysfunction of dopaminergic neurons in bDM mice. The number of intranuclear inclusions, which have been correlated with cell atrophy and/or death (Bates 2003; Hickey and Chesselet 2003), is also increased in bDM with respect to R6/1 mice. This effect is specific to the SN*pc*, as indicated by the fact that we did not detect any difference in the number of intranuclear aggregates in the striatum (Canals *et al.* 2004) or in the SN*pr* (present results) of bDM compared with R6/1 striata. Interestingly, we did not observe an increase in ubiquitin-positive intranuclear aggregates in bDM. Consistent with this, only a proportion of *htt* aggregates are ubiquitinated in human HD tissue (Gutekunst *et al.* 1999). Taken together, our findings may indicate that decreased BDNF expression interferes with the ubiquitin-mediated proteolytic pathway in the SN*pc*.

We next examined whether the reduced levels of BDNF expression in bDM has functional implications in the dopaminergic system. Our findings demonstrate that the reduction of BDNF expression does not affect the volume of the SN*pc* or the number of dopaminergic neurons. Compared with the uptake or transport of FG results, these findings suggest that the decrease of BDNF in bDM affects the functionality of dopaminergic neurons. Thus, we analyzed the contents of dopamine and the levels of D_1 and D_2 receptors. We observed a significant decrease of dopamine contents in bDM compared with R6/1 mice, which did not show reduction in dopamine content, as described previously (Petersen *et al.* 2002). These abnormal levels of dopamine in bDM could not be attributed to transport impairments because we examined dopamine content at 15 weeks of age, just before any effect on the transport or uptake of FG. These findings are in agreement with the results obtained when R6/1 and R6/2 lines were compared. Whereas no differences in dopamine content are detected in R6/1 mice (Petersen *et al.* 2002; present results), studies performed in homogenates of R6/2 mouse striata, in which BDNF is decreased (Zhang *et al.* 2003), demonstrated diminished levels of dopamine (Reynolds *et al.* 1999; Hickey *et al.* 2002). In addition, dopamine concentration in post-mortem striatal HD tissue has been shown to be decreased (Kish *et al.* 1987), a finding that can also be related to the reduced levels of BDNF (Ferrer *et al.* 2000). Thus, taken together, these results indicate that the reduced expression levels of this neurotrophin result in impairment of several dopaminergic functions.

Dopamine D_1 and D_2 receptor mRNAs and proteins show a pronounced reduction in human post-mortem HD tissue (Augood *et al.* 1997; Glass *et al.* 2000). We observed that bDM, like R6/2 transgenic mice (Cha *et al.* 1998), show a substantial decrease in D_1 and D_2 expression. However, our findings demonstrate that this down-regulation of the receptors does not have implications in terms of behavioural response. Thus, we did not observe any effect on the behavioural response to the dopamine receptor agonist the

apomorphine. Although this result was unexpected, it suggests that the reduced dopaminergic input induces sensitization of D_1 and/or D_2 receptors in the striatum in HD. Supersensitization of D_1 receptors has also been postulated in R6/2 mice, which shows decrease of dopamine receptor expression (Cha *et al.* 1998) but no decrease in immediate early gene expression induced by a D_1 agonist (Spektor *et al.* 2002).

When we examined motor behaviour after stimulation of the dopaminergic system with amphetamine, a drug that induces dopamine release, our results showed that in pre-symptomatic and symptomatic R6/1 mice, decreased BDNF expression results in a lower response to amphetamine. It is interesting that in BDNF heterozygous mice with normal *htt* the response to amphetamine is increased (Dluzen *et al.* 2001; present results). Therefore, the mutation of *htt* together with the reduced BDNF levels in bDM mice acts synergistically on dopamine synthesis and release. These findings suggest that presynaptic dopaminergic defects caused by decreased BDNF expression contribute to motor alterations in HD.

In conclusion, our present findings demonstrate that mutant *htt* induces a nigrostriatal dopaminergic dysfunction that is modulated by BDNF. Thus, BDNF may help to restore dopaminergic activity, which could be beneficial in short-term in reducing motor symptoms observed in HD.

Acknowledgements

We thank Dr Silvia Gines and Dr Marcy E. MacDonald for their help in western blot analysis of mutant Htt. We are very grateful to M. Teresa Muñoz, Ana López and Francesca Calderón for technical assistance, and Dr Emili Martínez for help with behavioural analysis. We are also grateful to Dr Amèrica Jiménez and the staff of the animal care (Facultat de Medicina, Universitat de Barcelona) for their help in mice care. This study was supported by the Ministerio de Ciencia y Tecnología (SAF2002-00314, to JA; SAF2002-00311, to JMC, Spain), 'redes temáticas de investigación cooperativa' (G03/167; G03/210; Ministerio de Sanidad y Consumo, Spain) and Fundació La Caixa (Spain). JRP is a fellow of the Ministerio de Educación y Ciencia (Spain) and MB of the University of Barcelona (Spain).

References

Agerman K., Hjerling-Leffler J., Blanchard M. P., Scarfone E., Canlon B., Nosrat C. and Ernfors P. (2003) BDNF gene replacement reveals multiple mechanisms for establishing neurotrophin specificity during sensory nervous system development. *Development* **130**, 1479–1491.

Aliaga E., Carcamo C., Abarca J., Tapia-Arancibia L. and Bustos G. (2000) Transient increase of brain derived neurotrophic factor mRNA expression in substantia nigra reticulata after partial lesion of the nigrostriatal dopaminergic pathway. *Brain Res. Mol. Brain Res.* **79**, 150–155.

Altar C. A. and DiStefano P. S. (1998) Neurotrophin trafficking by anterograde transport. *Trends Neurosci.* **21**, 433–437.

Antonini A., Leenders K. L., Spiegel R. *et al.* (1996) Striatal glucose metabolism and dopamine D2 receptor binding in asymptomatic gene carriers and patients with Huntington's disease. *Brain* **119**, 2085–2095.

Augood S. J., Faull R. L. and Emson P. C. (1997) Dopamine D1 and D2 receptor gene expression in the striatum in Huntington's disease. *Ann. Neurol.* **42**, 215–221.

Bates G. (2003) Huntingtin aggregation and toxicity in Huntington's disease. *Lancet* **361**, 1642–1644.

Bemelmans A. P., Horellou P., Pradier L., Brunet I., Colin P. and Mallet J. (1999) Brain-derived neurotrophic factor-mediated protection of striatal neurons in an excitotoxic rat model of Huntington's disease, as demonstrated by adenoviral gene transfer. *Hum. Gene Ther.* **10**, 2987–2997.

Bibb J. A., Yan Z., Svenningsson P., Snyder G. L., Pieribone V. A., Horiuchi A., Nairn A. C., Messer A. and Greengard P. (2000) Severe deficiencies in dopamine signaling in presymptomatic Huntington's disease mice. *Proc. Natl Acad. Sci. USA* **97**, 6809–6814.

Browne S. E. and Beal M. F. (2004) The energetics of Huntington's disease. *Neurochem. Res.* **29**, 531–546.

Canals J. M., Checa N., Marco S., Akerud P., Michels A., Perez-Navarro E., Tolosa E., Arenas E. and Alberch J. (2001) Expression of brain-derived neurotrophic factor in cortical neurons is regulated by striatal target area. *J. Neurosci.* **21**, 117–124.

Canals J. M., Pineda J. R., Torres-Peraza J. F., Bosch M., Martin-Ibanez R., Munoz M. T., Mengod G., Ernfors P. and Alberch J. (2004) Brain-derived neurotrophic factor regulates the onset and severity of motor dysfunction associated with enkephalinergic neuronal degeneration in Huntington's disease. *J. Neurosci.* **24**, 7727–7739.

Canudas A. M., Pezzi S., Canals J. M., Pallas M. and Alberch J. (2005) Endogenous brain derived neurotrophic factor protects dopaminergic nigral neurons against transneuronal degeneration induced by striatal excitotoxic injury. *Mol. Brain Res.* in press.

Cha J. H., Kosinski C. M., Kerner J. A., Alsdorf S. A., Mangiarini L., Davies S. W., Penney J. B., Bates G. P. and Young A. B. (1998) Altered brain neurotransmitter receptors in transgenic mice expressing a portion of an abnormal human huntington disease gene. *Proc. Natl Acad. Sci. USA* **95**, 6480–6485.

Dluzen D. E., Anderson L. I., McDermott J. L., Kucera J. and Walro J. M. (2002) Striatal dopamine output is compromised within +/- BDNF mice. *Synapse* **43**, 112–117.

Dluzen D. E., Gao X., Story G. M., Anderson L. I., Kucera J. and Walro J. M. (2001) Evaluation of nigrostriatal dopaminergic function in adult +/+ and +/- BDNF mutant mice. *Exp. Neurol.* **170**, 121–128.

Ernfors P., Lee K. F. and Jaenisch R. (1994) Mice lacking brain-derived neurotrophic factor develop with sensory deficits. *Nature* **368**, 147–150.

Ferrer I., Goutan E., Marin C., Rey M. J. and Ribalta T. (2000) Brain-derived neurotrophic factor in Huntington disease. *Brain Res.* **866**, 257–261.

Gauthier L. R., Charrin B. C., Borrell-Pages M. *et al.* (2004) Huntingtin controls neurotrophic support and survival of neurons by enhancing BDNF vesicular transport along microtubules. *Cell* **118**, 127–138.

Ginovart N., Lundin A., Farde L., Halldin C., Backman L., Swahn C. G., Pauli S. and Sedvall G. (1997) PET study of the pre- and post-synaptic dopaminergic markers for the neurodegenerative process in Huntington's disease. *Brain* **120**, 503–514.

Glass M., Dragunow M. and Faull R. L. (2000) The pattern of neurodegeneration in Huntington's disease: a comparative study of cannabinoid, dopamine, adenosine and GABA(A) receptor alterations in the human basal ganglia in Huntington's disease. *Neuroscience* **97**, 505–519.

Gutekunst C. A., Li S. H., Yi H., Mulroy J. S., Kuemmerle S., Jones R., Rye D., Ferrante R. J., Hersch S. M. and Li X. J. (1999) Nuclear and neuropil aggregates in Huntington's disease: relationship to neuropathology. *J. Neurosci.* **19**, 2522–2534.

Hickey M. A. and Chesselet M. F. (2003) Apoptosis in Huntington's disease. *Prog. Neuropsychopharmacol. Biol. Psychiatry.* **27**, 255–265.

Hickey M. A., Reynolds G. P. and Morton A. J. (2002) The role of dopamine in motor symptoms in the R6/2 transgenic mouse model of Huntington's disease. *J. Neurochem.* **81**, 46–59.

Hyman C., Hofer M., Barde Y. A., Juhasz M., Yancopoulos G. D., Squinto S. P. and Lindsay R. M. (1991) BDNF is a neurotrophic factor for dopaminergic neurons of the substantia nigra. *Nature* **350**, 230–232.

Kalchman M. A., Koide H. B., McCutcheon K. *et al.* (1997) HIP1, a human homologue of *S. cerevisiae* Sla2p, interacts with membrane-associated huntingtin in the brain. *Nat. Genet.* **16**, 44–53.

Kells A. P., Fong D. M., Dragunow M., During M. J., Young D. and Connor B. (2004) AAV-mediated gene delivery of BDNF or GDNF is neuroprotective in a model of Huntington disease. *Mol. Ther.* **9**, 682–688.

Kish S. J., Shannak K. and Hornykiewicz O. (1987) Elevated serotonin and reduced dopamine in subregionally divided Huntington's disease striatum. *Ann. Neurol.* **22**, 386–389.

Li H., Li S. H., Yu Z. X., Shelbourne P. and Li X. J. (2001) Huntingtin aggregate-associated axonal degeneration is an early pathological event in Huntington's disease mice. *J. Neurosci.* **21**, 8473–8481.

Li S. H., Gutekunst C. A., Hersch S. M. and Li X. J. (1998) Interaction of huntingtin-associated protein with dynactin P150Glued. *J. Neurosci.* **18**, 1261–1269.

Li X. J., Li S. H., Sharp A. H., Nucifora F. C. Jr, Schilling G., Lanahan A., Worley P., Snyder S. H. and Ross C. A. (1995) A huntingtin-associated protein enriched in brain with implications for pathology. *Nature* **378**, 398–402.

Mangiarini L., Sathasivam K., Seller M. *et al.* (1996) Exon 1 of the HD gene with an expanded CAG repeat is sufficient to cause a progressive neurological phenotype in transgenic mice. *Cell* **87**, 493–506.

Perez-Navarro E., Alberch J., Neveu I. and Arenas E. (1999) Brain-derived neurotrophic factor, neurotrophin-3 and neurotrophin-4/5 differentially regulate the phenotype and prevent degenerative changes in striatal projection neurons after excitotoxicity *in vivo*. *Neuroscience* **91**, 1257–1264.

Perez-Navarro E., Canudas A. M., Akerund P., Alberch J. and Arenas E. (2000) Brain-derived neurotrophic factor, neurotrophin-3, and neurotrophin-4/5 prevent the death of striatal projection neurons in a rodent model of Huntington's disease. *J. Neurochem.* **75**, 2190–2199.

Persichetti F., Trettel F., Huang C. C., Fraefel C., Timmers H. T., Gusella J. F. and MacDonald M. E. (1999) Mutant huntingtin forms *in vivo* complexes with distinct context-dependent conformations of the polyglutamine segment. *Neurobiol. Dis.* **6**, 364–375.

Petersen A., Puschban Z., Lotharius J., NicNiocaill B., Wiekop P., O'Connor W. T. and Brundin P. (2002) Evidence for dysfunction of the nigrostriatal pathway in the R6/1 line of transgenic Huntington's disease mice. *Neurobiol. Dis.* **11**, 134–146.

Ramanathan S., Hanley J. J., Deniau J. M. and Bolam J. P. (2002) Synaptic convergence of motor and somatosensory cortical afferents onto GABAergic interneurons in the rat striatum. *J. Neurosci.* **22**, 8158–8169.

Reynolds G. P., Dalton C. F., Tillery C. L., Mangiarini L., Davies S. W. and Bates G. P. (1999) Brain neurotransmitter deficits in mice transgenic for the Huntington's disease mutation. *J. Neurochem.* **72**, 1773–1776.

Rite I., Venero J. L., Tomas-Camardiel M., Machado A. and Cano J. (2003) Expression of BDNF mRNA in substantia nigra is dependent on target integrity and independent of neuronal activation. *J. Neurochem.* **87**, 709–721.

Rubinsztein D. C. (2002) Lessons from animal models of Huntington's disease. *Trends Genet.* **18**, 202–209.

Spektor B. S., Miller D. W., Hollingsworth Z. R., Kaneko Y. A., Solano S. M., Johnson J. M., Penney J. B. Jr, Young A. B. and Luthi-Carter R. (2002) Differential D1 and D2 receptor-mediated effects on immediate early gene induction in a transgenic mouse model of Huntington's disease. *Brain Res. Mol. Brain Res.* **102**, 118–128.

The Huntington's Disease Collaborative Research Group (1993) A novel gene containing a trinucleotide repeat that is expanded and unstable on Huntington's disease chromosomes. *Cell* **72**, 971–983.

Tomiyama M., Palacios J. M., Cortes R., Vilaro M. T. and Mengod G. (1997) Distribution of AMPA receptor subunit mRNAs in the human basal ganglia: an *in situ* hybridization study. *Brain Res. Mol. Brain Res.* **46**, 281–289.

Wanker E. E., Rovira C., Scherzinger E., Hasenbank R., Walter S., Tait D., Colicelli J. and Lehrach H. (1997) HIP-I: a huntingtin interacting protein isolated by the yeast two-hybrid system. *Hum. Mol. Genet.* **6**, 487–495.

Weeks R. A., Piccini P., Harding A. E. and Brooks D. J. (1996) Striatal D1 and D2 dopamine receptor loss in asymptomatic mutation carriers of Huntington's disease. *Ann. Neurol.* **40**, 49–54.

Zhang Y., Li M., Drozda M. *et al.* (2003) Depletion of wild-type huntingtin in mouse models of neurologic diseases. *J. Neurochem.* **87**, 101–106.

Zuccato C., Ciammola A., Rigamonti D. *et al.* (2001) Loss of huntingtin-mediated BDNF gene transcription in Huntington's disease. *Science* **293**, 493–498.

Zuccato C., Tartari M., Crotti A. *et al.* (2003) Huntingtin interacts with REST/NRSF to modulate the transcription of NRSE-controlled neuronal genes. *Nat. Genet.* **35**, 76–83.

Tercer trabajo

"Cystamine and cysteamine increase brain levels of BDNF in Huntington disease via HSJ1b and transglutaminase

Publicado en *The Journal of Clinical Investigation*

Research article

Cystamine and cysteamine increase brain levels of BDNF in Huntington disease via HSJ1b and transglutaminase

Maria Borrell-Pagès,[1] Josep M. Canals,[2] Fabrice P. Cordelières,[1] J. Alex Parker,[3] José R. Pineda,[2] Ghislaine Grange,[1] Elzbieta A. Bryson,[1] Martine Guillermier,[4] Etienne Hirsch,[5] Philippe Hantraye,[4] Michael E. Cheetham,[6] Christian Néri,[3] Jordi Alberch,[2] Emmanuel Brouillet,[4] Frédéric Saudou,[1] and Sandrine Humbert[1]

[1]Institut Curie, CNRS UMR 146, Orsay, France. [2]Departament de Biologia Cellular i Anatomia Patològica, Facultat de Medicina, Institut d'Investigacions Biomèdiques, Universitat de Barcelona, Barcelona, Spain. [3]INSERM, Avenir Group, Laboratory of Genomic Biology, Centre Paul Broca, Paris, France. [4]URA CEA/CNRS 2210, Service Hospitalier Frédéric Joliot and ImaGene program, Département de Recherches Médicales, Direction des Sciences du Vivant, CEA, Orsay, France. [5]INSERM U679, Neurologie et Thérapeutique Expérimentale, Hôpital de la Salpêtrière, Paris, France. [6]Division of Molecular and Cellular Neuroscience, Institute of Ophthalmology, University College London, London, United Kingdom.

There is no treatment for the neurodegenerative disorder Huntington disease (HD). Cystamine is a candidate drug; however, the mechanisms by which it operates remain unclear. We show here that cystamine increases levels of the heat shock DnaJ-containing protein 1b (HSJ1b) that are low in HD patients. HSJ1b inhibits polyQ-huntingtin–induced death of striatal neurons and neuronal dysfunction in *Caenorhabditis elegans*. This neuroprotective effect involves stimulation of the secretory pathway through formation of clathrin-coated vesicles containing brain-derived neurotrophic factor (BDNF). Cystamine increases BDNF secretion from the Golgi region that is blocked by reducing HSJ1b levels or by overexpressing transglutaminase. We demonstrate that cysteamine, the FDA-approved reduced form of cystamine, is neuroprotective in HD mice by increasing BDNF levels in brain. Finally, cysteamine increases serum levels of BDNF in mouse and primate models of HD. Therefore, cysteamine is a potential treatment for HD, and serum BDNF levels can be used as a biomarker for drug efficacy.

Introduction

Huntington disease (HD) is a devastating neurodegenerative disorder characterized by involuntary abnormal movements, personality changes, and dementia (1). The dominantly inherited causal gene encodes the huntingtin protein, which contains an abnormal polyglutamine (polyQ) expansion in HD patients. HD develops when the expansion exceeds 35 glutamine residues, and there is a strong inverse correlation between the number of residues and the age at onset. HD is characterized by the preferential dysfunction and death of striatal neurons in the brain and the presence of neuritic and intranuclear inclusions in neurons (2).

There is currently no effective treatment to prevent or delay disease progression, and death usually occurs within 10–20 years after the appearance of the first clinical symptoms. One of the most promising candidate drugs for HD is cystamine, a compound described as an in vitro transglutaminase (TGase) inhibitor. TGase is a calcium-dependent enzyme that catalyzes the formation of ε-(γ-glutamyl)lysine isopeptide bonds between a polypeptide-bound glutamine and a lysine of the protein substrate (3, 4). TGase is suspected of participating in HD pathogenesis (5). PolyQ-containing peptides and polyQ-huntingtin are substrates for TGase (6, 7). Moreover, TGase is upregulated in the brains of HD patients and of HD mice (8–11).

Given their enzymatic properties, TGases might promote aggregate formation in HD. The observations that TGase is recruited into neuronal intranuclear inclusions (NIIs) (10, 12) and that NIIs are reduced in a cystamine-treated mouse model of HD (10) are consistent with this idea. However, cystamine treatment of HD mice does not necessarily result in fewer NIIs (11), and an increase in NIIs is observed in HD mice that are deficient for 1 of the TGase isoenzymes, tissue TGase 2 (TGase 2) (13, 14). Nevertheless, both HD mice lacking TGase 2 and HD mice treated with cystamine have less neuronal death, improved motor performance, and prolonged survival (10, 11, 13–15). In addition to its role as an in vitro inhibitor of TGase, cystamine could act through other mechanisms (14, 16, 17). It inhibits caspase 3 activity and increases the levels of glutathione in cell models (18). It also increases the level of L-cysteine in cell models and animals (17, 19).

To understand better the beneficial effects of cystamine, Karpuj and colleagues treated HD mice with cystamine and analyzed large-scale profiles of transcription in the brain, where they identified genes whose transcription was specifically influenced by cystamine treatment (11). In particular, transcripts of DnaJ-type heat shock proteins (Hsps) were elevated upon cystamine treatment (11). Numerous other studies have highlighted the important role of Hsps in HD and in other polyQ disorders in cellular and animal models (for reviews, see refs. 20–22). Hsps are of particular relevance to HD not only because they prevent aggregation of mutant proteins and solubilize aggregated proteins but also because they promote ubiquitination and degradation of abnormal proteins and suppress the antiapoptotic program (22, 23). Cystamine might, therefore, be protective in HD by increasing the transcription of Hsps that, in turn, protect cells against polyQ-huntingtin–induced toxicity.

Nonstandard abbreviations used: BDNF, brain-derived neurotrophic factor; BFA, brefeldin A; CCV, clathrin-coated vesicle; HD, Huntington disease; hsc70, heat shock cognate 70 kDa; HSJ1, heat shock DnaJ-containing protein 1b; Hsp, heat shock protein; NII, neuronal intranuclear inclusion; 3NP, 3-nitropropionic acid; polyQ, polyglutamine; TGase, transglutaminase;TGase 2, tissue TGase 2; TGN, *trans*-Golgi network.

Conflict of interest: The authors have declared that no conflict of interest exists.

Citation for this article: *J. Clin. Invest.* doi:10.1172/JCI27607.

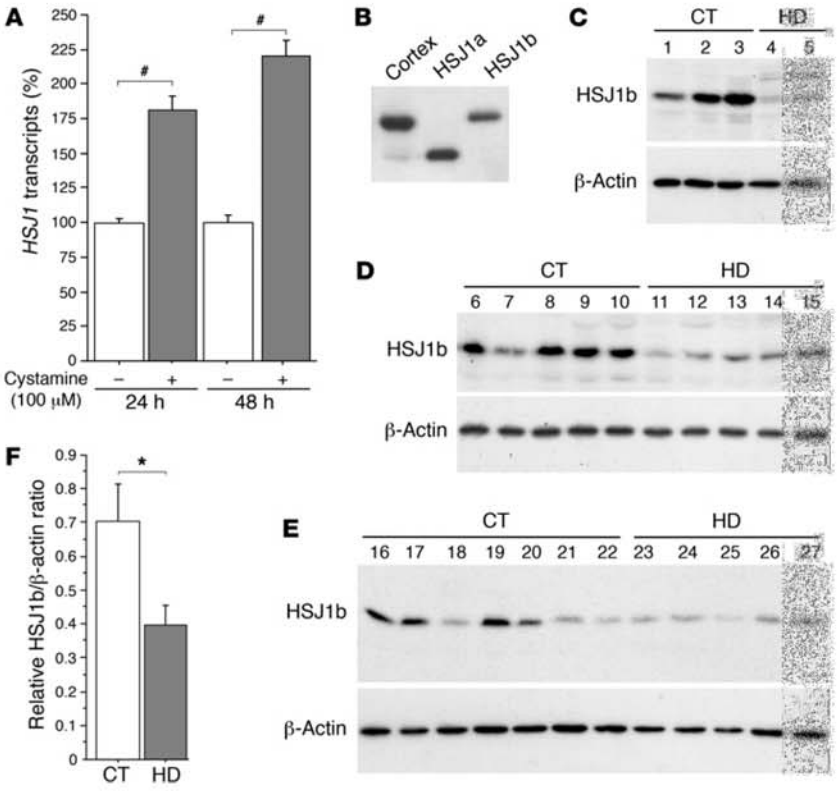

Figure 1
Cystamine increases *HSJ1* transcript levels in neuronal cells, while HSJ1b is decreased in postmortem brain extracts from HD patients. (**A**) Data revealed a statistically significant increase in *HSJ1* transcripts induced by cystamine treatment in comparison to control at 24 hours (Student's *t* test, $t_{[21]} = 5.77$; $P < 0.0001$) and at 48 hours (Student's *t* test, $t_{[10]} = 9.88$; $P < 0.0001$). (**B**) Protein extracts prepared from 1 control human cortical postmortem sample and from HEK 293T cells transfected with HSJ1a or HSJ1b were immunoblotted with an anti-HSJ1 antibody. The major brain isoform of HSJ1 proteins was the HSJ1b isoform. (**C**–**E**) Protein extracts were prepared from whole striatum (**C**), putamen (**D**), and caudate nucleus (**E**) of control (CT) and HD individuals and analyzed as in **B**. Immunoblotting with an anti–β-actin antibody was used as a control. (**F**) Quantification of the Western blots presented in **C**–**E** showed a statistically significant decrease in the protein level of HSJ1b in HD samples ($n = 12$) compared with control samples ($n = 15$) (Student's *t* test, $t_{[25]} = 2.33$; $P = 0.028$). $^{*}P < 0.05$, $^{\#}P < 0.0001$.

To study the protective mechanism elicited by cystamine, we focused on the *Homo sapiens* heat shock DnaJ-containing protein 1b (HSJ1b), which is enriched in the brain. We report that HSJ1b and cystamine are neuroprotective in HD by increasing the release of brain-derived neurotrophic factor (BDNF) — a trophic factor that is depleted in HD brains and is crucial for the survival of striatal neurons (24–27) — from neurons both in culture and in animals. We demonstrate that cystamine positively regulates BDNF release not only by increasing HSJ1 transcripts but also by inhibiting TGase. We next show that cysteamine, the FDA-approved reduced form of cystamine, is neuroprotective in HD mice by enhancing BDNF levels in brain. Indeed, changes in endogenous BDNF levels modulate the cystamine-induced neuroprotective effect in HD mice. Finally, BDNF blood levels are low in mice and primate models of HD and can be increased by injection of cysteamine. Our study provides not only new mechanisms by which cystamine promotes neuroprotection in HD, but also a potential new treatment for HD using its FDA-approved reduced form, cysteamine.

Results

HSJ1 transcripts are elevated upon cystamine treatment. To confirm that cystamine treatment leads to an increase in the amount of *HSJ1* transcripts, we treated mouse immortalized neuronal cells (28) with 100 μM cystamine for 24 or 48 hours, lysed the cells, isolated mRNAs, and performed real-time quantitative RT-PCR (real-time RT-PCR) using validated oligonucleotides (Figure 1A). We observed a statistically significant increase in HSJ1 transcripts of 1.7-fold after 24 hours treatment and of 2.2-fold after 48 hours (Figure 1A). Thus, *HSJ1* transcripts are elevated upon cystamine treatment of both neuronal cells and the R6/2 mouse model of HD (11).

HSJ1b — the predominant HSJ1 isoform in brain — is decreased in HD brains. The *HSJ1* gene generates, by alternate splicing, 2 proteins, HSJ1a and HSJ1b, that differ in their C termini. *HSJ1* mRNAs are enriched in brain, and HSJ1a and HSJ1b proteins are found in various regions such as cortex, cerebellum, striatum, and retina, with HSJ1b more abundant than HSJ1a (Figure 1, B–E) (29). To analyze the relevance of HSJ1 proteins in the context of HD, we determined their levels in postmortem samples of striatum from HD patients. Striatum that includes caudate nucleus and putamen is the most severely affected region in HD (1). By immunoblotting the samples with an antibody against HSJ1, we found a dramatic decrease in the level of HSJ1b protein in HD patients compared with control individuals (Figure 1, C–E). Anti–β-actin was used as a control for protein loading. HSJ1a was expressed at low or undetectable levels in both control and HD brain samples. We quantified the downregulation of HSJ1b and found it to be statistically significant (Figure 1F). These results show that the levels of HSJ1b, the main isoform of HSJ1 in brain, are reduced in the pathological situation and are of further support for a role of HSJ1b in HD pathogenesis. The postmortem samples represent late stages of the disease. Therefore, such a decrease could be attributed to the selective death of neurons expressing HSJ1b. However, these brain extracts show no profound modifications in the levels of calbindin, a specific marker of medium spiny neurons (data not shown). This suggests that the decreased levels of HSJ1b in postmortem samples are not merely a reflection of cell death.

HSJ1 proteins protect striatal neurons from polyQ-huntingtin–induced cell death. We next investigated whether HSJ1 proteins possess neuroprotective properties by studying a neuronal model of HD that recapitulates the main features of the disease (24). We transfected

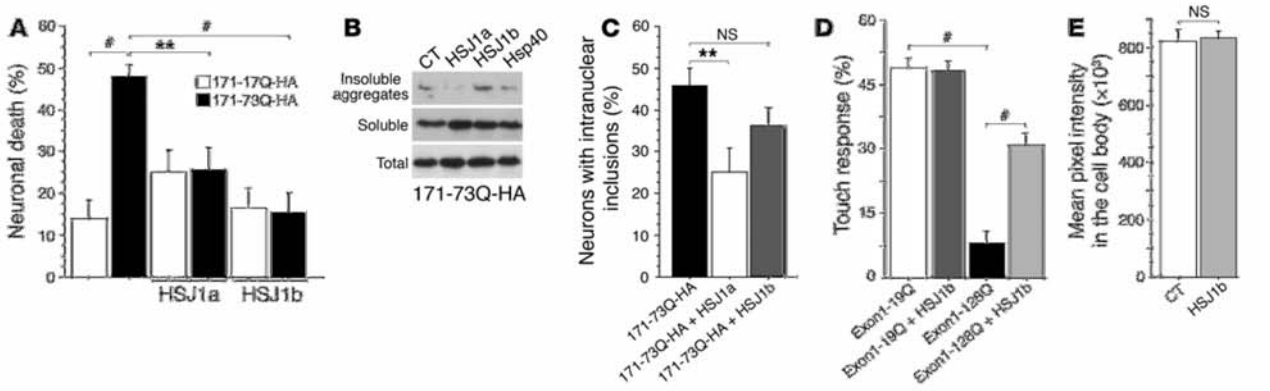

Figure 2

HSJ1 proteins and polyQ-huntingtin–induced toxicity and dysfunction. (**A**) Striatal neurons were transfected with 171-17Q-HA or 171-73Q-HA and HSJ1a, HSJ1b, or the corresponding empty vectors. Data (ANOVA, $F_{5,40} = 6.89$; $P < 0.0001$) demonstrated that cell death was significantly increased by 171-73Q-HA construct (post-hoc Fisher's test, $P < 0.01$) and blocked by cotransfection with HSJ1a (post-hoc Fisher's test, $P = 0.0043$) or HSJ1b (post-hoc Fisher's test, $P < 0.0001$). (**B**) Cell extracts prepared from 171-73Q-HA–transfected HEK 293T cells were analyzed by immunoblotting using an anti-HA antibody. (**C**) Striatal neurons were transfected with 171-17Q-HA or 171-73Q-HA together with HSJ1a, HSJ1b, or the corresponding empty vectors. Data (ANOVA, $F_{2,15} = 4.43$; $P = 0.031$) revealed a statistically significant decrease in the percentage of neurons with intranuclear inclusions in the presence of HSJ1a (post-hoc Fisher's test, $P = 0.0094$) but not of HSJ1b (NS). (**D**) Data (ANOVA, $F_{10,87} = 23.44$; $P < 0.0001$) revealed a statistically significant decrease in mechanosensation of touch receptor neurons in the tail of animals expressing the exon 1–128Q-GFP construct compared with neurons expressing exon 1–19Q-GFP (Student's t test, $t_{[16]} = 16.12$; $P < 0.0001$). Loss of touch response mediated by exon 1–128Q-GFP was inhibited by expression of HSJ1b (Student's t test, $t_{[16]} = 9.01$; $P < 0.0001$). (**E**) Morphometric analysis revealed no change in the aggregation of fusion proteins in the cell bodies of neurons from HSJ1b-expressing animals (Student's t test, $t_{[198]} = 1.22$; NS). $^{**}P < 0.01$, $^{\#}P < 0.001$.

primary cultures of striatal neurons with constructs encoding the first 171 amino acids of huntingtin with 17 (wild-type, 171-17Q-HA) or 73 glutamines (mutant, polyQ, 171-73Q-HA), either alone or in the presence of a construct expressing HSJ1a or HSJ1b, and analyzed neuronal death 24 hours after transfection (Figure 2A). As expected, the 171-73Q-HA construct induced a statistically significant increase in neuronal death compared with the 171-17Q-HA construct. Interestingly, HSJ1a and HSJ1b decreased neuronal death induced by the 171-73Q-HA fragment of huntingtin. These findings show that HSJ1 proteins exert a neuroprotective effect on polyQ-huntingtin–induced neuronal death.

HSJ1a but not HSJ1b reduces intranuclear inclusions. Hsps are known to assist in the refolding of misfolded proteins and/or in the transfer of such proteins to the proteasome for degradation (23, 30). Therefore, most Hsps reduce the aggregates in various HD models (22). Using an aggregation assay (31), we analyzed the effect of HSJ1 proteins on the formation of insoluble aggregates induced by the 171-73Q-HA fragment of huntingtin (Figure 2B). The DnaJ-type Hsp40 (HDJ2/HSDJ) was used as a positive control capable of solubilizing aggregates (20, 22). Surprisingly, HSJ1a and HSJ1b elicited different responses in this assay. Whereas HSJ1a reduced insoluble aggregates in a comparable manner to Hsp40, HSJ1b had no effect on the solubility of polyQ-huntingtin–induced aggregates. To confirm this differential response in a more physiological situation, we transfected primary cultures of striatal neurons with 171-73Q-HA and HSJ1a, HSJ1b, or the corresponding empty vector and scored the transfected neurons for the presence of NIIs (Figure 2C). Again, we found that whereas HSJ1a significantly reduced the formation of NIIs, HSJ1b had only a weak effect.

These findings suggest that HSJ1a acts as a "typical" chaperone that unfolds misfolded proteins, whereas HSJ1b has a beneficial effect on polyQ-huntingtin–induced neuronal death independent of polyQ aggregation. As HSJ1a is almost undetectable in brain (Figure 1), we focused our study on the predominant isoform, HSJ1b.

HSJ1b rescues mutant polyQ dysfunction in Caenorhabditis elegans neurons. To test whether HSJ1b may protect against the early phases of polyQ-huntingtin–induced neuronal dysfunction in vivo, we investigated the effects of HSJ1b in *C. elegans* transgenics that express an exon 1–like N-terminal fragment of huntingtin fused to GFP in their touch receptor neurons. This animal model of neuronal cell response to polyQ-expanded huntingtin shows polyQ-dependent neuronal dysfunction without cell death (32, 33). We generated transgenic strains of nematodes that express human HSJ1b in touch receptor neurons. Four independent stable lines were crossed with lines stably expressing a GFP-fused exon 1–like N-terminal fragment of huntingtin with 19 or 128 glutamines (exon 1–19Q-GFP or exon 1–28Q-GFP). Quantitative RT-PCR and Western blotting revealed no effect of HSJ1b on huntingtin transgene expression and protein levels (Supplemental Figure 1; supplemental material available online with this article; doi:10.1172/JCI27607DS1). We analyzed the touch response of the mutant polyQ and control worms in the absence or presence of HSJ1b. As previously reported (32, 33), animals expressing exon 1–128Q-GFP presented a statistically significant decrease in response to light touch at the tail compared with the exon 1–19Q-GFP–expressing worms (Figure 2D). Importantly, the loss of touch response induced by exon 1–128Q-GFP was inhibited by HSJ1b expression. In contrast, no statistical difference in cell body aggregation, measured as mean pixel intensity, was observed between exon 1–128Q-GFP strains and those with HSJ1b coexpression (Figure 2E). We conclude that HSJ1b has neuroprotective effects in vitro by inhibiting striatal neuronal death and in vivo by reducing neuronal cell dysfunction without any major effects on polyQ-huntingtin aggregation.

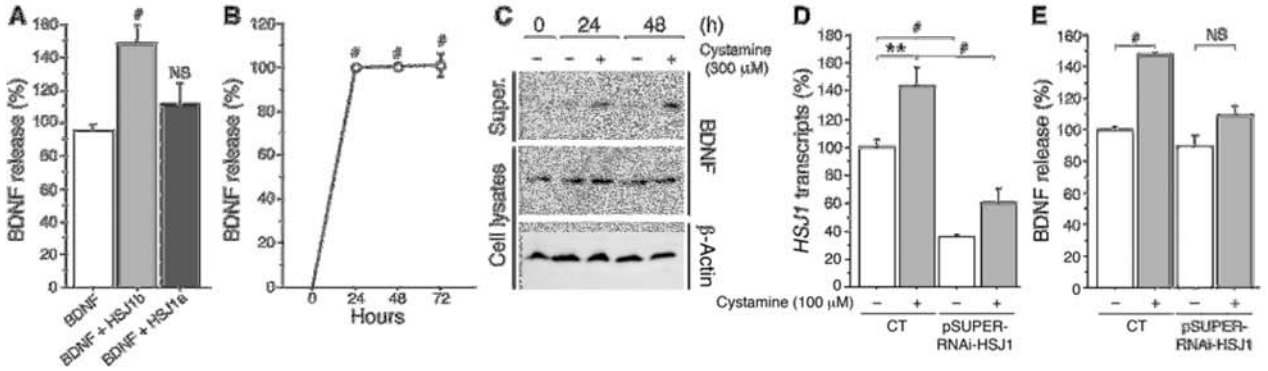

Figure 3

HSJ1b and cystamine increase BDNF release. (**A**) Neuronal cells were transfected with BDNF, HSJ1a, HSJ1b, or the corresponding empty vectors. Forty-eight hours after transfection, cells were washed with PBS and incubated for 30 minutes with DMEM, and supernatants (super.) were collected. Data (ANOVA, $F_{2,31} = 9.17$; $P = 0.0007$) revealed that HSJ1b (post-hoc Fisher's test, $P = 0.0002$), but not HSJ1a (NS), induced a statistically significant increase in BDNF release. (**B**) Data (ANOVA, $F_{3,39} = 323.66$; $P < 0.0001$) revealed a statistically significant increase in BDNF content in the supernatant of 100 μM cystamine-treated cells at 24, 48, and 72 hours (post-hoc Fisher's test, $P < 0.0001$). (**C**) Cells transfected with BDNF and treated with cystamine were analyzed by immunoblotting with anti-BDNF and anti–β-actin antibodies. (**D**) Data (ANOVA, $F_{3,29} = 26.01$; $P < 0.0001$) revealed a statistically significant decrease in *HSJ1* transcripts in cells transfected with siRNA-HSJ1 compared with control cells with or without cystamine treatment (post-hoc Fisher's test, $P < 0.0001$). Cystamine increased *HSJ1* transcripts in control conditions (post-hoc Fisher's test, $P = 0.002$) but not in the presence of siRNA-HSJ1 (NS). (**E**) Cystamine did not increase BDNF release when HSJ1b levels were lowered by RNAi-HSJ1 (ANOVA, $F_{3,19} = 7.59$; $P = 0.0016$). Cells were cotransfected with BDNF and pSUPER-RNAi-HSJ1 and treated with cystamine 48 hours after transfection. There was a significant increase in BDNF release in cystamine-treated cells compared with control cells (post-hoc Fisher's test, $P = 0.0005$). $^{**}P < 0.01$, $^{\#}P < 0.001$.

HSJ1b and cystamine promote BDNF release in neuronal cells. How does HSJ1b promote neuronal survival? Little is known about the function of HSJ1 proteins. We do know, however, that they interact with the Hsp70 family of proteins and stimulate their ATPase activity to regulate their substrate-binding capacities (34). Also, HSJ1 proteins inhibit the heat shock cognate 70 kDa (hsc70) protein. Since hsc70 is a constitutive Hsp70 that removes clathrin from clathrin-coated vesicles (CCVs), we hypothesized that HSJ1 proteins might play a role in regulating intracellular trafficking of CCVs (35). Indeed, huntingtin itself is implicated in clathrin-mediated endocytosis; it interacts with several proteins involved in this process, including HIP1, HIP12, PACSIN1, SH3GL3, and HIP14 (for a review, see ref. 36), and we recently demonstrated that huntingtin acts as a processivity factor to promote microtubule-based intracellular transport of BDNF-containing vesicles (27). In addition, the intracellular trafficking of BDNF-containing vesicles is altered, resulting in a decreased release of BDNF and subsequent neuronal toxicity.

We therefore analyzed whether HSJ1b protein regulates BDNF release in neuronal cells. To make sure that any effect on BDNF release was not due to a defect in BDNF transcription, we ectopically expressed BDNF under the control of the CMV promoter. In addition, the levels of BDNF in the supernatant were normalized to BDNF levels in cell lysates. Mouse neuronal cells were lipofected with vectors expressing BDNF, HSJ1b or HSJ1a, or the corresponding empty vector, and the amount of BDNF in the supernatant was assessed by ELISA (Figure 3A). Strikingly, HSJ1b significantly increased the amount of BDNF released, whereas HSJ1a had no effect. These results suggest that HSJ1b promotes neuronal survival by enhancing BDNF release in neuronal cells.

We next examined whether the effect of HSJ1b could be recapitulated by cystamine. Treating cells with cystamine for varying lengths of time led to increased BDNF release (Figure 3B). We also analyzed the amount of BDNF in cell lysates and supernatants by standard Western blotting (Figure 3C). While the levels of BDNF were similar in cell lysates, 24 and 48 hours of cystamine treatment resulted in increased BDNF release. These findings show that HSJ1b and cystamine increase BDNF release in neuronal cells. This effect was specific to HSJ1b, as HSJ1a did not modify BDNF release under the same conditions.

To determine whether the effect of cystamine on BDNF secretion requires HSJ1b, we used an RNA interference approach. We transfected neuronal cells with pSUPER-RNAi-HSJ1, which targets both HSJ1a and HSJ1b, as we could not identify RNAi discriminating between the 2 isoforms (data not shown). We used RT-PCR to demonstrate that pSUPER-RNAi-HSJ1 reduced *HSJ1* mRNA levels (Figure 3D). Strikingly, the ability of cystamine to increase BDNF release was lost in pSUPER-RNAi-HSJ1–transfected cells (Figure 3E) showing that the effect of cystamine on BDNF release requires HSJ1 proteins. As HSJ1a is almost undetectable in brain and has no effect on BDNF secretion (Figure 3A), the results of this experiment strongly support the notion that at least part of the effect of cystamine on BDNF release involves HSJ1b.

HSJ1b stimulates the secretory pathway. Clathrin is the main component of the protein coats that decorate the cytoplasmic face of vesicles budding from the plasma membrane, the *trans*-Golgi network (TGN), and endosomes (37). The clathrin coat is, therefore, an important target for regulating secretion and endocytosis. To understand how HSJ1b and cystamine might act through clathrin to promote BDNF release, we first analyzed the distribution of HSJ1b, BDNF, and clathrin by performing subcellular fractionation of neuronal cells expressing HSJ1b and BDNF-GFP constructs (Figure 4A). We found that these 3 proteins are enriched in the P3 fraction corresponding to small vesicles, confirming the distribution of BDNF and cofractionating with huntingtin (27). We also purified CCVs and found they were enriched in HSJ1b and

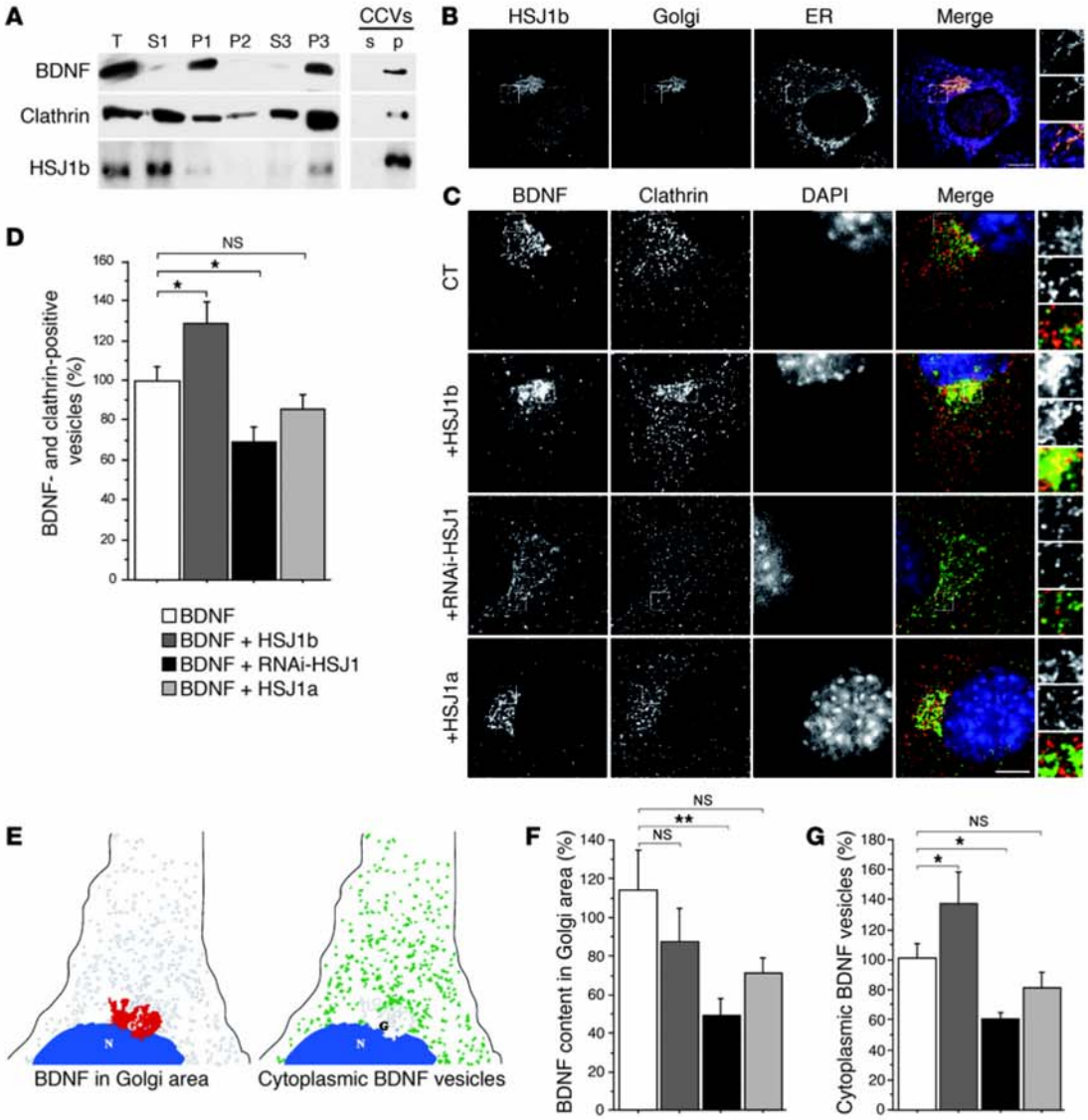

Figure 4

HSJ1b increases BDNF processing from the Golgi to the cytoplasm. (**A**) BDNF, clathrin, and HSJ1b were present in the same cellular compartments: small vesicle fraction (P3) and CCV fraction (p). (**B**) HSJ1b partially colocalized with the Golgi apparatus. (**C**) HSJ1b enhanced colocalization between BDNF and clathrin in the Golgi region, whereas RNAi-HSJ1 disrupted it. Scale bars: 10 μm. (**D**) Quantification (ANOVA, $F_{3,64} = 7.71$; $P = 0.0002$) revealed that expression of HSJ1b significantly increased the amount of BDNF vesicles that were clathrin positive compared with control cells (post-hoc Fisher's test, $P = 0.032$), while pSUPER-RNAi-HSJ1 significantly decreased it (post-hoc Fisher's test, $P = 0.019$). Overexpression of HSJ1a had no effect (NS). (**E**) Scheme showing the measurement of BDNF in the Golgi area (left) and in the cytoplasm (sorted vesicles, right). (**F**) Quantification (ANOVA, $F_{3,67} = 2,92$; $P = 0.04$) revealed that lowering HSJ1b by interference significantly decreased BDNF content in the Golgi area (post-hoc Fisher's test, $P = 0.005$). There was no difference between cells expressing HSJ1b or HSJ1a compared with control conditions (NS). (**G**) Quantification (ANOVA, $F_{3,47} = 5,84$; $P = 0.0018$) revealed that HSJ1b increased the amount of BDNF vesicles in the cytoplasm in comparison to control cells (post-hoc Fisher's test, $P = 0.048$), whereas pSUPER-RNAi-HSJ1 decreased it (post-hoc Fisher's test, $P = 0.038$). The difference was not significant in HSJ1a-overexpressing cells (NS). $^*P < 0.05$, $^{**}P < 0.01$.

BDNF. In addition, we found HSJ1b colocalizing with GMAP-210, a marker of the *cis*-Golgi (Figure 4B) (38) and with BDNF (Figure 5E). These results are consistent with a role for HSJ1b in the regulation of BDNF processing in the secretory pathway.

Since HSJ1b is known to regulate clathrin coating in vitro, we analyzed by immunofluorescence microscopy the subcellular location of BDNF relative to the location of endogenous clathrin (Figure 4C, upper panels). BDNF-containing vesicles and clathrin were both found predominantly in the Golgi region (as identified by immunostaining for GM130, another *cis*-Golgi marker; Figure 4C and data not shown). Increasing the levels of HSJ1b enhanced the colocalization of BDNF and clathrin, whereas reducing HSJ1b pro-

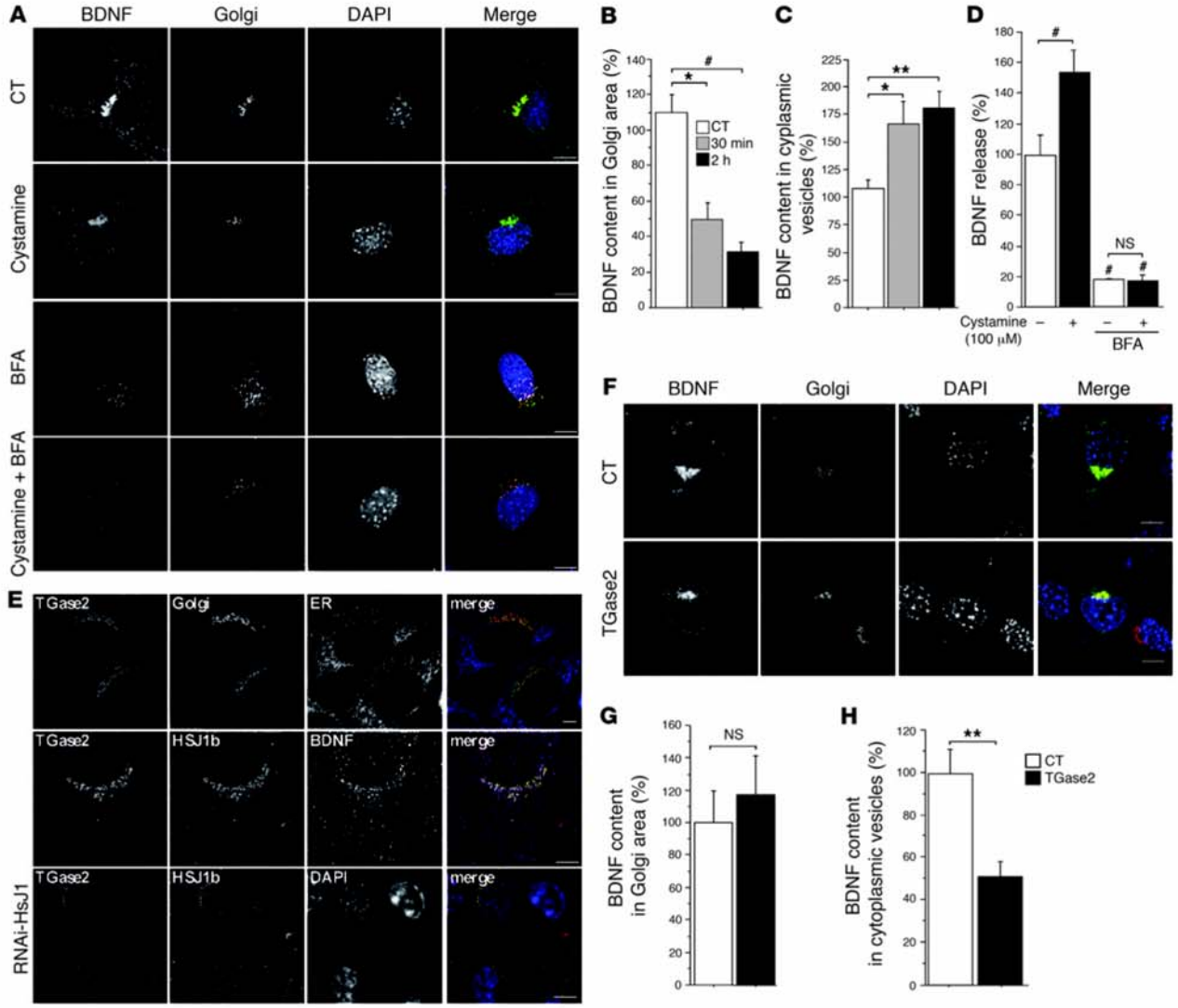

Figure 5

Cystamine and TGase 2 regulate BDNF secretion. (**A**) Cystamine treatment (100 μM, 30 minutes) of BDNF-GFP–transfected cells decreased colocalization between BDNF and GM130. BFA dispersed BDNF vesicles and GM130 with or without cystamine. (**B**) Quantification (ANOVA, $F_{2,46} = 7.10$; $P = 0.0021$) revealed that cystamine significantly decreased BDNF in the Golgi area compared with control cells at 30 minutes (post-hoc Fisher's test, $P = 0.011$) and 2 hours (post-hoc Fisher's test, $P = 0.0007$). (**C**) Data (ANOVA, $F_{2,46} = 4.83$; $P = 0.0125$) revealed that cystamine treatment significantly increased BDNF content in cytoplasmic vesicles compared with control cells at 30 minutes (post-hoc Fisher's test, $P = 0.021$) and 2 hours (post-hoc Fisher's test; $P = 0.0049$). (**D**) Data (ANOVA, $F_{3,32} = 45.6$; $P < 0.0001$) revealed that BFA significantly reduced BDNF release in control and cystamine-treated cells (post-hoc Fisher's test, $P < 0.0001$). Cystamine had an effect on control (post-hoc Fisher's test, $P < 0.006$) but not on BFA-treated cells (NS). (**E**) TGase 2 colocalization with HSJ1b at the Golgi (GMAP-210) was disrupted in pSUPER-RNAi-HSJ1–transfected cells. (**F**) TGase overexpression induced a decrease in cytoplasmic BDNF-containing vesicles. Scale bars: 10 μm. (**G**) TGase 2 did not modify BDNF content in the Golgi area compared with control cells (Student's t test, $t_{[13]} = 0.4$; NS). (**H**) TGase 2 induced a statistically significant decrease in cytoplasmic BDNF vesicles compared with control cells (Student's t test, $t_{[13]} = 3.4$; $P = 0.0051$). $^{*}P < 0.05$, $^{**}P < 0.01$, and $^{\#}P < 0.001$.

tein levels by RNA interference dramatically decreased it (Figure 4C, middle panels). Interestingly, decreasing HSJ1b protein levels also had an important impact on the intracellular distribution of clathrin, which appeared randomly distributed in the cytoplasm. HSJ1a had little or no effect on the colocalization of BDNF and clathrin. By quantifying the overlap between BDNF and clathrin, we found these effects to be statistically significant (Figure 4D). This increase in the clathrin coating of BDNF-containing vesicles in response to overexpression of HSJ1b is consistent with the fact that HSJ1b inhibits hsc70-catalyzed clathrin uncoating (35).

To understand how an increase in the clathrin coating of BDNF vesicles leads to an increase in the release of BDNF from neuronal cells, we measured the sorting of BDNF from the Golgi/TGN region into the cytoplasm by image analysis. We quantified the

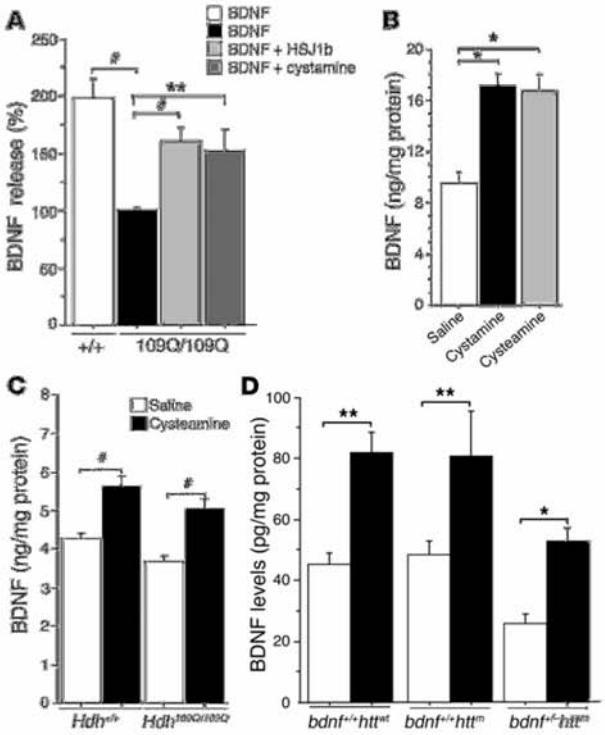

Figure 6
HSJ1b, cystamine, and cysteamine regulate BDNF levels in HD. (**A**) BDNF release was decreased (ANOVA, $F_{3,33} = 17.45$; $P < 0.0001$) in 109Q/109Q cells compared with control cells (post-hoc Fisher's test, $P < 0.0001$). This decrease was rescued when cells were transfected with HSJ1b (post-hoc Fisher's test, $P < 0.0001$) or treated with 100 μM cystamine for 30 minutes (post-hoc Fisher's test, $P = 0.001$). (**B**) Data (ANOVA, $F_{2,29} = 3.63$; $P = 0.0392$) revealed a statistically significant increase in the amount of BDNF in the brains of mice treated with cystamine (post-hoc Fisher's test, $P = 0.015$) or with cysteamine (post-hoc Fisher's test, $P = 0.04$) compared with controls. (**C**) Data (ANOVA, $F_{3,49} = 11.66$; $P < 0.0001$) revealed a statistically significant increase in the amount of BDNF in the brains of mice treated with cysteamine (post-hoc Fisher's test, $P < 0.001$). (**D**) Cysteamine increased BDNF levels in the striatum of the different genotypes (ANOVA, $F_{5,14} = 9.20$; $P < 0.0004$): wild-type animals (post-hoc Fisher's test, $P = 0.002$); *bdnf*$^{+/+}$*htt*^{m} mice (R6/1mice; post-hoc Fisher's test, $P = 0.009$); and *bdnf*$^{+/-}$*htt*^{m} mice (post-hoc Fisher's test, $P = 0.024$). $^{*}P < 0.05$, $^{**}P < 0.01$, and $^{\#}P < 0.001$.

intensity of the BDNF signal in the Golgi region (Figure 4E, left) and the number of cytoplasmic BDNF-containing vesicles of 67 nm–3.35 μm diameter (1–50 pixels) that correspond to vesicles budding from the Golgi/TGN region (Figure 4E, right). Reducing HSJ1 by RNA interference induced a statistically significant decrease in the BDNF content in the Golgi region (Figure 4F) and in the number of budding vesicles (Figure 4G). By contrast, HSJ1b overexpression increased the number of BDNF-containing vesicles in the cytoplasm. These findings indicate that HSJ1b is required for the formation of BDNF-containing vesicles.

Cystamine promotes BDNF secretion by an HSJ1b-dependent mechanism involving TGase inhibition. We have demonstrated that cystamine and HSJ1b increase BDNF release from neuronal cells and that the cystamine-induced BDNF release requires HSJ1b. We next treated neuronal cells with cystamine and analyzed the sorting of BDNF vesicles from the Golgi (Figure 5A). Analysis of 15–20 cells revealed that cystamine induced an extensive depletion of BDNF from the Golgi apparatus (Figure 5B) and increased the BDNF content of the vesicles (Figure 5C). These results indicate that cystamine promotes BDNF secretion by increasing the load of the neurotrophic factor in vesicles.

To verify that cystamine affects the secretion from the Golgi, we used brefeldin A (BFA), a fungal metabolite that is a potent inhibitor of Golgi vesicle fusion (39). BFA treatment led to dispersion of BDNF vesicles and, as expected, of the Golgi marker GM130 and was unaffected by cystamine treatment (Figure 5A, lower panels). We next analyzed BDNF release by ELISA in these conditions (Figure 5D). Strikingly, the ability of cystamine to increase BDNF release was lost in BFA-treated cells, demonstrating that the effect of cystamine on BDNF release requires secretion from the Golgi.

Because cystamine is well known to inhibit TGase in vitro, we tested the possibility that TGase might play a role in BDNF secretion. Several isoenzymes of TGase are found in the brain, of which TGase 2 is the most abundant. We found that TGase 2 partially colocalized with GMAP-210, with HSJ1b, and with BDNF (Figure 5E, upper and middle panels). We next analyzed whether TGase 2 localization depends on HSJ1b. Interestingly, reducing HSJ1b levels by RNA interference modified TGase 2 localization at the Golgi (Figure 5E, lower panels) and disrupted the Golgi (data not shown). We also assessed the consequences of increased TGase 2 activity on BDNF secretion. Cells were transfected with TGase 2 and treated with glutamate (5 μM, 30 minutes) to increase intracellular calcium concentration and subsequently activate the enzyme (40). In these conditions, BDNF remained in the Golgi area, whereas the number of BDNF-containing vesicles in the cytoplasm was reduced (Figure 5, F–H). These results demonstrate that TGase 2 inhibits BDNF processing. This observation is consistent with a report showing that TGase inhibitors stimulate catecholamine release from rat brain synaptosomes (41).

We have shown that cystamine induces BDNF release by increasing its processing from the Golgi/TGN region. We propose that cystamine acts at 2 levels: first, it stimulates the transcription of HSJ1b that is required for the sorting of BDNF-containing vesicles and second, it also increases BDNF processing by inhibiting TGase activity.

HSJ1b and cystamine rescue BDNF release defects induced by polyQ-huntingtin in cells and in HD mice. We determined the effect of HSJ1b and cystamine on BDNF release in the pathological situation. We used mouse neuronal cells derived from knock-in mice in which a 109-CAG expansion, encoding 109 glutamine residues, was inserted into the endogenous mouse huntingtin gene (109Q/109Q) (28). This cell line closely resembles the situation in HD patients as, in these cells, polyQ-huntingtin is expressed at endogenous levels. The level of BDNF released from these cells into the supernatant was significantly lower in 109Q/109Q cells compared with wild-

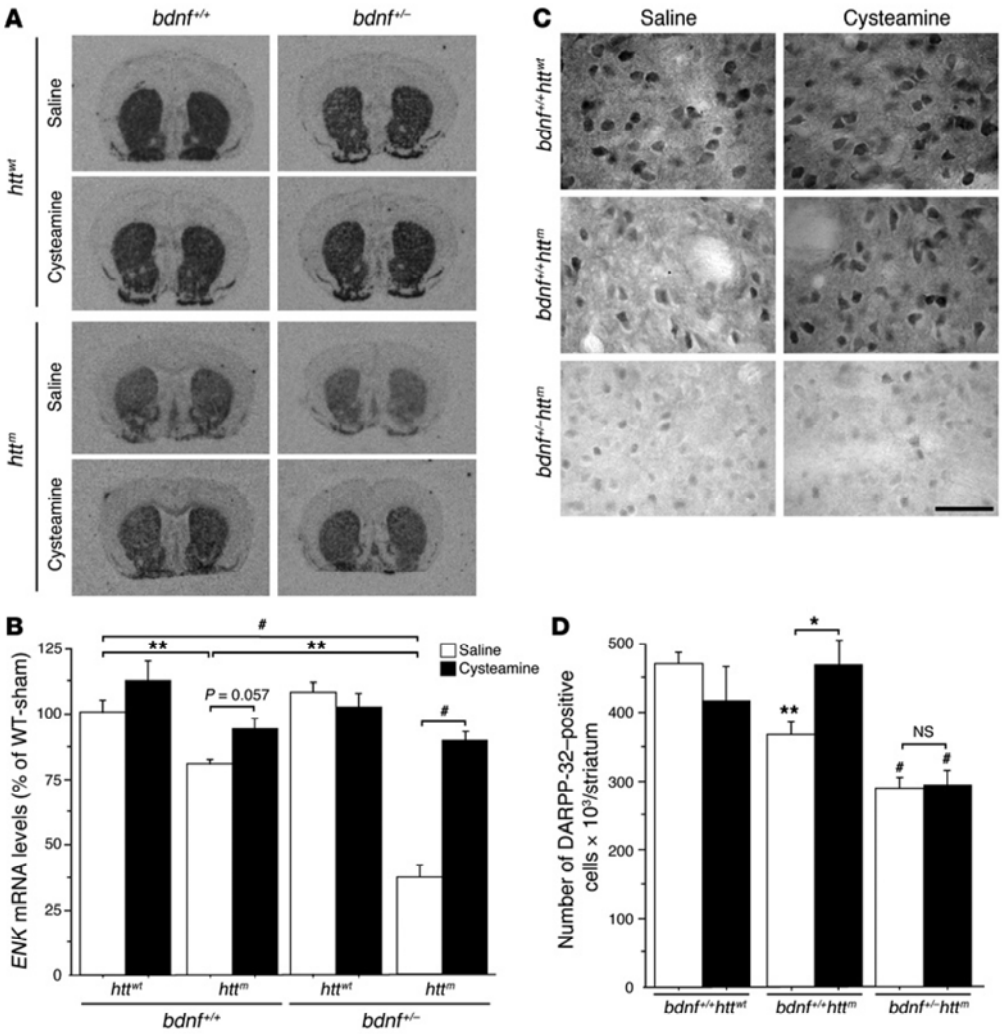

Figure 7

Cysteamine is neuroprotective in HD mice through a BDNF-dependent mechanism. (**A**) In situ hybridization revealed that *ENK* mRNA were reduced in R6/1 ($bdnf^{+/+}htt^{m}$) and dramatically reduced in $bdnf^{+/-}htt^{m}$ mice. At early stages, cysteamine treatment increased the levels of *ENK* mRNA in $bdnf^{+/+}htt^{m}$ and in $bdnf^{+/-}htt^{m}$ mice. (**B**) Quantification of *ENK* mRNA levels. WT-sham, wild-type saline-treated mice. (**C**) Cysteamine treatment of wild-type animals did not modify DARPP-32 immunostaining. In R6/1 animals, there was a decrease in the number of DARPP-32–positive cells that was recovered by cysteamine treatment. The loss of DARPP-32–positive neurons could not be prevented by cysteamine treatment in $bdnf^{+/-}htt^{m}$ mice. Scale bar: 50 μm. (**D**) Quantitative analysis of the changes in DARPP-32 immunostaining. $^{*}P < 0.05$, $^{**}P < 0.01$, and $^{\#}P < 0.001$; see statistical analysis in Methods.

type neuronal cells (Figure 6A). Interestingly, ectopic expression of HSJ1b or treatment with cystamine increased BDNF release from 109Q/109Q cells. Thus, the defect in BDNF release in a cellular model of HD can be rescued by HSJ1b or cystamine.

We next investigated whether cystamine regulates BDNF levels in the brain by injecting mice daily with cystamine. Mice were sacrificed after 7 days of treatment (30 minutes after the last injection), and the BDNF levels in brain extracts were measured. Treatment with cystamine resulted in an increase in brain BDNF level (Figure 6B). We also assessed in vivo the effect of the reduced form of cystamine, cysteamine. Unlike cystamine, cysteamine is an FDA-approved drug that is used to treat a rare childhood disorder called cystinosis (42), and tolerability of cysteamine was determined in HD patients (43, 44). Therefore, cysteamine might be used immediately after appropriate phase II clinical studies for use in HD patients. We analyzed the ability of cysteamine in comparison to cystamine to increase BDNF levels in the brain of treated mice and observed that cysteamine recapitulated the positive effect of cystamine on BDNF secretion in animals (Figure 6B). Having shown that cystamine and cysteamine are effective in wild-type mice, we tested the ability of cysteamine to regulate BDNF release in knock-in mice carrying a 109Q repeat in the *Hdh* locus that are homozygous for the mutation (45). We observed a small but not significant reduction ($P = 0.096$) in the brain levels of BDNF in $Hdh^{109Q/109Q}$ mice compared with their wild-type littermates (Figure 6C). Interestingly, cysteamine induced a significant increase in BDNF levels in HD knock-in mice.

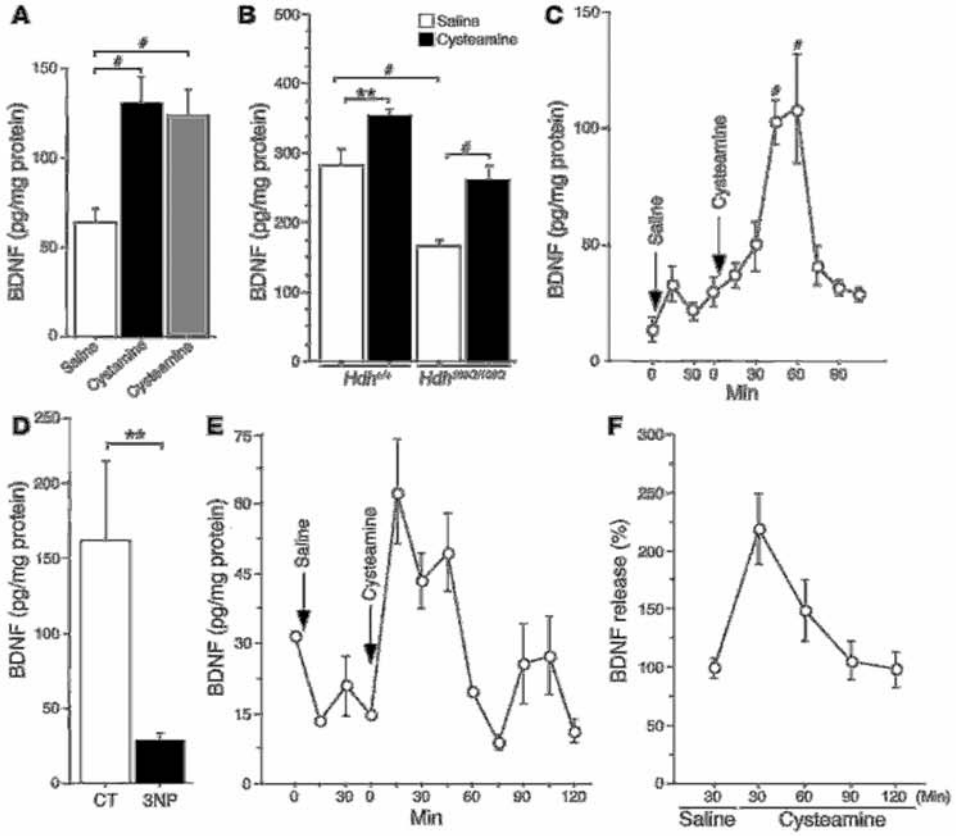

Figure 8

Cysteamine increases blood levels of BDNF in rodents and in a primate HD model. (**A**) Data (ANOVA, $F_{2,27}$ =17.13; $P < 0.0001$) revealed that the amount of BDNF in serum of mice treated with cystamine (post-hoc Fisher's test, $P < 0.0001$) or with cysteamine (post-hoc Fisher's test, $P < 0.0001$) was significantly increased. (**B**) The blood level of BDNF (ANOVA, $F_{3,50}$ =17.22; $P < 0.0001$) was reduced in *Hdh*$^{109Q/109Q}$ mice compared with wild-type littermates (post-hoc Fisher's test, $P = 0.0001$) and rescued by cysteamine. The amount of BDNF in the serum of wild-type mice (post-hoc Fisher's test, $P = 0.0099$) and *Hdh*$^{109Q/109Q}$ mice (post-hoc Fisher's test, $P = 0.0010$) was increased upon cysteamine treatment. (**C**) There was an increase of BDNF in serum of 4 cysteamine-treated rats (ANOVA, $F_{10,64} = 9.29$; $P < 0.0001$) after 45 minutes (post-hoc Fisher's test, $P < 0.0001$) and 60 minutes (post-hoc Fisher's test, $P < 0.0001$). (**D**) BDNF levels were reduced in the blood of 3NP-treated monkeys (Student's t test, $t_{[27]} = 3.05$; $P = 0.005$). $^{**}P < 0.01$ and $^{\#}P < 0.001$. Data are from 4 controls and three 3NP-treated monkeys. (**E** and **F**) Blood BDNF levels were increased in HD monkeys injected with cysteamine. (**E**) Representative results for 1 monkey are shown. (**F**) Graph represents the results for the 2 injected monkeys. Error bars represent SEM.

Cysteamine is neuroprotective in R6/1 mice by increasing BDNF levels. Strong evidence indicates that cystamine is neuroprotective in HD mouse models (10, 11, 14, 15). We aimed to assess whether cysteamine is neuroprotective in vivo and whether this depends on BDNF. For this purpose, we used a mouse model of HD, R6/1 mice, which show a much faster progression of disease phenotype compared with *Hdh*$^{109Q/109Q}$ mice (46, 47) and a double mutant line previously generated by crossing R6/1 mice with *bdnf* heterozygous mice (26). We first investigated whether cysteamine regulates BDNF levels in the striatum by injecting wild-type, R6/1 (*bdnf*$^{+/+}$*htt*^{m}), and double mutant mice (*bdnf*$^{+/-}$*htt*^{m}) daily for 7 days (Figure 6D). Although less efficiently in *bdnf*$^{+/-}$*htt*^{m} mice, this treatment induced an increase in striatal BDNF levels in the 3 mouse genotypes.

We next analyzed the effect of cysteamine treatment in different neuronal populations in these HD models at early (16 weeks) and late (26 weeks) stages of the disease. At 16 weeks, R6/1 mice are still presymptomatic, while double mutant (*bdnf*$^{+/-}$*htt*^{m}) mice already have a motor behavioral impairment. We analyzed the mice for enkephalin, a specific marker for striatopallidal neurons that are affected early in HD, and substance P, a marker for striatonigral neurons. At this early stage, enkephalin mRNA levels were not highly affected in R6/1 mice, whereas a much greater reduction was observed in *bdnf*$^{+/-}$*htt*^{m} mice (Figure 7, A and B) (26). Administration of cysteamine in double mutant mice increased the expression of enkephalin above the levels in sham-R6/1 and sham-*bdnf*$^{+/-}$*htt*^{m} mice. Cysteamine treatment did not modify the number of substance P–positive neurons in R6/1 mice or in double mutant mice above that in control mice (Supplemental Figure 2). These data show that cysteamine is neuroprotective in R6/1 mice at early stages.

We next determined changes in dopamine and cAMP-regulated phosphoprotein of a molecular mass of 32 kDa (DARPP-32), a specific marker for striatal projection neurons that is affected at the age of 26 weeks, but not at 16 weeks, in R6/1 mice. As expected, at 26 weeks, a decrease in DARPP-32–positive cells was observed in R6/1 compared with wild-type mice (Figure 7C). Interestingly, whereas cysteamine treatment prevented the reduction in the number of DARPP-32–positive cells in R6/1 mice, this treatment had no effect in R6/1 mice with disruption of *bdnf* (*bdnf*$^{+/-}$*htt*^{m} mice). We quantified these changes and found them to be statistically significant (Figure 7D).

Taken together, the results of experiments using enkephalin and DARPP-32 markers indicate that cysteamine is also neuroprotective in HD mice. This effect is similar to that of exogenous BDNF administration (26). Furthermore, these data demonstrate that this neuroprotective effect is dependent on the levels of endogenous BDNF.

Cystamine and cysteamine increase blood levels of BDNF in rodent and primate models of HD. We explored whether the positive effect of cystamine and cysteamine on BDNF secretion can also be seen in peripheral tissues. As with brain extracts, we observed a similar increase in BDNF levels in the blood of mice treated with cystamine or with cysteamine (Figure 8A). We next asked whether such chang-

es can be seen in *Hdh*$^{109Q/109Q}$ mice (Figure 8B). The blood of mice for which brain BDNF levels were measured (Figure 6C) was analyzed. Interestingly, a much greater reduction in the level of BDNF was detected in the serum of *Hdh*$^{109Q/109Q}$ mice compared with wild-type mice. As for brain levels, cysteamine also increased BDNF levels in *Hdh*$^{109Q/109Q}$ mice. We next characterized the pharmacokinetics of cysteamine's effect on BDNF levels in the blood of rats injected with cysteamine (Figure 8C). As in mice, blood BDNF levels also increased in response to cysteamine in rats. The maximum increase was reached 45–60 minutes after cysteamine administration, and BDNF levels returned to basal level after 90 minutes.

To further explore the effect of cysteamine in a situation that is close to human pathology, we chose a nonhuman primate model of HD produced by chronic systemic administration of the mitochondrial complex II inhibitor 3-nitropropionic acid (3NP). Chronic 3NP treatment produces striatal dysfunction and neurodegeneration in primates, leading to abnormal movements (including choreiform movements and dystonia) and frontal-type cognitive deficits that are highly reminiscent of HD (48, 49). We first asked whether BDNF levels were altered in the blood of 3NP-treated primates. We analyzed blood samples from 3NP-treated long-tailed macaques and observed a statistically significant decrease in peripheral BDNF when compared to control animals (Figure 8D).

Having shown that peripheral BDNF is decreased, we tested whether systemic injection of cysteamine would enhance BDNF levels in the primate model of HD. In two 3NP-treated macaques, we found that acute injection of cysteamine (100 mg/kg) rapidly induced an increase in BDNF blood levels (Figure 8, E and F). As in rats, the blood levels of BDNF peaked around 30 minutes after cysteamine injection and progressively returned to normal within 60 minutes, consistent with a transient but massive increase in BDNF release into the plasma compartment. This demonstrates that in a primate model of HD, BDNF peripheral levels are decreased and can be increased by administration of cysteamine.

Discussion

Cystamine is one of the very few candidate drugs being considered for the treatment of HD. Here we have investigated the molecular mechanisms of action of cystamine, and our study has revealed that an FDA-approved reduced form of cystamine produces very similar biological effects in vitro and in vivo. We demonstrate that part of the neuroprotective effect of cystamine is due to its promotion of secretion of the neuronal survival factor BDNF. Cystamine has 2 quite distinct actions in this regard. First, it increases the steady-state levels of the Hsp *HSJ1b* mRNA, which stimulates the secretory pathway through its action on CCV formation, and, second, it inhibits TGase, which has a negative effect on BDNF sorting.

HSJ1b belongs to the large family of DnaJ-like proteins that contain the typical Hsp40 chaperones HDJ1/Hsp40 and HDJ2/HSDJ. In most cases, these chaperones have been reported to reduce polyQ-induced aggregation and toxicity in various models (for reviews, see refs. 20–22). We found that HSJ1b functions in a qualitatively different way inasmuch as it appears not to prevent aggregation or the formation of NIIs. However, we found that HSJ1b is relevant to HD, as it strongly inhibits polyQ-huntingtin–induced neuronal death in vitro and rescues neuronal dysfunction in a nematode model of HD. Although we found that in mammalian cells, HSJ1b stimulates BDNF secretion, the exact mechanism by which HSJ1b operates in nematodes remains to be established. Indeed, BDNF is absent in nematodes. HSJ1b could, however, enhance the secretion of other specific *C. elegans* factors. In *C. elegans*, trophic factors other than BDNF exist. In particular, the mesencephalic, astrocyte-derived neurotrophic factor, MANF, is well conserved from *C. elegans* to humans and could be the target of HSJ1b (50). Furthermore, BDNF second messengers are conserved. Therefore, it is possible that HSJ1b acts through a pathway involving these molecules.

In mammalian cells the neuroprotective properties of HSJ1b are linked to its ability to enhance neurotrophic support. HSJ1b positively regulates the sorting of BDNF-containing vesicles from the Golgi/TGN, leading to an increase in BDNF release. These findings are in agreement with the function of HSJ1b in the inhibition of the uncoating of CCVs (35). Most of the vesicles budding from the Golgi/TGN region are CCVs, and assembly of the clathrin coat on the forming bud is an important step (37). HSJ1b could therefore promote the budding of BDNF-containing vesicles by stabilizing this assembly step. Consistent with this idea, we observed an increased percentage of BDNF-containing vesicles that were clathrin positive when HSJ1b expression was increased, whereas reducing HSJ1b levels decreased it. Interestingly, we found significantly less HSJ1b in postmortem brain extracts from HD patients than from control brains, suggesting a potential alteration in the processing of BDNF at the Golgi/TGN during HD pathogenesis. A defect in clathrin coating processes in HD is supported by the fact that huntingtin interacts with HIP1 and HIP12/HIP1R, 2 proteins that are components of clathrin coats and that regulate clathrin assembly by directly interacting with clathrin (51, 52). HSJ1b is thought to inhibit uncoating by interfering with the interactions of Hsc70 with specialized uncoating DnaJ-like proteins such as auxilin (35). Whether it also regulates the activity of huntingtin interactors such HIP1 remains to be determined.

The second consequence of cystamine treatment is promotion of the secretion of BDNF vesicles through a mechanism involving TGase. Our findings that TGase 2 colocalizes with BDNF at the Golgi and the observation that TGases regulate the secretion of BDNF is consistent with previous observations from the 1980s indicating a role of TGases in inhibiting secretion and/or release of various hormones and neurotransmitters such as insulin, serotonin, and dopamine (41, 53, 54). For instance, monodansylcadaverine (MDC), a potent TGase inhibitor, enhances dopamine release from rat brain synaptosomes in basal and in potassium-stimulated conditions (41). Moreover, reports that MDC blocks clathrin-mediated endocytosis (55, 56) accord with our finding that cystamine and TGases regulate the clathrin pathway.

We and others have reported a lack of BDNF support in HD that involves defects in BDNF synthesis (25) and transport (27). Our findings suggest that, in addition, a defect in BDNF sorting from the Golgi/TGN occurs in HD and that such BDNF processing is regulated by HSJ1b and TGases.

Cystamine was first described as a TGase inhibitor in vitro, and several studies are consistent with the possibility that cystamine is beneficial in HD by this mechanism (10, 11, 14, 15). However, whether cystamine is directly inhibiting TGase 2 in vivo remains to be clearly established. First, the reduced form of cystamine, cysteamine, could act as a competitive inhibitor of TGase 2 in vivo (57). Second, other metabolites of cystamine and cysteamine could mediate the neuroprotective effect, as they are rapidly metabolized and low to undetectable levels of cystamine and cysteamine are found in the brain of cystamine-treated mice (17). In addition, cystamine or its metabolites could act through a TGase-independent mechanism (16). Cystamine inhibits caspase 3 activity and

increases glutathione levels in cells (18). In vivo, the beneficial effect of cystamine could involve the increase in L-cysteine, which has antioxidant properties (17, 19).

We now show that cystamine and cysteamine target HSJ1b and TGase to increase the release of BDNF, a trophic factor that is depleted in HD and that is crucial for the survival of striatal neurons in HD. Our data further emphasize that cystamine or its metabolites acts at multiple levels to protect against polyQ-huntingtin–induced toxicity and therefore add to the motivation for optimizing a therapy with cystamine or related compounds.

We demonstrate that cysteamine is as efficient as cystamine in increasing levels of BDNF in the brain. We also report that cysteamine is neuroprotective in HD mice by increasing levels of BDNF in brain. BDNF levels can also be measured in blood as a biomarker for pathological stages. We found that in HD knock-in mice and in a primate model of HD, the levels of BDNF in serum were reduced compared with those in controls, whereas such decreases in brain BDNF could not be detected in HD knock-in mice and in R6/1 mice at 15 and 16 weeks of age. Interestingly, at these early stages, these mice do not show overt phenotypes (45, 46). This suggests that blood BDNF could be used to follow disease progression and validate the neuroprotective effects of drugs acting on BDNF levels.

We found cysteamine-induced release of BDNF in brain to be transient. This is consistent with the rapid clearance of cysteamine from the plasma of healthy individuals (58) and patients with nephropathic cystinosis (59) and suggests that, as for the treatment of nephropathic cystinosis, repeated doses of cysteamine at short intervals would be appropriate for the treatment of HD. Such limited and controlled release of BDNF is of particular interest for therapy, as an excessive stimulation of the BDNF/TrkB pathway leads to tumorigenesis in mice (60). Moreover, the efficacy of a repeated treatment is unlikely to diminish with time, as we found that the cysteamine-induced increase in brain and serum BDNF levels was still detected after 12 weeks continuous treatment (Supplemental Figure 3).

We propose the use of cysteamine as a therapeutic approach to treat HD. Indeed, the safety of cysteamine in humans is well documented, as cysteamine is used to treat cystinosis (42, 61). Moreover, the tolerated cysteamine dose has been evaluated in HD patients (43, 44). Finally, our findings indicate that the efficacy of cysteamine treatment in HD patients could be monitored by measuring serum levels of BDNF as a convenient biomarker.

Methods

Constructs. The vectors encoding BDNF, BDNF-GFP, Hsp40, and TGase 2 |have been described previously (62–64). The 171-17Q-HA and the 171-73Q-HA were obtained by inserting an HA tag into the XhoI-XbaI sites of the pcDNA-171-17Q and pcDNA-171-73Q, respectively (24). The oligonucleotides used were: 5′-TCGAGTACCCATACGATGTTCCAGATTACGCTTAAT-3′ and 5′-CTAGATTAAGCGTAATCTGGAACATCGTATGGGTAC-3′. The BamHI inserts of pBPSTR-1-HSJ1a and of pBPSTR-1-HSJ1b contained the sequences encoding human HSJ1a and HSJ1b, respectively (29), and were subcloned into the pcDNA3 vector (Invitrogen Corp.).

The RNA sequence targeting mouse *HSJ1* corresponds to the coding region 97–116 (GenBank accession number NM178055). The pSUPER-RNAi-HSJ1 construct was generated by inserting in the BbsI cloning site of pSuperhH1Neo (InvivoGen) the following annealed oligonucleotides: 5′-CAAAAAGACAAGAACCCGGATAATAGGTGGTATTATCCGGGTTCTTGT-3′ and 5′-TCCCGACAAGAACCCGGATAATACCACCTATTATCCGGGTTCTTGTCTT-3′.

Real-time RT-PCR. Forty-eight hours after transfection, neuronal cells (wild-type; ref. 28) were treated with 100 μM cystamine (Sigma-Aldrich) for 24 or 48 hours and lysed in TRIzol (Invitrogen Corp.). Total RNA was extracted, and samples were retrotranscribed using the First-Strand cDNA Synthesis Kit (Amersham Biosciences). cDNAs were then diluted 1:400 and submitted to RT-PCR (iQ SYBR Green Supermix; Bio-Rad) with the following HSJ1 oligonucleotides corresponding to the mouse coding region 1272–1387 (GenBank accession number NM178055): 5′-TCAGGCCCCTTCTTTACCTT-3′ and 5′-AAGGGTCTCCACTCCCAAAAG-3′. HPRT gene was used as an internal control and quantified with the following oligonucleotides: 5′-CACAGGACTAGAACACCTGC-3′ and 5′-GCTGGTGAAAAGGACCTCT-3′.

Results were analyzed using the ICycler apparatus (Bio-Rad). Data are from 4 separate quantitative RT-PCR experiments performed in triplicate from 2 independent mRNA preparations.

Human tissues. Human tissue samples 1–5 were from the Harvard Brain Tissue Resource Center (HBTRC) and correspond to brain numbers 4741, 4744, 4751, 4797, and 4740 as numbered by the HBTRC. Samples 1–3 were controls (age: 55.3 ± 1.9 years; postmortem delay: 23.8 ± 1.9 hours [mean ± SEM]). Samples 4 and 5 were from grade 3 and 4 HD brains, respectively (age: 63.5 ± 18.5 years; postmortem delay: 24.0 ± 2.0 hours). Human brain samples 6–27 were collected at the Salpêtrière. Samples 6–10 were putamen from controls (age: 72.6 ± 8.9 years; postmortem delay: 9.4 ± 2.1 hours). Samples 11–15 were putamen from symptomatic HD patients with family history (age: 65.6 ± 3.7 years; postmortem delay: 26.5 ± 7.4 hours). Samples 16–22 were caudate samples from controls (age: 79.4 ± 1.7 years; postmortem delay: 13.8 ± 3.0 hours). Samples 23–27 were caudate samples obtained from symptomatic HD patients with family history (age: 65.0 ± 4.0 years; postmortem delay: 25.2 ± 7.4 hours).

Brain samples were homogenized in NP40 lysis buffer (20 mM Tris-HCl pH 7.5, 150 mM NaCl, 2 mM EGTA, 1% Nonidet P-40, 10 mM β-glycerophosphate, 5 mM NaF, 1 mM NaPPi, 2 mM DTT, 1 mM sodium vanadate, 100 μM PMSF) and cleared by centrifugation at 6,000 *g* (15 minutes; 4°C). Fifty micrograms of homogenates were subjected to Western blot analysis. Quantifications of Western blots were performed and expressed relative to actin levels. Human biopsy samples were procured in accordance with the guidelines as adopted and promulgated by the NIH. Permission to perform the experiments with the samples was granted by the Scientific Advisory Board of the Harvard Brain Tissue Resource Center at McLean Hospital (Belmont, Massachusetts, USA).

Cell culture, transfection, and immunofluorescence. Primary cultures of striatal neurons were prepared from E17 Sprague-Dawley rats and transfected at 4 days in vitro by a modified calcium phosphate technique (24). Mouse neuronal cells derived from wild-type huntingtin mouse (neuronal cells, +/+) and from $Hdh^{109Q/109Q}$ knock-in mouse (109Q/109Q) were cultured as previously described (28) and transfected with Lipofectamine 2000 (Invitrogen Corp.). Human 293T cells were cultured in DMEM supplemented with 10% bovine calf serum. Transfected neuronal cells were grown on glass coverslips, fixed with 4% paraformaldehyde for 20 minutes, and immunostained as previously described (27). For experiments represented in Figures 4B and 5E, cells were fixed with methanol/acetone (vol/vol) at –20°C for 10 minutes.

Measurement of neuronal survival and intranuclear inclusions. Four days after plating, primary cultures of striatal neurons were transfected with wild-type or polyQ-huntingtin and GFP to identify the transfected cells. To be certain that each neuron synthesizing GFP also expressed the huntingtin construct, transfections were performed using a derived phosphate calcium method with a high ratio of huntingtin DNA to GFP DNA (10:1) (65). Under these conditions more than 95% of the GFP-positive neurons also expressed the huntingtin construct (data not shown). GFP-positive neurons were scored using fluorescence microscopy in a blinded manner 16 hours and 36 hours

after transfection. Cell death occurring within the GFP-positive cells was determined as the difference in the number of surviving neurons between the 2 time points and expressed as percentage of cell death. For intranuclear inclusions scoring, striatal neurons were transfected with vectors of interest and a plasmid encoding β-galactosidase (10:1). Neurons were fixed 5 days after transfection, immunostained, and analyzed for the presence of ubiquitin-positive intranuclear inclusions (anti–β-galactosidase, 1:300; 5 Prime–3 Prime Inc.; anti-ubiquitin, 1:100; Dako). Each graph represents 2–3 independent experiments performed in triplicate. Each bar in a given graph corresponds to the scoring of about 2,000 neurons in neuronal survival experiments and 500 neurons for inclusions scoring.

C. elegans assays. Nematode strains were handled following traditional methods (66). All strains were received from the Caenorhabditis Genetics Center, University of Minnesota. Construction of huntingtin transgenics, touch response assays, and visualization of neurons were carried out as described previously (32, 33). Transgenic strains expressing human HSJ1b were constructed by microinjection of *lin-15(n765ts)* animals with a mix of wild-type *lin-15* (50 ng/μl), *Pstr-1:GFP* (15 ng/μl), and *Pmec-7:HSJ1b* (15 ng/μl). Independent stable lines were established, and 4 lines with similar HSJ1b expression levels were chosen for further study. The 19Q-HSJ1b (n = 444) and 128Q-HSJ1b (n = 388) transgenics were obtained by crossing HSJ1b transgenics with lines expressing stably integrated *Pmec-3:htt57Q19:GFP* or *Pmec-3:htt57Q128:GFP*. Animals expressing control (exon 1–19Q-GFP) were 50.1% ± 2.4% touch sensitive at the tail, and animals expressing mutant transgene (exon 1–128Q-GFP) were 7% ± 1.1% touch sensitive. Data are from at least 3 independent experiments performed in triplicate.

Aggregation was observed in all strains expressing the exon 1–128Q-GFP transgene. Images of worm mechanosensory neurons were captured from at least 100 animals for each strain over 5 different trials. Aggregation was measured as average gray value using MetaView software (Molecular Devices). Data are from at least 3 independent experiments performed in triplicate.

Cell extracts, subcellular fractionation, preparation of CCVs, and Western blots. Cell extracts were obtained by lysing cells 48 hours after transfection with NP40 lysis buffer (2 minutes; 4°C). The extracts were sonicated and centrifuged at 11,000 *g* (15 minutes; 4°C). Proteins were loaded onto SDS-PAGE and subjected to Western blot analysis. For the experiment represented in Figure 2B, the samples were loaded without prior centrifugation. The aggregates remained in the stacking gel, whereas the soluble form migrated in the resolving gel. The aggregates were solubilized by formic acid treatment of the NP40 extracts (total) (31).

Subcellular fractionation was performed 48 hours after transfection as described previously (27). *T* represents the total extract, and fractions P1, P2, S3, and P3 were obtained using differential centrifugations: P1, initial pellet of homogenate; P2, crude synaptosomes; P3 and S3, high-speed pellet and supernatant of P2, respectively.

CCVs were purified from transfected cells (67). Cells were homogenized in buffer A [0.1 M 2-(N-morpholino)ethane-sulfonic acid, pH 6.5; 1 mM EGTA; 0.5 mM $MgCl_2$; 0.83 mM benzamidine; 0.23 mM phenylmethylsulfonyl fluoride; 0.5 μg/ml aprotinin; and 0.5 μg/ml leupeptin]. The homogenate was centrifuged at 17,800 *g* for 20 minutes, and the supernatant was collected and centrifuged at 56,100 *g* for 1 hour. The pellet was resuspended in buffer A, followed by dispersion through a 25-gauge needle. The resuspended pellet was loaded on top of a solution containing 8% sucrose in buffer A and centrifuged for 2 hours at 115,800 *g*. The supernatant (s) and the pellet containing the CCVs (p) were collected.

Antibodies. Antibodies used included: mouse monoclonal anti–β-actin AC15 (Sigma-Aldrich), anti-myc 9E10 (Calbiochem), anti–HA 16B12 (Covance Research Products Inc.), anti-clathrin, and anti-GM130 (BD Biosciences — Pharmingen); sheep polyclonal anti-HSJ1 (sHSJ1$^{1\text{-}277}$) (29); rabbit polyclonal anti-BDNF (Santa Cruz Biotechnology Inc.), anti-GFP (Chemicon International), and anti–endoplasmic reticulum (68); human polyclonal anti–GMAP-210 (38).

Anti-mouse and anti-rabbit secondary antibodies conjugated to HRP were purchased from Jackson ImmunoResearch Laboratories Inc. Anti-mouse and anti-rabbit secondary antibodies conjugated to Alexa Fluor (A488, A555, and A630) were from Invitrogen Corp. Pictures of fixed cells were captured with a 3D deconvolution imaging system.

Analysis of 3D images. The amount of clathrin-positive BDNF vesicles was quantified by measuring the colocalization between the 2 markers. Briefly, both clathrin and BDNF pictures were thresholded to segment vesicles and binarized. The percentage of colocalization was defined on binarized images as the ratio of clathrin-positive pixels overlapping BDNF-positive pixels to the total number of BDNF-positive pixels.

Quantification of Golgi area or vesicles that contained BDNF was achieved using the integrated morphometry analysis (IMA) from MetaMorph software version 6.2.6 (Molecular Devices). BDNF vesicles were defined by thresholding images to remove the background. Using an IMA size filter, objects ranging from 1–50 pixels (67 nm–3.35 μm diameter) were considered as vesicles and scored (cytoplasmic BDNF vesicles), whereas the bigger perinuclear structure was considered to be Golgi apparatus. The associated signal (pixel intensity) was recorded and corresponds to the quantity of BDNF in the defined structures (BDNF content in Golgi or BDNF content in cytoplasmic vesicles). Data are from at least 3 independent experiments, with a minimum of 5 cells analyzed per condition.

BDNF immunoenzyme assays. BDNF assays were performed 48 hours after lipofection of neuronal cells. Cells were washed with PBS and incubated 30 minutes with DMEM alone or DMEM containing 100 μM cystamine, and the supernatants were collected. For the time-course experiments, the incubation times with DMEM with or without cystamine were as stated. For BFA experiments, cells were first depolarized twice as previously described (27) in the absence or presence of BFA (5 μM). Cells were then washed and treated for 30 minutes with DMEM or cystamine (100 μM). The amount of BDNF was measured in supernatants and cell lysates using the BDNF Emax ImmunoAssay system (Promega). The data from transfected or treated cells are from at least 3 independent experiments performed in triplicate.

Animals. All experimental procedures were performed in strict accordance with the recommendations of the European Community (86/609/EEC) and the French National Committee (87/848) for care and use of laboratory animals. Live animal experiments were approved by the French Ethical Committee established by the Ministère de l'Agriculture et de la Forêt, Direction des Services Vétérinaires-Protection et Santé Animale (Evry, France).

R6/1 (*bdnf*$^{+/+}$*htt*^{m}) mice (46), BDNF heterozygous (*bdnf*$^{+/-}$*htt*$^{+/+}$) mice (69), and *bdnf*$^{+/-}$*htt*^{m} double-mutant mice (26) were used in this study. All experiments were performed on male littermates from the F_2 population to avoid strain and sex differences. Mice were housed together in numerical birth order in groups of mixed genotypes, and data were recorded for analysis by microchip mouse number. All experiments were conducted in a blinded manner with respect to genotype. Thirty minutes after the last administration of cysteamine (cysteamine bitartrate, or Cystagon [Orphan Europe], per os), 26- to 28-week-old mice (n = 4–5 per condition) were deeply anesthetized in a CO_2 chamber, and their striata were dissected out on ice and rapidly frozen using CO_2 pellets. Samples were then homogenized in lysis buffer (137 mM NaCl, 20 mM Tris-HCl, pH 8.0, 1% Igepal, 10% glycerol, 1 mM PMSF, 10 μg/ml aprotinin, 1 μg/ml leupeptin), sonicated, and centrifuged (10 minutes, 6,000 *g* at 4°C). BDNF contents were determined in duplicate by the Emax ImmunoAssay system using 300 μg of total protein for each point. C57BL/6 mice (males, age 5–6 weeks) were purchased from Charles River Laboratories. The *Hdh*^{109Q} mice (males, age 15 weeks) have been previously described (45). Treatments with cystamine (Sigma-Aldrich; intra-peritoneal injections) or cysteamine started on day 1 with 100 mg/kg

and were gradually increased to reach 300 mg/kg on day 7 (1 week). Mice were killed 30 minutes after the last administration. Blood was subjected to centrifugation (5 minutes; 2,700 *g*), and supernatant (serum) was kept. BDNF levels were determined using 600 μg of total protein (BDNF Emax ImmunoAssay system). A half frontal hemisphere of the brain was homogenized in NP40 lysis buffer and centrifuged 6,000 *g* (15 minutes; 4°C), and 100 μg of total protein of the supernatant was used to determine the amount of BDNF (BDNF Emax ImmunoAssay system).

Six-month-old male Sprague-Dawley rats (n = 4) weighing 550–580 g (Charles River Laboratories) were used for determination of the blood levels of BDNF at different time points before and after injection of either cysteamine (cysteamine dihydrochloride [Sigma-Aldrich]; 100 mg/kg; intramuscular injection) or its vehicle (physiological saline solution). For blood sampling, animals were anesthetized by inhalation of a mixture of isoflurane (1%), nitrous oxide (66%), and oxygen (33%). A catheter was inserted into and secured in the femoral vein. Blood samples (~300 μl) were collected every 15 minutes for 150 minutes.

Two long-tailed macaques (*Macaca fascicularis*) weighing 7.5 and 7 kg were treated for 14 months on a daily basis with slowly increasing doses of 3NP as previously described (49). At the time of blood collection, the 3NP dose was 30 mg/kg/d given in 2 daily injections (1 injection at 9 am, 1 injection at 5 pm). These 2 animals had no overt striatal degeneration as assessed by magnetic resonance (MR) imaging, but based on localized proton MR spectroscopy examination, they showed reduced tricarboxylic acid cycle turnover and depletion in *N*-acetyl-aspartate, glutamate, and GABA in the striatum. For blood sampling, the monkeys received a mixture of ketamine (15 mg/kg; Ketalar; PANPHARMA) and xylazine (1.5 mg/kg; Rompun; Bayer) before intubation. Animals were then anesthetized using an isoflurane/nitrous oxide mixture (1:66), controlled by an Ohmeda ventilator (Ohmeda OAV 7710; Datex-Ohmeda) with 33% oxygen. The tidal volume was adjusted to achieve stable end-tidal CO_2 tension between 38 and 40 mmHg.

After insertion of Teflon catheter into the saphena vein, blood samples (500 μl) were collected every 15 minutes for 45 minutes before cysteamine injection. Cysteamine treatment (cysteamine hydrochloride [Sigma-Aldrich], 100 mg/kg) was made by intramuscular injection in the hind limbs. Then blood samples were collected every 15 minutes for 120 minutes.

Immunohistochemistry. Cresyl violet staining and immunohistochemistry assays were performed on paraformaldehyde-fixed material as described previously (26). Administration of cysteamine or its vehicle was performed in 26-week-old mice (n = 4–5 per condition); 2 hours after the last administration, animals were deeply anesthetized and transcardially perfused with 4% paraformaldehyde solution in 0.1 M sodium phosphate, pH 7.2, at 15 days and 30 weeks of age. The brains were postfixed for 2 hours in the same solution, cryoprotected in increasing concentrations of sucrose/PBS (10–30%), and frozen in dry ice–cooled isopentane. Serial sections of 30 μm depth were obtained every 0.3 mm and were processed for cresyl violet staining and immunohistochemistry.

Sections were processed as free-floating for immunohistochemistry. To block endogenous peroxidases, sections were incubated for 30 minutes with PBS containing 10% methanol and 3% H_2O_2. Sections were washed 3 times in PBS and blocked for 1 hour with 2–10% normal serum in PBS. Tissue was then incubated with the anti–DARPP-32 antibody (1:10,000; Chemicon International) in PBS containing 2% normal goat serum for 16 hours at room temperature. Sections were washed 3 times and incubated with a biotinylated secondary antibody (1:200; Vector Laboratories) for 1–2 hours at room temperature in the same buffer as the primary antibody. The immunohistochemical reaction was developed using the VECTASTAIN ABC kit (Vector Laboratories). No signal was detected in controls that corresponded to the same treatment without the primary antibody.

Cell counts were performed in a blind manner with respect to genotype. Unbiased stereological counts of striatal cells were obtained from the entire neostriatum using Computer Assisted Stereology Toolbox (CAST) software (Olympus). The dissector counting method was employed to analyze coronal sections spaced 300 μm apart. The counting frames were randomly sampled. We counted the neuron-like cells in cresyl violet staining as the cells with a large nonpyknotic nucleus with clear nucleoli.

Quantification of DARPP-32–positive cells in the striatum of 3–4 animals per condition revealed significant differences (ANOVA, $F_{5,15}$ = 8.98; P < 0.0004 [P < 0.05 was considered statistically significant]). There was a significant difference in the number of DARPP-32–positive cells per striatum between $bdnf^{+/+}htt^{wt}$ mice and $bdnf^{+/+}htt^{m}$ mice (post-hoc Fisher's test, P = 0.003) and between $bdnf^{+/+}htt^{wt}$ mice and $bdnf^{+/-}htt^{m}$ mice with (post-hoc Fisher's test, P = 0.00022) or without cysteamine treatment (post-hoc Fisher's test, P = 0.00043). Cysteamine induced a significant increase in the number of DARPP-32–positive cells per striatum in $bdnf^{+/+}htt^{m}$ mice (post-hoc Fisher's test, P = 0.048) but not in $bdnf^{+/-}htt^{m}$ mice (post-hoc Fisher's test, NS).

In situ hybridization. Administration of cysteamine or its vehicle was performed in 17- to 18-week-old mice (n = 3–4). After 1 week, animals were killed 2 hours after the last administration, and brains were dissected out and frozen in dry-ice cooled isopentane. Sections were processed for in situ hybridization with radioactive oligonucleotide probes for preproenkephalin (PPE) as previously described (70). The slides were exposed to Biomax MR (Kodak) for 7 days. The expression of PPE was quantified on in situ hybridization films. Consecutive sections (18–20 sections/animal) were scanned, and mRNA levels were analyzed using the ImageJ program (http://rsb.info.nih.gov/ij/). The striatal area was determined according to anatomical landmarks, and the intensity was quantified. The background signal of the same adjacent area outside of the brain was subtracted.

Quantification of *ENK* mRNA levels in 3–4 animals per each condition revealed significant differences (ANOVA, $F_{7,16}$ = 17.71; P = 0.000002). There was a significant difference in *ENK* mRNA levels between $bdnf^{+/+}htt^{wt}$ mice and both $bdnf^{+/+}htt^{m}$ mice (post-hoc Fisher's test, P = 0.0084) and $bdnf^{+/-}htt^{m}$ mice (post-hoc Fisher's test, P = 0.000001); and between $bdnf^{+/+}htt^{m}$ mice and $bdnf^{+/-}htt^{m}$ mice (post-hoc Fisher's test, P = 0.0024). Cysteamine treatment induced an increase in *ENK* mRNA levels in $bdnf^{+/+}htt^{m}$ mice (post-hoc Fisher's test, P = 0.057) and in $bdnf^{+/-}htt^{m}$ mice (post-hoc Fisher's test, P = 0.0002).

Acknowledgments

We greatly acknowledge V.C. Wheeler and M.E. MacDonald for Hdh^{109Q} mice; G.V. Johnson and H.Y. Zoghbi for constructs; Ana López for her help in mice care; E. Coudrier and M. Bornens for antibodies; the Institut Curie Imaging Facility; the Huntington French Speaking Group for valuable discussions; S. Julien-Grille, H. Medyouf, and members of the Saudou/Humbert laboratory for help and comments. We gratefully acknowledge Harvard Brain Tissue Resource Center, supported in part by Public Health Service grant number MH/NS 31862, for providing human brain tissue. This research was supported by the Association pour la Recherche sur le Cancer (ARC 3665, to S. Humbert), Fondation pour la Recherche Médicale and Fondation BNP Paribas (to F. Saudou), HighQ Foundation (to J.A. Parker, C. Néri, F. Saudou, and S. Humbert), Association Française contre les Myopathies (AFM; to F. Saudou), Provital — P. Chevalier (to F. Saudou and S. Humbert), INSERM (to C. Néri), the Ministerio de Educación y Ciencia (to J. Alberch and J.M.

Canals), and Fundació La Caixa (to J. Alberch). J.R. Pineda is a fellow of the Ministerio de Educación y Ciencia (Spain). M. Borrell-Pagès is supported by an EMBO long-term fellowship. F. Saudou is a recipient of an EMBO Young Investigator award and is an INSERM/Assistance Publique —Hôpitaux de Paris investigator. S. Humbert is an INSERM investigator.

Address correspondence to: F. Saudou and S. Humbert, Institut Curie — UMR146 CNRS, Bat. 110, Centre Universitaire, Orsay, 91400, France. Phone: 33-169-86-30-24; Fax: 33-169-07-45-25; E-mail: frederic.saudou@curie.u-psud.fr (F. Saudou). Phone: 33-169-86-30-69; Fax: 33-169-07-45-25; E-mail: sandrine.humbert@curie.u-psud.fr (S. Humbert).

Received for publication December 7, 2005, and accepted in revised form February 14, 2006.

Josep M. Canals, Fabrice P. Cordelières, and J. Alex Parker contributed equally to this work.

1. Young, A.B. 2003. Huntingtin in health and disease. *J. Clin. Invest.* **111**:299–302. doi:10.1172/JCI200317742.
2. MacDonald, M.E., Gines, S., Gusella, J.F., and Wheeler, V.C. 2003. Huntington's disease. *Neuromolecular Med.* **4**:7–20.
3. Melino, G., and Piacentini, M. 1998. 'Tissue' transglutaminase in cell death: a downstream or a multifunctional upstream effector? *FEBS Lett.* **430**:59–63.
4. Lesort, M., Tucholski, J., Miller, M.L., and Johnson, G.V. 2000. Tissue transglutaminase: a possible role in neurodegenerative diseases. *Prog. Neurobiol.* **61**:439–463.
5. Green, H. 1993. Human genetic diseases due to codon reiteration: relationship to an evolutionary mechanism. *Cell.* **74**:955–956.
6. Cooper, A.J.L., et al. 1997. Polyglutamine domains are substrates of tissue transglutaminase - does transglutaminase play a role in expanded Cag/Poly-Q neurodegenerative diseases? *J. Neurochem.* **69**:431–434.
7. Kahlem, P., Green, H., and Djian, P. 1998. Transglutaminase action imitates Huntington's disease: selective polymerization of huntingtin containing expanded polyglutamine. *Mol. Cell.* **1**:595–601.
8. Karpuj, M.V., et al. 1999. Transglutaminase aggregates huntingtin into nonamyloidogenic polymers, and its enzymatic activity increases in Huntington's disease brain nuclei. *Proc. Natl. Acad. Sci. U. S. A.* **96**:7388–7393.
9. Lesort, M., Chun, W., Johnson, G.V., and Ferrante, R.J. 1999. Tissue transglutaminase is increased in Huntington's disease brain. *J. Neurochem.* **73**:2018–2027.
10. Dedeoglu, A., et al. 2002. Therapeutic effects of cystamine in a murine model of Huntington's disease. *J. Neurosci.* **22**:8942–8950.
11. Karpuj, M.V., et al. 2002. Prolonged survival and decreased abnormal movements in transgenic model of Huntington disease, with administration of the transglutaminase inhibitor cystamine. *Nat. Med.* **8**:143–149.
12. Zainelli, G.M., Ross, C.A., Troncoso, J.C., and Muma, N.A. 2003. Transglutaminase cross-links in intranuclear inclusions in Huntington disease. *J. Neuropathol. Exp. Neurol.* **62**:14–24.
13. Mastroberardino, P.G., et al. 2002. 'Tissue' transglutaminase ablation reduces neuronal death and prolongs survival in a mouse model of Huntington's disease. *Cell Death Differ.* **9**:873–880.
14. Bailey, C.D., and Johnson, G.V. 2005. Tissue transglutaminase contributes to disease progression in the R6/2 Huntington's disease mouse model via aggregate-independent mechanisms. *J. Neurochem.* **92**:83–92.
15. Wang, X., et al. 2005. Cerebral PET imaging and histological evidence of transglutaminase inhibitor cystamine induced neuroprotection in transgenic R6/2 mouse model of Huntington's disease. *J. Neurol. Sci.* **231**:57–66.
16. Bailey, C.D., and Johnson, G.V. 2005. The protective effects of cystamine in the R6/2 Huntington's disease mouse involve mechanisms other than the inhibition of tissue transglutaminase. *Neurobiol. Aging.* doi:10.1016/j.neurobiolaging.2005.04.001.
17. Pinto, J.T., et al. 2005. Treatment of YAC128 mice and their wild-type littermates with cystamine does not lead to its accumulation in plasma or brain: implications for the treatment of Huntington disease. *J. Neurochem.* **94**:1087–1101.
18. Lesort, M., Lee, M., Tucholski, J., and Johnson, G.V. 2003. Cystamine inhibits caspase activity. Implications for the treatment of polyglutamine disorders. *J. Biol. Chem.* **278**:3825–3830.
19. Fox, J.H., et al. 2004. Cystamine increases L-cysteine levels in Huntington's disease transgenic mouse brain and in a PC12 model of polyglutamine aggregation. *J. Neurochem.* **91**:413–422.
20. Opal, P., and Zoghbi, H.Y. 2002. The role of chaperones in polyglutamine disease. *Trends Mol. Med.* **8**:232–236.
21. Bonini, N.M. 2002. Chaperoning brain degeneration. *Proc. Natl. Acad. Sci. U. S. A.* **99**:16407–16411.
22. Muchowski, P.J., and Wacker, J.L. 2005. Modulation of neurodegeneration by molecular chaperones. *Nat. Rev. Neurosci.* **6**:11–22.
23. Sherman, M.Y., and Goldberg, A.L. 2001. Cellular defenses against unfolded proteins: a cell biologist thinks about neurodegenerative diseases. *Neuron.* **29**:15–32.
24. Saudou, F., Finkbeiner, S., Devys, D., and Greenberg, M.E. 1998. Huntingtin acts in the nucleus to induce apoptosis but death does not correlate with the formation of intranuclear inclusions. *Cell.* **95**:55–66.
25. Zuccato, C., et al. 2001. Loss of huntingtin-mediated BDNF gene transcription in Huntington's disease. *Science.* **293**:493–498.
26. Canals, J.M., et al. 2004. Brain-derived neurotrophic factor regulates the onset and severity of motor dysfunction associated with enkephalinergic neuronal degeneration in Huntington's disease. *J. Neurosci.* **24**:7727–7739.
27. Gauthier, L.R., et al. 2004. Huntingtin controls neurotrophic support and survival of neurons by enhancing BDNF vesicular transport along microtubules. *Cell.* **118**:127–138.
28. Trettel, F., et al. 2000. Dominant phenotypes produced by the HD mutation in STHdh(Q111) striatal cells. *Hum. Mol. Genet.* **9**:2799–2809.
29. Chapple, J.P., and Cheetham, M.E. 2003. The chaperone environment at the cytoplasmic face of the endoplasmic reticulum can modulate rhodopsin processing and inclusion formation. *J. Biol. Chem.* **278**:19087–19094.
30. Sakahira, H., Breuer, P., Hayer-Hartl, M.K., and Hartl, F.U. 2002. Molecular chaperones as modulators of polyglutamine protein aggregation and toxicity. *Proc. Natl. Acad. Sci. U. S. A.* **99**:16412–16418.
31. Hazeki, N., Tukamoto, T., Goto, J., and Kanazawa, I. 2000. Formic acid dissolves aggregates of an N-terminal huntingtin fragment containing an expanded polyglutamine tract: applying to quantification of protein components of the aggregates. *Biochem. Biophys. Res. Commun.* **277**:386–393.
32. Parker, J.A., et al. 2001. Expanded polyglutamines in Caenorhabditis elegans cause axonal abnormalities and severe dysfunction of PLM mechanosensory neurons without cell death. *Proc. Natl. Acad. Sci. U. S. A.* **98**:13318–13323.
33. Parker, J.A., et al. 2005. Resveratrol rescues mutant polyglutamine cytotoxicity in nematode and mammalian neurons. *Nat. Genet.* **37**:349–350.
34. Cheetham, M.E., Jackson, A.P., and Anderton, B.H. 1994. Regulation of 70-kDa heat-shock-protein ATPase activity and substrate binding by human DNAJ-like proteins, HSJ1a and HSJ1b. *Eur. J. Biochem.* **226**:99–107.
35. Cheetham, M.E., Anderton, B.H., and Jackson, A.P. 1996. Inhibition of hsc70-catalysed clathrin uncoating by HSJ1 proteins. *Biochem. J.* **319**:103–108.
36. Harjes, P., and Wanker, E.E. 2003. The hunt for huntingtin function: interaction partners tell many different stories. *Trends Biochem. Sci.* **28**:425–433.
37. Gleeson, P.A., Lock, J.G., Luke, M.R., and Stow, J.L. 2004. Domains of the TGN: coats, tethers and G proteins. *Traffic.* **5**:315–326.
38. Infante, C., Ramos-Morales, F., Fedriani, C., Bornens, M., and Rios, R.M. 1999. GMAP-210, a cis-Golgi network-associated protein, is a minus end microtubule-binding protein. *J. Cell Biol.* **145**:83–98.
39. Klausner, R.D., Donaldson, J.G., and Lippincott-Schwartz, J. 1992. Brefeldin A: insights into the control of membrane traffic and organelle structure. *J. Cell Biol.* **116**:1071–1080.
40. Campisi, A., et al. 2003. Glutamate-induced increases in transglutaminase activity in primary cultures of astroglial cells. *Brain Res.* **978**:24–30.
41. Pastuszko, A., Wilson, D.F., and Erecinska, M. 1986. A role for transglutaminase in neurotransmitter release by rat brain synaptosomes. *J. Neurochem.* **46**:499–508.
42. Gahl, W.A., Thoene, J.G., and Schneider, J.A. 2002. Cystinosis. *N. Engl. J. Med.* **347**:111–121.
43. Shults, C., et al. 1986. Huntington's disease: effect of cysteamine, a somatostatin-depleting agent. *Neurology.* **36**:1099–1102.
44. Dubinsky, R., and Gray, C. 2005. CYTE-I-HD: phase I dose finding and tolerability study of cysteamine (Cystagon) in Huntington's disease. *Mov. Disord.* doi:10.1002/mds.20756.
45. Wheeler, V.C., et al. 2000. Long glutamine tracts cause nuclear localization of a novel form of huntingtin in medium spiny striatal neurons in HdhQ92 and HdhQ111 knock- in mice. *Hum. Mol. Genet.* **9**:503–513.
46. Mangiarini, L., et al. 1996. Exon 1 of the HD gene with an expanded CAG repeat is sufficient to cause a progressive neurological phenotype in transgenic mice. *Cell.* **87**:493–506.
47. Wheeler, V.C., et al. 2002. Early phenotypes that presage late-onset neurodegenerative disease allow testing of modifiers in Hdh CAG knock-in mice. *Hum. Mol. Genet.* **11**:633–640.
48. Brouillet, E., et al. 1995. Chronic mitochondrial energy impairment produces selective striatal degeneration and abnormal choreiform movements in primates. *Proc. Natl. Acad. Sci. U. S. A.* **92**:7105–7109.
49. Palfi, S., et al. 1998. Fetal striatal allografts reverse cognitive deficits in a primate model of Huntington disease. *Nat. Med.* **4**:963–966.
50. Petrova, P., et al. 2003. MANF: a new mesencephalic, astrocyte-derived neurotrophic factor with selectivity for dopaminergic neurons. *J. Mol. Neurosci.* **20**:173–188.

51. Legendre-Guillemin, V., et al. 2005. Huntingtin interacting protein 1 (HIP1) regulates clathrin assembly through direct binding to the regulatory region of the clathrin light chain. *J. Biol. Chem.* **280**:6101–6108.
52. Chen, C.Y., and Brodsky, F.M. 2005. Huntingtin-interacting protein 1 (Hip1) and Hip1-related protein (Hip1R) bind the conserved sequence of clathrin light chains and thereby influence clathrin assembly in vitro and actin distribution in vivo. *J. Biol. Chem.* **280**:6109–6117.
53. Bungay, P.J., Potter, J.M., and Griffin, M. 1984. The inhibition of glucose-stimulated insulin secretion by primary amines. A role for transglutaminase in the secretory mechanism. *Biochem. J.* **219**:819–827.
54. Gobbi, M., Frittoli, E., and Mennini, T. 1996. Role of transglutaminase in [3H]5-HT release from synaptosomes and in the inhibitory effect of tetanus toxin. *Neurochem. Int.* **29**:129–134.
55. Davies, P.J., et al. 1984. Studies on the effects of dansylcadaverine and related compounds on receptor-mediated endocytosis in cultured cells. *Diabetes Care.* **7**:35–41.
56. Howe, C.L., Valletta, J.S., Rusnak, A.S., and Mobley, W.C. 2001. NGF signaling from clathrin-coated vesicles: evidence that signaling endosomes serve as a platform for the Ras-MAPK pathway. *Neuron.* **32**:801–814.
57. Jeitner, T.M., Delikatny, E.J., Ahlqvist, J., Capper, H., and Cooper, A.J. 2005. Mechanism for the inhibition of transglutaminase 2 by cystamine. *Biochem. Pharmacol.* **69**:961–970.
58. Tenneze, L., Daurat, V., Tibi, A., Chaumet-Riffaud, P., and Funck-Brentano, C. 1999. A study of the relative bioavailability of cysteamine hydrochloride, cysteamine bitartrate and phosphocysteamine in healthy adult male volunteers. *Br. J. Clin. Pharmacol.* **47**:49–52.
59. Belldina, E.B., Huang, M.Y., Schneider, J.A., Brundage, R.C., and Tracy, T.S. 2003. Steady-state pharmacokinetics and pharmacodynamics of cysteamine bitartrate in paediatric nephropathic cystinosis patients. *Br. J. Clin. Pharmacol.* **56**:520–525.
60. Douma, S., et al. 2004. Suppression of anoikis and induction of metastasis by the neurotrophic receptor TrkB. *Nature.* **430**:1034–1039.
61. Kleta, R., et al. 2004. Long-term follow-up of well-treated nephropathic cystinosis patients. *J. Pediatr.* **145**:555–560.
62. Chun, W., et al. 2001. Tissue transglutaminase selectively modifies proteins associated with truncated mutant huntingtin in intact cells. *Neurobiol. Dis.* **8**:391–404.
63. Cummings, C.J., et al. 1998. Chaperone suppression of aggregation and altered subcellular proteasome localization imply protein misfolding in SCA1. *Nat. Genet.* **19**:148–154.
64. Haubensak, W., Narz, F., Heumann, R., and Lessmann, V. 1998. BDNF-GFP containing secretory granules are localized in the vicinity of synaptic junctions of cultured cortical neurons. *J. Cell Sci.* **111**:1483–1493.
65. Humbert, S., et al. 2002. The IGF-1/Akt pathway is neuroprotective in Huntington's disease and involves Huntingtin phosphorylation by Akt. *Dev. Cell.* **2**:831–837.
66. Brenner, S. 1974. The genetics of Caenorhabditis elegans. *Genetics.* **77**:71–94.
67. Metzler, M., et al. 2001. HIP1 functions in clathrin-mediated endocytosis through binding to clathrin and adaptor protein 2. *J. Biol. Chem.* **276**:39271–39276.
68. Louvard, D., Reggio, H., and Warren, G. 1982. Antibodies to the Golgi complex and the rough endoplasmic reticulum. *J. Cell Biol.* **92**:92–107.
69. Ernfors, P., Lee, K.F., and Jaenisch, R. 1994. Mice lacking brain-derived neurotrophic factor develop with sensory deficits. *Nature.* **368**:147–150.
70. Perez-Navarro, E., Alberch, J., Neveu, I., and Arenas, E. 1999. Brain-derived neurotrophic factor, neurotrophin-3 and neurotrophin-4/5 differentially regulate the phenotype and prevent degenerative changes in striatal projection neurons after excitotoxicity in vivo. *Neuroscience.* **91**:1257–1264.

Cuarto trabajo

"Neuroprotection by GDNF-secreting stem cells

in a Huntington's disease model:

optical neuroimage tracking of brain-grafted cells"

Publicado en *Gene Therapy*

Gene Therapy (2006), 1–11

www.nature.com/gt

ORIGINAL ARTICLE

Neuroprotection by GDNF-secreting stem cells in a Huntington's disease model: optical neuroimage tracking of brain-grafted cells

JR Pineda[1], N Rubio[2], P Akerud[3], N Urbán[1], L Badimon[2], E Arenas[3], J Alberch[1], J Blanco[2] and JM Canals[1]

[1]Departament de Biologia Cel·lular i Anatomia Patològica, Facultat de Medicina, IDIBAPS, Universitat de Barcelona, Barcelona, Spain; [2]Cardiovascular Research Center, ICCC-CSIC, Hospital de Sant Pau, Barcelona, Spain; [3]Laboratory of Molecular Neurobiology, Department of Medical Biochemistry and Biophysics, Karolinska Institute, Stockholm, Sweden

The use of stem cells for reconstructive or neuroprotective strategies can benefit from new advances in neuroimaging techniques to track grafted cells. In the present work, we analyze the potential of a neural stem cell (NSC) line, which stably expresses the glial cell line-derived neurotrophic factor (GDNF) and the firefly luciferase gene (GDNF/Luc-NSC), for cell therapy in a Huntington's disease mouse model. Our results show that detection of light photons is an effective method to quantify the proliferation rate and to characterize the migration pathways of transplanted NSCs. Intravenous administration of luciferine, the luciferase substract, into the grafted animals allowed the detection of implanted cells in real time by an optical neuroimaging methodology, overpassing the limits of serial histological analyses. We observed that transplanted GDNF/Luc-NSCs survive after grafting and expand more when transplanted in quinolinate-lesioned nude mouse striata than when transplanted in non-lesioned mice. We also demonstrate that GDNF/Luc-NSCs prevent the degeneration of striatal neurons in the excitotoxic mouse model of Huntington's disease and reduce the amphetamine-induced rotational behavior in mice bearing unilateral lesions.

Gene Therapy advance online publication, 31 August 2006; doi:10.1038/sj.gt.3302847

Keywords: *neurodegenerative disorders; striatum; cell grafting; neurotrophic factors; neuroprotection; non-invasive imaging*

Introduction

Cell transplantation is one of the most promising approaches for the prevention and restoration of neural degeneration. Owing to their capacity to integrate in the host brain, stem cells releasing neuroprotective molecules have been proposed for *ex vivo* gene therapy.[1,2] The use of genetically engineered neural stem cells (NSCs) delivering glial cell line-derived neurotrophic factor (GDNF) in an animal model of Parkinson's disease to reduce disease progression has been previously described.[3] GDNF has also stimulated great interest as a therapeutic candidate for Huntington's disease (HD) owing to its high expression in the striatum.[4] To exert its biological activities, GDNF signals through a two-component receptor complex consisting of the c-Ret and the GDNF family receptor-α.[5–7] These receptor subunits are expressed in the striatum and are upregulated after an excitotoxic lesion, suggesting an endogenous protective role after neuronal damage of this brain nucleus.[8] In fact, administration of exogenous GDNF, throughout the grafting of a fibroblast cell line genetically modified to constitutively release this trophic factor, protects striatal neuronal populations against quinolinate (QUIN).[9–11] However, the methodology used in these studies cannot be used for chronic pathologies because fibroblasts make tumors after brain transplants.[12] Thus, the use of NSCs for cell therapy in HD can constitute a powerful tool for releasing neurotrophic factors to protect striatal neurons in this movement disorder.

A common problem in cell therapy using NSCs is that cells cannot be tracked *in vivo* after grafting into the brain. Thus, in models of neurodegenerative disorders, tracking of stem cells over long periods of time is limited by the need to use histological procedures and multiple animals for each time point examined. *In vivo*, non-invasive imaging is an emerging methodology that allows the use of multiple luciferase reporters. Bioluminescent markers have been used successfully to non-invasively track local tumor growth and the development of metastasis in a variety of organs of living mice.[13–15] Owing to the absence of endogenous light-producing reactions in most mammal tissues, the use of bioluminescence markers for *in vivo* imaging is advantageous over the use of fluorescent reporters.[15] The luciferase from *Photinus pyralis* catalyzes the oxidation of luciferine, in the presence of ATP and oxygen, generating light

Correspondence: Dr JM Canals, Departament de Biologia Cel·lular i Anatomia Patològica, Facultat de Medicina, IDIBAPS, Universitat de Barcelona, C/Casanova, 143, E-08036 Barcelona, Spain.
E-mail: jmcanals@ub.edu
Received 16 February 2006; revised 10 July 2006; accepted 10 July 2006

photons and oxyluciferine.[13] The use of a high-sensitivity video camera to detect photons that traverse mouse tissues after luciferine administration has allowed repeated non-invasive imaging of luciferase-expressing tumors and metastases.[16]

In the present work, we have adopted optical imaging procedures to monitor the fate of NSCs grafted into the brain of living mice during neuroprotective studies. To do this, we have generated the luciferase-expressing cell line GDNF/Luc-NSC using a retroviral vector for stable expression of transgenes. Our results demonstrate that *in vivo* optical neuroimaging allows tracking of light-producing GDNF/Luc-NSCs grafted into QUIN-lesioned mouse brains. We also show that intrastriatal grafting of GDNF/Luc-NSCs protects striatal neurons against excitotoxicity, resulting in the prevention of locomotor impairment in a mouse model of HD.

Results

Light production by NSCs engineered to express enhanced green fluorescent protein (eGFP)-luciferase

C17.2-neural stem cells (NSCs) were transduced using the peGFP-CMV/luc construct (Figure 1a) to obtain the eGFP and luciferase-expressing c17.2/Luc-NSC subline. A standard plot of luciferase activity measured in cell homogenates using a luminometer, relative light units (RLUs) vs number of cells, resulted in a linear graph ($R^2 = 0.987$; Figure 1b) showing that light measurements can be used to estimate cell numbers.

The amount of light produced by a known number of c17.2/Luc-NSCs was also measured in tissue culture plates using a high-efficiency cooled charge-couple device (CCD) camera system (Figure 1c and d; ORCA-2BT; Hammamatsu Photonics, Hammamatsu City, Japan). Plots of light emission vs cell numbers were linear through the range of cells tested ($R^2 = 0.993$; Figure 1c). The slope of this linear regression, 8.732, indicated the number of RLU per cell. Assay sensitivity was defined as the number of cells required to generate a quantity of light equivalent to two times the standard deviation of background noise.[17] Our results show that the average of the standard deviations of photons (RLUs) detected from each of the predetermined numbers of cells is 75. Thus, the minimal differences in the number of cells that can be statistically detected is approximately 17 NSCs ($(75 \times 2)/8.732$).

With this instrument, the sensitivity for detection of small numbers of cells could be significantly increased by the aggregated reading of groups of CCD pixels (binning), resulting in a reduction of noise (binning 8×8 (range 10–2000: $R^2 = 0.993$); Figure 1d inset). However, binning reduces the linearity of intense signals, owing to the saturation of light detectors (range 10–10 000; $R^2 = 0.959$; Figure 1d).

We also tested whether differentiation of c17.2/Luc-NSCs affects their light production capacity. EGFP expression was maintained after differentiation in the non-mitogenic N2 medium, during at least 14 days, the longest period tested (Figure 1e). In addition, our results also demonstrated that differentiated cells maintain luciferase expression (Figure 1f). No differences in light emission were detected between the same number of proliferating and differentiated c17.2/Luc-NSCs (Figure 1f).

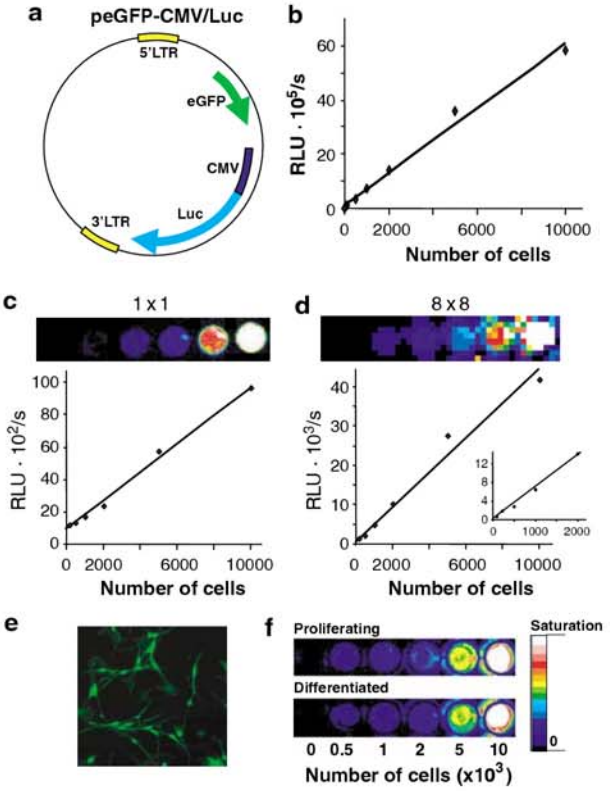

Figure 1 Transduction of the c17.2-NSC lines with retroviral vector peGFP-CMV/Luc for expression of the enhanced green fluorescent protein (eGFP) and luciferase (Luc) genes. (**a**) Schematic representation of the peGFP-CMV/Luc retroviral vector. Constitutive expression of eGFP and luciferase genes is controlled by the retroviral LTR and the CMV promoters, respectively. (**b–d**) Standard plots of light produced (RLUs) by predetermined numbers of c17.2/Luc-NSCs *in vitro*. (**b**) Light production was measured using a bench top luminometer, $R^2 = 0.999$ ($n = 3$). (**c, d**) Emitted light was recorded using the ORCA-2BT imaging system: (**c**) 1×1 binning, $R^2 = 0.993$ ($n = 6$; cell range 10–10 000); (**d**) 8×8 binning, $R^2 = 0.959$ ($n = 6$) (cell range 10–10 000); (**d**) inset, binning 8×8 (cell range 10–2000), $R^2 = 0.993$. In the 1×1 binned images, pixels correspond to single CCD pixels; in the 8×8 binned images, pixels correspond to clusters of 8×8 CCD pixels. (**e**) Expression of eGFP in C17.2/Luc-NSCs after differentiation in N2 medium. (**f**) Light production by C17.2/Luc-NSCs after differentiation in N2 medium. An arbitrary color scale is used to indicate relative light intensities from black (lower) to white (higher) (WASABI, Hammamatsu Photonics). R, correlation coefficient. RLUs, relative light units.

Quantification and tracking of brain-engrafted NSCs by optical neuroimaging

C17.2/Luc-NSCs grafted into the brains of nude mice could be easily detected *in vivo* using the imaging system (Figure 2). To establish the sensitivity range, nude mice were bilaterally inoculated with 10 000 and 5000 c17.2/Luc-NSCs. Light emission by the grafted NSCs was imaged between minutes 6 and 10 following either intraperitoneal (i.p.) or intravenous (i.v.) inoculation of D-luciferine (100 mg/kg). Intravenous inoculation of luciferine increased light detection sensitivity by approximately 220–240% when compared to the

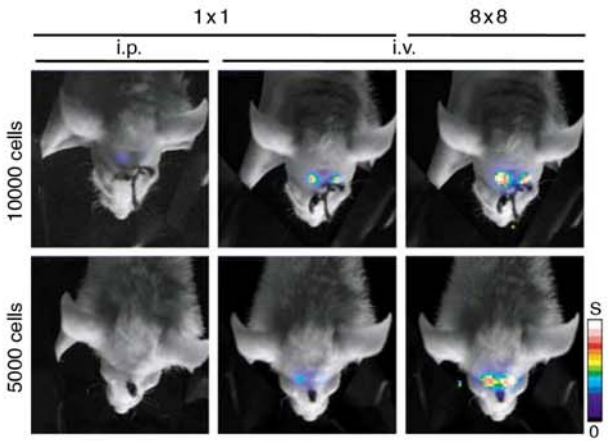

Figure 2 *In vivo* optical images of luciferase-expressing NSCs transplanted into mice striatum, recorded using the ORCAB-2BT imaging system. I.v. inoculation of luciferine results in a 220–240% increase in light production, relative to i.p. inoculation. 8×8 binning results in a 4–5-fold increase in sensitivity, relative to 1×1 binning. i.v., intravenous injection; i.p. intraperitoneal injection. 1×1 binning, the image pixels correspond to single CCD pixels; 8×8 binning, the image pixels correspond to clusters of 8×8 CCD pixels.

detection sensitivity after i.p. injection of luciferine (Figure 2). These findings show that i.v. injected luciferine reaches the brain region efficiently via the vascular system. Interestingly, c17.2/Luc-NSCs were detected from the second day after transplantation (Figure 3b), but no light emission was observed in any condition 1 day after the implantation of NSCs into the brain (Figure 3a). Histological analysis of the NSC-grafted brains showed that at this short time post grafting, cells were still at the inoculation sites (Figure 3c). However, at the second day, c17.2/Luc-NSCs are more dispersed and integrated in the brain tissue (Figure 3d). Thus, a plausible explanation for the lack of light production the first day post inoculation could be an inefficient supply of luciferine to the cells, owing to the absence of an established vascular system. In fact, the coinjection of c17.2/Luc-NSCs with luciferine allowed the detection of light when imaged just after grafting (data not shown), demonstrating that when luciferine reaches the transplanted cells, light emission can be easily detected.

To determine whether *in vivo* optical neuroimaging could be used to quantify low numbers of brain-engrafted cells and their proliferation rate, known numbers, ranging from 100 to 10 000, of c17.2/Luc-NSCs were intrastriatally injected in nude mice. The animals were imaged at 1 week post-engraftment, when grafted NSCs can easily be detected by optical neuroimage (Figure 3e). Plot of light production vs the number of transplanted c17.2/Luc-NSCs were linear through the tested range of cell numbers ($R^2 = 0.986$; Figure 3f). The slope of the resulting linear regression plot, a measure of the amount of light/(cell $\times$ min), indicated that the c17.2/Luc-NSCs transplanted into the striatum-generated 9.97 RLU/min/grafted cell. The minimal number of transplanted c17.2/Luc-NSCs that we could detect was 500 cells per striatum at the highest sensitivity possible (8×8 binning; Figure 3e and f).

To better determine the correlation between the number of c17.2/Luc-NSCs present in transplanted mouse brains and the RLU recorded, at 6 weeks post-engraftment, mice grafted with different numbers of c17.2/Luc-NSCs were imaged, to measure light emission, and in the same day they were processed for histology (see Material and methods for details). We performed stereological counting of eGFP-positive c17.2/Luc-NSCs in the brain sections from animals grafted with different number of c17.2/Luc-NSCs. These experiments, which allowed us to compare the RLU with the exact number of cells in each mice, demonstrated a lineal correlation between RLU/min and the number of eGFP-positive cells ($R^2 = 0.958$; Figure 3g). The slope of the linear plot indicated that each eGFP-positive c17.2/Luc-NSC produced 7.42 RLU/min, a number consistent, considering the experimental constraints, with that found for cells 1 week post grafting.

Repetitive imaging of the same animal allowed determination of the proliferation rate for implanted c17.2/Luc-NSCs (Figure 3h), based on the changes in light emission. Light from transplanted cells detected by optical neuroimaging of the same animal 1 week and 6 weeks post implantation (Figure 3h) showed an increase in intensity that varied depending on the number of transplanted cells. We observed that mice engrafted with a lower number of c17.2/Luc-NSCs had a larger increase in light emission than mice engrafted with a larger number of cells (data not shown). These increase in light emission also correlated with a time-dependent increase in stereologically counted eGFP-positive c17.2/Luc-NSCs. As with the case for light production, the increase in eGFP counts was also larger for mice grafted with the lower than for those grafted with the larger numbers of cells (number of population doublings vs number of grafted cells: 9.94, 500 grafted cells; 9.25, 1000 grafted cells; 8.57, 2000 grafted cells; 6.46, 10 000 grafted cells). The proliferation rate of c17.2/Luc-NSCs after grafting was similar to that detected for the parental cell line c17.2-NSC (data not shown), suggesting that the expression of eGFP and luciferase does not affect the proliferation of NSCs after grafting.

Light detection may be affected by the amount of tissue intervening between the cells and the CCD camera. It seems not to be a problem in small animals like mice, although one should expect noticeable impairments in larger animals.

Migratory behavior of implanted cells

To test the possibility that implanted c17.2/Luc-NSCs would migrate and could be detected using optical neuroimaging, we implanted 5000 c17.2/Luc-NSCs in the rostral migratory stream (Figure 4a), a well-characterized migratory pathway for NSCs of the subventricular zone.[18] Light emission images taken 1 week after grafting showed the cells localized at the grafting site (Figure 4b). However, 6 weeks post grafting, the light signal at the injected sites was reduced and a new light spot was detected in the olfactory bulb region (Figure 4c), suggesting that grafted cells migrated from the original implantation site (Figure 4b). Histological analysis of the light-producing brain area showed eGFP-positive c17.2/Luc-NSCs (Figure 4d) in the granular and glomerular cell layers of the olfactory bulb, the natural migration target for NSCs from the subventricular zone.[18] Some eGFP-

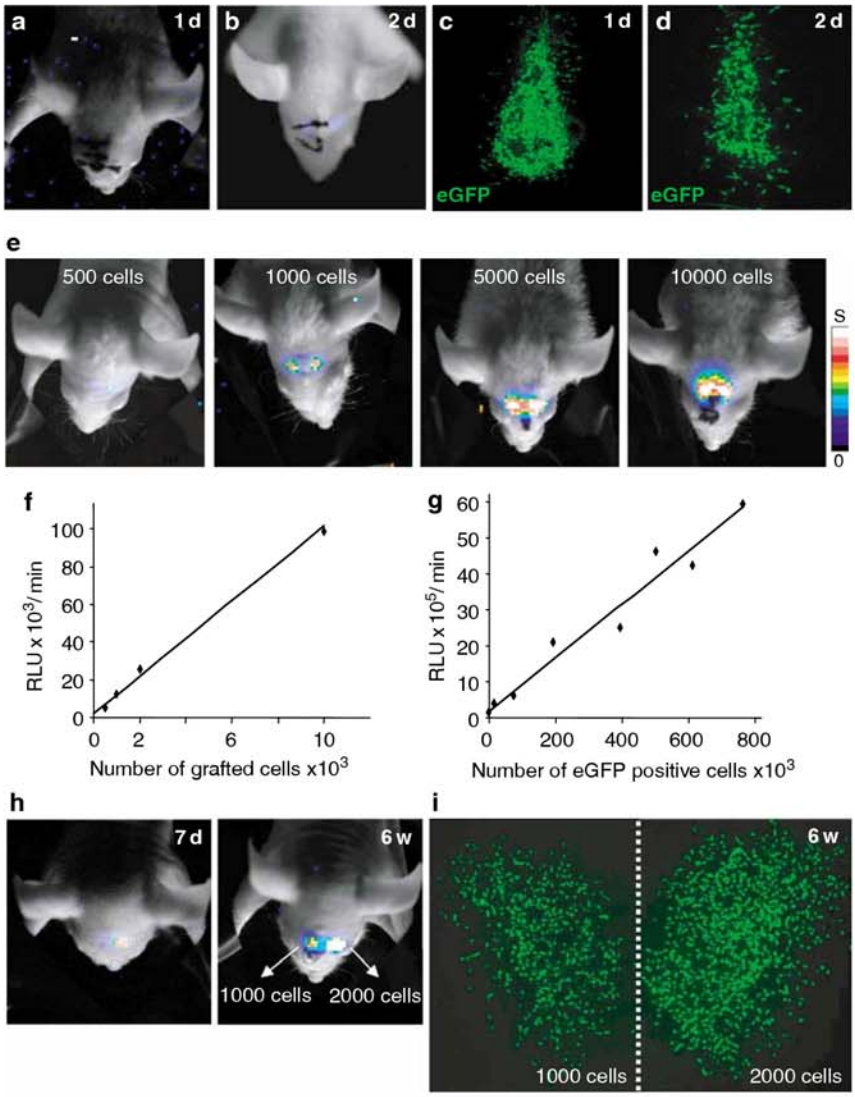

Figure 3 Non-invasive optical neuroimaging allows the quantification of brain-transplanted NSCs. (**a**, **b**) Optical neuroimages taken 1 and 2 days post cell inoculation, demonstrating that light emission can be detected from the second day. (**c**, **d**) Morphological pictures of eGFP-expressing c17.2/Luc-NSCs 1 and 2 days post brain grafting. (**e**) Optical images from mice bilaterally grafted with increasing numbers (500–10 000) of c17.2/Luc-NSCs acquired 1 week post grafting. Each mouse was grafted with an equal number of cells in each hemisphere. (**f**) Plot of the number of neuroimage recorded light events 1 week after grafting (ordinate; RLU/min) vs the number of implanted cells, $R^2 = 0.986$ ($n = 4$). (**g**) Plot of the number of neuroimage recorded light events (ordinate; RLU/min) vs the number of eGFP-positive cells (histological procedure) at the same day (see Material and methods for details), $R^2 = 0.958$ ($n = 4$). (**h**) Optical neuroimages of 1000, right hemisphere, and 2000, left hemisphere, c17.2/Luc-NSCs implanted in the host striatum. Pictures were taken from the same mouse at 1 and 6 weeks post grafting, respectively. (**i**) Morphological analysis of postmortem samples from mouse in (**h**), 6 weeks after intrastriatal grafting. RLU, relative light units.

positive cells were also detected throughout the *corpus callosum* (data not shown) corresponding to low levels of light detected in the forebrain by optical imaging (Figure 4c).

Optical neuroimaging to monitor NSCs in neuroprotective studies

GDNF-expressing c17.2-NSCs (GDNF-NSC) and mock-transfected c17.2 (MT-NSC) described by Akerud *et al.*,[3] were transduced with the peGFP-CMV/luc construct (GDNF/Luc-NSC and MT/Luc-NSC, respectively). Both GDNF/Luc-NSCs and MT/Luc-NSCs produced similar amounts of light/cell, and in linear proportion to cell number (data not shown).

Expression of eGFP and luciferase had no effect on the capacity of GDNF-NSCs for GDNF expression. Our analysis showed that while the parental cell line (GDNF-NSC) secreted 19.9 ± 3.77 ng of GDNF per 10^6 cells in 1 day, the GDNF/Luc-NSC cell line produced a very similar quantity, 18.42 ± 2.1 ng of GDNF per 10^6 cells in 1 day (Figure 5a). The expression of eGFP and luciferase did not alter the morphology or the fate of the GDNF-NSC lines, and all characteristic phenotypes, including neurons and glia, were detected in differentiated GDNF/Luc-NSCs (Figure 5b).

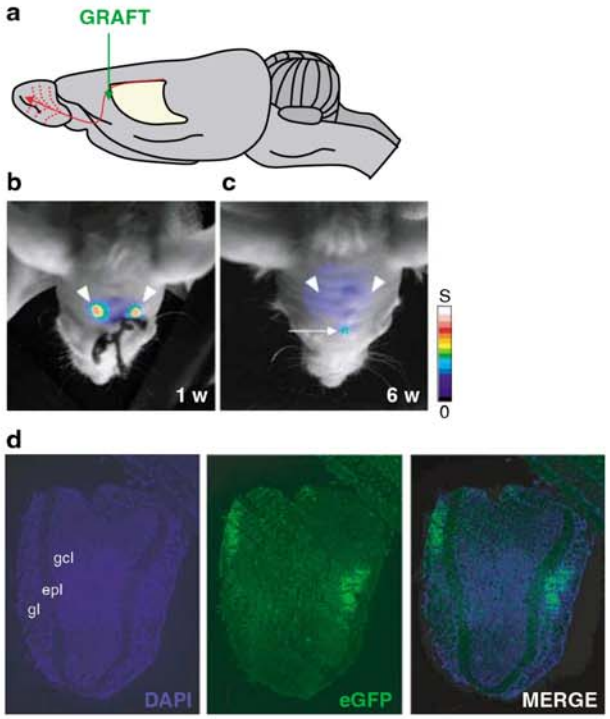

Figure 4 Tracking of NSC migration by *in vivo* optical neuroimaging. (**a**) Diagram showing the rostral migratory stream of endogenous NSCs, from the subventricular zone to the olfactory bulb. (**b**) Optical neuroimage of c17.2/Luc-NSCs transplanted in the mouse rostral migratory stream, acquired 1 week post grafting. (**c**) Bioluminscent spot (arrow) detected over the olfactory bulb of the same mouse 6 weeks post grafting. The arrows-heads indicate the grafting sites. (**d**) Histological analysis showing eGFP-positive c17.2/Luc-NSCs in the olfactory bulb. Counterstaining with DAPI (blue) shows the presence of eGFP-expressing cells in the glomerular and granular cell layers, the natural migration target for NSCs of the subventricular zone ($n=3$).

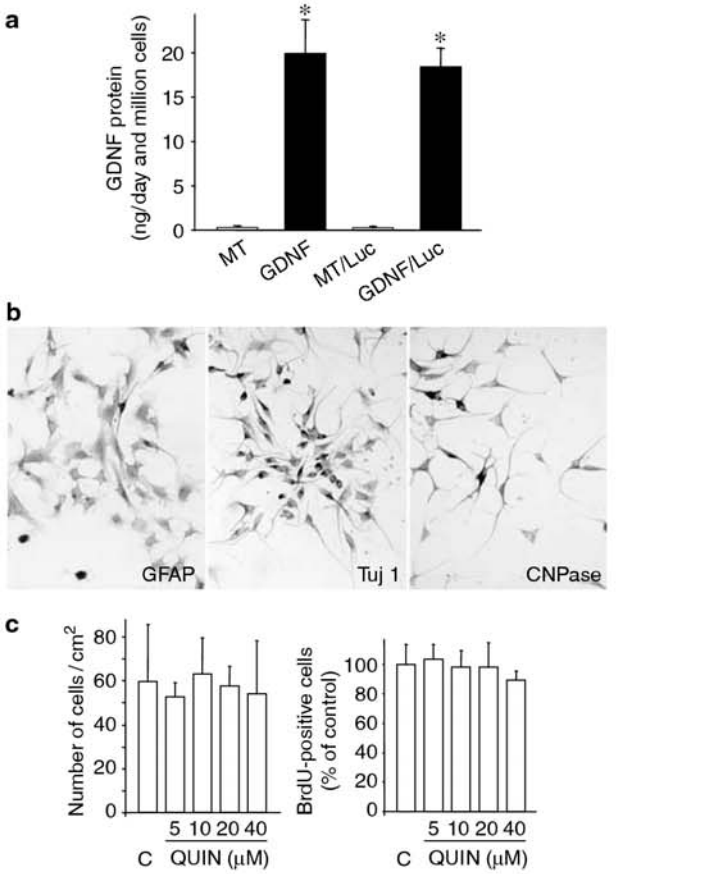

Figure 5 Expression of Luciferase and eGFP genes does not modify the GDNF-expression level in the NSC lines. (**a**) Comparison by ELISA analysis of the GDNF expression levels for eGFP-Luc-transduced, MT/Luc-NSC (MT/Luc), GDNF/Luc-NSC (GDNF/Luc) and non-transduced MT-NSC (MT) and GDNF-NSC (GDNF) cell lines. Values are expressed as ng of GDNF per 10^6 cells during 1 day (mean ± standard error of the mean (s.e.m.), $n=5$). Statistical analysis was performed using one-way ANOVA followed by the least significant differences (L.S.D.) *t post hoc* test, $^*P<0.01$. (**b**) *In vitro* culture in N2-supplemented medium showing *in vitro* differentiation of GDNF/Luc-NSCs to neurons (Tuj1), astrocytes (GFAP) and oligodendrocytes (CNPase). (**c**) The survival or proliferation of c17.2/Luc-NSCs treated with different doses of QUIN. Following the treatment with the indicated doses of QUIN, the number of cells/cm² as well as the number of BrdU-positive neurons/cm² was counted (Con.: Control, 0 μM QUIN).

To analyze the effects of NSCs in a QUIN model of HD, we first studied the effect of this *N*-methyl-D-aspartate (NMDA)-receptor agonist on cultures of c17.2/Luc-NSCs. QUIN treatment did not affect the viability and/or proliferation of c17.2/Luc-NSCs (Figure 5c). However, we observed differences in the behavior of c17.2/Luc-NSC implanted in QUIN-lesioned and non-lesioned striata. Mice were bilaterally grafted ($n=4$–5 per group) with GDNF/Luc-NSCs or MT/Luc-NSCs. The following day, left striata received an injection of QUIN and during the following 14 days the mice were monitored periodically by optical neuroimaging. The analysis revealed that light emission from both GDNF/Luc-NSCs and MT/Luc-NSCs was 59–69% higher in lesioned striata than in sham-treated (phosphate-buffered saline; PBS) ones (Figure 6a and b). This result was also confirmed by histological analysis, which showed higher numbers of eGFP-positive NSCs in QUIN-lesioned mice than in PBS-treated mice (Figure 6c and d; QUIN-mice, 272 ± 29% with respect to sham-treated mice, 100 ± 10%). In addition, the graft volume, measured 15 days after grafting, in QUIN-lesioned mice, was a 195 ± 0.1% larger than in PBS-injected mice (100 ± 6%). The analysis of cell proliferation at the second day post-engraftment showed that QUIN-lesioned mice had a proliferation rate of a 1575 ± 330% with respect to PBS-injected mice (100 ± 17%). However, no differences in proliferation capacity were detected by optical neuroimaging between GDNF/Luc-NSCs and MT/Luc-NSCs (data not shown). Taken together, these findings demonstrate that NSCs have a higher proliferation rate when transplanted into lesioned striata than in sham-operated controls. This effect cannot be attributed to a direct action of QUIN on NSCs, as we did not detect any effect of QUIN on NSCs in culture (Figure 5c).

We next tested whether QUIN lesion affected the fate of transplanted NSCs or the production of GDNF. We have previously described that GDNF-NSCs predominantly colocalize with CNPase staining, a marker for oligodendrocytes.[3] We now observe that while most of the GDNF/Luc-NSCs were also positive for CNPase

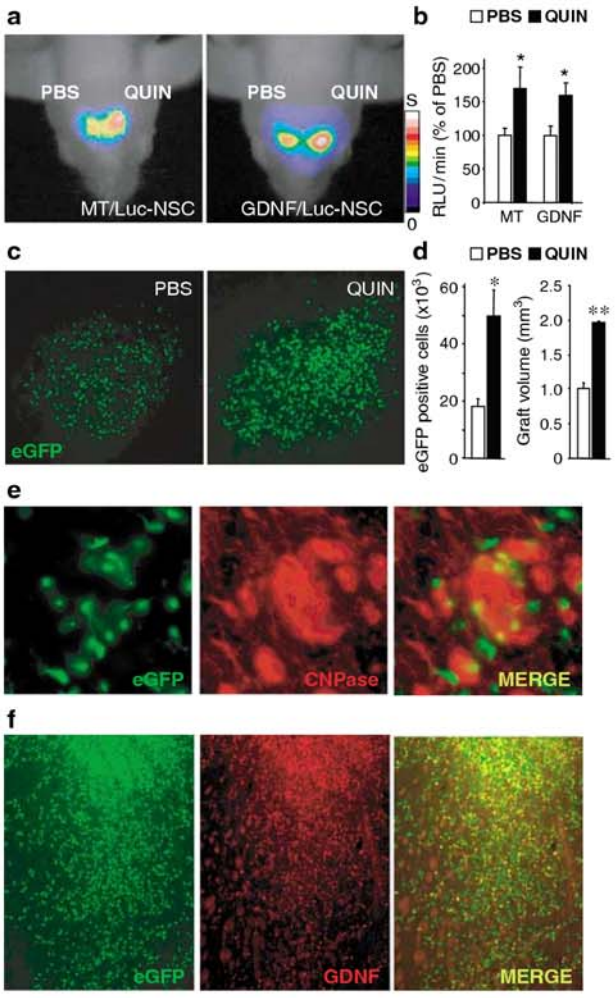

Figure 6 QUIN lesion of the striata induces proliferation of both MT/Luc-NSCs and GDNF/Luc-NSCs, but has no effect on cell fate or GDNF expression level. (**a**) *In vivo* optical neuroimages 15 days after cell implantation showing light production from MT/Luc-NSCs and GDNF/Luc-NSCs, in QUIN-lesioned striatum (QUIN; left hemisphere) and PBS-treated controls (PBS; right hemisphere). (**b**) Quantification of light events produced by MT/Luc-NSCs and GDNF/Luc-NSCs grafted in QUIN-lesioned than in PBS-treated mice. Results shown the mean of three mice, normalized to the average of the sham-treated hemispheres. Error bars represent the s.e.m. Statistical analysis was performed using one-way ANOVA followed by the L.S.D. *post hoc* test. $^{*}P<0.05$. (**c**) Morphological analysis of eGFP-positive NSCs in animals that received GDNF/Luc-NSCs, in the QUIN-lesioned (QUIN) and in the PBS-injected (PBS) striata. (**d**) Quantification of the total number of eGFP-positive GDNF/Luc-NSCs and the graft volume of QUIN- or PBS-treated hemispheres from (**d**). Results shown represent the mean of three mice and are normalized to the average of sham hemispheres. Error bars represent the s.e.m. Statistical analysis was performed using one-way ANOVA followed by the L.S.D. *post hoc* test. $^{*}P<0.05$, $^{**}P<0.005$. (**e**) Colocalization of implanted GDNF/Luc-NSCs and oligodendrocytic marker (CNPase), 14 days following a striatal lesion with QUIN. (**f**) Expression of GDNF by implanted GDNF/Luc-NSCs 14 days following striatal QUIN lesion.

immunolabeling after QUIN injection (Figure 6e), very few transplanted GDNF/Luc-NSCs had become neurons or astrocytes (data not shown). In addition, GDNF/Luc-NSCs maintained a high production of GDNF after grafting into the striatum, as was shown by double immunohistochemistry (Figure 6f).

GDNF/Luc-NSCs protect striatal neurons in a QUIN model of HD

The neuroprotective effect of GDNF/Luc-NSCs against intrastriatal injection of QUIN was tested by counting the number of neuronal nuclei (NeuN)-positive neurons 14 days after the lesion was induced (Figure 7). The injection of QUIN in non-grafted mice reduced the total number of striatal neurons to 14%, relative to non-lesioned mice (QUIN lesioned, 345.3 ± 49.3 cells/mm^2; non-lesioned, 2473.5 ± 311.8 cells/mm^2) (Figure 7). A similar reduction in the number of neurons was detected in striata transplanted with MT/Luc-NSCs before the QUIN-lesion, in which the number of NeuN-positive neurons was reduced to 16%, relative to non-injected striata (389.6 ± 59.2 cells/mm^2) (Figure 7). However, mice that received GDNF/Luc-NSCs 1 day before the QUIN-lesion showed a smaller reduction in the number of striatal neurons, and up to 27% of them were preserved, relative to non-injected controls (663.4 ± 66.5 cells/mm^2) (Figure 7). Thus, the number of protected striatal neurons after QUIN lesion in GDNF/Luc-NSCs-grafted mice is 190% higher than that observed in QUIN-lesioned mice, grafted or not with MT/Luc-NSC (663.4 in GDNF/Luc-NSCs vs 345.3 or 389.6 in non- or MT/Luc-NSC-grafted mice).

Intrastriatal grafting of GDNF/Luc-NSCs prevents behavior impairment induced by QUIN lesions

To determine whether the neuronal protective effects of GDNF/Luc-NSCs correlated with functional improvements, we assayed the grafted mice for amphetamine-stimulated circling behavior. Control mice that received a unilateral striatal QUIN lesion but no cell grafting showed asymmetric behavior after the i.p. administration of the dopaminergic indirect agonist. The number of net rotations was partially reduced by previous grafting of GDNF/Luc-NSCs (Figure 8). However, the protective effect was not observed in animals transplanted with MT/Luc-NSCs (Figure 8). The reduction in the number of net rotations in animals grafted with GDNF/Luc-NSCs was of 54.3+8.2% relative to non-grafted QUIN-lesioned mice and of 52.8+13.3% relative to MT/Luc-NSCs-grafted mice. Thus, our findings demonstrated that GDNF/Luc-NSCs partially prevent the behavioral deficits induced in the excitotoxic lesion model of HD.

Discussion

Studies using NSC transplants to remediate neurodegenerative disorders could benefit from the development of neuroimaging procedures to track cells implanted in the brain of living animal models. In the current work, we show that NSCs expressing luciferase implanted into the brain of nude mice can be tracked, quantified and characterized *in vivo* by neuroimaging of optical photons generated by the luciferase–luciferine reaction, without the need for skull and skin withdrawal. This technique allows the study of the neuroprotective effects of GDNF-overexpressing NSCs in the excitotoxic model of HD.

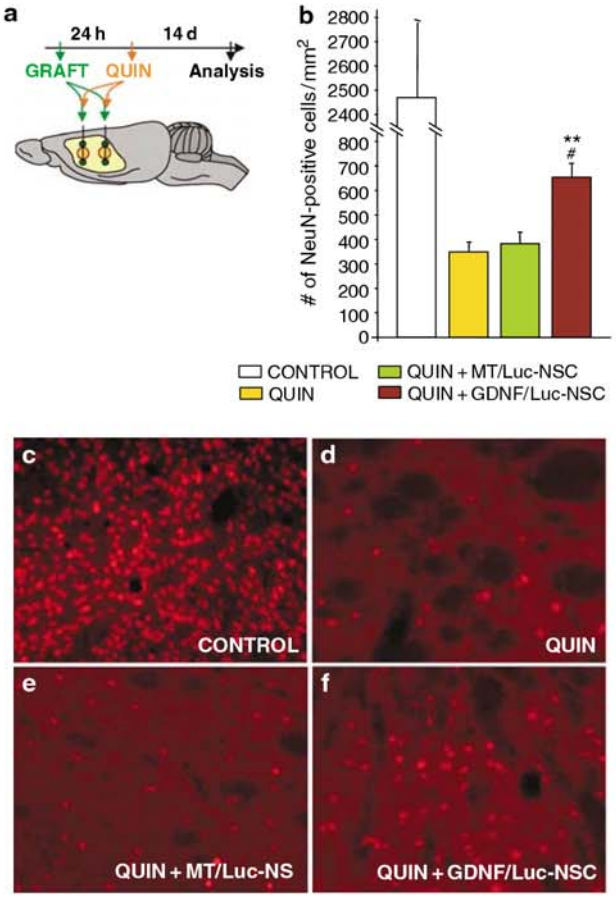

Figure 7 GDNF secreted by NSCs protect striatal neurons from excitotoxicity. (**a**) Schematic representation of NSC graft and QUIN-lesion strategy for neuroprotective studies. (**b**) Histogram showing the number of NeuN-positive cells in the brains of QUIN-lesioned mice treated or not with either non-expressing MT/Luc-NSCs or GDNF-expressing GDNF/Luc-NSCs, control mice receive no lesions. Results are expressed as the mean of six mice. Error bars represent the s.e.m. Statistical analysis was performed using one-way ANOVA followed by the L.S.D. *post hoc* test. $^{**}P<0.005$ relative to control, non-lesioned mice; $^{\#}P<0.05$ relative to QUIN. (**c**–**f**) Detection of NeuN-positive cells in the brains of mice 14 days after treatments: (**c**) ungrafted and non-lesioned; (**d**) ungrafted but QUIN-lesioned; (**e**) MT/Luc-NSCs grafted and QUIN-lesioned and (**f**) GDNF/Luc-NSC grafted and QUIN-lesioned.

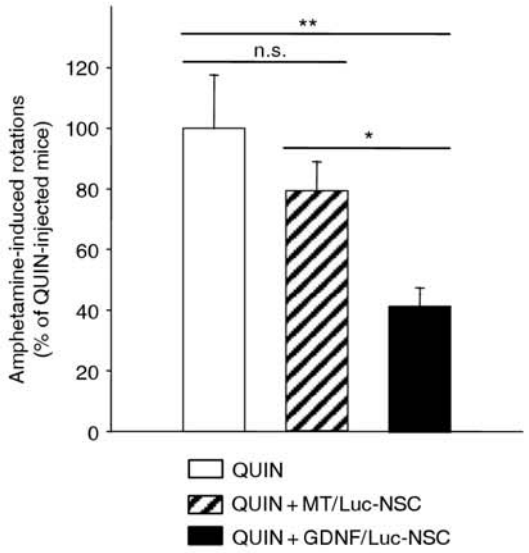

Figure 8 GDNF/Luc-NSCs grafting reverses the amphetamine-induced rotational behavior in QUIN lesions mice. Results are expressed as the mean of six mice. Error bars represent the s.e.m. Statistical analysis was performed using one-way ANOVA followed by the L.S.D. *post hoc* test. $^{*}P<0.05$; $^{**}P<0.005$ relative to QUIN-lesioned mice that received no cell implants.

GDNF protects striatal projection neurons and improves behavioral abnormalities.

Optical luminescent neuroimaging is a sensitive approach for the detection of implanted cells, which benefits from the absence of competing endogenous light-producing reactions in the brain. This method allowed us to detect a minimum number of about 500 intrastriatal grafted NSCs, a number slightly higher than that detected by other non-invasive techniques such as magnetic resonance imaging (MRI). Although Stroh *et al.*[19] reported the detection of approximately 10 magnetically labeled cells using MRI, this neuroimaging technique does not allow the quantification of transplanted cells or the evaluation of their proliferation capacity.[19] The advantage of luciferase labeling is that the number of light photons produced by the labeled cells can be used to determine their number. Thus, in the current experiments, the number of photons emitted by luciferase-expressing NSCs correlated linearly with the number of cells counted *in vitro*. *In vivo*, a similar linear correlation was shown between the amount of light recorded by the imaging system and the number of brain-engrafted NSCs stably expressing luciferase. Our findings also demonstrate a linear correlation between cell number estimates, calculated from light recorded by optical neuroimaging, and the results of independent stereological cell counts in the same animal.

Implanted NSCs showed migratory behavior, homing to the granular and glomerular cell layers of the olfactory bulb when they were grafted in the rostral migratory stream, the natural migratory pathway for NSCs of the subventricular zone. Therefore, optical bioluminescent imaging can be used as a quantitative method for tracking luciferase-expressing NSCs implanted in the brains of live animals.

Genetic markers also have additional advantages over other methods used for tracking stem cells *in vivo* such as magnetic particles for MRI. Exogenous non-replicating markers are diluted in the proliferating cell population and, what is more problematic; the label released by dead cells can be taken up again by neighboring cells when the tagged transplanted ones die. Keeping with this view, we have previously observed ^{3}H-thymidine-positive astrocytes in brains transplanted with dead pre-labeled cells, suggesting that endogenous brain cells acquire non-biodegradable markers (Canals, Akerud and Arenas, unpublished results). Importantly, while we observed that the expression of luciferase and eGFP genes does not alter the differentiation of NSCs *in vitro* and *in vivo*, it has been reported that differentiation of mesenchymal stem cells is altered after magnetic labeling.[20,21]

We next analyzed the cell behavior of the GDNF/Luc-NSCs when transplanted in a mouse excitotoxic model of

HD.[22] We show that expression of eGFP and luciferase genes did not affect the levels of GDNF expression, which were maintained after the cells had survived in the brain for at least a 15-day period. Similarly, the expression of eGFP and luciferase or the repetitive administration of luciferine and light emission analysis during the life of the mice did not modify the fate determination of these NSCs. In addition, *in vivo* optical imaging showed that NSCs transplanted in QUIN-lesioned striata proliferate more than cells transplanted into intact striata, a result corroborated by histological analysis of eGFP-expressing cells and in agreement with previously published data.[23] These proliferative responses is not a direct effect of QUIN on NSCs and suggest that the implanted cells are well integrated in brain tissue and respond to endogenous signals.

We finally demonstrated that transplanted GDNF/Luc-NSCs protect striatal neurons from excitotoxicity and partially reverse behavioral impairments in this severe mouse model of HD. We have previously described that GDNF and other trophic factors are good neuroprotective factors for HD.[5] As we show here and in previous work,[3] implanted GDNF/Luc-NSCs disperse widely in the striatum where, under the control of a mammalian promoter, express and administer GDNF for long periods of time. These results indicate that this strategy provides a suitable vehicle for delivery of neuroprotective factors, determinant in the treatment of this neurodegenerative disorder and useful as a tool for development of therapeutic approaches.

In conclusion, we find that optical neuroimaging can be advantageously used to sensitively detect and quantify cells implanted in the brain of live animals, allowing studies of their proliferation and homing behavior. What is more, we were able to show that NSCs-mediated release of GDNF protects striatal neurons and may constitute a useful therapeutic strategy in the treatment of HD.

Materials and methods

Cell culture and transduction

C17.2-NSCs and GDNFexpressing c17.2-NSCs (GDNF-NSC) or mock-transfected c17.2-NSCs (MT-NSC) were cultured as described previously by Akerud *et al*.[3] Cells in the proliferation state were transduced, as described Baum *et al*.,[24] with the retroviral construct peGFP-CMVluc, for expression of eGFP and *Photinus pyralis* luciferase (Luc). Positive eGFP-expressing cells, the top 2%, were purified by cell sorting using a fluorescence-activated cell sorting (FACS; MoFlo Flow Cytometer; Cytomation Inc., Fort Collins, CO, USA). The resulting cell pools, c17.2/Luc-NSC, GDNF/Luc-NSC and MT/Luc-NSC, respectively, were expanded in Dulbecco's modified Eagle's medium (DMEM; Gibco-BRL, Renfrewshire, Scotland, UK) supplemented with 10% fetal calf serum (Gibco-BRL), 5% horse serum (Gibco-BRL), and 2 mM glutamine (Sigma-Aldrich, Steinheim, Germany) in standard conditions (37°C, 5% CO_2). Cells were split (1:10) when they reached 80–90% of confluence.

To differentiate NSC lines *in vitro*, cells were grown for 1 week in N2-supplemented DMEM-F12 (1:1 mixture of F12 and DMEM containing: 10 ng/ml insulin, 100 μg/ml transferine, 100 mM putrescine, 20 nM progesterone, 30 nM selenium, 6 mg/ml glucose and 1 mg/ml bovine serum albumin (BSA)), in poly-D-lysine (Sigma-Aldrich)-coated dishes.

In order to analyze the proliferation rate in culture after QUIN administration, c17.2/Luc-NSCs were treated with different doses of QUIN (0, 5, 10, 20 or 40 μM) and 48 h later we perform an extended pulse of 5-bromodeoxyuridine (BrdU; Roche Diagnostics GmbH, Mannheim, Germany) as described elsewhere.[25] The mitotic marker was added to the culture at 3 μg/ml during a 24 h period and the cultures were fixed with 4% paraformaldehyde. After three washes with PBS, cells were treated with HCl 2 M for 30 min, followed by four washes in PBS. The cell cultures were then processed for immunocytochemistry for detection of BrdU using an anti-BrdU antibody (1:50; Dako A/S, Glostrup, Germany). Immunocytochemistries were counterstained with 4′,6-diamidino-2-phenylindole (DAPI; Sigma-Aldrich) to visualize and count the total number of cells.

Animal procedures

Nude mice (Swiss nu/nu; 25–35 g) were from Charles River Laboratories (Les Oncins, France). Nude mice were used because previous work had shown better cell survival in these animals,[3] because they do not produce immunological rejection. The animals were maintained with unlimited access to food and water, at constant temperature (19–22°C) and humidity (40–50%) on a 12:12 h light/dark cycle. All animal-related procedures were performed in accordance with the National Institute of Health Guide Lines for the care and use of laboratory animals, with the approval of the animal care committee of the University of Barcelona and the Generalitat de Catalunya.

For cell grafting, animals were anesthetized with pentobarbital (50 mg/kg i.p.), placed in a Stoelting stereotaxic apparatus (Wood Dale, IL) with the incisor bar at −3 mm. GDNF/Luc-NSC and MT/Luc-NSC cells in the actively growing phase were washed twice with Hank's Balanced Salt Solution, trypsinized and dissociated with a fire-polished Pasteur pipette, pelleted and then resuspended in DMEM at the indicated concentration. GDNF/Luc-NSC or MT/Luc-NSC were grafted in four locations at the following coordinates (in millimeters); anteroposterior (AP), +0.8 and +0.33; lateral (L), $\pm$1.8 and $\pm$2 from bregma and dorsoventral (DV), −2.55 and −2.75 from dura. Cell grafting was performed unilaterally or bilaterally as indicated. Cell viability was >95% at the end of the transplantation session, as determined by the trypan blue dye exclusion. At 1 day after the grafting procedure, mice were striatally lesioned with 2×0.5 μl of 10 mg/ml QUIN (20 nmols; Sigma-Aldrich) in the left hemisphere at the following coordinates; AP, +0.8 and +0.33; L, +1.8 and +2 from bregma and DV, −2.65 from dura.

To follow the proliferation of grafted NSCs, we treated three bilateral grafted mice with BrdU (50 mg/kg) 1 day following QUIN or PBS injection. After 24 h, mice were deeply anaesthetized in a CO_2 chamber and transcardially perfused with a 4% paraformaldehyde solution in 0.1 M sodium phosphate, pH 7.2. Brain tissue was post-fixed for 2 h in the same solution, cryoprotected with 10% sucrose in PBS and frozen in dry ice-cooled isopentane. Sections were treated with 2 M HCl

and processed for immunohistochemistry as describe Bosch *et al*.[25]

Three animals were grafted in the rostral migratory stream (AP, +1.5 and L, +0.7 from bregma; and DV −2.3 from dura) in order to examine the migration potential of NSCs.

Enzyme-linked immunosorbent assay (ELISA)

To study GDNF secretion, cells were cultured in 24-well plates for 24 h in differentiation medium. The medium was collected and the cells in each well were counted. GDNF contents was determined in 50 μl duplicates of cell culture supernatants, after a 1:1 dilution with block or sample buffer, using the Emax ImmunoAssay system (Promega, Madison, WI, USA), according to the manufacturer's instructions. Duplicates of serial dilutions containing recombinant GDNF (0–1000 pg/ml) were also analyzed in order to generate a standard curve. Results were expressed as ng of GDNF per 10^6 cells per day.

In vitro *luciferase assay*

Cell lysates were prepared by performing a one freeze–thaw cycle in Reporter Lysis Buffer (RLB; Promega). To generate light vs cell number standard curves and calculate the linear regression coefficient, luciferase-expressing NSCs were diluted serially from 10 to 10 000 cells and analyzed for light generation ($n=3$). Luciferase activity in cells was measured by chemiluminescence, using the standard luciferase assay kit (Promega). Light production was measured using a Turner Designs luminometer model TD 20/20, after the addition of 100 μl of luciferase assay reagent (Promega) to 20 μl of cell lysate. Light detector measurements were expressed in RLU.

Non-invasive *in vivo* optical imaging was performed using a high-sensitive CCD camera (ORCA-2BT Imaging System; Hammamatsu Photonics). To correlate the recorded light intensities with the numbers of cells, standard curves were generated by measuring light produced by 100 to 10 000 cell serial dilutions in 24-well plates ($n=6$). Images were captured, using the ORCA-2BT system.

In vivo *optical neuroimaging*

In vivo optical neuroimaging of intrastriatally grafted nude mice was performed as described previously by El Hilali *et al*.[16] Mice were anesthetized with a mixture of droperidol (Roche, Basel, Switzerland) 6 mg/kg and midazolam (Rovi S.A., Madrid, Spain) 12 mg/kg. For imaging, the mice were i.p. or i.v. inoculated with 150 μl of an aqueous solution of D-luciferine (100 mg/kg; Promega) and placed at 247 mm distance from the camera objective in the detection chamber of a high-efficiency ORCA-2BT Imaging System, Hammamatsu Photonics) provided with a C4742-98-LWG-MOD camera and a 512 × 512 pixel, charge-couple device (CCD) cooled at −80°C. Images were acquired during 1 min period, routinely starting 4 min after luciferine administration. Light measurements were expressed as RLUs. Immediately after image acquisition, while the animal remained in the same position, another image of the animal was obtained using an ambient light. As indicated in some experiments, to increase detection sensitivity, the reading noise of the recorded signal was reduced by an 8 × 8 binning of the camera CCD. Quantification and analysis of photons recorded in images was carried out using the WASABI image analysis software (Hammamatsu Photonics). The Orca system records absolute light events detected by the CCD in the image memory. The gray scale/color values displayed by the WASABI image processing software are chosen to best represent the range of values in the image memory. This necessity arises from the fact that computer monitors cannot display accurately the complete range of values that the image memory can store. However, the scale is always the same within the experiment. Thus, a given color in an image always represents the same range of light intensity recorded by the Orca system CCD output.

In order to establish the correlation between the number of transplanted cells and the emitted light, a standard curve was generated by grafting predetermined numbers of c17.2/Luc-NSCs in the brains of mice ($n=4$). Data are represented as the number of RLUs vs number of grafted cells. The slope of the linear regression curve is the number of *in vivo* RLU/min per transplanted cell.

Immunostaning

C17.2/Luc-NSC, GDNF/Luc-NSC or MT/Luc-NSC were induced to differentiate *in vitro* on glass cover slips using non-mitotic medium, N_2. After 7 days of culture, cells were fixed with 4% paraformaldehyde in PBS for 45 min at room temperature. Immunostaining was performed as described elsewhere.[25] In brief, samples were incubated for 30 min with PBS containing 0.3% Triton X-100 and 30% normal horse serum (NHS; Gibco-BRL). Thereafter, the cover slips were incubated overnight at 4°C in PBS containing 0.3% Triton X-100 and 5% NHS, and the corresponding primary antibodies. The following antibodies and dilutions were used: anti-GFAP (glial fibrillary acidic protein; 1:400; Sigma-Aldrich), anti-Tuj1 (1:250; Sigma-Aldrich), anti-CNPase (1:250, Chemicon, Temecula, CA, USA). Following three washes with PBS, the cultures were incubated for 2 h at room temperature with the appropriate biotinylated secondary antibody. The signal was developed using the avidin–biotin complex procedure (ABC; Pierce, Rockford, IL, USA), and finally visualized with 3,3′-diaminobenzidine.

For immunohistochemistry, at day 15 post implantation, nude mice were deeply anaesthetized in a CO_2 chamber and transcardially perfused with a 4% paraformaldehyde solution in 0.1 M sodium phosphate, pH 7.2. Brain tissue was post-fixed for 2 h in the same solution, cryoprotected with 10% sucrose in PBS and frozen in dry ice-cooled isopentane. Serial coronal cryostat sections (30 μm thick) through the whole striatum were collected as free-floating in PBS and processed for immunohistochemistry as described elsewhere.[25] After three rinses with PBS, slices were incubated with NH_4Cl 50 mM to reduce background autofluorescence. Tissue was permeabilized with PBS-T buffer (PBS containing 0.3% Triton X-100, 1.5% NHS and 1% BSA) at room temperature for 1 h. After washing in PBS, the slices were incubated overnight at 4°C with the corresponding primary antibodies and dilutions: anti-GFAP (1:400; Sigma-Aldrich), anti-NeuN (1:100; Chemicon), anti-CNPase (1:250, Chemicon), anti-GDNF (1:20, R&D Systems, Inc., Minneapolis, MN, USA), which were combined with the anti-GFP (1:400; Abcam Ltd, Cambridge, UK) to detect the transplanted cells. Samples were then incubated for 2 h at room temperature with

the appropriate secondary antibody: FITC-conjugated anti-rabbit (1:100; Vector laboratories, Burlingame, CA, USA) and Texas Red-conjugated anti-mouse (1:200; Jackson Immunoresearch Laboratories Inc., West Grove, PE, USA). Tissue sections were mounted with Mowiol (Calbiochem, Darmstadt, Germany) and visualized using a fluorescent microscope. No signal was detected in controls in which the primary antibodies were omitted.

Stereological cell counting

All cell counts were performed using a blind-coded procedure. In cell cultures, DAPI-positive nuclei were counted as the total number of cells. Total cell number and BrdU-positive neurons were counted after fluorescent immunocytochemistry in four independent cultures. Several fields comprising 5% of the cover slip surface were randomly chosen using the Computer Assisted Stereology Toolbox (CAST) software (Olympus Danmark A/S, Ballerup, Denmark), and the numbers of positive cells were counted for each staining.

In order to correlate light recorded by optical neuroimaging with the number of transplanted cells in the same animal, eGFP-expressing cells were counted using a stereological method. Light emission was first recorded using the Orca system as described above. At 2 h after imaging, the animals were processed for immunohistochemistry, also as described, and eGFP-positive cells were counted ($n=8$). Only cells showing a clear eGFP-positive cytoplasm were counted as positive. Unbiased stereological counts were obtained from the entire graft using the CAST software (Olympus Danmark A/S) as described previously by Canals *et al*.[26] The amount of light recorded from each animal, expressed as RLU/min, was plotted vs the number of eGFP-positive NSCs counted. To analyze the graft volume, the area including the eGFP-positive NSCs in each section was outlined and the volume was calculated by multiplying the sum of all the outlined areas (square millimeters) by the distance between successive sections (0.3 mm).

BrdU-positive cells were counted in the selected graft area using the stereological dissector (CAST, Olympus Danmark A/S). Results were expressed as the average of three mice per condition tested and normalized to the mean of sham-grafted mice.

To count the spared striatal neurons after QUIN lesion in grafted and non-grafted mice, we performed a double immunohistochemistry for NeuN and eGFP ($n=6$). NeuN-positive cells in overall striatum area were counted as described previously by Canals *et al*.[26] The few cells that were simultaneously positive for NeuN and eGFP were excluded from the cell counts. Stereological counts were obtained from the entire neostriatum using the CAST software (Olympus Danmark A/S). The dissector counting method was employed to analyze coronal sections spaced 98 μm apart. The counted frames were randomly sampled.

Behavioral measurements

Turning behavioral testing was performed 14 days after striatal QUIN-induced lesions in mice grafted unilaterally with GDNF/Luc-NSC or MT/Luc-NSC and in non-grafted animals. Groups of mice grafted with GDNF/Luc-NSCs or MT/Luc-NSCs, and non-grafted mice were mixed and data were recorded using a blind procedure. Mice were injected i.p. with amphetamine (2.5 mg/kg) to induce turning behavior as described previously by Akerud *et al*.[3] At 20 min after injection, the number of rotations was scored during 5 min. Values were expressed as the number of full turns, and were normalized relative to the average number of turns of non-grafted QUIN-lesioned mice.

Acknowledgements

We thank M Teresa Muñoz and Ana López for technical assistance, and Dr Jaume Comas from the Cell Separation Unit of the Serveis Científico-Tècnics (Universitat de Barcelona) for their support and advice with the cell sorting procedures We thank Dr Evan Y Snyder for the generous gift of the c17.2 cell line. We are also grateful to Dr Amèrica Jiménez and the staff of the animal facility (Facultat de Medicina, Universitat de Barcelona) for their help with mice care. This study was supported by grants from the Ministerio de Educación y Ciencia (SAF2005-01335, JA; SAF2005-00147, JMC; Spain), the Ministerio de Sanidad y Consumo (Redes Temáticas de Investigación Coorporativa: G03/167 and G03/210 and FIS: PI040659; Spain), Fundació La Caixa (Spain) and the Network of excellence for Diagnostic Molecular Imaging (DiMI; Sixth Framework, European Community). JRP is a fellow from the Spanish Ministerio de Educación y Ciencia and NU is a fellow from CIRIT, Generalitat de Catalunya (Spain).

References

1 Arenas E. Stem cells in the treatment of Parkinson's disease. *Brain Res Bull* 2002; **57**: 795–808.
2 Alberch J, Perez-Navarro E, Canals JM. Neuroprotection by neurotrophins and GDNF family members in the excitotoxic model of Huntington's disease. *Brain Res Bull* 2002; **57**: 817–822.
3 Akerud P, Canals JM, Snyder EY, Arenas E. Neuroprotection through delivery of glial cell line-derived neurotrophic factor by neural stem cells in a mouse model of Parkinson's disease. *J Neurosci* 2001; **21**: 8108–8118.
4 Pochon NA, Menoud A, Tseng JL, Zurn AD, Aebischer P. Neuronal GDNF expression in the adult rat nervous system identified by *in situ* hybridization. *Eur J Neurosci* 1997; **9**: 463–471.
5 Alberch J, Perez-Navarro E, Canals JM. Neurotrophic factors in Huntington's disease. *Prog Brain Res* 2004; **146**: 195–229.
6 Enomoto H. Regulation of neural development by glial cell line-derived neurotrophic factor family ligands. *Anat Sci Int* 2005; **80**: 42–52.
7 Airaksinen MS, Saarma M. The GDNF family: signalling, biological functions and therapeutic value. *Nat Rev Neurosci* 2002; **3**: 383–394.
8 Marco S, Canudas AM, Canals JM, Gavalda N, Perez-Navarro E, Alberch J. Excitatory amino acids differentially regulate the expression of GDNF, neurturin, and their receptors in the adult rat striatum. *Exp Neurol* 2002; **174**: 243–252.
9 Perez-Navarro E, Arenas E, Reiriz J, Calvo N, Alberch J. Glial cell line-derived neurotrophic factor protects striatal calbindin-immunoreactive neurons from excitotoxic damage. *Neuroscience* 1996; **75**: 345–352.
10 Perez-Navarro E, Arenas E, Marco S, Alberch J. Intrastriatal grafting of a GDNF-producing cell line protects striatonigral neurons from quinolinic acid excitotoxicity *in vivo*. *Eur J Neurosci* 1999; **11**: 241–249.

11 Araujo DM, Hilt DC. Glial cell line-derived neurotrophic factor attenuates the excitotoxin-induced behavioral and neurochemical deficits in a rodent model of Huntington's disease. *Neuroscience* 1997; **81**: 1099–1110.
12 Hoffman D, Breakefield XO, Short MP, Aebischer P. Transplantation of a polymer-encapsulated cell line genetically engineered to release NGF. *Exp Neurol* 1993; **122**: 100–106.
13 Sala-Newby GB, Kendall JM, Jones H, Taylor KM, Badminton MN, Llewellyn DH, Campbell AK. Bioluminescent and chemiluminescent indicators for molecular signaling and function in living cells. In: Mason WT (ed). *Fluorescent and Luminescent Probes for Biological Activity: a Practical Guide to Technology for Quantitative Real-Time Analysis (Biological Techniques)*. Academic Press: London, 1996, pp 58–82.
14 Rubio N, Villacampa MM, El HN, Blanco J. Metastatic burden in nude mice organs measured using prostate tumor PC-3 cells expressing the luciferase gene as a quantifiable tumor cell marker. *Prostate* 2000; **44**: 133–143.
15 Massoud TF, Gambhir SS. Molecular imaging in living subjects: seeing fundamental biological processes in a new light. *Genes Dev* 2003; **17**: 545–580.
16 El Hilali N, Rubio N, Martinez-Villacampa M, Blanco J. Combined noninvasive imaging and luminometric quantification of luciferase-labeled human prostate tumors and metastases. *Lab Invest* 2002; **82**: 1563–1571.
17 Rubio N, Villacampa MM, Blanco J. Traffic to lymph nodes of PC-3 prostate tumor cells in nude mice visualized using the luciferase gene as a tumor cell marker. *Lab Invest* 1998; **78**: 1315–1325.
18 Avarez-Buylla A, Garcia-Verdugo JM. Neurogenesis in adult subventricular zone. *J Neurosci* 2002; **22**: 629–634.
19 Stroh A, Faber C, Neuberger T, Lorenz P, Sieland K, Jakob PM *et al*. *In vivo* detection limits of magnetically labeled embryonic stem cells in the rat brain using high-field (17.6T) magnetic resonance imaging. *Neuroimage* 2005; **24**: 635–645.
20 Kostura L, Kraitchman DL, Mackay AM, Pittenger MF, Bulte JW. Feridex labeling of mesenchymal stem cells inhibits chondrogenesis but not adipogenesis or osteogenesis. *NMR Biomed* 2004; **17**: 513–517.
21 Bulte JW, Kraitchman DL, Mackay AM, Pittenger MF. Chondrogenic differentiation of mesenchymal stem cells is inhibited after magnetic labeling with ferumoxides. *Blood* 2004; **104**: 3410–3412.
22 Beal MF, Ferrante RJ, Swartz KJ, Kowall NW. Chronic quinolinic acid lesions in rats closely resemble Huntington's disease. *J Neurosci* 1991; **11**: 1649–1659.
23 Lundberg C, Martinez-Serrano A, Cattaneo E, McKay RD, Bjorklund A. Survival, integration, and differentiation of neural stem cell lines after transplantation to the adult rat striatum. *Exp Neurol* 1997; **145**: 342–360.
24 Baum C, Hegewisch-Becker S, Eckert HG, Stocking C, Ostertag W. Novel retroviral vectors for efficient expression of the multidrug resistance (mdr-1) gene in early hematopoietic cells. *J Virol* 1995; **69**: 7541–7547.
25 Bosch M, Pineda JR, Sunol C, Petriz J, Cattaneo E, Alberch J *et al*. Induction of GABAergic phenotype in a neural stem cell line for transplantation in an excitotoxic model of Huntington's disease. *Exp Neurol* 2004; **190**: 42–58.
26 Canals JM, Pineda JR, Torres-Peraza JF, Bosch M, Martin-Ibanez R, Munoz MT *et al*. Brain-derived neurotrophic factor regulates the onset and severity of motor dysfunction associated with enkephalinergic neuronal degeneration in Huntington's disease. *J Neurosci* 2004; **24**: 7727–7739.

Quinto trabajo

"Induction of GABAergic phenotype in a neural stem cell line for transplantation in an excitotoxic model of Huntington's disease"

Publicado en *Experimental Neurology*

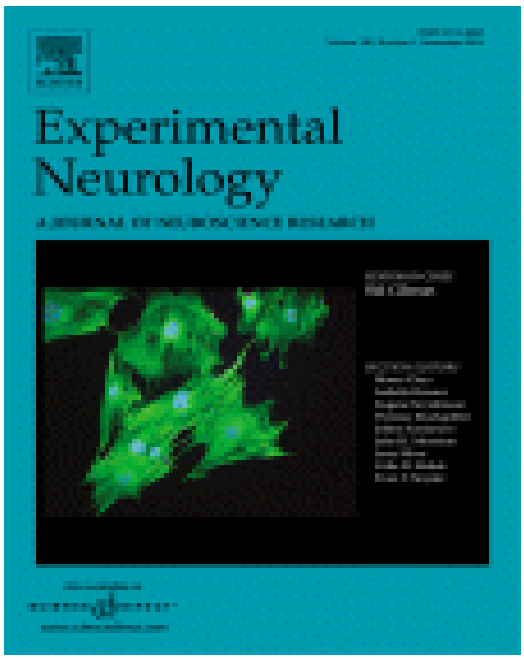

Available online at www.sciencedirect.com

SCIENCE DIRECT

Experimental Neurology 190 (2004) 42–58

Experimental Neurology

www.elsevier.com/locate/yexnr

Induction of GABAergic phenotype in a neural stem cell line for transplantation in an excitotoxic model of Huntington's disease

Miquel Bosch[a], José R. Pineda[a], Cristina Suñol[b], Jordi Petriz[c], Elena Cattaneo[d], Jordi Alberch[a], Josep M. Canals[a,*]

[a]*Departament de Biologia Cel·lular i Anatomia Patològica, Facultat de Medicina, Institut d'Investigacions Biomèdiques August Pi i Sunyer (IDIBAPS), Universitat de Barcelona, E-08036 Barcelona, Spain*

[b]*Department of Neurochemistry, Institut d'Investigacions Biomèdiques de Barcelona, Consejo Superior de Investigaciones Cientificas, CSIC-IDIBAPS, E-08036 Barcelona, Spain*

[c]*Àrea de Criopreservació, Hospital Clinic, IDIBAPS, E-08036 Barcelona, Spain*

[d]*Department of Pharmacological Sciences, Center of Excellence on Neurodegenerative Diseases, University of Milan, Milan, Italy*

Received 27 April 2004; revised 16 June 2004; accepted 22 June 2004

Abstract

The implementation of cell replacement therapies for Huntington's disease using multipotent neural stem cells (NSCs) requires the specific differentiation into γ-aminobutyric acid (GABA) neuronal subtype before transplantation. Here we present an efficient culture procedure that induces stable GABAergic neurons from the immortalized striatal neural stem cell line ST14A. This process requires sequential retinoic acid treatment and KCl depolarization. Initial addition of 10 μM retinoic acid increased cell survival and promoted neuronal differentiation. Subsequent stimulation with 40 mM KCl induced specific differentiation into GABAergic neurons, yielding 74% of total cultured cells. KCl-evoked Ca^{2+} influx reduced cell proliferation and nestin expression, and induced neurite outgrowth and GABAergic markers as well as GABA contents, release, and uptake. Characterization of the integration, survival, and phenotype of these predifferentiated GABAergic neurons following transplantation into the adult brain in a model of Huntington's disease revealed long-term survival in quinolinate-lesioned striata. Under these conditions, cells maintained their GABAergic phenotype and elaborated neurite processes with synaptic contacts with endogenous neurons. In conclusion, we have generated a homogeneous population of functional GABAergic neurons from a neural stem cell line, which survive and maintain their acquired fate in vivo. These data may lend support to the possibility of cell replacement therapies for Huntington's disease using neural stem cells.

Keywords: Cell replacement; GABA; Differentiation; Retinoic acid; KCl; GABA release; GABA uptake; Striatum

Introduction

Cell replacement therapies are currently being proposed for the treatment of a wide variety of diseases characterized by the loss of a specific cellular subtype, including diabetes, cardiomyopathies, and neurodegenerative disorders. Several clinical trials using implantation of fetal cells have already been performed in patients suffering from Parkinson's and Huntington's disease (HD) (for review, see Bjorklund and Lindvall, 2000; Watts and Dunnett, 2000). However, the use of human fetal tissue for cell therapy implies some technical and ethical concerns. Consequently, the use of neural stem cells (NSCs) from different origins is currently under intense investigation (Arenas, 2002; Baetge, 1993; Rossi and Cattaneo, 2002). Transplantation of undifferentiated NSCs into adult hosts results in good survival and

* Corresponding author. Departament de Biologia Cel·lular i Anatomia Patològica, Facultat de Medicina, Institut d'Investigacions Biomèdiques August Pi i Sunyer (IDIBAPS), Universitat de Barcelona, Casanova 143, E-08036 Barcelona, Spain. Fax: +34 934 021 907.

E-mail address: jmcanals@ub.edu (J.M. Canals).

0014-4886/$ - see front matter © 2004 Elsevier Inc. All rights reserved.
doi:10.1016/j.expneurol.2004.06.027

integration. However, control of their fate determination is poor and very few neurons are generated, with even less of the desired phenotype (Lundberg et al., 1997; Martinez-Serrano and Bjorklund, 1997; Rubio et al., 2000; Snyder et al., 1997). Thus, it appears necessary to control the process of differentiation before cell replacement therapy. In vitro predifferentiated dopaminergic cells from NSCs and embryonic stem cells have successfully been transplanted in models of Parkinson's disease (Barberi et al., 2003; Kim et al., 2002; Wagner et al., 1999). However, there is currently no data relating to transplantation of differentiated NSCs for HD.

HD is a hereditary neurodegenerative disorder caused by a CAG expansion within the huntingtin gene (The Huntington's Disease Collaborative Research Group, 1993). This mutation leads to selective death of GABAergic projection neurons in the striatum (Vonsattel and DiFiglia, 1998). Glutamate is the main excitatory input to these striatal projection neurons. It has been postulated that excessive stimulation of *N*-Methyl-D-aspartate (NMDA)-glutamate receptors is involved in the pathophysiology of this movement disorder. In fact, overstimulation of the NMDA receptor with agonists such as quinolinate (QA) has been extensively used to reproduce the biochemical deficits observed in Huntington's disease (Beal et al., 1991). To date, there is no effective treatment to stop or reverse the progression of HD. Intrastriatal transplantation of GABAergic neurons might replace the population of lost cells and recover the functionality of the damaged circuit (Bjorklund and Lindvall, 2000). Striatal GABAergic projection neurons arise from the lateral ganglionic eminence located in the subventricular zone of the developing telencephalon (Campbell, 2003). However, little is known about the signals and molecular mechanisms controlling their differentiation and generation. Intrinsic cues are characterized by spatial and temporally restricted expression of developmental control genes (Campbell, 2003; Hamasaki et al., 2003; Jain et al., 2001; Redies et al., 2002). Striatal precursors also respond to epigenetic factors in specific temporal windows. Previous in vitro studies have suggested that neuronal activity (Ciccolini et al., 2003; Gu and Spitzer, 1995; Patz et al., 2003; Watt et al., 2000) and neurotrophins (Barberi et al., 2003; Mizuno et al., 1994; Yamada et al., 2002) could also play an important role in the acquisition and maturation of GABAergic phenotype.

In the present work, we have induced the differentiation of GABAergic neurons in vitro for transplantation into QA-lesioned rat striata. For this purpose, we used the ST14A NSC line, which was generated by immortalization of striatal progenitor cells at embryonic day (E) 14 with a temperature-sensitive oncogene (Cattaneo and Conti, 1998). We promoted the GABAergic phenotype by sequential exposure to epigenetic signals. Addition of retinoic acid (RA) followed by a KCl-driven depolarization generated a homogeneous population of functional GABAergic neurons. These differentiated NSCs survive for at least 7 months and stably maintain their neuronal and GABAergic phenotype after transplantation.

Materials and methods

Cell culture and differentiation protocol

We used a clone of the ST14A cell line, retrovirally transduced with the PINCO vector, which expresses the enhanced green fluorescent protein (EGFP) (Conti et al., 2001). Cells were grown at the permissive temperature of 33 °C in Dulbecco's Modified Eagle Medium (DMEM; Gibco-BRL, Renfrewshire, Scotland, UK) supplemented with 10% fetal calf serum (FCS; Gibco-BRL), as previously described (Cattaneo and Conti, 1998). To induce differentiation, cells were seeded at 39 °C at a density of 2.5×10^4 cells/cm^2 on coverslips precoated with 0.002% poly-ornithine (Sigma, St Louis, MO, USA) in 24-well plates. N2-supplemented MEM-F12 (Gibco-BRL) was used to plate the cells under serum-free conditions. In these culture conditions, we tested the caspase inhibitor z-VAD-FMK (50–100 μM; Calbiochem, San Diego, CA), mitogenic factors, such as epidermal growth factor (EGF; 10 mg/ml; Promega, Madison, WI) and basic or acidic fibroblast growth factor (aFGF and bFGF; 20–40 mg/ml; Promega), and neurotrophic factors [brain-derived neurotrophic factor (BDNF), neurotrophin-3 (NT-3), glial-derived neurotrophic factor (GDNF), or neurturin (NTRN); 10 or 50 ng/ml; Preprotech EC Ltd., London, UK] for survival improvement at the non-permissive temperature of 39 °C.

In some experiments, ST14A cells were co-cultured with postnatal day 1 striatal astrocytes or cultured with astrocyte-conditioned medium. Purification of these rat glial cells from the striatum was performed according to a standard protocol (McCarthy and de Vellis, 1980). After replating, astrocytes were grown to confluence in serum-containing medium and changed to N2-supplemented MEM-F12. After 4 days in vitro (DIV), or simultaneously, co-cultures were initiated in this medium as previously described (Wagner et al., 1999). Alternatively, ST14A cells were cultured in conditioned medium from 4 DIV-confluent astrocyte cultures.

For minimal serum condition assays, ST14A cells were plated in B27-MEM medium (Gibco-BRL) supplemented with 1% FCS at 39 °C. This medium was removed after 2 DIV and replaced with N2-supplemented MEM-F12 medium containing 0.5% FCS. Some cells were maintained in these culture conditions, which we will refer as 'basal-conditioned medium', until DIV 15. To assay neuronal differentiation, we added all-trans RA (10 μM; Sigma) to basal-conditioned medium from DIV 2 to 7 (Fig. 1A). Five days later (DIV 7), this medium was changed to N2-0.5% FCS, with or without the addition of KCl (40 mM; Merck,

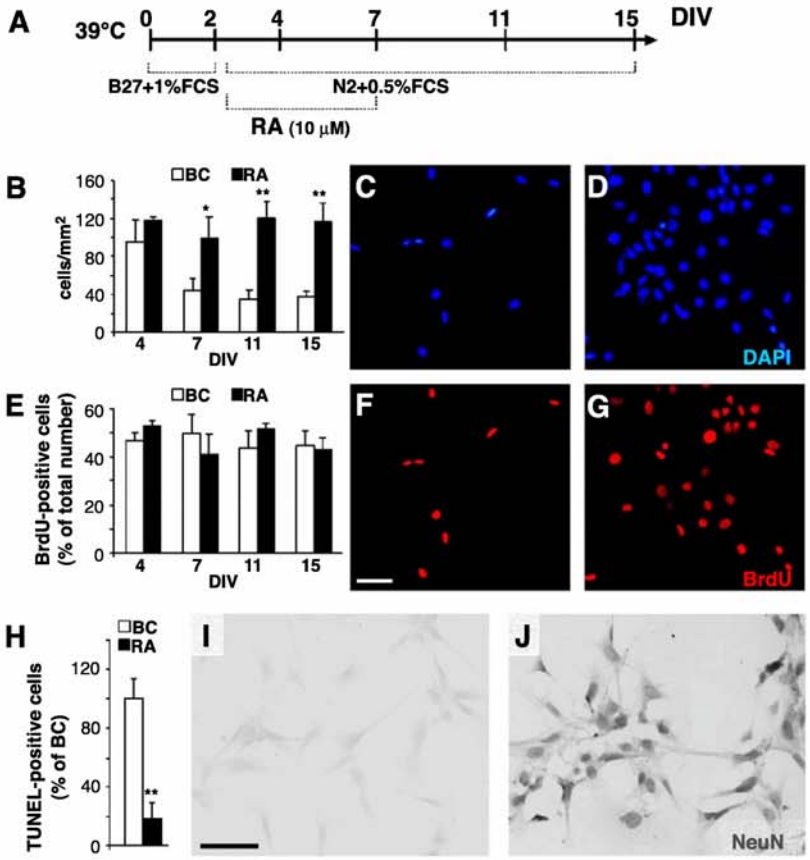

Fig. 1. Retinoic acid improves cell survival and induces neuronal phenotype in ST14A cells. (A) Scheme of the in vitro culture conditions for the differentiation of ST14A NSCs at 39°C. RA (10 μM) was added to the basal-conditioned medium from 2 to 7 DIV. (B) RA increases cell number at 7, 11, and 15 DIV with respect to basal-conditioned medium (BC) cultures. (C and D) Representative fluorescent photomicrographs showing DAPI staining of basal cultures (C) or RA-treated cultures (D) at 15 DIV. (E) The increase in cell number is not due to an increased rate of proliferation, because the number of cells that incorporate BrdU does not change in any of the conditions. (F and G) Photomicrographs from the same field as C and D show BrdU-immunostained nuclei in basal-conditioned medium (F) or in RA-treated cultures (G). (H) The differences in the number of cells between RA-treated (RA) and nontreated cultures (BC) are related to a reduction of cell death in RA-treated cells. (I–J) RA treatment also increases immunostaining for the mature neuronal marker NeuN at 7 DIV in almost all cells in the culture (J). This increase is not detected in basal-conditioned medium (I). $*P < 0.05$, $**P < 0.005$ with respect to basal cultures. Scale bars represent 40 μm.

Barcelona, Spain), BDNF, NT-3, GDNF, or NTRN (all at 50 ng/ml; Preprotech EC Ltd.; Fig 2A). To assay the time course of the KCl effect, in some cultures 40 mM KCl medium was replaced with basal-conditioned medium at DIV 8, 9, or 11. In controls, KCl was added to non-RA-treated cultures at DIV 7. At 15 DIV, cells from all culture conditions were fixed and processed for morphological analyses.

Intracellular Ca^{2+} determination

Cells were plated on poly-ornithine-precoated 1.8 cm^2 surface-area-chambered cover glasses (Lab-Tek Nalge Nunc International) at 2.5×10^4 cells/cm^2 and cultured according to the RA differentiation protocol or the basal-conditioned medium. At 7 DIV, cells were rinsed and incubated with 2 μM Fluo-4 acetoxymethyl ester and 0.02% Pluronic acid (Molecular Probes, Leiden, The Netherlands) in basal-conditioned medium for 30 min at room temperature. Three 5-min rinses in basal-conditioned medium were performed at 37°C to allow hydrolysis of the ester. Intracellular Ca^{2+} levels were measured in individual cell bodies at 39°C using a Leica TCS SL laser-scanning confocal spectral microscope (Leica Microsystems Heidelberg GmbH, Manheim, Germany) with Argon and HeNe lasers attached to a Leica DMIRE2 inverted microscope equipped with an incubation system with temperature and CO_2 control. Images were acquired using a 63× oil immersion objective lens (NA 1.32), 488 nm laser line, excitation beam splitter RSP 500, and emission range detection at 500–600 nm, and processed using the Image Processing Leica Confocal Software. For depolarization experiments, images were recorded every 5 s over a 10-min period. At 110 s, KCl was added to a concentration of 40 mM. Calcium concentration was calculated as described elsewhere (Kao et al., 1989), assuming a K_d of 345 nM. F_{max} values were obtained in

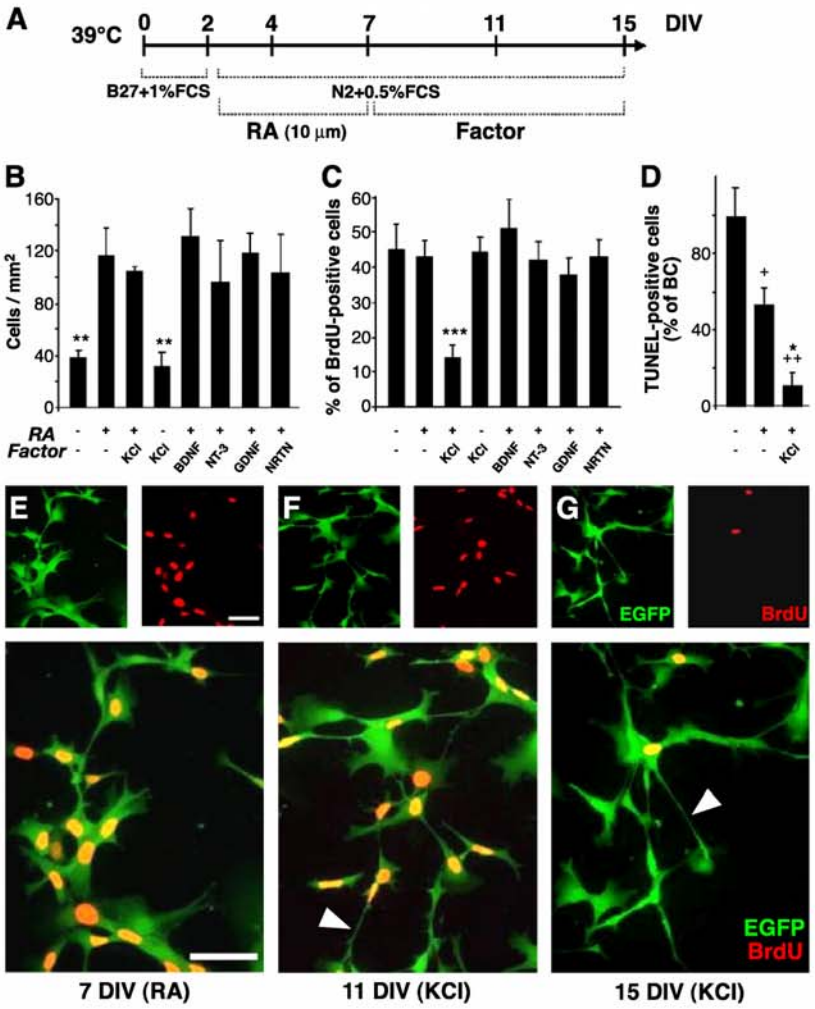

Fig. 2. Addition of 40 mM KCl decreases cell proliferation. (A) Sequential treatment was applied to ST14A cultures: each tested factor was added from 7 to 15 DIV after 5 days of RA treatment. (B) None of the assayed factors change the number of cells with respect to RA treatment at 15 DIV. (C) Addition of 40 mM KCl significantly reduces the number of BrdU-positive cells at 15 DIV, whereas neurotrophic factors (50 ng/ml) have no effect. (D) At this culture stage, treatment with RA alone reduces cell death in a 47% and the sequential treatment with RA and KCl decreases the number of dying cells in a 89%. (E–G) Fluorescence photomicrographs of EGFP and BrdU immunostaining showing the reduction in the number of proliferative cells observed at 15 DIV (G). KCl also promotes the outgrowth of neurite-like processes (arrowheads) at 11 DIV (F) and 15 DIV (G). $^{+}P < 0.05$, $^{++}P < 0.005$ respect to basal-conditioned medium; $*P < 0.05$, $**P < 0.005$, $***P < 0.001$ with respect to RA treatment. Scale bars represent 40 μm.

the presence of 50 μM ionomycin and F_{min} after addition of 15 mM EGTA. All values were normalized with respect to initial baseline intensity and the endogenous EGFP fluorescence was subtracted in each cell body analyzed. Other calcium indicators with emissions different from that of EGFP were discarded due to the high degree of compartmentalization. Fluo-4 emission upon Ca^{2+} binding was sufficiently intense to detect changes in calcium concentrations above the EGFP signal. To analyze the long-term effects of KCl on the elaboration of neurites, images were captured every 20 s over a period of five consecutive hours after depolarization.

To block the influx of extracellular calcium, 1.5 mM EGTA was added at 7 DIV to basal or high KCl medium cultures. This medium was replaced 1 day later with N2-0.5% FCS medium. Assessment of the number of postmitotic cells and morphological analyses were performed at 15 DIV.

BrdU treatment

To analyze the proliferative populations in the culture, we treated the cells with an extended pulse of 5-bromodeoxyuridine (BrdU; 3 μg/ml; Roche Diagnostics GmbH, Mannheim, Germany). The mitotic marker was added to the culture at 3, 6, 10, and 14 DIV. Twenty-four hours after, cultures were fixed with 4% paraformaldehyde. After three washes with phosphate-buffered saline (PBS), cells were treated with 2 M HCl for 30 min, followed by four washes in PBS. The cell cultures were then processed for immunocytochemistry to detect BrdU.

Measurement of GABA contents, release, and uptake

The endogenous levels of γ-aminobutyric acid (GABA) in each condition were measured by high performance liquid chromatography (HPLC) at 15 DIV. Cells were collected in cold 0.25 M perchloric acid and frozen to −20°C until analysis. On the day of the analysis, samples were homogenized, centrifuged 30 min at 16,000 × *g* at 4°C, and supernatants were brought to pH 8 with NaOH. GABA content was determined by HPLC analysis and fluorimetric determination of the *o*-phthaldialdehyde derivative as described (Suñol et al., 1988) with minor modifications. Separation of endogenous GABA was carried out in a reverse-phase C_{18} column (Tracer Nucleosil C_{18} 5-μm particle size, 10 × 0.4 cm; Teknokroma S.C.C.L., Sant Cugat del Vallès, Spain) using a mobile phase containing 0.1 M sodium acetate, 5.5 mM triethylamine (pH 3.15), and 28.6% acetonitrile at a flow rate of 0.8 ml/min. GABA content was calculated after fluorometric detection (excitation/emission: 360/450 nm) using an external standard method. Results were expressed as pmol of GABA in each well. Values are expressed as the mean of 3 wells from three independent cultures ± standard error of the mean (SEM).

For GABA release and uptake, we used 4-Amino-*n*-[2,3-^{3}H] butyric acid ([^{3}H]GABA; Amersham Biosciences UK Limited, Buckinghamshire, UK). [^{3}H]GABA uptake experiments were performed as described (Weiss, 1988). Briefly, cells were preincubated at 37°C in Krebs-Ringer-HEPES buffer (KRH; containing in mM: NaCl, 125; KCl, 4.8; $MgSO_4$, 1.2; KH_2PO_4, 1.2; $CaCl_2$, 2.2; glucose, 5.6; HEPES, 25, pH 7.4), then incubated for 30 min at 37°C with 20 nM [^{3}H]GABA (93 Ci/mmol) in KRH and rinsed three times with cold KRH (4°C). Thereafter, cells were lysed with 400 μl of 0.1 M NaOH and the total number of counts per minute (cpm) was measured in scintillation liquid. Values are calculated as the percentage of basal conditions cultures and represented as the mean ± SEM from 12 wells from three independent cultures.

For [^{3}H]GABA release experiments, cells were preincubated for 10 min at 37°C in KRH buffer supplemented with 100 μM γ-vinyl-GABA (GVG; Merrell Dow Research Institute, Strasbourg, France) and then incubated for 30 min at 37°C with 20 nM [^{3}H]GABA in KRH with GVG as described elsewhere (Belhage et al., 1993). All next incubations were done in 200 μl KRH with GVG during 3 min at 37°C. After three washes (refereed as basal levels), cells were depolarized for 3 min with ionomycin (0.1 μM; Sigma) to evoke Ca^{2+}-dependent neurotransmitter release as described previously (Katsura et al., 2002), and the medium was collected. We used ionomycin to depolarize the differentiated cells because they were already cultured in 40 mM KCl. As it has been previously described (Katsura et al., 2002), the concentration of ionomycin used in this study did not affect cell viability as assessed by trypan blue dye exclusion (>90% at the end of the experiment in each condition). Some experiments were processed in Ca^{2+}-free medium supplemented with 1.5 mM EGTA. Cells were washed for three additional times and each aliquot, including the initial rinses (basal levels; time 0), the depolarization (time 3 min), and the post-depolarization rinses (times 6, 9, and 12 min), was counted in scintillation liquid. Values represent the mean ± SEM from 4 wells from three independent cultures and are expressed as the percentage of the initial basal levels.

Transplantation procedures

An overall scheme of cell differentiation and grafting is shown in Fig. 5A. Adult male Sprague–Dawley OFA-Hairless rats (150–200 g; Charles River Laboratories, Les Oncins, France) were used to minimize immunological rejection. Rats were anesthetized with pentobarbital (50 mg/kg ip), placed in a David Kopf stereotaxic apparatus, and microinjected with quinolinate (QA; 68 nmol; Sigma) into the left striatum at two coordinates, as described elsewhere (Canals et al., 2001). Seven days after QA lesion, rats received cell grafts of predifferentiated cells. ST14A cells were differentiated until 11 DIV following in vitro sequential treatment with RA and KCl or cultured in basal-conditioned medium. Cells were trypsinized, pelleted, and resuspended in B27:MEM 1:1 containing 22 U/ml of DNAse (Sigma) at 3000 cells/μl. This methodology did not affect cell viability which was >98% just before grafting in all differentiation conditions (basal-conditioned medium, and RA- and KCl-treated cultures), as determined by trypan blue dye exclusion method. To follow them after EGFP downregulation, in some experiments cells were prelabeled in vitro with a 24-h pulse of BrdU performed at 10 DIV. Anesthetized rats were unilaterally or bilaterally microinjected with 9000 cells per striatum (1500 cells per deposit at 0.5 μl/min) following six coordinates: anteroposterior (AP),+2.8, lateral (L), ±2.4; AP, +1.8, L, ±2.9; and AP,+0.8, L, ±3.5 from bregma; dorsoventral (DV) −5.3 and −4.3 from dura, with the incisor bar at −5 mm. Cell viability was >90% at the end of the transplantation session, as determined by the trypan blue dye exclusion method.

After surgery, animals were housed separately with access to food and water *ad libitum* at constant temperature (19–22°C) and humidity (40–50%) on a 12-h light–dark cycle. All animal-related procedures were in accordance with the National Institute of Health Guide for the care and use of laboratory animals and approved by the local animal care committee of the University of Barcelona (67/02) and by the Generalitat de Catalunya.

Circling behavior

On the day before, and 1 and 5 weeks after unilateral cell transplantation, QA-lesioned rats were assayed for circling behavior in response to apomorphine stimulation. Rats were injected subcutaneously with apomorphine (0.5 mg/kg), placed in circular cages, and tethered to an automated

rotometer as described elsewhere (Marin et al., 2003). Rats were allowed 15 min to habituate to the rotometer before the administration of apomorphine. A computer recorded the number of complete (360°) turns made during the 15-min period and the values were expressed as net total numbers of full turns (n = 6–7).

Immunostaining

Immunostaining was performed using the following antibodies: anti-BrdU (1:50; Dako A/S, Glostrup, Germany), anti-NeuN (1:100; Chemicon, Temecula, CA), anti-Nestin (Rat 401; 1:38; Developmental Studies Hybridoma Bank, University of Iowa, Iowa), anti-GABA (1:100; Sigma), anti-β-III-tubulin (Tuj1; 1:400; Sigma), anti-GFAP (1:400; Sigma), anti-glutamic acid decarboxilase (GAD)65 (1:100; Sigma), anti-vesicular GABA transporter (v-GAT; 1:100; Synaptic Systems GmbH, Goettingen, Germany), anti-RIP (1:50; Developmental Studies Hybridoma Bank), anti-O4 (1:25; Chemicon), anti-CD11b clone OX-42 (1:50; Serotec Ltd, Kidlington, Oxford, UK), anti-GFP (1:200; Abcam Ltd, Cambridge, UK), anti-synapsin I (1:300; Chemicon), and anti-synaptotagmin (1:300; Synaptic Systems GmbH). Cultures were fixed with 4% paraformaldehyde in 0.1 M phosphate buffer (pH 7.4) for 45 min at 4, 7, 11, and 15 DIV. After a 30-min preincubation in PBS containing 0.3% Triton X-100 and 30% normal horse serum (NHS; Gibco-BRL), coverslips were incubated overnight at 4°C in PBS containing 0.3% Triton X-100 and 5% NHS with the corresponding primary antibodies. After three PBS washes, cultures were incubated for 2 h at room temperature with the appropriate biotinylated secondary antibody. The signal was developed using the avidin–biotin complex method (ABC; Pierce, Rockford, IL) and finally visualized with 3,3′-diaminobenzidine.

For immunohistochemistry, 3, 6, or 12 days after transplants, rats were transcardially perfused with 4% paraformaldehyde in 0.1 M phosphate buffer (pH 7.4). Brains were removed, postfixed for 2 h at 4°C in the same solution, cryoprotected in PBS containing 30% sucrose, and frozen in dry ice-cooled isopentane. Serial coronal cryostat sections (30 μm thick) through the whole striatum were collected as free-floating sections in PBS and processed for immunohistochemistry as described elsewhere (Canals et al., 2001). Briefly, autofluorescence was blocked with 50 mM NH_4Cl, tissue was permeabilized with PBS-T buffer [PBS containing 0.3% Triton X-100 (except for RIP antibody where we used 2%), 1.5% NHS, and 1% BSA] at room temperature for 1 h. Incubation with primary antibodies was performed overnight at 4°C in the same PBS-T buffer. For fluorescence immunodetection, we used the following secondary antibodies: FITC-conjugated anti-rabbit (1:100; Vector laboratories, Burlingame, CA) and Texas Red-conjugated anti-mouse (1:200; Jackson Immunoresearch Laboratories Inc., West Grove, PE).

Some cultures and sections were counterstained with 4′,6-diamidino-2-phenylindole (DAPI; Sigma) to visualize and count the total number of cells. All treatments were performed in parallel using the same reaction and exposure times for an optimal comparison between the assayed conditions. No signal was detected in controls in which primary antibodies were not added.

In situ detection of cell death

Cell death was detected in cell culture and in tissue sections using the in situ Apoptosis Detection System (Promega), as described elsewhere (Perez-Navarro et al., 2000). Cells were fixed with 4% paraformaldehyde in 0.1 M phosphate buffer (pH 7.4) at 4 and 15 DIV, and processed following manufacturer instructions. For detection of cell death in transplanted tissue, rats were transcardially perfused with 4% paraformaldehyde in 0.1 M phosphate buffer (pH 7.4) 3 and 6 days after transplants. Brains were removed, postfixed for 2 h at 4°C in the same solution, cryoprotected in PBS containing 30% sucrose, and frozen in dry ice-cooled isopentane. Cryostat-cut coronal sections were serially collected on silane-coated slides and processed to detect DNA fragmentation. After cell death detection with the TdT-mediated dUTP Nick-End Labeling (TUNEL) technique, cell cultures and sections were processed for immunohistochemistry against EGFP to detect the transplanted cells, as described above. Finally, tissue sections were mounted with Mowiol (Calbiochem) and visualized by fluorescence microscopy.

Cell counting

All cell counts were performed on blind-coded samples. In cell cultures, DAPI-positive nuclei were counted as the total number of cells in each condition at 4, 7, 11, and 15 DIV. Total cell number and BrdU-positive neurons were counted after fluorescent immunocytochemistry in 4 wells from four independent cultures. Positive cells for DNA fragmentation detected by the TUNEL assay were counted at 4 and 15 DIV from 4 wells of three independent experiments treated with basal-conditioned medium, RA or RA and KCl. Nestin- or GABA-positive cells at 15 DIV were counted under brightfield and compared with the phase contrast counts of total cells in the same field from three independent experiments. Several fields comprising 5% of the coverslip surface were randomly chosen using the Computer Assisted Stereology Toolbox (CAST) software (Olympus Danmark A/S, Ballerup, Denmark) and the number of positive cells was counted for each condition.

For in vivo counts of the grafted cells, every seventh coronal section (30 μm thick) across the striatum was processed for immunohistochemistry against EGFP and counterstained with DAPI. The total number of grafted cells per striatum was estimated by calculating the total number of EGFP-positive cells per section and multiplying these

values by seven in each animal. Values were corrected using the Abercrombie method (Abercrombie, 1946). The final numbers were expressed as the mean of four animals ± SEM. The number of dying transplanted cells was calculated as the percentage of TUNEL-positive cells with respect to the total number of EGFP-positive cells.

For statistical analysis, we performed a Student's *t* test for independent samples.

Detection of the EGFP gene by PCR

Six days, 45 days, or 7 months post-transplantation, rats were deeply anesthetized in a CO_2 chamber, their brains were quickly removed, and their striata were dissected out for PCR analysis. DNA from grafted, lesioned, or intact striata as well as for a confluent plate of proliferating ST14A cells was extracted by a deproteinization method (Akerud et al., 2001) and resuspended in nuclease-free H_2O. One microgram of DNA was added to a final 25-μl volume of PCR reaction mixture composed of 1× PCR buffer (Ecogene SRL, Madrid, Spain), 2 mM $MgCl_2$, 0.12 mM dNTPs, 50 nM of each primer, and 2 units of EcoTaq Plus DNA Polymerase (Ecogene). The PCR reaction was run at an annealing temperature of 58°C for 40 cycles. The forward primer (5′-ATGGTGAGCAAGGGCGAG-3′) and the reverse primer (5′-CTTGTACAGCTCGTCCATGCC-3′) recognized the gene for the egfp (GenBank: U57609). A product of 700 bp was amplified and resolved on 2% agarose gels.

Results

Retinoic acid improves cell survival and induces a neuronal phenotype in ST14A cells

We differentiated ST14A cells at the nonpermissive temperature of 39°C in N2 medium supplemented with minimal FCS (0.5%), in which a survival of more than 15 DIV was achieved (Fig. 1A). Under these culture conditions, addition of 10 μM RA from 2 to 7 DIV resulted in an improvement of cell survival. RA treatment caused an increase in cell number of 125 ± 35% at 7 DIV, 244 ± 37% at 11 DIV, and 206 ± 41% at 15 DIV over non-RA-treated cultures (basal-conditioned medium; Figs. 1B–D). This increase was not due to an enhancement of the proliferation rate because the number of cells that incorporated BrdU was the same in both conditions at all time points examined (Figs. 1E–G). Thus, we next examined if the addition of RA decreased cell death in our cultures. We examined by TUNEL assay the number of dying cells 2 days after RA administration. We observed a massive cell death in basal-conditioned medium-treated cells. However, the addition of RA reduced apoptotic cells by 81.4 ± 10.3%, indicating that RA was acting as a survival factor (Fig. 1H). Moreover, RA treatment significantly increased NeuN signal in almost all cells in the culture from 7 DIV (Figs. 1I–J), which was stable until 15 DIV, the last time point examined. No immunostaining was observed for glial markers such as the astrocytic marker GFAP, the oligodendroglial markers RIP and O4, or the microglial marker OX42, in any condition or at any time point examined (data not shown). In contrast, addition of the broad-spectrum caspase inhibitor z-VAD-FMK (50–100 μM) or mitogenic agents such as bFGF, aFGF, or EGF (10–20 ng/ml) did not delay cell death at 39°C in N2 medium. Similarly, co-culture of ST14A cells with neonatal striatal astrocytes did not modify cell survival, differentiation, or proliferation (data not shown).

KCl depolarization decreases cell proliferation and induces neurite outgrowth in a Ca^{2+}-dependent manner

In an effort to further differentiate cells, we assayed sequential treatment with 10 μM RA (from DIV 2 to 7) and distinct factors (from DIV 7 to 15; Fig. 2A). The neurotrophic factors BDNF, NT3, GDNF, and NTRN were added at concentrations of 10–50 ng/ml but did not modify the total number of cells (Fig. 2B) or the proliferation rate (Fig. 2C) with respect to controls treated with RA alone at any time point. However, depolarizing concentrations of KCl substantially reduced the rate of proliferation at 15 DIV. Exposure to 40 mM KCl diminished the number of BrdU-positive cells by 67 ± 9.8% with respect to RA treatment alone (Figs. 2C and F–G). Interestingly, sequential addition of RA and KCl did not alter the total number of cells (Fig. 2B), indicating that this treatment increased the survival of postmitotic cells. Thus, we examined the number of TUNEL-positive cells at 15 DIV. Our experiments demonstrated that both RA and KCl act as survival factors because they reduced cell death observed in basal-conditioned medium by 47.0 ± 9.9% and 89.7 ± 7.7%, respectively (Fig. 2D). KCl treatment also increased neurite outgrowth, in terms of both number and length, in many cells in the culture (Figs. 2F–G and 3F). Furthermore, the decrease in the number of proliferative cells caused by KCl treatment did not occur in non-RA-treated cells (Fig. 2C). To study whether the KCl effect was a chronic or an acute response, we treated cells with KCl for 1, 2, 4, and 8 days (Fig. 3A). These experiments revealed that 1 day of KCl treatment was sufficient to decrease cell proliferation at 15 DIV (Fig. 3B).

Analysis of the role of Ca^{2+} in the KCl-induced effects revealed that after KCl depolarization the intracellular levels of Ca^{2+} increased by about 900% in RA-treated and non-treated cells (Figs. 3D–E). However, KCl administration had a strong effect on the elaboration and maturation of neurite-like processes only in cells that had received prior treatment with RA (Fig. 3F), but not in untreated cells (data not shown). Addition of the calcium chelator EGTA completely blocked the decrease in proliferation following addition of KCl (Figs. 3B–C). Furthermore, administration of EGTA also inhibited the elaboration of these neurite-like processes (Fig. 3C, compare with Figs. 2E–G).

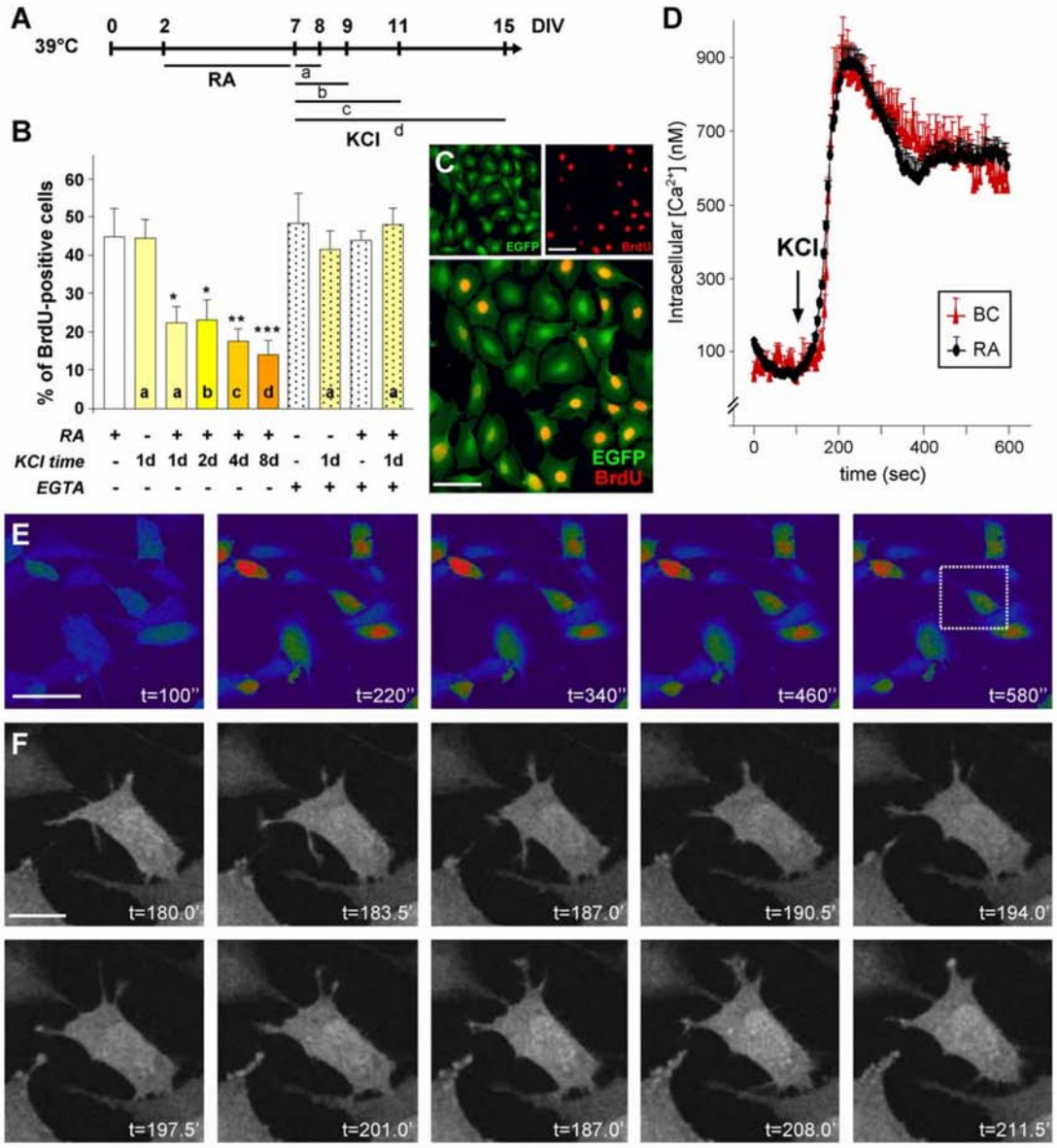

Fig. 3. Ca^{2+} influx participates in KCl effects. (A) KCl was added for 1 (a), 2 (b), 4 (c), or 8 days (d) after RA treatment. (B) The number of BrdU-positive cells was counted at 15 DIV. One day of exposure to KCl (a) is sufficient to decrease the number of proliferative cells in RA-treated cultures but not in basal-conditioned medium. Addition of 1.5 mM EGTA for 1 day completely abolished this effect. (C) Fluorescence photomicrographs of EGFP and BrdU immunostaining showing that addition of EGTA inhibits not only the decrease in cell proliferation but also the formation of neurite-like processes. (D–E) Calcium measurements show that RA-treated and basal-conditioned medium cultures respond to the addition of 40 mM KCl with a 9-fold increase in intracellular $[Ca^{2+}]$. Data are represented as the mean ± SEM of the $[Ca^{2+}]$ values of at least 25 cells from three independent cultures. (E) Fluo-4 fluorescence intensity increases after KCl addition and thereafter reaches a plateau (see also supplemental video 1). (F) Images of the cell contained in the square drawn in C taken 3 h after KCl addition show the dynamics of the formation of neurite-like processes (see also supplemental video 2). This phenomenon was observed in RA-treated but not basal-conditioned medium cultures. $*P < 0.05$; $**P < 0.005$; $***P < 0.001$ with respect to RA treatment. Scale bars: C and E, 40 μm; F, 10 μm.

KCl depolarization induces the acquisition of a functional GABAergic phenotype

Next, we looked for changes in cellular phenotype induced by exposure to KCl. After the sequential addition of RA and KCl, the number of nestin-positive cells decreased by 49 ± 11% with respect to RA treatment alone (Figs. 4A and C). This effect was not observed in cells cultured in basal-conditioned medium or treated with RA alone (Figs. 4A and C). Furthermore, we found that addition of KCl in RA-treated cells increased the number of GABA-positive cells to 74 ± 8% of total cells at 15 DIV (Figs. 4B and D). The intensity of the immunostaining was also enhanced. 41 ± 1% of these GABA-positive cells

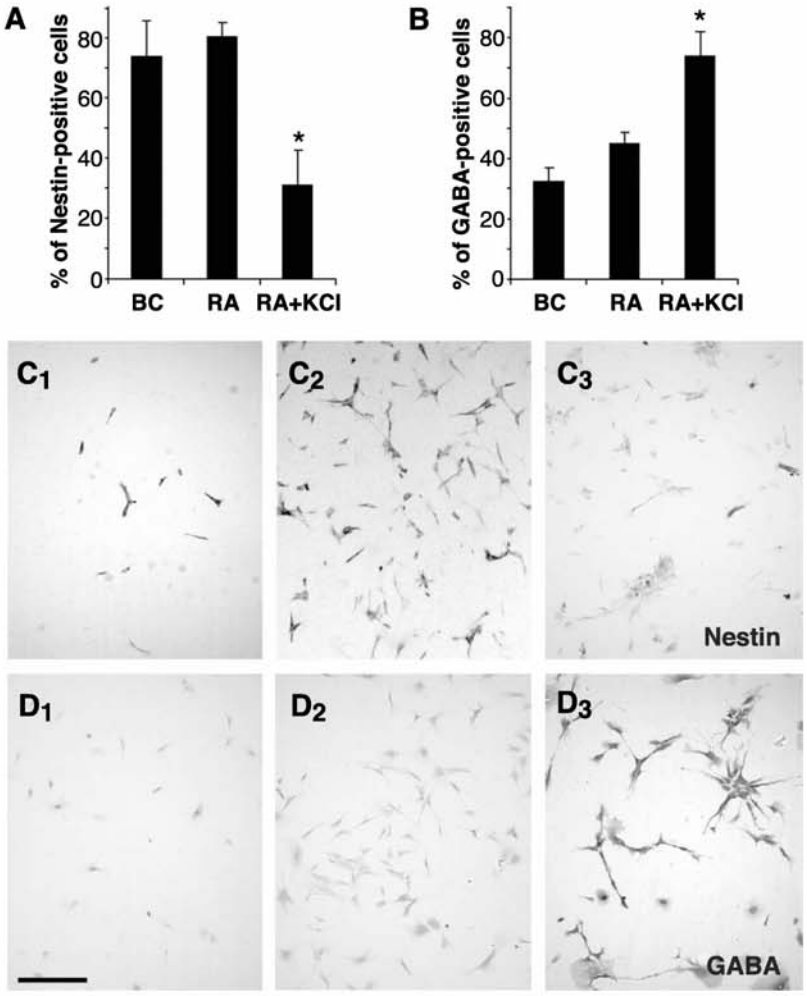

Fig. 4. Addition of KCl decreases the expression of Nestin and increases the immunostaining for GABA. (A) KCl treatment (40 mM) from 7 to 15 DIV reduces the number of Nestin-positive cells with respect to RA treatment. (B) KCl treatment significantly increases the number of GABA-positive cells to 74% of total cells at 15 DIV. (C) Photomicrographs showing the decrease in Nestin expression observed in RA- and KCl-treated cultures (C3) compared with basal-conditioned medium (C1) and RA-treated cultures (C2) at 15 DIV. (D) Representative photomicrographs showing the increased intensity of GABA immunostaining observed in cells treated with RA and KCl (D3) but not in basal-conditioned medium (D1) or cultures treated with RA alone (D2) at 15 DIV. *$P < 0.05$ with respect to basal and RA cultures. Scale bar represents 120 μm.

showed very strong immunostaining. These differentiated cells were also positive for tubulin βIII and MAP2ab (data not shown). In basal-conditioned medium and RA-treated cultures at 15 DIV, GABA immunoreactivity was detected in 32 ± 5% and 45 ± 4% of the cells, respectively (Figs. 4B and D). Only 16 ± 2% and 18 ± 8% of cells showed high levels of GABA immunostaining in basal-conditioned medium and in RA-treated cultures, respectively. Treatment of cells with KCl for 1 or 2 days was insufficient to detect changes in GABA immunostaining (34 ± 5% and 28 ± 9%, respectively). The minimal period of KCl administration to show a positive effect on GABA expression after RA pretreatment was 4 DIV, after which 68 ± 10% of cells were positive. This enhancement of GABA immunostaining was not detected in cultures exposed to neurotrophic factors at any time point examined. No staining for glial markers (GFAP, O4, RIP, or OX42) was observed after the differentiation protocol (data not shown).

To further examine the GABAergic characteristics of differentiated cells, we performed immunohistochemistry against GAD and v-GAT, the proteins that synthesize and package GABA into synaptic vesicles, respectively. These experiments showed that differentiated cells with sequential treatment with RA and KCl were positive for both markers (Figs. 5A and B), suggesting that these neurons can synthesize and release GABA. Thus, we next examined these functional properties. We demonstrated by HPLC that differentiated cells with RA and KCl were able to synthesize GABA because we detected high levels of neurotransmitter contents in these neurons. Cells differentiated with RA and KCl contained 19.8 ± 3.1 pmol/well of GABA, about 7-fold the amount of basal-conditioned cells (2.61 ± 0.94 pmol/

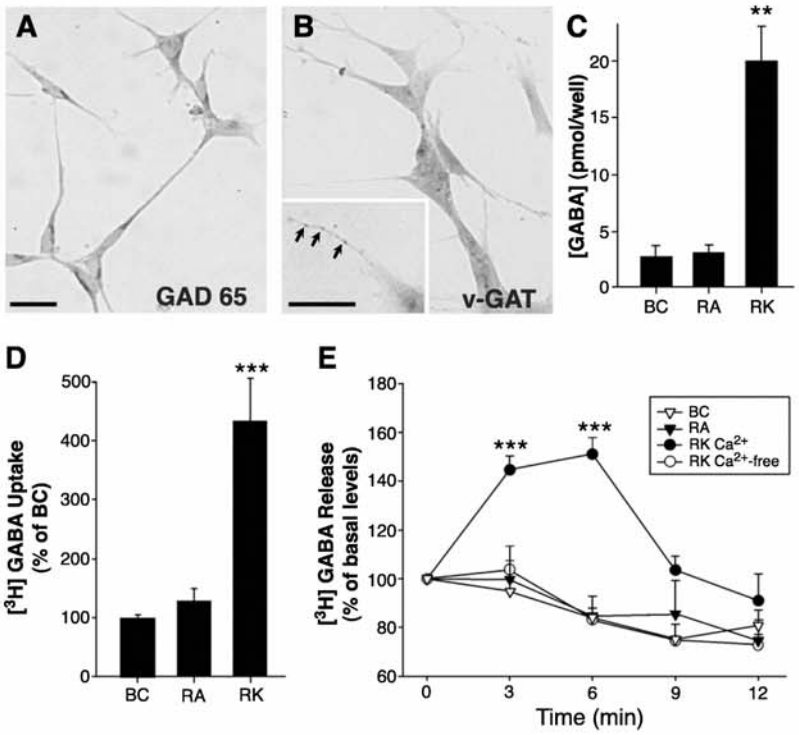

Fig. 5. KCl treatment induces a functional GABAergic phenotype. (A) RA and KCl sequential treatment induces a strong immunostaining for GAD 65. (B) Cells are also immunostained for the vesicular GABA transporter v-GAT in the cytoplasm and in neuritic processes (arrows in inset). (C) Total GABA content was quantified by HPLC at 15 DIV in basal condition cultures (BC), in RA-treated cells (RA), and in cultures differentiated with the sequential addition of RA and KCl (RK). The intracellular GABA content increased 7-fold in RK-treated cells with respect to BC and RA cells. (D) In addition, cells differentiated with sequential treatment with RA and KCl (RK) showed a 4-fold increase in [^{3}H]GABA uptake with respect to basal-conditioned medium or RA-treated cells. (E) These differentiated GABAergic neurons were also able to release GABA after ionomycin depolarization in a calcium-dependent manner. Only RA- and KCl-treated cells (RK Ca^{2+}) were able to release [^{3}H]GABA in the presence of Ca^{2+}. This release is inhibited in the absence of calcium in the medium (RK Ca^{2+}-free). $^{**}P < 0.005$ and $^{***}P < 0.001$ with respect to BC and RA. Scale bar represents 20 μm.

well) or RA-treated cells (2.92 ± 0.69 pmol/well) (Fig. 5C). We also examined the capacity of differentiated cells to uptake and release GABA. Our findings showed that NSC treated with basal-conditioned medium or with RA alone uptaked very low levels of [^{3}H]GABA whereas differentiated cells with RA and KCl were able to uptake 336 ± 73% more GABA than basal-conditioned medium-treated cells and 234 ± 56% with respect to RA-treated cells (Fig. 5D). Furthermore, these cells were able to release GABA after depolarization in a Ca^{2+}-dependent manner (Fig. 5E). Cells cultured in basal-conditioned medium or treated with RA-alone did not show GABA release. Taken together, these data indicate that sequential treatment with RA and KCl promotes cell maturation to a postmitotic functional GABAergic phenotype in the ST14A NSC line.

Survival of predifferentiated ST14A cells after transplantation in a Huntington's disease rat model

Next, we studied the integration of these predifferentiated striatal neural stem cells upon transplantation into adult rats. ST14A cells were differentiated by sequential treatment with RA and KCl or cultured in basal-conditioned medium until 11 DIV, when cells were already committed to a GABAergic phenotype, and then implanted into QA-lesioned or intact striata (Fig. 6A).

Three days after transplantation, EGFP-positive cells could be detected in all of the grafts, but there was an approximately 2-fold increase in cell survival in RA- and KCl-predifferentiated cells compared with those grown in basal-conditioned medium (Fig. 6B). There were no differences in survival or differentiation between cells transplanted in QA-lesioned or non-lesioned striata (Fig. 6B).

We detected very few EGFP-positive cells 6 days after transplantation and no EGFP-positive cells after 12 days. This could be due to a massive cell death from day 3 to 6, or alternatively, to a downregulation of EGFP expression. When we performed a TUNEL assay to count the number of dying cells, only 3.9 ± 2.1% of transplanted cells were TUNEL positive 3 days after transplantation (Fig. 6C) and no positive cells were detected 6 days after transplantation (data not shown). As an alternative detection method for grafted cells beyond the third day, we prelabeled cells in culture with a 24-h pulse of BrdU before grafting. Three days after transplantation, about half of the EGFP-positive cells were also positive for BrdU staining (Fig. 6D). At 6 days postgraft, a

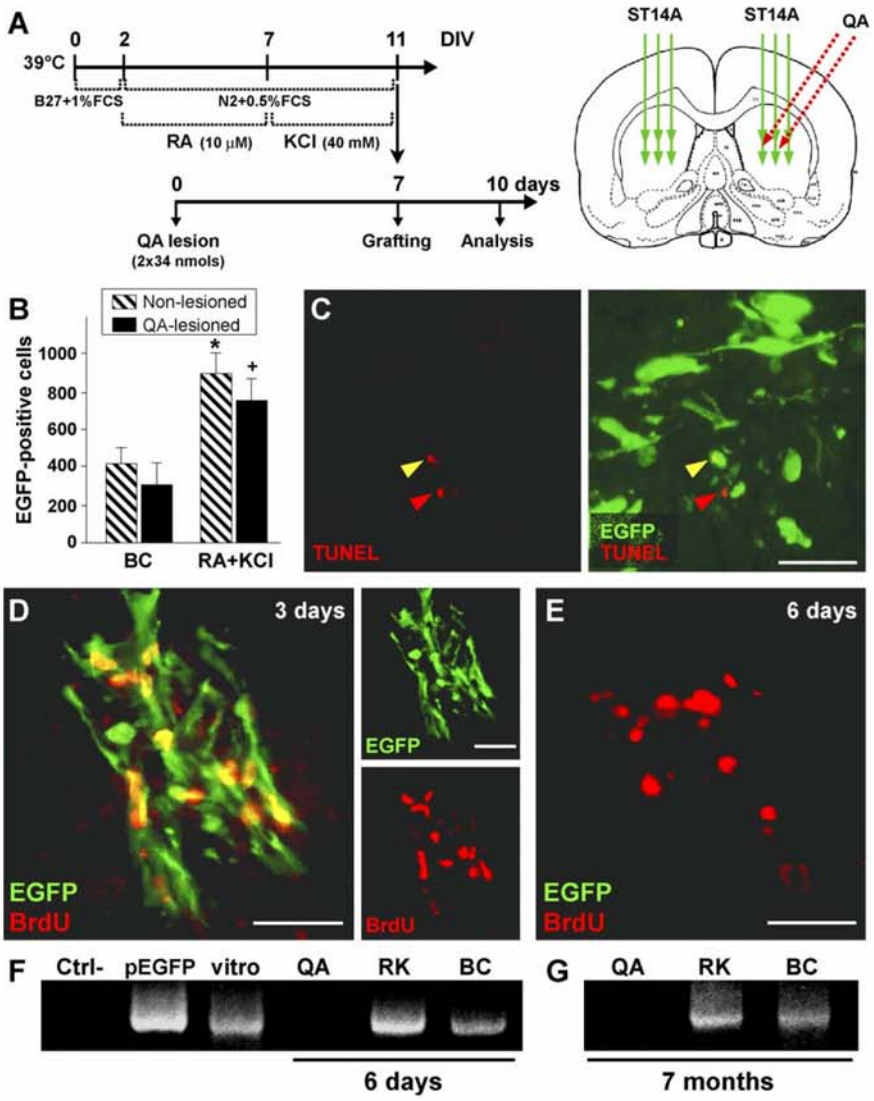

Fig. 6. Survival of predifferentiated ST14A cells after transplantation in a Huntington's disease model. (A) Scheme of the grafting procedure: cells were cultured until 11 DIV following sequential treatment or cultured in basal-conditioned medium, and then grafted in a QA-lesioned or non-lesioned striatum. (B) Three days after transplantation, grafts of RA- and KCl-treated cells contained twice the number of EGFP-positive cells as those performed with untreated cells in both non-lesioned and QA-injected rats. (C) Three days after cell transplantation, very few cells were detected positive for TUNEL assay (arrowheads). We detected apoptotic cells that colocalize with EGFP-positive cells (yellow arrowhead) and with EGFP-negative cells (red arrowhead). (D–E) To detect grafted cells beyond EGFP downregulation, they were prelabeled with a 24-h pulse of BrdU added at 10 DIV. (D) Three days after transplantation, we observed cells double immunostained for EGFP and BrdU. (E) A similar number of BrdU-positive nuclei can be seen in the graft site 6 days postgrafting. However, we observed a complete downregulation of the EGFP marker at this time point. (F and G) Detection of the EGFP gene by PCR indicates long-term survival of grafted NSCs. (F) Representative gel showing the presence of the specific band of the EGFP gene in lesioned striata grafted with RA- and KCl-treated cells (lane RK) or with basal-conditioned medium-treated cells (lane BC). The EGFP gene was not detected in non-grafted, lesioned rats (lane QA). Positive controls for the PCR are the plasmid containing the EGFP sequence (lane pEGFP) and DNA extracted from proliferative ST14A cells in vitro (lane 'vitro'). (G) ST14A cells survive until 7 months after transplantation. The specific band of the EGFP gene was found in grafted striata with RA- and KCl-treated cells (RK) and with untreated cells (BC). $^{*,+}P < 0.05$ respect to BC. Scale bars represents 30 μm.

similar number of BrdU-positive nuclei were found in the graft site although they were negative for EGFP (Fig. 6E). These findings indicate that expression of EGFP was down-regulated in vivo. A similar phenomenon has been described previously in other cellular models (Akerud et al., 2001; Martinez-Serrano and Bjorklund, 1997). To further confirm the presence of ST14A cells beyond 3 days postgraft, we examined the presence of the EGFP gene by PCR. Six days after transplantation, the specific band corresponding to the EGFP gene was detected in lesioned striata transplanted with predifferentiated or control cells (Fig. 6F). In long-term experiments, the EGFP gene was also detected by PCR in the striata of all transplanted animals at 1.5 months (data not shown) and 7 months postgrafting (Fig. 6G).

In vitro predifferentiated ST14A cells maintain their neuronal GABAergic phenotype and elaborate neurites with synaptic contacts after transplantation

We analyzed the fate that these predifferentiated cells acquired 3 days after transplantation in QA-lesioned or non-lesioned striata. Almost all grafted cells showed immunostaining for the neuronal marker β-III-tubulin (Tuj1; Fig. 7A). Similar staining was observed in cells pretreated with RA and KCl or with the basal-conditioned medium. Interestingly, cells predifferentiated with RA and KCl treatment were strongly positive for GABA (Fig. 7B) and GAD immunostaining (Fig. 7C), whereas non-treated cells were not positive for these markers (data not shown). No EGFP-positive cells co-localized with glial markers, such as the astrocytic marker GFAP (Fig. 7D) or the oligodendro-

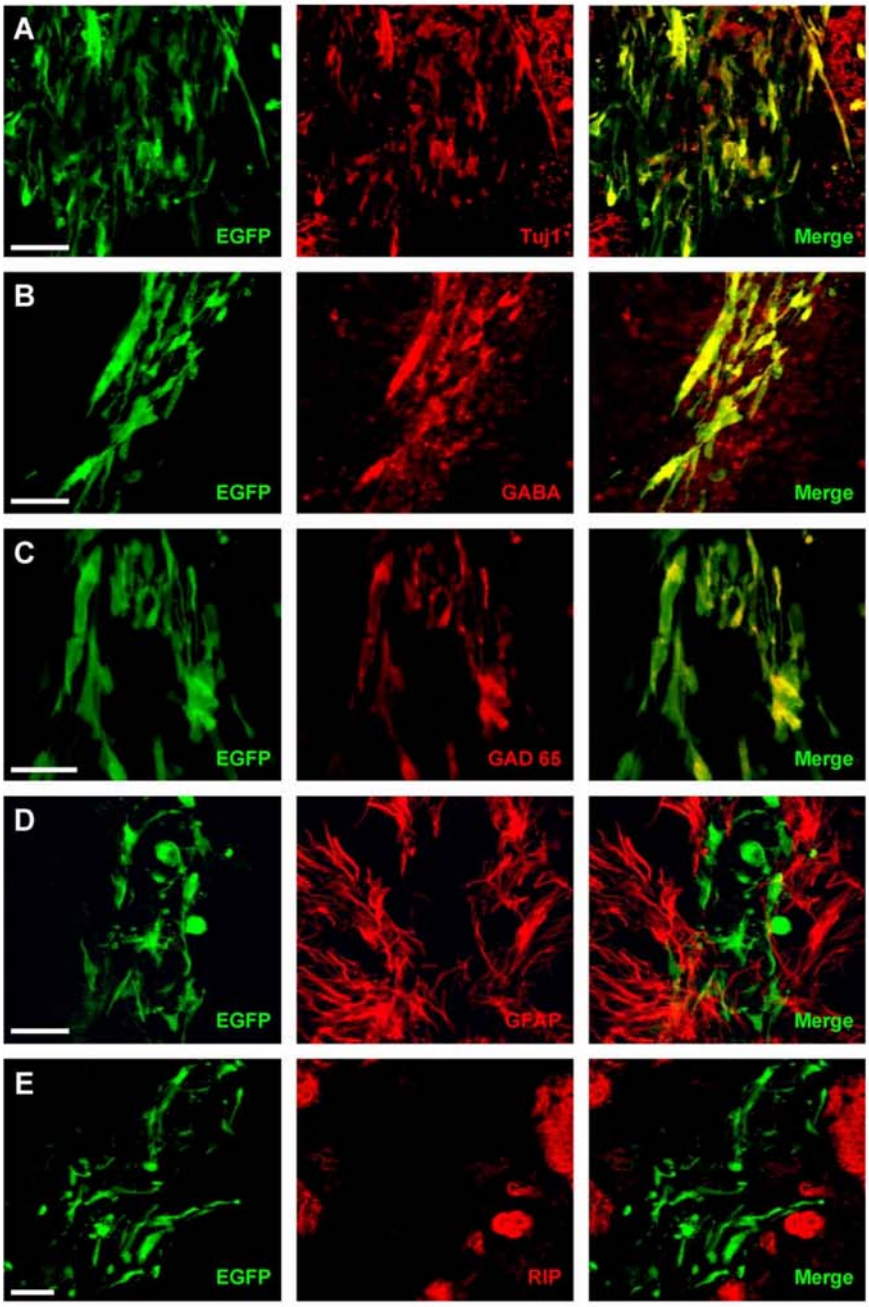

Fig. 7. In vitro-predifferentiated ST14A cells maintain their neuronal GABAergic phenotype after transplantation. Phenotypic analysis of RA- and KCl-treated cells 3 days after transplantation in QA-lesioned rat striata reveals that (A) they show immunoreactivity for the neuronal marker Tuj1, (B) they are immunopositive for GABA and (C) GAD 65, and (D) no EGFP-positive cells colocalized with the astrocytic marker GFAP or (E) the oligodendritic marker RIP. Scale bars represent 20 μm.

glial marker RIP (Fig. 7E). In addition, transplanted cells were not detectable by antibodies against the immature neural marker Nestin (data not shown). Similar results were observed in cells grafted into QA-lesioned or in intact striata. No signal was observed in the absence of the primary antibodies in any case.

We observed that cells predifferentiated with sequential treatment with RA and KCl elaborated long neurite-like processes after transplantation (Fig. 8A). However, cells pretreated with the basal-conditioned medium did not show neurite-like processes in vivo (Fig. 8A, inset). Our findings also showed that the soma and the processes of the transplanted GABAergic cells were surrounded by numerous synaptic contacts as assessed by the close presence of synaptic vesicle proteins (vSNARE proteins; for review: Trimble, 1998) such as synapsin I (Fig. 8B) and synaptotagmin (Fig. 8C). These findings suggest that grafted predifferentiated cells received synaptic inputs from host neurons. In addition, we observe colocalization of EGFP-positive structures with synaptotagmin-positive vesicles (Fig. 8D), indicating that our predifferentiated GABAergic cells may also elaborate synaptic contacts. Similar structures were also observed positive for v-GAT (Fig. 8E). Taken together, these findings suggest that predifferentiated cells with the RA and KCl established pre- and postsynaptic contacts with endogenous striatal cells after transplantation.

Thus, we next examined whether transplantation of these predifferentiated GABAergic cells could attenuate the circling behavior of unilaterally lesioned rats. For this purpose, rats were intrastriatally injected with QA and 1 week later, they received ipsilateral implantation of basal-conditioned medium-treated cells or RA- and KCl-differentiated cells. As a control, some QA-injected rats received vehicle alone. Rats were stimulated with apomorphine and

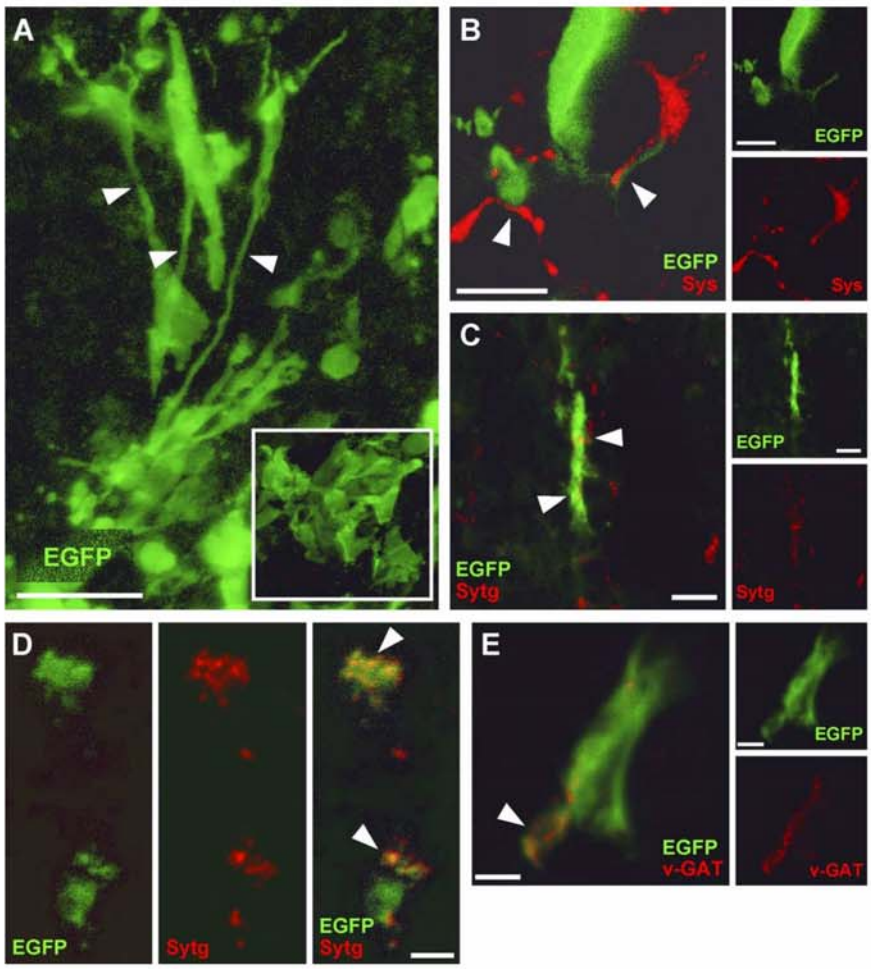

Fig. 8. Predifferentiated cells elaborate neurite-like processes and synaptic connections. (A) Three days after transplantation, immunohistochemistry against EGFP reveals the presence of long neurite-like processes (arrowheads) in transplanted cells predifferentiated with RA and KCl, but not in grafts with basal-conditioned medium-treated cells (inset). (B and C) Double immunohistochemistry shows the presence of synaptic vesicle proteins such as synapsin I (Sys; B) and synaptotagmin (Sytg; C) close to EGFP-positive cells, soma, and processes. (D and E) These synaptic vesicle proteins, such as synaptotagmin (Sytg, D), are also localized inside the EGFP-positive terminal-like structures, which also contain v-GAT-immunopositive vesicles (E). Scale bars represent A, 16 μm; B and C, 5 μm; D and E, 1 μm.

the number of rotations was automatically recorded in a blind-coded way. All animals showed similar rotations 1 day before cell transplantation. One and five weeks after grafting experiments, QA-lesioned animals transplanted with cells pretreated in the basal-conditioned medium reduce the number of rotations by 13% and 32% with respect to non-grafted animals, 1 and 5 weeks after grafting, respectively. However, rats that receive predifferentiated GABAergic cells reduced the net number of turns by 58% and 64% with respect to non-grafted rats, 1 and 5 weeks after grafting, respectively. These findings suggest that our GABAergic cells might produce beneficial effects in this rat model.

Discussion

In the present work, we obtained a population of postmitotic GABAergic neurons from a striatal NSC line by manipulation of the external medium conditions. Striatal NSCs were exposed to sequential treatment with RA and depolarizing concentrations of KCl. RA induced a neuronal phenotype and enhanced cell survival, whereas administration of 40 mM KCl decreased proliferation and nestin expression, and promoted differentiation into functional GABAergic neurons. We have also demonstrated that transplantation of these differentiated GABAergic neurons into adult rat striata is feasible, with long-term survival, maintenance of the in vitro induced GABAergic phenotype, and elaboration of extensive neurite outgrowth with synaptic contacts.

In agreement with our findings, it has been reported previously that RA promotes the survival of different neural progenitors (Henion and Weston, 1994; Kornyei et al., 1998), probably by increasing anti-apoptotic proteins such as Bcl-2 (Daadi et al., 2001; Hanada et al., 1993). RA has also been described as a potent inducer of neuronal differentiation (Dinsmore et al., 1996; Encinas et al., 2000; Maden, 2002; Palmer et al., 1997). Here we show that after 5-day RA treatment, ST14A cells increase NeuN expression, a marker of mature neurons. Similarly, it has been shown that RA treatment of neural progenitor cells derived from E9 mouse increases the NeuN signal from day 5 in culture (Herberth et al., 2002). RA receptors are already expressed at E12.5 in the developing striatum (Ruberte et al., 1993) and E13.5 primary neuronal cultures from the lateral ganglionic eminence enhance their striatal neuronal characteristics after RA treatment (Toresson et al., 1999). However, we observed that RA alone is not sufficient to induce an increase in the GABAergic phenotype of ST14A stem cells. Therefore, factors other than RA found in striatal primary cultures must also participate in the maturation of striatal precursors. It has been proposed that glial cells from the lateral ganglionic eminence are a major source of retinoids in the developing telencephalon (Toresson et al., 1999). In addition, astrocytes promote survival and differentiation of neurons (Song et al., 2002), including dopaminergic neurons (Wagner et al., 1999). However, in our experiments, co-culture with astrocytes did not increase ST14A cell viability or differentiation, suggesting that other factors are necessary for the specification of GABAergic identity.

Neurotrophins have also been implicated in the differentiation of striatal neurons, depending on the developmental stage. Previous results from our group demonstrated that nestin-positive progenitors present in striatal cultures do not respond to BDNF (Gavalda et al., 2004). This finding, together with the present results, which show no effect of neurotrophins on the differentiation of ST14A cell line derived from E14 striatal progenitors, indicates that these neurotrophins may instead play a role in later stages of maturation. BDNF, NT-3, and NT-4 have been reported to promote the maturation of GABAergic striatal cells in E17–E19 embryonic primary cultures (Mizuno et al., 1994; Ventimiglia et al., 1995). Furthermore, Barberi et al. (2003) reported an in vitro procedure for the generation of GABAergic neurons from embryonic stem cells in which terminal differentiation is driven by the late addition of BDNF and NT-4. In fact, it has been shown that BDNF expression increases during postnatal brain development (Checa et al., 2000).

Synaptic activity is a potent inducer of neuronal differentiation. Thus, we analyzed whether ST14A striatal precursors respond to stimulation by neuronal activity. We observed that exposure to depolarizing concentrations of KCl downregulates the immature neural marker nestin and increases the number of postmitotic neurons with extensive neurite outgrowth. It is well documented that neuronal activity induces dendritic growth (for review; Wong and Ghosh, 2002). However, some reports show contradictory data about the anti- or pro-mitotic effect of the induction of neural activity. Although most studies demonstrate that depolarization caused by KCl or glutamate decreases the mitotic activity of neuronal precursors (Antonopoulos et al., 1997; Cui and Bulleit, 1998; Haydar et al., 2000; LoTurco et al., 1995), other authors have shown an increase of proliferation in neural progenitors after depolarization (Borodinsky and Fiszman, 1998; Haydar et al., 2000). These differences may be due to developmental stage (Haydar et al., 2000), because it has been shown that extracellular K^+ levels influence the proliferation of neural progenitors in a stage-dependent manner (Herberth et al., 2002). The neuronal activity induced by KCl promotes calcium influx in our striatal NSC cultures. Interestingly, this increase in calcium levels induces the generation of postmitotic neurons and neurite outgrowth only in NeuN–positive cells generated by prior treatment with RA. Thus, we next characterized the fate of these mature neurons after sequential treatment with RA and KCl. Our experiments showed that 74% of neurons become GABAergic, similar to the percentage of GABAergic neurons present in a striatal primary culture (Gavalda et al., 2004; Mizuno et al., 1994). These differentiated NSC have the morphological and the

biochemical parameters of fully differentiated functional GABAergic neurons, including GABA synthesis, uptake, and release. These findings agree with previous studies showing the effect of KCl-induced depolarization and global spontaneous calcium spikes on the GABAergic phenotype in neurosphere-derived precursors (Ciccolini et al., 2003) and embryonic *Xenopus* spinal cord neurons (Gu and Spitzer, 1995; Spitzer et al., 1993).

To study the stability and integration of our in vitro-differentiated ST14A cells, we transplanted them into the adult rat brain. Many reports show that transplantation of NSCs into the embryonic or neonatal host brain results in a site-specific fate acquisition (Doering and Snyder, 2000; Englund et al., 2002; Lundberg et al., 2002; Snyder et al., 1992). The phenotypic fate of the graft and its functional integration into the host tissue will depend on their origin as well as the implantation site. It is well known that specific neuronal differentiation of grafted cells depends on host age, being much less efficient in the adult brain. Many studies show that undifferentiated cells achieve a glial phenotype or remain undifferentiated after grafting into the adult brain (Lundberg et al., 1997; Rubio et al., 2000). Thus, an in vitro predifferentiation into the desired phenotype before transplantation is necessary (Bjorklund and Lindvall, 2000; Rossi and Cattaneo, 2002). Predifferentiation cells toward a GABAergic phenotype can be useful as cell therapy for Huntington's disease. Therefore, we transplanted cells committed to a GABAergic phenotype. Our experiments demonstrate that predifferentiated cells maintain their in vitro acquired GABAergic phenotype and elaborate long neurite extensions 3 days after transplantation in both the intact and QA-lesioned striatum. Moreover, none of the predifferentiated cells had differentiated toward a glial phenotype. Although we observe a complete downregulation of the EGFP marker gene, which precludes a long-term analysis of their phenotype, grafted cells survive at least until 7 months post-transplantation. It is clear that an important step for getting a functional transplant is that cells receive and elaborate synaptic contacts (Rossi and Cattaneo, 2002). In our model, predifferentiated cells established synaptic contacts with host cells, suggesting that grafted GABAergic cells are functionally integrated. In fact, preliminary behavioral results showed that animals transplanted with predifferentiated GABAergic neurons have a trend to improve their circling-behavior respect to sham-treated rats. However, further experiments are required to characterize the exact number of cells and the distribution of cell transplantation to better improve their functionality.

In conclusion, this work provides data that support the feasibility of controlling the process of differentiation of NSCs for cell replacement approaches. We generated a homogenous population of mature GABAergic neurons in vitro, which stably maintain their phenotype after transplantation in a Huntington's disease rat model. The controlled generation of GABAergic neurons from NSCs could be useful not only for the treatment of Huntington's disease, but also as a local administration of GABA in those nuclei where a tonic inhibition could be beneficial, such as the subthalamic nucleus in Parkinson's disease.

Acknowledgments

We would like to thank M.T. Muñoz for technical assistance, Dr. Maria Calvo and Anna Bosch of the Serveis Científico-Tècnics (University of Barcelona) for their support and advice on the use of confocal microscopy, Dr. Francesc Tebar for his help in EGFP PCR experiments, Dr. Joan Blasi for his help in synaptic vesicle proteins characterization, and Robin Rycroft for linguistic advice. The Rat-401 and the Rip monoclonal antibodies developed by Susan Hockfield were obtained from the Developmental Studies Hybridoma Bank developed under the auspices of the NICHD and maintained by the Department of Biological Science, University of Iowa, Iowa City, IA. This study was supported by the Ministerio de Ciencia y Tecnología (SAF2002-00314, J.A.; SAF2002-00311, J.M.C. Spain), 'redes temáticas de investigación coorporativa' (G03/167; G03/210; Ministerio de Sanidad y Consumo, Spain), and Fundació La Caixa. M.B. is a fellow of the Universitat de Barcelona (Spain) and J.R.P. of the Ministerio de Educación, Cultura y Deporte (Spain).

References

Abercrombie, M., 1946. Estimation of nuclear populations from microtome sections. Anat. Rec. 94, 239–247.

Akerud, P., Canals, J.M., Snyder, E.Y., Arenas, E., 2001. Neuroprotection through delivery of glial cell line-derived neurotrophic factor by neural stem cells in a mouse model of Parkinson's disease. J. Neurosci. 21, 8108–8118.

Antonopoulos, J., Pappas, I.S., Parnavelas, J.G., 1997. Activation of the GABAA receptor inhibits the proliferative effects of bFGF in cortical progenitor cells. Eur. J. Neurosci. 9, 291–298.

Arenas, E., 2002. Stem cells in the treatment of Parkinson's disease. Brain Res. Bull. 57, 795–808.

Baetge, E.E., 1993. Neural stem cells for CNS transplantation. Ann. N. Y. Acad. Sci. 695, 285–291.

Barberi, T., Klivenyi, P., Calingasan, N.Y., Lee, H., Kawamata, H., Loonam, K., Perrier, A.L., Bruses, J., Rubio, M.E., Topf, N., Tabar, V., Harrison, N.L., Beal, M.F., Moore, M.A., Studer, L., 2003. Neural subtype specification of fertilization and nuclear transfer embryonic stem cells and application in parkinsonian mice. Nat. Biotechnol. 21, 1200–1207.

Beal, M.F., Ferrante, R.J., Swartz, K.J., Kowall, N.W., 1991. Chronic quinolinic acid lesions in rats closely resemble Huntington's disease. J. Neurosci. 11, 1649–1659.

Belhage, B., Hansen, G.H., Schousboe, A., 1993. Depolarization by K+ and glutamate activates different neurotransmitter release mechanisms in GABAergic neurons: vesicular versus non-vesicular release of GABA. Neuroscience 54, 1019–1034.

Bjorklund, A., Lindvall, O., 2000. Cell replacement therapies for central nervous system disorders. Nat. Neurosci. 3, 537–544.

Borodinsky, L.N., Fiszman, M.L., 1998. Extracellular potassium concentration regulates proliferation of immature cerebellar granule cells. Brain Res. Dev. Brain Res. 107, 43–48.

Campbell, K., 2003. Dorsal–ventral patterning in the mammalian telencephalon. Curr. Opin. Neurobiol. 13, 50–56.
Canals, J.M., Checa, N., Marco, S., Akerud, P., Michels, A., Perez-Navarro, E., Tolosa, E., Arenas, E., Alberch, J., 2001. Expression of brain-derived neurotrophic factor in cortical neurons is regulated by striatal target area. J. Neurosci. 21, 117–124.
Cattaneo, E., Conti, L., 1998. Generation and characterization of embryonic striatal conditionally immortalized ST14A cells. J. Neurosci. Res. 53, 223–234.
Checa, N., Canals, J.M., Alberch, J., 2000. Developmental regulation of BDNF and NT-3 expression by quinolinic acid in the striatum and its main connections. Exp. Neurol. 165, 118–124.
Ciccolini, F., Collins, T.J., Sudhoelter, J., Lipp, P., Berridge, M.J., Bootman, M.D., 2003. Local and global spontaneous calcium events regulate neurite outgrowth and onset of GABAergic phenotype during neural precursor differentiation. J. Neurosci. 23, 103–111.
Conti, L., Sipione, S., Magrassi, L., Bonfanti, L., Rigamonti, D., Pettirossi, V., Peschanski, M., Haddad, B., Pelicci, P., Milanesi, G., Pelicci, G., Cattaneo, E., 2001. Shc signaling in differentiating neural progenitor cells. Nat. Neurosci. 4, 579–586.
Cui, H., Bulleit, R.F., 1998. Potassium chloride inhibits proliferation of cerebellar granule neuron progenitors. Brain Res., Dev. Brain Res. 106, 129–135.
Daadi, M.M., Saporta, S., Willing, A.E., Zigova, T., McGrogan, M.P., Sanberg, P.R., 2001. In vitro induction and in vivo expression of bcl-2 in the hNT neurons. Brain Res. Bull. 56, 147–152.
Dinsmore, J., Ratliff, J., Deacon, T., Pakzaban, P., Jacoby, D., Galpern, W., Isacson, O., 1996. Embryonic stem cells differentiated in vitro as a novel source of cells for transplantation. Cell Transplant. 5, 131–143.
Doering, L.C., Snyder, E.Y., 2000. Cholinergic expression by a neural stem cell line grafted to the adult medial septum/diagonal band complex. J. Neurosci. Res. 61, 597–604.
Encinas, M., Iglesias, M., Liu, Y., Wang, H., Muhaisen, A., Cena, V., Gallego, C., Comella, J.X., 2000. Sequential treatment of SH-SY5Y cells with retinoic acid and brain-derived neurotrophic factor gives rise to fully differentiated, neurotrophic factor-dependent, human neuron-like cells. J. Neurochem. 75, 991–1003.
Englund, U., Fricker-Gates, R.A., Lundberg, C., Bjorklund, A., Wictorin, K., 2002. Transplantation of human neural progenitor cells into the neonatal rat brain: extensive migration and differentiation with long-distance axonal projections. Exp. Neurol. 173, 1–21.
Gavalda, N., Perez-Navarro, E., Gratacos, E., Comella, J.X., Alberch, J., 2004. Differential involvement of phosphatidylinositol 3-kinase and p42/p44 mitogen activated protein kinase pathways in brain-derived neurotrophic factor-induced trophic effects on cultured striatal neurons. Mol. Cell. Neurosci. 25, 460–468.
Gu, X., Spitzer, N.C., 1995. Distinct aspects of neuronal differentiation encoded by frequency of spontaneous Ca2+ transients. Nature 375, 784–787.
Hamasaki, T., Goto, S., Nishikawa, S., Ushio, Y., 2003. Neuronal cell migration for the developmental formation of the mammalian striatum. Brain Res., Brain Res. Rev. 41, 1–12.
Hanada, M., Krajewski, S., Tanaka, S., Cazals-Hatem, D., Spengler, B.A., Ross, R.A., Biedler, J.L., Reed, J.C., 1993. Regulation of Bcl-2 oncoprotein levels with differentiation of human neuroblastoma cells. Cancer Res. 53, 4978–4986.
Haydar, T.F., Wang, F., Schwartz, M.L., Rakic, P., 2000. Differential modulation of proliferation in the neocortical ventricular and subventricular zones. J. Neurosci. 20, 5764–5774.
Henion, P.D., Weston, J.A., 1994. Retinoic acid selectively promotes the survival and proliferation of neurogenic precursors in cultured neural crest cell populations. Dev. Biol. 161, 243–250.
Herberth, B., Pataki, A., Jelitai, M., Schlett, K., Deak, F., Spat, A., Madarasz, E., 2002. Changes of KCl sensitivity of proliferating neural progenitors during in vitro neurogenesis. J. Neurosci. Res. 67, 574–582.
Jain, M., Armstrong, R.J., Barker, R.A., Rosser, A.E., 2001. Cellular and molecular aspects of striatal development. Brain Res. Bull. 55, 533–540.
Kao, J.P., Harootunian, A.T., Tsien, R.Y., 1989. Photochemically generated cytosolic calcium pulses and their detection by fluo-3. J. Biol. Chem. 264, 8179–8184.
Katsura, M., Shuto, K., Mohri, Y., Shigeto, M., Ohkuma, S., 2002. Functional significance of nitric oxide in ionomycin-evoked [3H]GABA release from mouse cerebral cortical neurons. J. Neurochem. 81, 130–141.
Kim, J.H., Auerbach, J.M., Rodriguez-Gomez, J.A., Velasco, I., Gavin, D., Lumelsky, N., Lee, S.H., Nguyen, J., Sanchez-Pernaute, R., Bankiewicz, K., McKay, R., 2002. Dopamine neurons derived from embryonic stem cells function in an animal model of Parkinson's disease. Nature 418, 50–56.
Kornyei, Z., Toth, B., Tretter, L., Madarasz, E., 1998. Effects of retinoic acid on rat forebrain cells derived from embryonic and perinatal rats. Neurochem. Int. 33, 541–549.
LoTurco, J.J., Owens, D.F., Heath, M.J., Davis, M.B., Kriegstein, A.R., 1995. GABA and glutamate depolarize cortical progenitor cells and inhibit DNA synthesis. Neuron 15, 1287–1298.
Lundberg, C., Martinez-Serrano, A., Cattaneo, E., McKay, R.D., Bjorklund, A., 1997. Survival, integration, and differentiation of neural stem cell lines after transplantation to the adult rat striatum. Exp. Neurol. 145, 342–360.
Lundberg, C., Englund, U., Trono, D., Bjorklund, A., Wictorin, K., 2002. Differentiation of the RN33B cell line into forebrain projection neurons after transplantation into the neonatal rat brain. Exp. Neurol. 175, 370–387.
Maden, M., 2002. Retinoic acid and limb regeneration—A personal view. Int. J. Dev. Biol. 46, 883–886.
Marin, C., Bove, J., Bonastre, M., Tolosa, E., 2003. Effect of acute and chronic administration of U50,488, a kappa opioid receptor agonist, in 6-OHDA-lesioned rats chronically treated with levodopa. Exp. Neurol. 183, 66–73.
Martinez-Serrano, A., Bjorklund, A., 1997. Immortalized neural progenitor cells for CNS gene transfer and repair. Trends Neurosci. 20, 530–538.
McCarthy, K.D., de Vellis, J., 1980. Preparation of separate astroglial and oligodendroglial cell cultures from rat cerebral tissue. J. Cell Biol. 85, 890–902.
Mizuno, K., Carnahan, J., Nawa, H., 1994. Brain-derived neurotrophic factor promotes differentiation of striatal GABAergic neurons. Dev. Biol. 165, 243–256.
Palmer, T.D., Takahashi, J., Gage, F.H., 1997. The adult rat hippocampus contains primordial neural stem cells. Mol. Cell. Neurosci. 8, 389–404.
Patz, S., Wirth, M.J., Gorba, T., Klostermann, O., Wahle, P., 2003. Neuronal activity and neurotrophic factors regulate GAD-65/67 mRNA and protein expression in organotypic cultures of rat visual cortex. Eur. J. Neurosci. 18, 1–12.
Perez-Navarro, E., Canudas, A.M., Akerund, P., Alberch, J., Arenas, E., 2000. Brain-derived neurotrophic factor, neurotrophin-3, and neurotrophin-4/5 prevent the death of striatal projection neurons in a rodent model of Huntington's disease. J. Neurochem. 75, 2190–2199.
Redies, C., Kovjanic, D., Heyers, D., Medina, L., Hirano, S., Suzuki, S.T., Puelles, L., 2002. Patch/matrix patterns of gray matter differentiation in the telencephalon of chicken and mouse. Brain Res. Bull. 57, 489–493.
Rossi, F., Cattaneo, E., 2002. Opinion: neural stem cell therapy for neurological diseases: dreams and reality. Nat. Rev., Neurosci. 3, 401–409.
Ruberte, E., Friederich, V., Chambon, P., Morriss-Kay, G., 1993. Retinoic acid receptors and cellular retinoid binding proteins. III. Their differential transcript distribution during mouse nervous system development. Development 118, 267–282.
Rubio, F.J., Bueno, C., Villa, A., Navarro, B., Martinez-Serrano, A., 2000. Genetically perpetuated human neural stem cells engraft and differentiate into the adult mammalian brain. Mol. Cell. Neurosci. 16, 1–13.

Snyder, E.Y., Deitcher, D.L., Walsh, C., Arnold-Aldea, S., Hartwieg, E.A., Cepko, C.L., 1992. Multipotent neural cell lines can engraft and participate in development of mouse cerebellum. Cell 68, 33–51.

Snyder, E.Y., Yoon, C., Flax, J.D., Macklis, J.D., 1997. Multipotent neural precursors can differentiate toward replacement of neurons undergoing targeted apoptotic degeneration in adult mouse neocortex. Proc. Natl. Acad. Sci. U. S. A. 94, 11663–11668.

Song, H., Stevens, C.F., Gage, F.H., 2002. Astroglia induce neurogenesis from adult neural stem cells. Nature 417, 39–44.

Spitzer, N.C., Debaca, R.C., Allen, K.A., Holliday, J., 1993. Calcium dependence of differentiation of GABA immunoreactivity in spinal neurons. J. Comp. Neurol. 337, 168–175.

Suñol, C., Artigas, F., Tusell, J.M., Gelpi, E., 1988. High-performance liquid chromatography-fluorescence detection method for endogenous gamma-aminobutyric acid validated by mass spectrometric and gas chromatographic techniques. Anal. Chem. 60, 649–651.

The Huntington's Disease Collaborative Research Group, 1993. A novel gene containing a trinucleotide repeat that is expanded and unstable on Huntington's disease chromosomes. Cell 72, 971–983.

Toresson, H., Mata, d.U., Fagerstrom, C., Perlmann, T., Campbell, K., 1999. Retinoids are produced by glia in the lateral ganglionic eminence and regulate striatal neuron differentiation. Development 126, 1317–1326.

Trimble, W.S., 1998. Synaptic vesicle proteins: a molecular study. In: Lazarovici, P. (Ed.), Cellular and Molecular Mechanism of Toxin Action. Harwood, Amsterdam, pp. 3–43.

Ventimiglia, R., Mather, P.E., Jones, B.E., Lindsay, R.M., 1995. The neurotrophins BDNF, NT-3 and NT-4/5 promote survival and morphological and biochemical differentiation of striatal neurons in vitro. Eur. J. Neurosci. 7, 213–222.

Vonsattel, J.P., DiFiglia, M., 1998. Huntington disease. J. Neuropathol. Exp. Neurol. 57, 369–384.

Wagner, J., Akerud, P., Castro, D.S., Holm, P.C., Canals, J.M., Snyder, E.Y., Perlmann, T., Arenas, E., 1999. Induction of a midbrain dopaminergic phenotype in Nurr1-overexpressing neural stem cells by type 1 astrocytes. Nat. Biotechnol. 17, 653–659.

Watt, S.D., Gu, X., Smith, R.D., Spitzer, N.C., 2000. Specific frequencies of spontaneous Ca2+ transients upregulate GAD 67 transcripts in embryonic spinal neurons. Mol. Cell. Neurosci. 16, 376–387.

Watts, C., Dunnett, S.B., 2000. Towards a protocol for the preparation and delivery of striatal tissue for clinical trials of transplantation in Huntington's disease. Cell Transplant. 9, 223–234.

Weiss, S., 1988. Excitatory amino acid-evoked release of gamma-[3H]aminobutyric acid from striatal neurons in primary culture. J. Neurochem. 51, 435–441.

Wong, R.O., Ghosh, A., 2002. Activity-dependent regulation of dendritic growth and patterning. Nat. Rev., Neurosci. 3, 803–812.

Yamada, M.K., Nakanishi, K., Ohba, S., Nakamura, T., Ikegaya, Y., Nishiyama, N., Matsuki, N., 2002. Brain-derived neurotrophic factor promotes the maturation of GABAergic mechanisms in cultured hippocampal neurons. J. Neurosci. 22, 7580–7585.